

Alma Mater Studiorum – Università di Bologna

DOTTORATO DI RICERCA IN

**Ingegneria Civile, Chimica, Ambientale e dei
Materiali**

Ciclo XXIX

Settore Concorsuale di afferenza: 08/B3

Settore Scientifico disciplinare: ICAR/09

TITOLO TESI

**The development of a new hysteretic device:
The Crescent Shaped Brace**

Presentata da: Antoine Dib

Coordinatore Dottorato

Luca Vittuari

Relatore

Tomaso Trombetti

Correlatore

Stefano Silvestri

Esame finale anno 2017

“We are all pilgrims who seek Italy”

Johann Wolfgang von **Goethe**

*Thanks to my parents, I have a life
And thanks to Italy, I know how to enjoy it*

ACKNOWLEDGMENTS

The legend says that when God finished his work in the sixth day, he went to relax in his paradise, but he left his shoe somewhere on the earth. The story does not stop here; it continues and says that everyone touches this shoe, may gain magical powers and takes whatever he wants from the paradise.

Being fascinated by this legend since my childhood, I decided to search for the God's shoe to have the magical powers. But unfortunately, the relation between every legend and every child is destined to fade with time; and my case was not so different. I grow up and I forgot this legend.

Until one day, I received a mail from Dunia-Beam project, congratulating me that I won a full scholarship, three years in Italy, at the Alma Mater Studiorum, to have a PhD degree in civil engineering. And then, after arriving to Italy, I discovered that the legend was not a legend, and the God's Shoe was not an invention and the magical powers are not a lie. Yes, everything was true; really, I am telling you the truth!!! I discovered that Italy is the God's Shoe, and that Italians are the fortunate people to touch this shoe and take from the paradise wherever they want: they took the beauty, the art, best artists, best food, best fashion, best life, best nature, best cars...and best engineers!

For this reason, with the text of this thesis completed in my hands, I would like to express my gratitude to every one helped me to believe again in legends: my supervisor, Prof. Tomaso Trombetti, a great person who changed in me the way of seeing the world of engineering with his creativity and authenticity of thinking. I also would like to thank my co-supervisor, Prof. Stefano Silvestri, another great humble person who significantly contributed to the development of this thesis. A big hug is dedicated to my friends and colleagues, with whom I shared a lot of moments: Michele for all his support and help in this thesis, and of course for all the coffee breaks we spent together. How can I forgot all the laughs I had with Simo (who discovered as well how many types of laughs I have), LA Martucia, Luca, Giada, Diego, Roby and all

the friends I spent with them beautiful moments and had amazing dinners, Spritz and Cotolette.

A big big “thank you” goes to all my friends, who always supported me and helped me to discover myself in parallel with my PhD program. And so, thank you Hiba, Liuba, Christina, Clelia, Pietro, Tim-Noah, Donatella, Davide, Silvia, Alessandro, Wal, Federico, Michelangelo, Olgu, Angela, Sarah... and all the other friends I don't explicitly mention here.

Final thanks to my family for the absolute confidence in me and the constant support even via calls....

What can I say more? Maybe a final Thumb up!!!

Ah yes, I forgot to tell you that during my childhood, I was fascinated about another legend as well, a man who discovered a secret passage to go and play with Superheroes in Paradise, I hope to find this passage as soon as possible!!!

Bologna, 31/03/2017

Antoine

ABSTRACT

Negli ultimi cinquant'anni, molti studi e ricerche sono stati condotti nell'ambito di sistemi di isolamento sismico, tecnologie innovative di resistenza al terremoto e smorzamenti supplementari, con lo scopo di fornire all'ingegneria strutturale degli strumenti atti ad incrementare notevolmente le prestazioni sismiche delle strutture.

Il "Crescent Shaped Braces" (CSB) è un nuovo dispositivo isteretico in acciaio da introdurre in combinazione diagonale in strutture intelaiate, recentemente proposto dal nostro gruppo di ricerca dell'Università di Bologna nell'ambito del Performance Based Seismic Design.

Contrariamente al convenzionale sistema di controventamento concentrico diagonal, il CSB consente al progettista di scegliere la rigidezza laterale indipendentemente dalla resistenza allo snervamento del dispositivo, grazie alla sua peculiare forma ad-hoc.

Nella presente tesi, viene trattato lo studio del dispositivo CSB. Sono stati sviluppati modelli analitici al fine di descrivere la risposta del sistema a carichi di trazione e compressione, sia nella prima fase elastica che dopo il raggiungimento del limite a snervamento. Al fine di validare i risultati ottenuti dalla modellazione analitica e valutare la capacità del sistema sottoposto a carico ciclico, sono state condotte diverse simulazioni numeriche utilizzando più software di calcolo. Inoltre, sono stati effettuati test sperimentali, consistenti in prove monotone pseudo-statiche e prove cicliche, su tredici dispositivi campioni realizzati in scala con diverse sezioni trasversali. La risposta complessiva sperimentale in termini di rigidezza, resistenza, duttilità e instabilità globale è stata confrontata con i risultati ottenuti dalle analisi analitiche e numeriche. È stato rilevato che il comportamento complessivo del dispositivo CSB, mostrato dalle prove sperimentali, viene colto adeguatamente dal modello analitico sviluppato e che, i software commerciali utilizzati sono sufficientemente adatti a simularne la risposta isteretica.

Dopo aver valutato le capacità strutturali del Crescent Shaped Brace, un nuovo concetto di progettazione sismica è stato sviluppato nell'ambito del Performance Based Seismic Design e il sistema "enhanced first story". Esso si basa sulla separazione tra Sistema Resistente Verticale (VRS) e Sistema Resistente Orizzontale (HRS) al fine di ottenere una certa "objective curve" della struttura. Sulla base di questa nuova concezione strutturale, un esempio applicativo di dispositivo HRS è stato studiato con lo scopo di sfruttare i vantaggi offerti dall'uso del CSB come sistema di dissipazione sismica. Infine, sono stati presentati ulteriori utilizzi indicativi del CSB, non solo come elemento dissipativo al livello del primo piano ("enhanced first story"), ma anche come collegamento orizzontale, rinforzo angolare per giunti trave-colonna ed elementi dissipativi di facciata.

Parole chiave: Crescent Shaped Braces, Nuovi Dispositivi di Dissipazione Isteretica, Performance Based Seismic Design, Sistema Resistente Orizzontale, Nuovo Approccio Sismico, Objective Curve, Curva di Capacità

ABSTRACT

Over the last fifty years, extensive researches have been conducted in the field of seismic isolation systems, innovative earthquake resisting systems and supplemental damping, showing a potential step towards the boosting of the seismic performance of buildings.

The Crescent Shaped Braces (CSB) is a new simple steel hysteretic device, recently proposed by our group of research at the University of Bologna to be used as an enhanced diagonal brace in framed structures, within the Performance Based Seismic Design framework. By making use of CSBs as lateral resisting system and contrarily to the conventional concentric stiff diagonal braces, the CSB allows the practical designer to choose the lateral stiffness independently from the yield strength of the device, due to its peculiar ad-hoc shape.

In the present thesis, a complete study referring to the crescent shaped brace has been presented. Analytical formulas have been developed to describe the behavior of such devices under tensile and compressive loads, in elastic and post-yielding phases. The same device has been studied through extensive numerical simulations to assess the seismic capacity and its response under cyclic loads. As well, the main results of experimental tests conducted on thirteen scaled CSB specimens realized with different cross-sections are presented. Both monotonic pseudo-static tests and cyclic tests have been performed in order to further assess the seismic behavior of such devices. The overall experimental response in terms of stiffness, strength, ductility and global instability is compared with the design formulations and with the results of numerical simulations developed with commercial software. It is shown that the overall experimental behavior of CSB is well captured by the design formulas and that commercial software are suitable to simulate the hysteretic response of such device.

After the validation of the analytical formulas and the hysteretic capacities of the Crescent Shaped Braces, a new seismic concept has been proposed within the

Performance Based Seismic Design and the concept of the enhanced first story. It relies on the total separation between the Vertical Resisting System (VRS) and the Horizontal Resisting System (HRS) in order to attain a certain objective curve of the structure. An applicative example has been studied following this concept and exploiting the advantages of the CSBs as seismic dissipative devices, to be used for the HRS.

Some indicative use of the CSB have been presented, not just as dissipative elements in the level of the first story, as well as horizontal link, angle reinforcement for beam-column joints and façade dissipative elements.

Keywords: Crescent Shaped Braces, New Hysteretic Dissipative Devices, Performance Based Seismic Design, Horizontal Resisting System, New Seismic Approach, Objective Curve, Capacity curve

Table of contents

ACKNOWLEDGMENTS	v
ABSTRACT	i
ABSTRACT	iii
Table of contents	v
List of Figures.....	ix
List of Tables	xii
1. Introduction	1
1.1. Background and Motivations	1
1.2. Problem Description.....	3
1.3. Organization and objectives of the thesis.....	4
PART A: Seismic Philosophies Design and Dissipative Techniques	8
2. Seismic Protection of Structures	10
2.1. Introduction	10
2.2. Traditional Philosophy of a Seismic Design	13
2.3. Modern approach through structure control: energy dissipation systems.....	14
2.3.1. Active Control System.....	17
2.3.2. Semi-Active and Hybrid Control System	18
2.3.3. Passive Control System	19
2.4. Hysteretic Dampers	22
2.5. Conclusions	25
3. Seismic Design Philosophies and Concepts.....	27
3.1. Introduction	27
3.2. Traditional and New Approaches of Seismic Design	28
3.2.1. Traditional Method	28
3.2.2. Innovative Methods	29
3.3. Capacity Spectrum Curve.....	33
3.4. The Proposed Method	34
3.5. Conclusions	37

4.	The Proposed Method and the Objective Curve	39
4.1.	The Structural Concept.....	39
4.2.	Vertical System	41
4.3.	Desired Objective Curve	44
4.4.	Horizontal System	44
4.5.	CSB Devices To Fulfill The Performance Objectives	46
4.6.	Conclusions	51
	PART B: Constitutive Behavior of the Crescent Shaped Brace.....	54
5.	Behavior of CSB: Analytical Developments	56
5.1.	Introduction	56
5.2.	Geometrical and Mechanical Properties	56
5.3.	Equilibrium Equations.....	59
5.4.	The linear elastic behavior	59
5.5.	the post elastic behavior	62
5.6.	Applicative Example	63
5.6.1.	Behavior under Tensile Loads	64
5.6.2.	Behavior under Compressive Loads.....	73
5.7.	The Double CSB Equations	78
5.8.	Conclusions	79
6.	Behavior of CSB: Numerical Simulation.....	81
6.1.	Introduction	81
6.2.	Behaviour under Tensile Loads.....	83
6.3.	Behaviour under Compressive Loads	84
6.4.	Influence of The Cross Section	86
6.5.	Influence of The Coupled CSB	88
6.6.	Influence of The Double CSB.....	90
6.7.	The Material Behavior	93
6.8.	Conclusions	94
7.	Behavior of CSB: Experimental Tests	97
7.1.	Description of the Experimental Tests	97
7.1.1.	Geometrical and mechanical properties of the specimens.....	97

7.1.2.	Test set-up and protocols	100
7.1.3.	Main goals of the experimental tests	107
7.2.	The Force – DIsplacement response	109
7.3.	The Effect of Welding on The Crescent Shaped Brace.....	124
7.3.1.	Analysis of the tensional state	124
7.3.2.	Identification of the situation of highest stress and calculation of the maximum stress in the tensile cycle.....	125
7.3.3.	Identification of the situation of the highest stress and the calculation of the maximum stress in the compression cycle.....	126
7.3.4.	Remarks	126
7.4.	Assessment of The Ductility Capacity	127
7.5.	Energy Dissipation Capacity	128
7.6.	Local Deformations Through The DIC Technique	132
7.6.1.	The digital image correlation (DIC)	132
7.6.2.	The deformation fields through the DIC technique	134
7.7.	Conclusions	138
8.	Analytical Numerical Experimental Correlation Study	141
8.1.	The Numerical Results	141
8.2.	The Force-Displacement Curves	142
8.3.	The Material Behavior	144
8.4.	Conclusions	146
	PART C: Design Solutions and Procedures	150
9.	Possible Dispositions of The Crescent Shaped Braces	152
9.1.	The First Soft Story Concept.....	152
9.2.	The Strongback or Backbone Concept.....	157
9.3.	Other solution (external facades, single disposition, double disposition).....	160
9.3.1.	CSB AS A BEAM-COLUMN JOINT.....	161
9.3.2.	CSB AS A HORIZONTAL LINK.....	161
9.3.3.	CSB AS DISSIPATIVE DEVICES ALONG THE STRUCTURE.....	162
10.	Design Procedure	165
10.1.	Introduction	165

10.2. The Proposed Approach and The Concept of the First Storey Isolation.....	165
10.3. Applicative Example	177
10.3.1. Load Analysis	180
10.3.2. Numerical Application:.....	181
10.4. Conclusions	187
11. Conclusions and Future Developments.....	188
11.1. Main Conclusions.....	188
11.2. Future Developments	191
Appendix A: Calculation of δ (under flexion) of a system composed of single element with two different inertia.....	192
References	194

List of Figures

Figure 2.1 The seismic energy dissipation concept.....	11
Figure 2.2 Categories of structural seismic protections	13
Figure 2.3 Influence of base isolation	15
Figure 2.4 Influence of viscous dampers.....	16
Figure 2.5 Active Control System Working Chart.....	17
Figure 2.6 Semi-Active Control System Working Chart	18
Figure 2.7 Hybrid Control System Working Chart	19
Figure 2.8 Passive Control System Working Chart.....	20
Figure 2.9. A viscous damper inserted inside a residential building.....	21
Figure 2.10 The TMD inserted in the Taipei Tower	22
Figure 2.11 An example of a Rotational Friction Damper	24
Figure 2.12 Example of Concentrated Dissipative Braces	25
Figure 3.1 The Performance Based Seismic Design Objectives	31
Figure 3.2 The desired Objective Curve Normalized in terms of F_y and δ_y	36
Figure 4.1 An example of a soft or weak first story building.....	41
Figure 4.2 The difference between the VRS capacity curve and the objective curve	45
Figure 4.3 The CSB are inserted at the first level based on the concept of enhanced first story ..	47
Figure 4.4 The building designed to verify the PBSO objectives using CSB	48
Figure 4.5 The Castel Hill School in Bisignano.....	49
Figure 4.6 The behavior difference between the naked and the equipped structure in X direction	50
Figure 4.7 Example of the inserted CSB in X direction.....	50
Figure 4.8 The behavior difference between the naked and the equipped structure in Y direction	51
Figure 5.1 A single Crescent Shaped Brace	56
Figure 5.2 A single Crescent shaped Brace inserted in a frame	57
Figure 5.3 Geometrical characteristics of a CSB device	59
Figure 5.4 The stress-strain steel behavior	64
Figure 5.5 the deformation of a CSB device under tensile loads	65
Figure 5.6 The change of the section characteristics after the yielding point	67
Figure 5.7 Analytical response of a rectangular cross section CSB device under tensile loads ...	73
Figure 5.8 The deformation of a CSB device under compression.....	74
Figure 5.9 Analytical response of a CSB device under compressive loads	78
Figure 5.10 Double CSB devices inserted together.....	78
Figure 5.11 The force acting on one half of one CSB device from a double disposition	79
Figure 6.1 The Menegotto-Pinto Model.....	82
Figure 6.2 Force-Displacement curve of a rectangular cross section CSB under tensile loads	84
Figure 6.3 Force-Displacement curve of a rectangular CSB under compressive loads	85
Figure 6.4 The tensile response of different cross section CSBs	87
Figure 6.5 The compressive response of different cross section CSBs.....	88
Figure 6.6 A couple CSBs inserted in a generic frame	89
Figure 6.7 The behavior force-displacement of coupled CSBs inserted in a generic frame	90
Figure 6.8 The Force(kN)-Displacement(m) curve (grey) of a single circular cross section CSB under tensile loads	90

Figure 6.9 The Force-Displacement curve (grey) of a double circular cross section CSB under tensile loads	91
Figure 6.10 The Force(kN)-Displacement(m) curve (grey) of a single circular cross section CSB under compressive loads.....	92
Figure 6.11 The Force(kN)-Displacement(m) curve (grey) of a double circular cross section CSB under compressive loads.....	92
Figure 6.12 The material response under cyclic loading (ABAQUS).....	93
Figure 7.1 Six Specimens (rectangular and circular cross section) before testing with ends details	99
Figure 7.2 RW1R, RR1R, TW1R before testing with welding details	100
Figure 7.3 The universal traction machine	101
Figure 7.4 Details of the bolts used at the extremities.....	101
Figure 7.5 The typical loading protocols: left) traction, middle) compression, right) reversed..	104
Figure 7.6 RR2R, RW2R, RW3R and TW2R before testing	108
Figure 7.7 RW2R inserted in the test machine during the test loading	108
Figure 7.8 The adopted measures for the rectangular cross section specimens	109
Figure 7.9 The force-displacement response of R1T	110
Figure 7.10 The force-displacement response of R2C	111
Figure 7.11 The force-displacement response of R3R	111
Figure 7.12 The applied dimensions for circular cross section specimens	112
Figure 7.13 The force-displacement response of C1T	113
Figure 7.14 The ovalisation of the bolt hole.....	114
Figure 7.15 The force-displacement response of C2C	114
Figure 7.16 The force-displacement response of C3R	115
Figure 7.17 The applied geometry of the welded rectangular cross section specimens.....	116
Figure 7.18 The force-displacement response of RW1(C+T)	117
Figure 7.19 The force-displacement response of RW2R	118
Figure 7.20 The force-displacement response of RW3R	119
Figure 7.21 The applied geometry for the rectangular cross section with ribs specimens.....	119
Figure 7.22 The force-displacement response of RR1R.....	120
Figure 7.23 The force-displacement response of RR2R.....	121
Figure 7.24 The applied geometry for the tubular cross section specimen	122
Figure 7.25 The force-displacement response of TW1R.....	123
Figure 7.26 The force-displacement response of TW2R.....	123
Figure 7.27 The RW1 before being welded	124
Figure 7.28 Ductility capacity of the R3R specimen left) in tension, Right) in compression....	128
Figure 7.29 Ductility capacity of the C3R specimen left) in tension, Right) in compression....	128
Figure 7.30 R3R equivalent damping ratio Left) Tension; Right) Compression	129
Figure 7.31 C3R equivalent damping ratio Left) Tension; Right) Compression	130
Figure 7.32 RR1R equivalent damping ratio Left) Tension; right) Compression.....	130
Figure 7.33 RW2R equivalent damping ratio Left) Tension; Right) Compression	131
Figure 7.34 TW2R equivalent damping ratio Left) Tension; Right) Compression.....	131
Figure 7.35 Basic concept of the image correlation	133
Figure 7.36 R3R and RW1R colored to be tested by the DIC technique	134
Figure 7.37 The results by the DIC technique of the RW1R specimen	134
Figure 7.38 The correspondent DIC technique results to the force-displacement behavior curve of the specimen C1T	135

Figure 7.39 The correspondent DIC technique results to the force-displacement behavior curve of the specimen C2C.....	136
Figure 7.40 The material behavior of the C3R specimen under reversed test.....	137
Figure 8.1 The force-displacement curve under tensile loads.....	143
Figure 8.2 The force-displacement curve under compressive loads.....	144
Figure 8.3 Comparison between numerical and real material behavior.....	145
Figure 8.4 Comparison between numerical and real material behavior.....	146
Figure 9.1 Possible dispositions of the CSB: from left to right: first story isolation, Diagonal dissipative elements, double diagonal dissipative elements, and horizontal links.....	152
Figure 9.2 An example of a residential building with a weak first story.....	153
Figure 9.3 The above residential building idealized as a SDOF with the mass of the upper-structure m	153
Figure 9.4 The proposed approach is the combination of the Fintel & Khan concept and the PBSO.....	155
Figure 9.5 The idealization of a building as a simple oscillator or SDOF.....	155
Figure 9.6 Difference between the response of a backbone and soft first story structures.....	158
Figure 9.7 Different backbone structures types.....	158
Figure 9.8 Crescent Shaped Brace Element can be used as horizontal link or angle reinforcement.....	161
Figure 9.9 VIII Agosto Building in Bologna City.....	162
Figure 9.10 single coupled CSBs inserted in VIII Agosto building.....	163
Figure 9.11 A double coupled CSB devices inserted in a frame as a Pall Friction Damper.....	163
Figure 9.12 VIII Agosto enhance by double CSB devices.....	164
Figure 10.1 The SDOF idealization of the ‘enhanced first story’ isolated structure.....	166
Figure 10.2 The objective curve in terms of stiffness, strength ductility and earthquake levels.....	168
Figure 10.3 The different resisting systems of the proposed approach.....	173
Figure 10.4 CSB inserted in a frame.....	174
Figure 10.5 Coupled CSB inserted in an ‘enhanced first-story’ building.....	175
Figure 10.6 Flow-chart of the proposed procedure.....	176
Figure 10.7 Plan and Facades of the first floor of the studied example.....	178
Figure 10.8 Plan Details.....	179
Figure 10.9 VRS Capacity curve.....	181
Figure 10.10 The objective curve (black), VRS capacity curve (Red) and the HRS capacity curve (Blue).....	184
Figure 10.11 the total response F-d of a couple of CSB, one is stretched under tensile loads, the other is compressed under compressive loads (cross section HE240B, $d/L=0.1$).....	185
Figure 10.12 Capacity curve of the Horizontal Resisting System (HRS) composed of four couples of Crescent shaped Braces stretched/compressed in every direction.....	186

List of Tables

Table 5-1 i/h of typical steel profiles.....	58
Table 5-2 Deformation values under elastic tensile loads.....	65
Table 5-3 Deformation values under elastic tensile loads (second method).....	66
Table 5-4 Deformation values of CSB device under post-elastic tensile loads.....	71
Table 5-5 Deformation values of CSB device under plastic tensile loads.....	71
Table 5-6 The values of the hardening response of a (4.14x1.5 cm) CSB devcice.....	72
Table 5-7 Deformations value of a CSB device udner elastic compressive loads.....	76
Table 5-8 Deformation values of a CSB device under post-elastic compressive loads.....	77
Table 6-1 Geometrical and mechaniccal properties of the studied profiles.....	86
Table 7-1 Geometrical properties of the studied specimens.....	99
Table 7-2 The applied protocol at the R1T specimen.....	104
Table 7-3 The applied protocol at the R2C specimen.....	104
Table 7-4 The applied protocol at the R3R specimen.....	105
Table 7-5 The applied protocol at the C1T specimen.....	105
Table 7-6 The applied protocol at the C2C specimen.....	105
Table 7-7 The applied protocol at the C3R specimen.....	105
Table 7-8 The applied protocol at the RW1(C+T) specimen.....	106
Table 7-9 The applied protocol at the RW2R specimen.....	106
Table 7-10 The applied protocol at the RW3R specimen.....	106
Table 7-11 The applied protocol at the RR1R specimen.....	106
Table 7-12 The applied protocol at the RR2R specimen.....	107
Table 7-13 The applied protocol at the TW1R specimen.....	107
Table 7-14 The applied protocol at the TW2R specimen.....	107
Table 8-1 Comparison between analytical and experimental numerical results.....	142
Table 10-1 the performance objectives.....	168
Table 10-2 Parameters to define the seismic hazard for the city of Bologna.....	179

1. Introduction

1.1. BACKGROUND AND MOTIVATIONS

Life after an earthquake is definitely different than life before it: losses of lives, parents, friends, houses, properties... are sufficient to change way of life and print it with bad memories... Thus, the society trust engineers to build them facilities like houses, roads, offices, hospitals, theatres, dams... in a way that can afford a disaster like earthquakes and remain afterward functional without any loss.

Regarding numbers, the problem of earthquakes is not the live losses anymore, an average of 10,000 people die each year from earthquakes compared to 1,300,000 deaths by car accidents.

Looking to the number of death on the Italian territory for the last 20 years due to earthquakes, which is around 687 death (309 due to the L'Aquila earthquake 2009 and 295 under the Amatrice Earthquake 2016), with an average of 35 death per year, it is evident that this number is less than the number of victims of car accidents for example in the same country, which is 3753 just for the year 2013.

In japan for example, the number of deaths due to earthquakes in last 20 years is around 16022 deaths (15894 due to 2011 Earthquake, one of the biggest worldwide earthquakes) with an average of 801 deaths per year in front of 5971 deaths by car accident for the year 2013.

The real problem is the changes induced after a ground motion, the number of deaths after just one event and the collapse of buildings, apartments and even full villages. These changes cost the government/ civil communities a big amount of money. For example a UNESCO study gives damage losses amounting to \$10,000,000,000 from 1926 to 1950 due to earthquakes.

Putting a part that a big number of earthquake deaths are not related directly to structural failure but as well to fire, weather climate, nonstructural collapse... the old idea behind the structural seismic design that life safety is the goal of engineers and

society, is an under estimate goal of design and the new philosophies of design are more ambitious than the old concept. [31], [68], [80]

Thus, it is not strange to say that structural dynamics is the topic of the 21st century. It took almost the entire 20th century to bring the civil structural engineering profession to the point where buildings and other structures can be analyzed with a reasonable degree of confidence to evaluate their performance to real civil engineering types of forcing functions. The first part of the 20th century was primarily devoted to developing a basic theoretical foundation that incorporated the principles of mathematics and mechanics using very simple idealizations of structures. The result was that starting from the 1960s, structural analysis moved onto a much more sophisticated and accurate phase where it incorporated the mathematics of matrix methods and numerical analysis to develop analytical models of structures. This led to modern finite element methods of structural analysis using high-speed digital computers.

Recently, the Performance Based Seismic Design has been proposed as the most up-to-date methodology to predict the response of any structure under different types of ground motion, from fully operational response under frequent earthquakes to near collapse response under rare ones. [14], [17], [67]

In order to design a structure to withstand different levels of earthquakes, the correspondent actions acting on it must be specified. The amplitudes of the possible actions that will occur during the life of the structure cannot be known in a deterministic way. Thus a reliable estimation of their maximum expected values is important, since the cost of construction, and therefore the economic viability of the project depends on a safe and cost efficient final product. [13], [14],[49], [65]

Factors such as the dynamic characteristics of earthquakes, their duration and the effects of site conditions are all external to a building. No matter how well or poorly designed, a building has no control over those effects. A combination of factors such as the structural configuration of a building, its materials of construction and dynamic characteristics, as well as the quality of its structural design and construction, greatly influence how a building responds to any shaking it experiences. Therefore, it is better

to turn the attention to those aspects of a building itself that largely determine its seismic response.[14]

To have more precise idea about these forces, many procedures were developed to know the seismic forces: for regular building, an Equivalent Static Force method has been developed; for irregular buildings, Dynamic analyses are used. [13], [17], [30], [42]

Conventionally designed and constructed, earthquake-resistant buildings rely on significant inelastic actions or energy dissipation in selected components of the framing system in the design earthquake. For common used moment-resisting frames, inelastic action should occur in the beams near the columns and in the beam-column panel zones: both zones form part of the gravity-load-resisting system. Inelastic actions results in damage, which is often substantial in scope and difficult to repair. Damage to gravity-load-resisting system can result in significant direct and indirect (business interruption) losses. [31], [42],

The desire to avoid damage to components of gravity-load-resisting frames in buildings leads to add energy dissipation systems, to build frames focusing the energy dissipation during an earthquake into those disposable elements specifically designed for this purpose and to substantially reduce energy dissipation in the gravity-load-resisting frame. As energy dissipators do not form part of the gravity frame and can be replaced after an earthquake without compromising the structural integrity of the frame, passive metallic yielding, viscoelastic and viscous energy dissipators are now available in the marketplace.

1.2. PROBLEM DESCRIPTION

Not just researches aim was to describe mathematically the seismic behavior of any structure, but it was devoted to find solutions to the stability of the structure under any ground motion. Even though, many design philosophies have been proposed since modern Earthquake Engineering has been established in the 1960, they can be generally classified as traditional or innovative solutions. While traditional solutions mainly relies upon strength, stiffness and ductility capacities of frames, bracings and

walls, more innovative solutions are based on the use of energy dissipation devices or base isolation devices which absorb/ reduce the input energy which is transmitted to the structure by the earthquake ground motion.[13], [43], [49], [51],

Seismic Dampers are one among the solutions and they are used in place of structural elements, like diagonal braces, for controlling seismic damage in structures. They partly absorb the seismic energy and reduce the motion of buildings.

One of the design strategies allowing the achievement of multiple performance objectives is based on the conceptual separation of the vertical resisting system from the horizontal resisting system. Clearly, in order to design a structure behaving closely to the desired “objective curve” [49], the lateral resisting system must be conceived in order to be very flexible in terms of its stiffness, strength and ductility. In the recent years, researches have been focused on enhanced bracing systems, one of them, is the Crescent Shaped Braces, studied in this thesis. This device, thanks to its peculiar shape, allows design its lateral stiffness independently from its initial yield strength thus appearing suitable to be used for an enhanced lateral resisting system. Not just the independency between stiffness and strength is the only characteristic of the Crescent shaped Brace, the ductility which presents, and the last hardening behavior which avoid collapse under P-Delta effect, altogether form a good point for this device to be inserted in buildings, giving engineers a lot of independents parameters to play with.[26], [27], [55], [56], [64]

In the present thesis, the results of the experimental tests performed on scaled prototypes are presented and compared with analytical and numerical predictions, developed formerly and finishes with some examples of how the device can be inserted in a real building and all its possible dispositions.

1.3. ORGANIZATION AND OBJECTIVES OF THE THESIS

The thesis is organized in three parts: part A, part B and part C. Part A focuses on energy dissipation systems in the field of seismic engineering and is composed of three chapters: chapter 2 , chapter 3 and chapter 4. Part B is devoted to the study of on a new hysteretic dissipative device, the Crescent shaped Brace (CSB), and shows analytically (chapter 5), numerically (chapter 6) and experimentally (chapter 7) its constitutive

behavior and an overall comparison between the three results of the previous chapters (chapter 8), part C tries, through its two chapters (chapter 9 and chapter 10) to show some possible implementation of the CSB in real building cases.

The objective of part A is to have an overview above the field of seismic engineering dissipative elements, the development of seismic concepts and philosophies that are behind the Crescent Shaped Brace and a proposal of a new method of design based on the recent researches in the field of seismic engineering which push our team of research to develop this new device.

In details, chapter 2 presents a quick view over the earthquake resistance methods in seismic engineering world, from passive to active, semi active and other classical solutions. In details, passive devices and especially hysteretic ones are more investigated because the studied element in this thesis, the Crescent Shaped Brace, is classified under this category of devices.

Chapter 3 is a general presentation of the seismic design philosophies existing in the engineering world, traditional method which is the Force Based Design (FBD) and new ones like the Performance Based Seismic Design (PBSD) and the Direct Displacement Based Design (DDBD). Referring to the philosophy of the Performance Based Seismic Design, we proposed a new method to be admitted for structural design combining the objectives target of the PBSD and the capacity curve of the structure.

Chapter 4 explains in detail how it is possible to reach our new proposed method, separating between vertical resistant system and horizontal resisting system, where the last one can be reached by inserting special types of devices, as the Crescent Shaped Brace. An ultimate paragraph will be dedicated to show that those new elements, that we are going to study in part B, are able to fulfill the imposed seismic objectives showing previous studies done in the academic world.

The objective of part B is to assess the constitutive behavior of the Crescent Shaped Brace as well as its seismic and dissipative performances through analytical studies, numerical models and experimental campaigns.

Chapter 5 presents the analytical studies developed to understand the behavior of the new hysteretic device under imposed forces. It describes in detail its geometrical and

mechanical properties, the linear elastic and the post yielding behaviors, and trying to describe as well the softening and hardening responses.

Chapter 6 is a numerical study of the crescent shaped brace device both under tensile and compressive loads. The linear elastic and post elastic fields are described using SeismoStruct program. The influence of the cross section and of the inclination of the element has been studied in a second phase. The behavior of a simple crescent shaped brace, double elements and coupled ones are studied in details which can be useful for part C and the applicative example.

Chapter 7 presents a large experimental campaign carried out on 13 specimens in four different phases between 2014 and 2016. Through the experimental campaign, cyclic tensile, cyclic compressive and cyclic reversed tests are assessed on different types of cross sections: fully rectangular, fully rectangular with ribs, fully circular, tubular and welded fully rectangular cross sections. The chapter provides an interpretation of the experimental results and the force displacement behavior obtained from the tests. Ductility and energy dissipation capacities are studied and local deformations are investigated through the DIC technique.

Part B finishes with chapter 8 which is a comparison between the results of the previous chapter. In this chapter, it is clearly explained that the analytical equations developed in chapter 5 do not describe exactly the plastic behavior of the element, while numerical models can describe pretty good even they do not take in consideration the imperfection of the specimens. However, the whole results are really close one to each other and can describe clearly the new device.

Part C is the applicative part of the crescent shaped brace. It shows many possible displacements of the element into an existing or new building.

It starts with chapter 9, which shows how this element can be inserted in a real building. It can be inserted as horizontal resistant system in a first soft story structure, or it can be inserted as horizontal link between two different structures for seismic motives.

Chapters 10 contain the applicative example to show, in practice, how the design should be carried out using the crescent shaped braces as passive hysteretic dissipative elements through the building. First, the proposed concept is presented and the

corresponding steps are described, so that the entire numerical hypothesis are explained and justified. Then, the studied example is presented and the retrofit intervention is designed based on the concept admitted. The results of the analyses performed on the model of the original structure are presented. In chapter 10, the soft story concept, proposed by Fintel and Khan, was the main idea of the retrofitting, thus the flexible crescent shaped braces are used just in the ground floor while the upper structure is stiffened by concentrated braces.

Finally, Chapter 11 summarizes the main findings of the previous chapters. Recommendations for future research topics are as well provided.

PART A: Seismic Philosophies Design and Dissipative Techniques

Part A is a general introduction to introduce a new hysteretic dissipative device, the Crescent Shaped Brace (CSB) developed in part B and to a new design procedure introduced later in part C. To frame the CSB device, chapter 2 has the role to explain all possible energy dissipation techniques available now in the market of the seismic engineering with a special attention to the category of passive dissipative devices and hysteretic ones to which the CSB belongs.

Instead, chapter 3 is a brief review of the traditional and new seismic concepts used by designer to make there seismic decisions. At the end of this chapter, we proposed a new method to be used for seismic calculation. Chapter 4 develops conceptually this method based on a total separation between Horizontal resisting system and Vertical resisting system. This chapter ends with some examples of structures that were enhanced by CSB.

2. Seismic Protection of Structures

2.1. INTRODUCTION

While designing a structure to withstand an earthquake force, it is important to know the forces value acting on it in order to design properly the resisting elements. However, this knowledge is not easy because it depends on many factors: earthquake size, energy transmitted to the structure, distance of the fault to the structure, geological factors, even the structure itself...[4], [14], [15]

The main idea behind any seismic design is to know the amount of energy imparted into a structure during an earthquake ground motions, to design the structure in a way to handle this energy without or with the less possible damages and finally to construct the structure respecting the corresponding design.[1], [4], [14]

The investment in constructed facilities includes many components in addition to the structure. In fact, in most applications the cost of the structure is less than one fourth of the cost of the total investment (depend on way of life), and in industrial facilities this ratio may be even less. However, the survival of the entire investment depends on the survival of the structure. That is why the structural engineer has a critical responsibility and needs to be well informed about the behavior of the structure. [47], [52]

Thus, the seismic design of structures cannot be developed ignoring the energy approach of the design issue.

The load action of dynamic type introduces into a structural system certain amount of energy. The input energy is converted into stored energy and dissipated energy.

$$E_I \leq E_S + E_D$$

The energy E_S is stored in two distinct ways:

$$E_S = E_E + E_K$$

- E_E is the elastic strain energy

- E_K is the kinetic energy

Regarding the energy dissipated E_D , the dissipation occurs through two different mechanisms:

$$E_D = E_H + E_V$$

- E_H is the energy dissipated by hysteretic or plastic deformation (associated with strength that depend only on the deformation)

- E_V is the energy dissipated through viscous damping

In few worlds, it is possible to divide those energies into two types, reversible which includes the elastic and viscous energies, and irreversible which corresponds to the kinetic and hysteretic energies.

$$E_I \leq \underbrace{E_E + E_V}_{\text{Reversible}} + \underbrace{E_K + E_H}_{\text{Irreversible}}$$

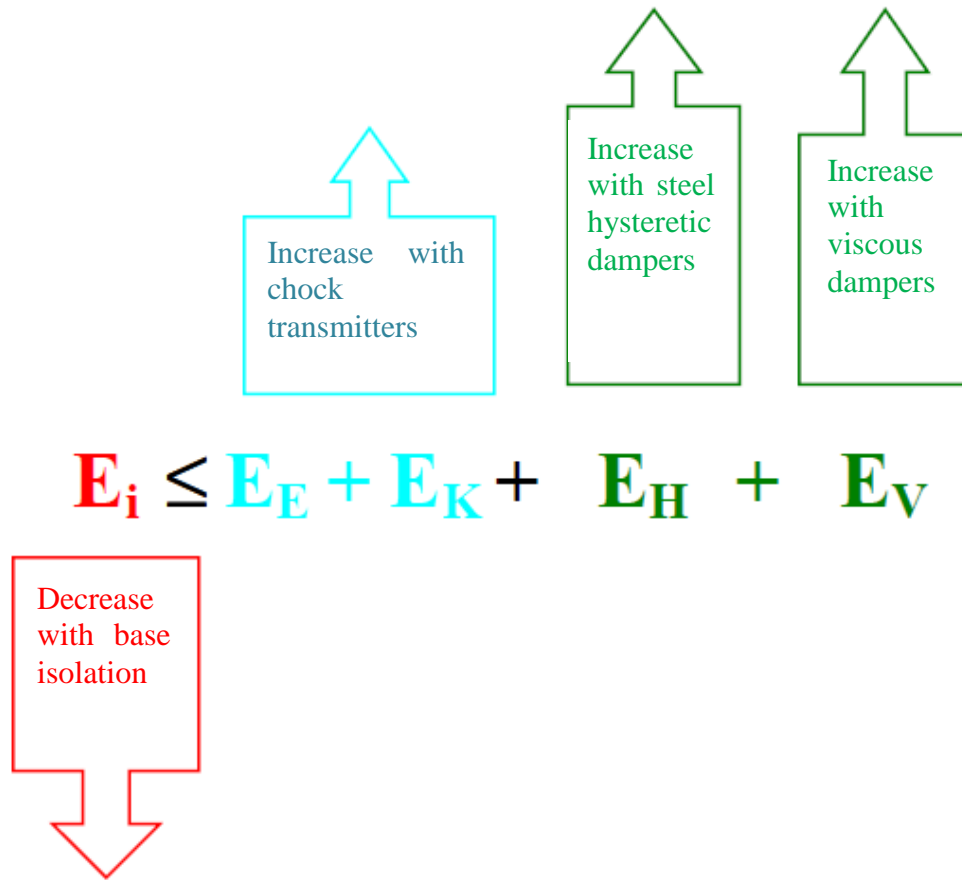


Figure 2.1 The seismic energy dissipation concept

The reduction of the horizontal seismic response, independently on the type of the structures or the materials used, and without counting all possible techniques, can be reached using one of those two isolation strategies or by combining them:

- 1- Increasing the relative period of the construction, taking it to the zone of small acceleration response (damping system)

2- Limiting the maximum horizontal force occurred (base isolation...), [2], [3], [14], [17], [22]

The presence of the dissipation energy, for the same amount of input energy, means that less elastic stresses are applied on the structure with linear elastic behavior.

The traditional building systems (Reinforced concrete, steel structure, masonry building...) rely on ductility to reduce the seismic action to SLU entities.

Substantially, the ductility allows reducing the effects of the earthquake energy through the dissipated energy in form of damage, properly studied, into the structural and non-structural elements.[17], [22], [76], [77],

The innovative seismic designs pursue the reduction of the effects of the earthquake without counting on the energy dissipation which arises from damage of structural and non-structural elements. They rather provide the insertion of devices suitably designed to dissipate the input energy input preserving like this the structure. [17]

The use of a system properly designed to resist seismic actions introduces a new problem, explicitly the need of providing within the structures a double-resistant systems.

Instead of adjusting the structural system to withstand the vertical loads, together with the seismic forces, it is getting the idea to insert a specific resistant system for the horizontal actions which are integrated in parallel with those for the vertical actions. [35]

In general, it is possible to define two areas where the isolation system is active:

The infrastructure, it is the part of the building including the foundations where in general the horizontal deformability is negligible and the upper-structure.

After centuries where traditional ways of dissipation through plastic hinges and damages were by default the only existing techniques of energy degeneracy, many technical means are been developed for the energy absorption of the earthquake: base isolation, thus the energy is absorbed on the level of the foundation, the soft first storey concept idealized by Fintel and khan, so the energy is absorbed by the first shock

absorbing soft storey and the isolation systems: like dampers, passive, active and semi active devices...[71], [76]

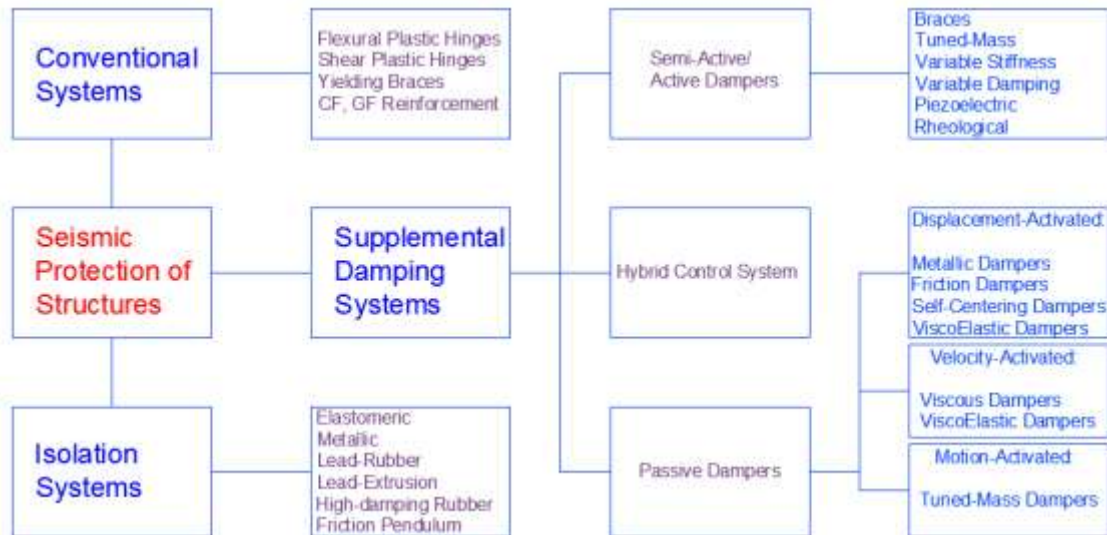


Figure 2.2 Categories of structural seismic protections

2.2. TRADITIONAL PHILOSOPHY OF A SEISMIC DESIGN

The traditional seismic design philosophy is based on energy dissipation through inelastic but stable mechanisms. These mechanisms can be accomplished through axial tension-yielding compression-buckling of brace elements, through flexural hinging of columns, walls and beams, and through shear hinging of steel elements. The energy dissipated through those mechanisms can lead to a good seismic performance, if proper capacity design principles are enforced. To notice that the hysteretic energy used to dissipate the seismic input energy in these systems corresponds directly to structural (and non-structural) damage, and is accepted as long as the structure is able to carry the gravity load and its vertical capacity is not jeopardized. [17]

Moment resisting frames are favored for their earthquake resistance capability because properly detailed frames have stable ductile behavior under repeated reversing loads. However, they are very flexible and it is often economically difficult to develop enough stiffness to control storey-drifts and deflections to prevent non-structural damage.

It is worth to give one example of traditional technique of seismic design to add rigidity to the moment resisting frames: the concrete shear walls. This technique as any technique has its own advantages and disadvantages.

The main advantages can be summarized as follow: the concrete is a low cost and effective building material, especially for wall construction. Concrete walls can be detailed with boundary elements and field steel for reliable, ductile cyclic response. Due to the high stiffness of concrete shear walls, the expected inelastic drifts should decrease for a structure designed to have such elements. [14]

In general, any advantage gained by added stiffness is negated by the increased amount of energy input, and thus place higher demand on strength and ductility which is sensitive in reinforced concrete to detailing and quality control.[17]

Regarding other disadvantages, from structural point of view, shear walls located at the core would develop a large overturning moments in narrow elements, which lead to high uplift forces and hence expensive foundations. As well, if walls would be clustered around the center of the floor plate (usually near elevators), this leads to torsional flexibility of the building, and large drifts from accidental mass eccentricity. To not forget that once located, they have to continue from top to foundation. It can be not a suitable solution for existing and fully operational buildings. [14], [17]

Another conventional construction method is the braced steel frames known to be economical and effective in controlling lateral deflections under wind and moderate earthquakes. Instead, during a major ground motion, the performance of these structures is poor. Being stiffer, they invite higher lateral inertial forces and the energy dissipation capacity of the brace is very limited. [17]

2.3. MODERN APPROACH THROUGH STRUCTURE CONTROL: ENERGY DISSIPATION SYSTEMS

During an earthquake, high energy is applied on the structure. Once applied, the energy is absorbed by the structure or amortized by other devices. If the structure is free of damping (traditional philosophy), its vibration will be continuously, but due to the presence of special devices, vibration will be reduced. As mentioned before, seismic

structures progression pursues the reduction of the effects of the earthquake without counting on the damage of structural and non-structural elements. They rather provide the insertion of devices suitably designed to dissipate the input energy. Lateral force reduction can be achieved by inserting special devices under the structure like base isolation or by the use of dampers. [17], [33], [36], [66]

Damping reduces structural response (acceleration and displacement): damping effect at high periods is not counted on spectrum amount; as well as at low periods, it has low effect on response acceleration. Figure 2.3 and Figure 2.4 show the effect of damping increasing in the periods from 0.3 to 2.5 seconds.

Among the advantages of using dampers we can infer to high energy absorbance, easy to install and replace them not counting the coordination to other structure members.

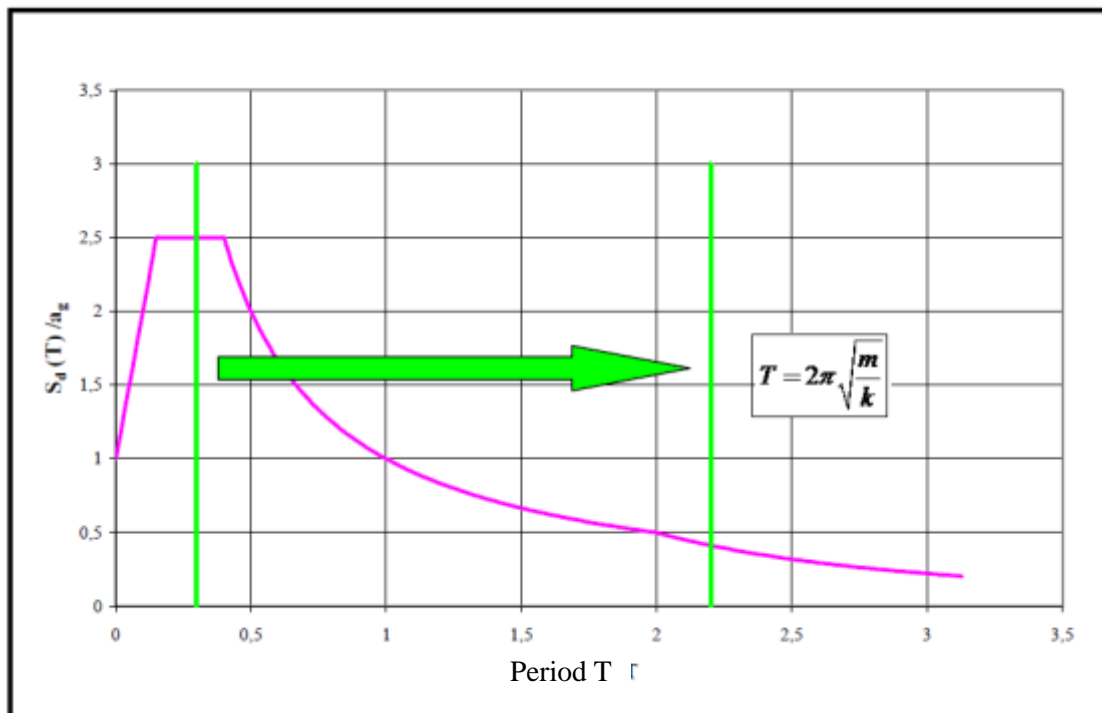


Figure 2.3 Influence of base isolation

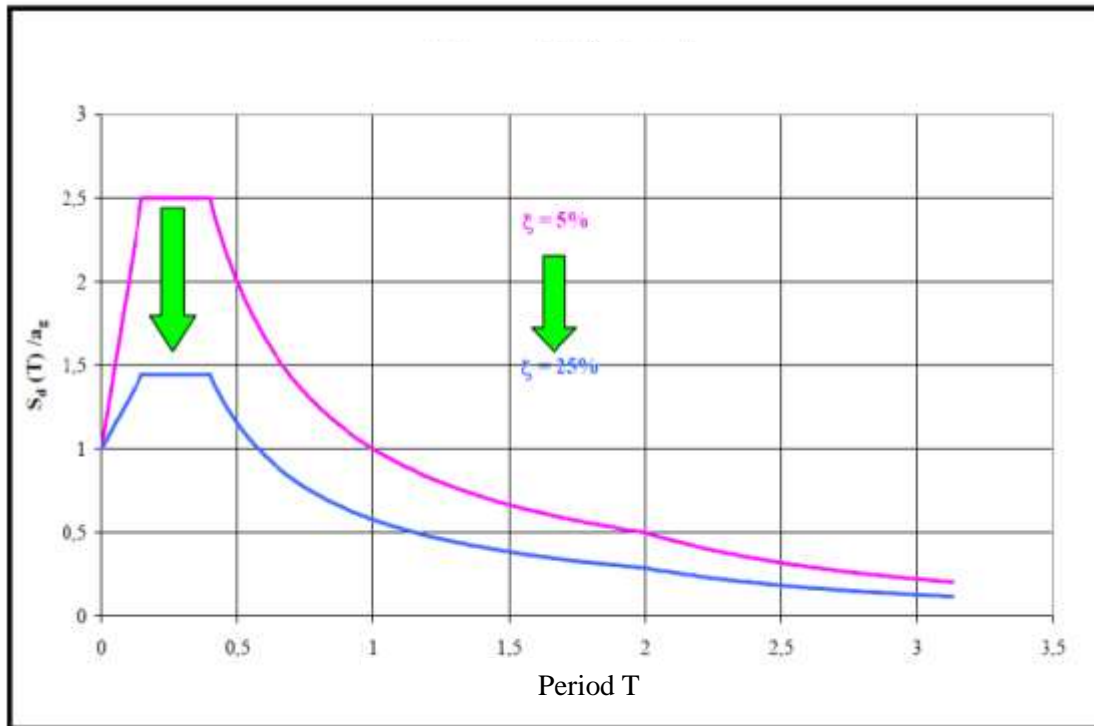


Figure 2.4 Influence of viscous dampers

Damping system is the collection of structural elements that includes all the individual damping devices, all structural elements or bracing required to transfer forces from damping devices to the base of the structure, and the structural elements required to transfer forces from damping devices to the seismic force-resisting system.[17]

In both cases, the isolation performance can be improved, by dissipating through the isolation system, the mechanical energy transmitted from the ground level to the construction.

Damping device is a flexible structural element of the damping system that dissipates energy due to relative motion of each end of the device. They include all pins, bolts, gusset plates, brace extensions, and other components required to connect damping devices to the other elements of the structure. Damping devices may be classified as either displacement-dependent or velocity-dependent, or a combination thereof, and may be configured to act in either a linear or nonlinear manner. [14], [15], [17], [33], [37], [59]

In this section, referring to Figure 2.2, supplemental damping system will be discussed. Thus, active, semi-active, hybrid and passive control systems will be presented and some overview of each technique will be given.

2.3.1. Active Control System

Active vibration control uses some kind of sensor to measure the motion or force or acceleration etc. of the structure and a powered actuator to generate a force to resist the unwanted motion. There is also some kind of logic that controls the actuator so it pushes in the right direction at the right time to reduce the unwanted action.[17]

Typically, an active control system is composed of three integrated components: i) a monitoring system that is able to sense the state of the structure and to record the associated data through an electronic data acquisition system; ii) a control system that receives the data from the monitoring system and decides on the countermeasures to be applied and iii) an actuating system that physically applies these countermeasures to the structure. Therefore, active systems require a continuous external power source to operate properly (Haysami et al)).[17]

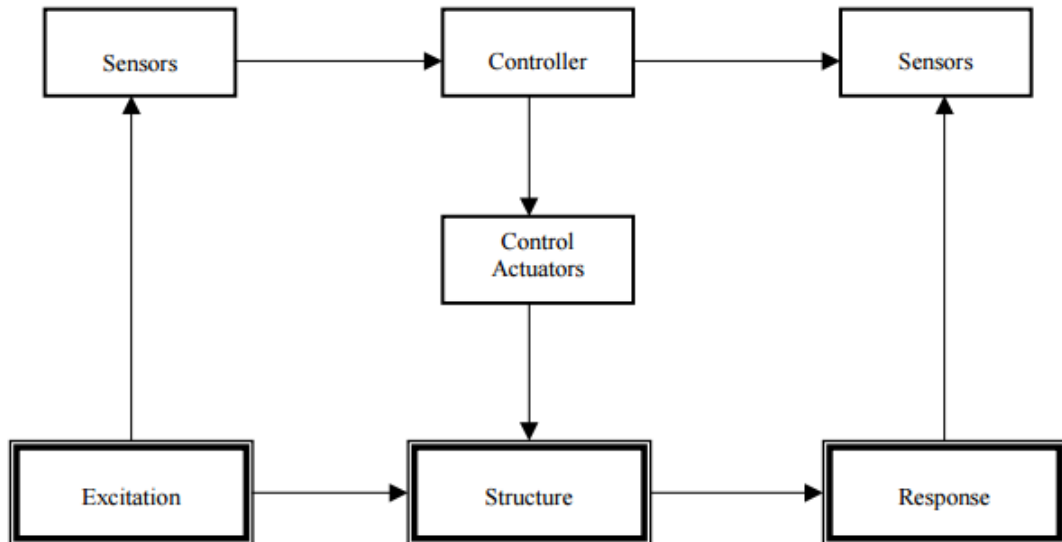


Figure 2.5 Active Control System Working Chart

This dependence on external power sources has been a significant limitation on the seismic application of active systems. During a strong earthquake, the electric

transmission and distribution systems can fail. Even backup electrical generating systems can be damaged. Furthermore, the control algorithm may become unstable during strong seismic shaking and/or operating conditions. These concerns have limited the implementation of active and semi-active systems for seismic control of civil engineering structures worldwide. Japan is the only exception where active systems have been implemented in several buildings. [17],

2.3.2. Semi-Active and Hybrid Control System

Semi-active systems are in the same category as active systems except that they require a relatively small amount of external energy without the need for a global monitoring system. The control is limited to modifying the local properties of the dampers, such as the geometry of the orifices in a fluid damper, which eliminates the possibility of instability. Because of this low dependence on external power sources and the removal of instability concerns, research on semi-active systems has intensified in recent years. These systems, however, have not yet enjoyed widespread applications in North America and Europe. [17]

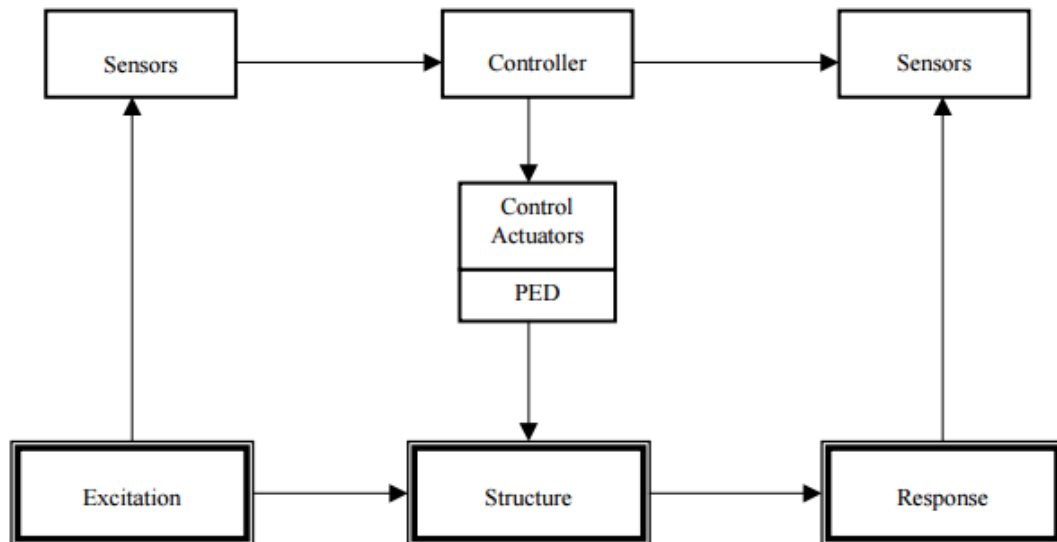


Figure 2.6 Semi-Active Control System Working Chart

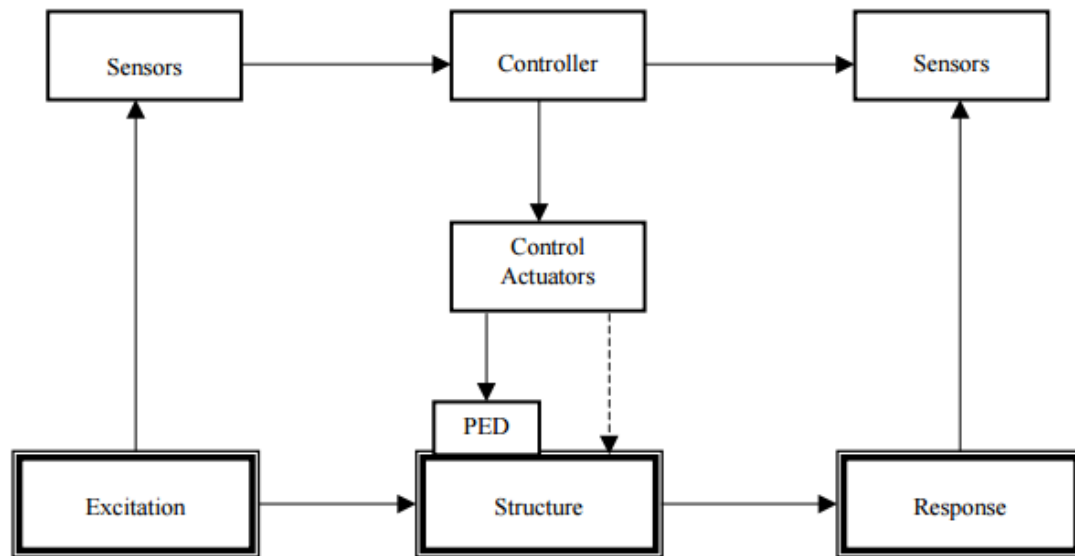


Figure 2.7 Hybrid Control System Working Chart

The term of hybrid control systems is used for a hybrid using of active and passive control systems. Semi-active systems are extracted from active control systems. In these cases, the required output energy is lower than active control system. And it is only the producer of electric pulse to provide control system. Semi active control components dose not add mechanical additional energy to structure system (which includes structural and stimulus control), so the stability of input and output connections are guaranteed. Semi-active control components often can be seen as passive control components. Particularly, more resistant or depreciate forces are produced by internal mechanism based on feedback output sensor. So the combination ability of the best active and passive systems or against less reduction of desired components and due to low power, have high control ability. Semi-active systems are an attractive alternative for active and hybrid systems.[17], [26], [71]

2.3.3. Passive Control System

Passive systems, on the other hand, as their name indicates, operate without external computers, power supply or actuators. As it shown in Figure 2.8, “passive systems have properties that cannot be modified during the seismic response of the structure.” Once they are implanted into a structure, the seismic input energy contained in a narrow

frequency band is dissipated through the fixed characteristics of the passive dampers shown to be effective, robust and economical solutions. “The implementation of passive systems has outdistanced significantly the implementation of active systems.”[17], [23]

Maybe one impediment to the widespread use of passive energy dissipation systems have been the lack of robust and validated guidelines for the modeling, analysis, design and testing of the dampers. [10]

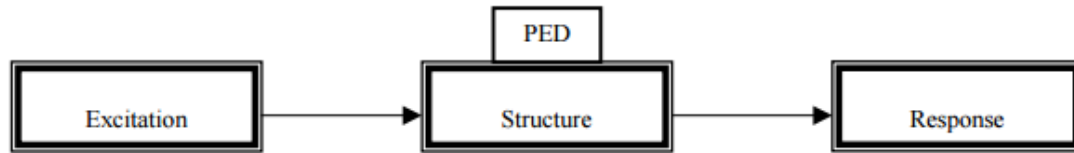


Figure 2.8 Passive Control System Working Chart

Passive energy dissipating systems can be divided into three different categories: displacement-activated devices, velocity-activated devices, and motion-activated devices. Note that some systems, such as viscoelastic dampers, can be classified both as displacement and velocity-activated device. [44], [50], [61]

Displacement-activated devices are characterized that their force response is primarily a function of the relative displacement between each end of the device, in another words the relative displacements occur simultaneously with the maximum internal forces. The response is substantially independent of the relative velocity between each of the devices and/ or the excitation frequency. Typical dampers falling in this category include metallic dampers, friction dampers and self-centering dampers.[17], [24]

Velocity-activated devices dissipate energy through the relative velocities that occur between their connected points. The force-displacement response of these dampers usually depends on the frequency of the motion. Also, the forces generated by these devices in the structure are usually out-of-phase with the internal forces resulting from shaking. Therefore, the maximum forces generated by the dampers do not occur simultaneously with the maximum internal forces corresponding to the peak transient deformations of the structure. This results in lower design forces for structural

members where the devices installed as well as in lower design forces for the foundations. Typical dampers falling in this category include purely viscous and visco-elastic dampers. [17], [41]



Figure 2.9. A viscous damper inserted inside a residential building

A motion-activated device disturbs the flow of energy in the structure through the vibration of a secondary system. Tuned-Mass Dampers (TMDs) are examples of motion-activated devices. A TMD is a relatively small secondary mass-spring-dashpot system that is attached to a structure in order to reduce its dynamic response. The secondary system is tuned to be in resonance with the main structure on which it is installed. Under a dynamic excitation, the TMD resonates at the same frequency as the main structure but out-of-phase from it, thereby diverting the input energy from the main structure into itself. The input energy is dissipated by the inertia forces applied by the TMD on the main structure. These systems, usually installed on the roofs of buildings, have been proven effective in reducing wind-induced vibrations in high-rise buildings and floor vibrations induced by occupant activity (Haysami et al).[12], [17], [53], [54]

For example, inside Taipei World Financial Center in Taiwan is the largest and heaviest regulated damper (TMD) which is installed globally. And they act as a big pendulum, a big steel core that is moved slowly in front and rear of each movement of building. This is an engineering feat and is able to limit the vibration of a tall building above 500 meter. A steel core with 5.5 m diameter and 728 tons weight are suspended with 8 cables from the top floors of the tower. And they are visible between floors 88 and 92. And it is one of the tallest structures in the world which are located about 200 meters from main fault line and wind and earthquake are serious problems for this

structure. In fact, tourists could even take photos from this TMD during Sishan earthquake. (Haysami et al)



Figure 2.10 The TMD inserted in the Taipei Tower

In this 101-story towers, this steel core able to bear 1.5 meter movement in each direction. And they reduce the vibration range about 30 to 40%.

2.4. HYSTERETIC DAMPERS

One of the most efficient dissipation mechanisms of the energy transmitted to structures through earthquakes is one that takes advantage of the plastic deformability of the metal elements, from here born the idea of entrusting the seismic energy dissipation devices able to undergo large plastic deformation cycles, and then dissipate to hysteresis a high amount of energy. [17]

Some of the hysteretic devices that have demonstrated a particularly desirable behavior are here briefly recalled. The Added Damping – Added Stiffness (ADAS) device, originally manufactured by Bechtel Corporation in the 1980s, is usually installed between the apex of a chevron brace and the underside of the beam. The Triangular Added Damping – Added Stiffness (TADAS) device is a variation of the original ADAS device which makes use of triangular plates as dissipative steel elements. In the mid-1970s, Lead Extrusion Devices (LED) were proposed in New Zeland (Robinson and Greenbank 1976) taking advantage of the stable and repeatable hysteretic behavior of a lead element. The Buckling Restrained Brace (BRB), as the unbounded brace

manufactured by Nippon Steel Corporation in the early 1980s, consists in a steel member encased in a tube filled with concrete that prevents the buckling.

Even if the market is full of different types of hysteretic devices, all of them are intended to provide better and more reliable seismic performance than that of a conventional structure at the expense of the seismic load energy dissipation. In general, there are four major groups of hysteretic dampers used for the purpose, namely: 1-Fluid viscous dampers (FVDs) 2-Viscoelastic dampers (VEDs) 3-Friction dampers (FDs) 4-Metallic yielding dampers (MYDs). Hysteretic philosophy is used in Isolation Systems and Supplemental Damping systems.

Friction dampers belong to the displacement-activated supplemental damping systems. Steel dampers take advantage of the hysteretic behavior of the material exceeding its yielding point. Particularly desirable properties of these devices are a stable hysteretic behavior, the ability in sustaining an adequate number of cyclic loading-unloading (low-cycle fatigue), long term reliability and low sensitivity to environmental temperature.

The friction brake is widely used to extract kinetic energy from a moving body as it is the most effective, reliable and economical mean to dissipate energy. Friction-dampers are suitable for different kinds of constructions: 1) concrete shear walls, 2) braced steel and/or concrete frame; 3) low rise buildings and 4) clad-frame construction.

Pall friction dampers are simple and fool-proof in construction and inexpensive in cost. Basically, these consist of series of steel plates which are specially treated to develop most reliable friction. These plates are clamped together with high strength steel bolts and allowed to slip at a predetermined load. Their performances are reliable, repeatable and possess large rectangular hysteresis loops with negligible fade over several cycles of reversals that can be encountered in successive earthquake. Much greater quantity of energy can be disposed of in friction than any other method involving the damaging process of yielding of steel or viscoelastic materials. [58]



Figure 2.11 An example of a Rotational Friction Damper

Unlike viscoelastic materials, their performance is not affected by temperature, velocity and stiffness degradation due to aging. The maximum earthquake force with friction-dampers is well defined when compared to viscous or viscoelastic dampers in which it varies with the velocity and displacement across the device.[58]

Unlike devices that dissipate energy by the damaging process of yielding of steel plates, these do not need repair or replacement after the earthquake. Also, yielding devices may develop premature fracture due to fatigue caused by frequent occurrence of wind loadings and hence require regular inspection. Pall friction dampers need no maintenance over the life of the building and are always ready to do their job regardless of how many times they have performed.[17], [58]

Friction dampers are designed not to slip during wind storms or moderate earthquakes. During severe seismic excitations, friction dampers slip at a predetermined optimum load before yielding occurs in other structural members and dissipate a major portion of the seismic energy. This allows the building to remain elastic or at least yielding is delayed to be available during catastrophic conditions. By selecting the proper slip load, it is possible to ‘tune’ the response of the structure to an optimum value. Parametric dynamic studies have shown that the optimum slip load is independent of the time-history of the earthquake motion and is rather a structural property. Also, within a variation of $\pm 20\%$ of slip load, the seismic response is not significantly affected. Another interesting feature of friction damped buildings is that their natural period varies with the amplitude of vibration i.e. the severity of earthquake. Hence the phenomenon of resonance or quasi-resonance for future earthquakes is avoided.

These friction dampers have successfully gone through rigorous proof-testing on shake tables in Canada and the United States. The response of friction-damped braced frame was much superior to that of moment-resisting frame and moment-resisting braced frame. [25], [39], [44], [58], [62],[78]

Yielding Dampers are simple dampers that energy is absorbed by metallic components that yield and in this method we allow our metal components to reach yield point like using steel brace in concrete frame or steel frame.[17]



Figure 2.12 Example of Concentrated Dissipative Braces

2.5. CONCLUSIONS

The main objective of this chapter was to introduce all present strategies to be followed to reduce the damageable effects of earthquakes on structures.

The first concept is that earthquake forces are an energy form, the less is this energy, and the less are the seismic forces acting into the structure.

This energy can be reduced before entering the structure and this is the concept of the technique of base isolation system, which is sufficient for selected type of structures and not flexible structures ($T > 1\text{sec.}$) or buildings of soft and/or weak soils. Isolation is

not an economic technique and high costs limit its use, especially for retrofitting existing buildings.

In the case where the base isolation system cannot be used, the energy can be dissipated into the structure. This dissipation follows two possible ways: I) The first one is the traditional one which means the dissipation of energy through plastic hinges, structural and non-structural damages profiting from the ductility of the materials, or by increasing the strength of the structure by implementing carbon or glass fibers or by designing moment resisting frames or inserting shear walls. II) The second possible way is to insert supplemental damping systems to dissipate this energy: in the structure like passive, active or semi active dampers or hybrid control system. It is possible as well to insert a new external structure, like dissipative towers, implemented by dissipators and connected by specific links to the concerned structure to take out this unwelcomed energy.

At the end, many factors restrained engineers to choose between many techniques to avoid damages: ground factors, shape and type of the structure, technical problems, economical cost, time of intervention...But of course, the worst seismic prevention is much better than keeping the structure without any intervention.

3. Seismic Design Philosophies and Concepts

3.1. INTRODUCTION

The objective of this chapter is to investigate all possible design seismic philosophies and to reap the key benefits of the methods and application technologies mentioned and integrate them into a single approach proposal.

In previous chapter, we highlighted on different techniques to be inserted in any desired structure to dissipate earthquake energy. In this chapter, brief overviews of traditional and new approaches of seismic design are described in a way that we can understand from where our calculation should start and which characteristics of the structure are important to take into consideration in order to develop the design. The Force Based seismic Design (FBD) is the more representative of the traditional seismic philosophies and it is considered as the basis of the most modern design codes and new approaches like the Performance Based Seismic Design (PBSD), characterized by its different levels of design, and the Direct Displacement Based seismic Design (DDBD), which unlike force based design, it uses displacement as the designed target.

The purpose of Performance-Based Seismic Design (PBSD) is to give a realistic assessment of how a structure will perform when subjected to either particular or generalized earthquake ground motion. While applying the DDBD, structures should be designed so that it could reach the targeted design displacement rather than to be bounded by a certain displacement limitation.[17], [35], [55]

In another section, the Capacity Spectrum Method (CSM) is described. It is a procedure that can be applied to the PBSD. The procedure compares the capacity of the structure (in the form of a pushover curve) with the demands on the structure (in the form of a response spectrum). The graphical intersection of the two curves approximates the response of the structure. [15], [17], [32], [72],

3.2. TRADITIONAL AND NEW APPROACHES OF SEISMIC DESIGN

3.2.1. Traditional Method

In traditional seismic structural design, for example the force based design (FBD), force is the most important parameter in the design. FBD born trying to imitate the traditional approach used for static design structures. It uses the estimated initial stiffness to determine structural period and the distribution of forces among members. Force is directly related to structural stiffness and displacement during elastic stage. However, for structures in plastic condition, the relationship is complex. Engineers usually reduce the calculated elastic force level due to ductility possessed by the structures. [17]

Ductility enables structures to deform inelastically to the required deformation without loss of strength. If the resistance of the structure is less than the applied force, or if their deformations exceed the limitation, then redesign should be taken. The interdependency between strength and stiffness as well as between strength and ductility cause FBD hardly to be compatible with modern philosophies like performance based seismic design where structural performance is measured by specific displacement for a certain earthquake level. [17], [35], [56]

Thus, the seismic provisions based on the force-based seismic design procedure must be considered as minimum requirements, providing the degree of seismic safety that has been considered reasonable up to now... the force-based seismic design approach is simple to apply to a single performance level and is economically viable since the design base shear V is lower than the strength that would be required if the structure were to remain elastic during the design seismic event. [17]

However, other different issues are related to this methodology and some of them are indicated below:

- The Force-Based Design suffers from various problems. First of all, this approach is based on an estimation of the initial stiffness to determine the period and the distribution of the design forces between the different structural elements; this approach is a condition in itself. As from the moment that the stiffness depends on the resistance of the elements, cannot be known until the design process is not complete;

- The seismic forces are distributed between the various structural elements on the basis of the initial stiffness; this is incorrect because it would mean that different elements can be conducted at yielding simultaneously;
- The Force-Based Design is based on the assumption that for a given type of structures and for a given material is sufficient only one reduction factor of the forces (based on the capacity of ductility);
- Resistant system designed to support vertical loads is also designed to withstand horizontal loads arising from seismic actions.

In addition, it should be emphasized that the seismic design is a very complex problem, because the seismic action is influenced by the dynamic response of the structural system. [17]

In conclusion, you may notice that the seismic design of the structures is based on the fact that the dynamic response of the structural system is evaluated in a passive sense and indeed is not governed to optimize it; in fact, the structural system that is initially designed to carry only the vertical loads, is then also arranged to carry the horizontal loads.

The limitations of the Force-based seismic design procedure and the fact that is related to one single performance level do not allow for an adequate assessment of the seismic safety when considering the various limit-states that modern structures may have to confront during their service life. Recent innovative contributions have been developed in the field of seismic design and intend to control the dynamic response of the structural system. [17]

3.2.2. Innovative Methods

Innovative methods which have been developed recently in the design seismic structures are listed below and then described briefly:

- 1) Performance Based Seismic Design "PBSD";
- 2) Direct Displacement Based Design "DDBD";
- 3) Static Non-Linear Analysis Methods or pushover method;
- 4) Nonlinear Dynamic Analysis;

1) Performance Based Seismic Design "PBSD"

The Performance Based Seismic Design (PBSD) was introduced by PEER through the Vision 2000 document of 1995. The intent of the Performance Based Seismic Design is to provide designers with a method that allows them to design, build and maintain the buildings in such a way that these are able to carry certain performance if exposed to certain levels of seismic intensity, or they are able to satisfy predetermined "performance targets." The objectives Performance "(Performance Objectives) thus arise from the union of so-called "Performance levels" and the so-called "levels of seismic intensity" planned and described in the Vision2000 document, and may be more or less stringent according to the importance of the structure itself.

The Performance Based Design arises therefore as a new approach to seismic design, but also as an approach of direct type, in that it allows earthquake professionals or designers to quantify seismic risk in terms that are meaningful to the decision makers or customers and then decision-makers make informed decisions that define a rational course of action for the earthquake professionals. [17], [35], [56]

It is possible to summarize the steps to follow while performing a performance based seismic design in 5 steps: i). Performance definition, ii) Evaluation approach, iii) Analysis, iv). Mathematical modeling, v). Acceptance criteria.

The performance definition is shown in Figure 3.1. A Performance Objective has two components: performance level (horizontal) and hazard or ground motion level (vertical). The association of the two levels forms what we call the performance objective. Performance levels are discrete damage states selected among all possible damage states that a building could experience as a result of earthquake response. It can be fully functional, immediate occupancy or collapse prevention... Hazard levels indicate the probability that a given value of a ground motion parameter, for example peak ground acceleration, will be exceeded over a certain period of time.

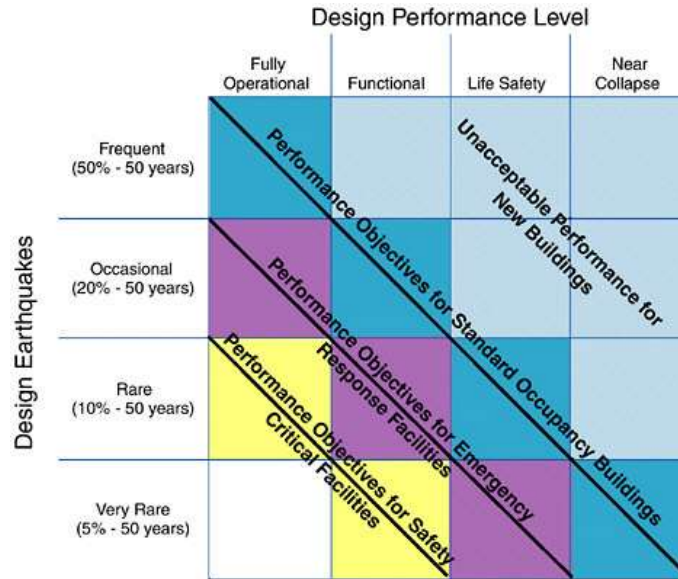


Figure 3.1 The Performance Based Seismic Design Objectives

The PBSO is based on four performance states:

- Fully Operational: continuous service, negligible structural and nonstructural damage
- Operational: most operations and functions can be immediately resumed, the structure is safe for occupancy, essential operations are protected, but non-essential ones may be disrupted. Repair is required to restore some non-essential services, but the damage is light
- Life Safety: moderate damage, but the structure is stable. Selected building systems, features and contents may be protected, as well as life safety, but the building may be evacuated for following earthquakes. Repair is possible, but might be economically unfeasible
- Near Collapse: severe damage, but structural collapse is prevented, while nonstructural elements might fall.

As well as for the performance levels, also four levels of earthquake intensity were quantitatively described, in probabilistic terms:

- Frequent Earthquake: recurrence interval of 50 years, with a probability of occurrence of 50% in 50 years
- Occasional Earthquake: recurrence interval of 225 years, with a probability of occurrence of 20% in 50 years
- Rare Earthquake: recurrence interval of 475 years, with a probability of occurrence of 10% in 50 years

- Very Rare Earthquake: recurrence interval of 950 years, with a probability of occurrence of 5% in 50 years.

Therefore a performance objective for a design should more correctly be stated as:

A certain level of confidence (i.e. 95%) that the structure will remain fully operational for frequent earthquake hazards with 50% probability of exceedance in 50 years.

Once the performance objective is determined, the structural analysis is used to predict the value of various structural response parameters: Interstory drift, axial force...

Then, analysis can be performed following one of those methods: i). Linear static procedure; ii) Linear dynamic procedure; iii) Nonlinear static procedure; iv) Nonlinear dynamic procedure. Once the analyses are done, a mathematical model is done verifying the frame configuration, connections, horizontal torsion, foundations, diaphragms, P-Delta effects, vertical ground motion...

2) Direct Displacement Based Design "DDBD"

The Direct Displacement Based Design, (DDBD), was originally introduced by Nigel Priestly and subsequently was developed in collaboration with G. M. Calvi with the purpose to overcome the deficiencies inherent in the conventional Force-Based Design. The fundamental difference with respect to the Force-Based Design concerns the fact that the DDBD characterizes such structures so that they can be designed by making use of the model to a single degree of freedom (single-degree-of-freedom, SDOF), which allows to represent the performance of the structure on the basis of the maximum response in terms of displacement, contrary to the traditional approach which instead occurs with the initial elastic characteristics of the structure itself. In other words it can be said that the Direct Displacement-Based Design replaces the real structure, which in general can be a multi-degree of freedom system (multi-degree-of-freedom, MDOF), with a simple equivalent oscillator and that this equivalence is realized on the basis of the maximum displacement of the structure itself. The basic philosophy behind this approach is to design a structure capable of achieving a given performance (identified by a certain limit state for the structure itself) under an earthquake of a defined intensity (characterized by a precise probability of occurrence). [17], [56]

In summary from the two presents new approaches presented, the intent of Performance Based Seismic design is to produce structures with predictable performance levels. To achieve this, non-linear analysis procedures are used. The most realistic procedure is the response history analysis. This method is complicated. Thus, simplified non-linear analyses have been developed.

Adaptive load pattern is a pattern of Pushover curve where the loads change while the structure is displaced. [15], [17]

3) Static Non-Linear Analysis

PBSD has activated a significant research work aimed at better characterizing structural performance levels. This aspect of this methodology is the most challenging since engineers should take rational decisions on what constitutes damage in a complex structure. Thus, an advanced design was developed to understand the response of structures in the nonlinear range. Nonlinear Static Analysis method was already an established method in the offshore platform industry. It is able to capture local nonlinearities effects and by increasing the levels of lateral loads, the behavior is detected until a target displacement or the total collapse is reached. This pushover analysis relies on an estimate based on the strength envelope of the system. This method works well for regular and not tall buildings [16], [17], [28].

4) Dynamic Non-Linear Analyses

For very tall and/or irregular structures, the nonlinear dynamic analyses can be implemented. It can be used as well at the end of the design for verification determinations. In both cases, a ground motion input must be represented by an ensemble of acceleration time-histories, recorded or synthetic, but compatible with the seismic hazard at the construction site.[11], [17]

3.3. CAPACITY SPECTRUM CURVE

The Capacity Spectrum Method (CSM) is a procedure that can be applied to PBSD. The CSM was first introduced in the 1970s as a rapid evaluation procedure in a pilot project for assessing seismic vulnerability of buildings at the Puget Sound Naval

Shipyards. In the 1980s, it was used as a procedure to find a correlation between earthquake ground motion and building performance. The method was also developed into a design verification procedure for the Tri-services (Army, Navy, and Air Force) “Seismic Design Guidelines for Essential Buildings” manual. The procedure compares the capacity of the structure (in the form of a pushover curve) with the demands on the structure (in the form of a response spectrum). The graphical intersection of the two curves approximates the response of the structure. In order to account for non-linear inelastic behaviour of the structural system, effective viscous damping values are applied to the linear-elastic response spectrum similar to an inelastic response spectrum. In the mid-1990s, the Tri-services manual was updated.[17], [81]

By converting the base shears and roof displacements from a non-linear pushover to equivalent spectral accelerations and displacements, and superimposing an earthquake demand curve, the non-linear pushover becomes a capacity spectrum. The earthquake demand curve is represented by response spectra, plotted with different levels of “effective” or “surrogate” viscous damping (e.g. 5%, 10%, 15%, 20% and sometimes 30% to approximate the reduction in structural response due to the increasing levels of damage). By determining the point, where this capacity spectrum “breaks through” the earthquake demand, engineers can develop an estimate of the spectral acceleration, displacement, and damage that may occur for specific structure responding to a given earthquake. A number of changes have been proposed to the capacity spectrum method that increase the complexity and computational effort associated with this method, usually requiring iteration to find the “exact” point where the capacity spectrum intersects the “correct” level of damping. By formatting the results in the acceleration-displacement response-spectrum format in lieu of the traditional spectral acceleration (S_a) versus period (T) format, the graphical and intuitive nature of the capacity spectrum method become even more apparent. [17]

3.4. THE PROPOSED METHOD

Within the PBSM and the CSM, we developed an original seismic design approach, aimed at obtaining the desired “objective curve”. For common building structures, the

following performance objectives are typically required (the so called “basic objectives”, with reference to the Vision 2000 document):

- PO-1: “Frequent Earthquake (FE) intensity level + Fully Operational (FO) performance level”: under a frequent earthquake negligible damage for both structural and non-structural elements can occur, and facilities can continue with no disruption;
- PO-2: “Occasional Earthquake (OE) intensity level + Operational (O) performance level”: under an occasional earthquake negligible damage for structural elements and moderate damage for the non-structural ones can occur, and facilities continue in operation with minor damage and minor disruption only in non-essential services;
- PO-3: “Rare Earthquake (RE) intensity level + Life-Safe (LS) performance level”: life safety is substantially protected, and damage to structural and non-structural elements is moderate to extensive;
- PO-4: “Very-Rare Earthquake (V-RE) intensity level + Near-Collapse (NC) performance level”: life safety is at risk, and damage is severe but structural collapse is prevented.

These performance objectives can be translated into specific requirements for a steel bracing system:

- imposing the PO-1 gives a specific requirement on the initial elastic lateral stiffness;
- imposing the PO-2 gives a specific requirement on the yield strength;
- imposing the PO-3 gives a specific requirement on the ductility capacity;
- imposing the PO-4 gives a specific requirement on the post-yielding hardening behavior.

These multiple requests can be generally represented by the “objective curve”, whose qualitative shape is showed in Figure 3.2.

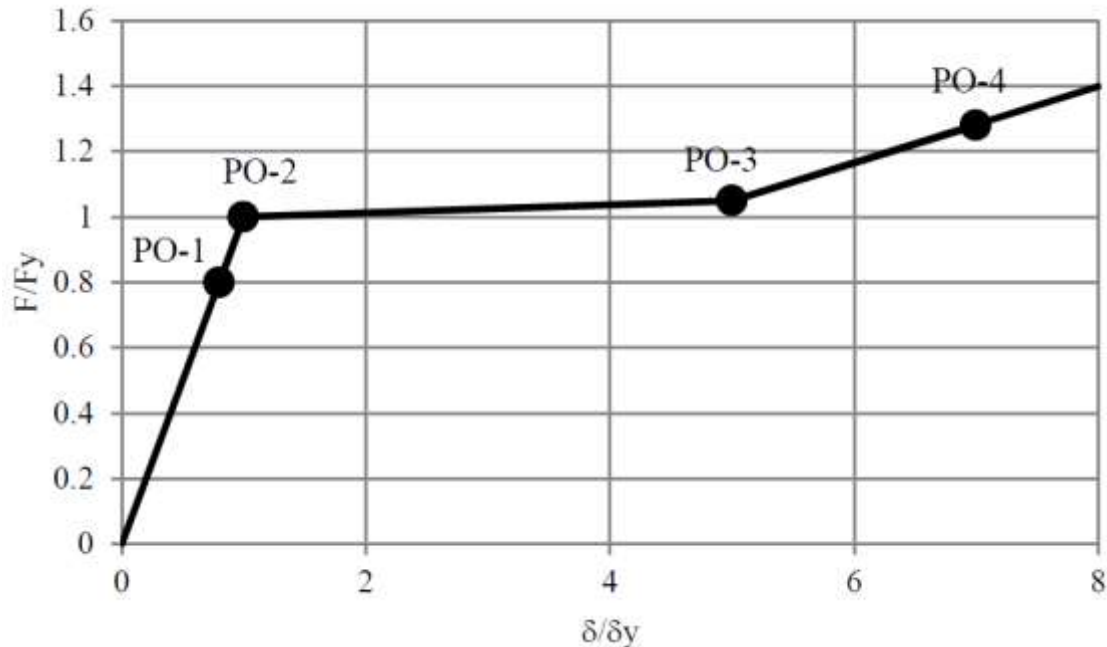


Figure 3.2 The desired Objective Curve Normalized in terms of F_y and δ_y

The purpose of Performance-Based Seismic Design (PBSD) is to give a realistic assessment of how a structure will perform when subjected to either particular or generalized earthquake ground motion. While the code design provides a pseudo capacity to resist a prescribed lateral force, this force level is substantially less than that to which a building may be subjected during a postulated major earthquake. It is assumed that the structure will be able to withstand the major earthquake ground motion by components yielding into the inelastic range, absorbing energy, and acting in a ductile manner as well as by a multitude of other actions and effects not explicitly considered in code applications .[35]

Although the code requires special ductile detailing, it does not provide a means to determine how the structure will actually perform under severe earthquake conditions. [17], [35], [55], [56], [57], [74], [75], [82]

3.5. CONCLUSIONS

The main objective of this chapter was to familiarize engineers with different possible approaches to overcome a seismic design.

The main aim of course of each structural philosophy is to ensure adequate safety by avoiding catastrophic failures and loss of life. This is the main objective of the force-based seismic design which was considered in this chapter as a traditional approach. In fact, the FBD has a lot of limitations: putting a part the assumption that for a given type of structures only one reduction factor is sufficient and that different elements can be conducted at yielding simultaneously, it suffers especially from the fact that is related to one single performance level which does not allow for an adequate assessment of the seismic safety when considering the various limit-states that modern structures may have to confront during their service life.

Thus, recent innovative contributions have been developed in the field of seismic design and they have been showed briefly in this chapter.

An innovative approach was presented and it was the Direct Displacement Based Seismic Design DDBD. The fundamental difference with respect to the Force-Based Design concerns the fact that the DDBD characterizes such structures so that they can be designed by making use of the model to a single degree of freedom. For SDOF structures (like the soft first story idealized by Fintel and Khan, or backbone structures...) this procedure is straightforward, whereas for MDOF structures, and before defining the equivalent SDOF structure, an assumption on the deflected shape of the system at the target deformation must be made.

Another approach was showed and it is the Performance Based Seismic Design. It is a modern approach which take into consideration not just the life safety, but also economic parameters, like the cost of damage to equipment and the cost associated with the loss of operation following a moderate or strong earthquake. In another words, the intent of Performance Based Seismic design is to produce structures with predictable performance levels.

Nonlinear static or pushover analysis is one of the methods used in practice to predict the maximum deformation capacity of the structure. Exploiting this idea, it allows for a better estimate of the maximum deformations under a given level of earthquake. This

method works perfectly for regular structures. However, for tall or irregular structure, a non-linear dynamic analysis is needed, and many performance levels can be applied to a structure and designers, using this method can construct the target curve.

In chapter two the main objective was to show all possible dissipative techniques to be used in a structure to avoid collapse or damage. In this chapter different approaches were presented to set crescent seismic levels depending on the level of the earthquake. For this reason, we presented a new approach, taking advantages of the performance targets of the PBSB and the CSC, as a new methodology for approaching seismic design. The objective of the next chapter will be to concretize our new approach and show possible solutions to reach it in real cases, which one of them will be the Crescent Shaped Brace, the main subject of this thesis.

4. The Proposed Method and the Objective Curve

4.1. THE STRUCTURAL CONCEPT

The objective of this chapter is to reap the key benefits of the methods and application technologies mentioned and integrate them into a single approach project. This approach presents a particular type of structure, reduced in single degree of freedom, equipped with two resistant systems, a structural vertical system with the main role of resisting only vertical loads, and a parallel horizontal resisting system which is inserted to resist horizontal forces.

As we shall see, a structural typology of this type in general presents the following advantages:

- Allows the designer to split the structural system to vertical actions from that of the horizontal actions resistant system;
- Facilitates the modelling of the structure in the analysis phase, as it can be assimilated (at least in first approximation) to a simple oscillator.

It is clear that in a given structural design, a central role is taken by the horizontal resistant system whose optimal characteristics will result from the meeting of different pre-established performance objectives. In general the vertical resistant system may simply be dimensioned only for the vertical static loads and the system of stiffening of the superstructure will be sized at the end of the design on the basis of the actual characteristics of the other two resistant systems. [14], [15], [17]

In few words, the proposed method can be summarized as follow:

1. Sizing of the system resistant to vertical actions for static loads and determining the capacity curve of the vertical actions only durable system;
2. Determination of the objective curve (capacity curve of the whole structure) on the basis of pre-established performance goals;

3. Determination of the capacity curve of the system resistant to horizontal actions through the difference between the objective curve (determined in step 2) and the capacity curve of the vertical resistant system (determined in step 1);
4. Choice of the number and the type of dissipative elements that will constitute the system resistant to horizontal actions, on the basis of the determined capacity curve at section 3;
5. Control of the fulfillment of all performance targets based on the capacity curve of the horizontal resistant system, now fully dimensioned.
6. Final verification of the dimensioned structure using nonlinear dynamic analyzes of appropriate accelerograms spectrum.

The use and the consequences of failure of the structure may also be of concern in the design. These factors are included in the specification of the seismic design forces. There are two commonly used procedures for specifying seismic design forces: The "Equivalent Static Force Procedure" and "Dynamic Analysis". In the equivalent static force procedure, the inertial forces are specified as static forces using empirical formulas. The empirical formulas do not explicitly account for the "dynamic characteristics" of the particular structure being designed or analyzed. The formulas were, however, developed to adequately represent the dynamic behavior of what are called "regular" structures, which have a reasonably uniform distribution of mass and stiffness. For such structures, the equivalent static force procedure is most often adequate. Structures that do not fit into this category are called "irregular". Common irregularities include large floor-to-floor variation in mass or center of mass and soft stories. Therefore, the use of the empirical formulas, used in the equivalent static force procedure may lead to erroneous results. In these cases, a dynamic analysis should be used to specify and distribute the seismic design forces. [11], [40], [73], [79]



Figure 4.1 An example of a soft or weak first story building

Below we will be examined the main aspects of the procedure; and to fix the ideas, we will assume that the system resistant to vertical actions and that is resistant to horizontal actions exhibit both elastic – perfectly plastic behavior. However, to count the effects of the second order and to guarantee against the collapse of the structure, it is appropriate that at least the system resistant to horizontal actions presents a significantly hardening behavior.

4.2. VERTICAL SYSTEM

Thanks to the substantial independence of roles between the different resistant systems (horizontal and vertical)), it is possible to size the resistant system to vertical actions (beams and columns) from the beginning of the design, without the need to perform any specific preventive seismic analysis. Therefore this vertical system can be considered known from the start of the design and its capacity curve concerning the force – displacement can be detected.

In this regard, it will be interesting to determine the force – displacement curve of the columns of the ground floor, as the performance of such floor will be governed by the contributions of these columns and of the inserted dissipative elements that constitute

the horizontal resistant system. However, since the columns are dimensioned from the beginning of the design based on static vertical loads, it will be up to the ground floor bracing elements to cover the planed performance targets.

The resistant vertical system has been assumed to be a vertical frame with hinged beams to the continuous columns which are hinged in their turn to the base. Such static scheme, in itself labile, naturally has sense just because of the presence of the other two lateral resistant systems (ground floor and superstructure). In general, depending on the constraints at the two ends, the columns of the ground floor would be in an intermediate situation between two static schemes:

1. A cantilever beam elastically constrained to the extreme top shelf and hinged to the base;
2. A fixed beam to the base and bounded to the upper end with a sliding interlocking (which it simulates the infinite stiffness of the beams of the first floor).

Assuming that the columns of the ground floor are all equal and have the same static scheme, the horizontal displacement of each of them may in any event be expressed in the form:

$$\delta = \frac{FH^3}{c_1 EJ}$$

Supposing c_1 a constant depending on the static scheme (for example, $c_1 = 3$ for perfectly fixed cantilever, $c_1 = 12$ for the schema fixed end – sliding fixed end), E is the Young's modulus or the modulus of elasticity of steel and J the moment of inertia in the considered direction; therefore the rigidity of the columns, supposed we have n columns, is given by:

$$K_V = nc_1 \frac{EJ}{H^3} \quad \text{Eq4.1}$$

As for the moment in the most stressed zone of the column, it will be possible in general write:

$$M = \frac{FH}{c_2}$$

Where c_2 is a numerical coefficient depending on the static scheme (for example $c_2 = 1$ for a perfectly fixed cantilever and $c_2 = 2$ for the fixed end - sliding fixed end). At the elastic limit, it is possible to write:

$$\sigma = \frac{N}{A} + \frac{M}{W} = f_y$$

having

$$M_y = W(f_y - \sigma_N) = Wf_y \left(1 - \frac{\sigma_N}{f_y}\right) = \alpha_N Wf_y$$

Where

$$\sigma_N = N/A \text{ and } \alpha_N = 1 - \sigma_N/f_y < 1$$

Thus, by implying $M = M_y$ when $F = F_{y,v}$ we obtain:

$$\frac{F_{y,v}H}{C_2} = Wf_{y,red}$$

Thus

$$F_{y,v} = \frac{c_2 W f_{y,red} H}{H} \quad \text{Eq.4.2}$$

While the displacement at the elastic limit $\delta_{y,v}$ of the columns can be determined as

$$\delta_{y,v} = \frac{(F_{y,v}H)H^2}{c_1 E J} = \frac{\alpha_N W f_y H^2}{c_1 c_2 E J} = \frac{2\alpha_N}{c_1 c_2} \varepsilon_y \frac{H^2}{h} \quad \text{Eq 4.3}$$

With $W = 2J/h$ where h is the size of the section in the considered direction.

In the case of different columns or with different static formulas patterns, equations (4.1), (4.2) and (4.3) will have to be suitably modified; nonetheless at the end of the dimensioning of the vertical resistant system, it will be possible to have the values of the elastic stiffness K_V , the elastic limit resistance $F_{y,v}$ and the elastic displacement $\delta_{y,v}$ and to plot in the plane $F - \delta$ capacity curve.

In general, we may have $K_V < K$, since the rigidity of the vertical system may not be able alone to meet the performance target. In this case, it is precisely required an additional bracing system resistant to the horizontal actions. However, it is necessarily to have $\delta_{y,v} \geq \delta_y$, otherwise, it would mean that the columns of the ground floor exceeds the elastic limit for an earthquake lower than the intensity of an occasional one.

From Eq 4.3, it is further noted that, with noticed values of α_N and H , and in order to have higher value of $\delta_{y,v}$ we should:

- Use static patterns for which the product c_1c_2 is the minimum possible (providing the hinges at the base of the columns);
- Use a steel with higher ε_y (or equivalently, higher f_y);
- Use of profiles with reduced h (like the case of double-T sections, HE type of series B or M).

4.3. DESIRED OBJECTIVE CURVE

The desired objective curve is determined based on the performance objectives explained within the Performance Based Seismic Design. It is not possible to give a general description of this curve which depends on each type of structure, each site construction and other different considerations. In general, the structure will present an elastic behavior under a frequent earthquake (on the edge between elastic and plastic field without exploiting excessively the ductility of the structural element). In those two cases, the serviceability limit state is the range within it the structure reacts.

Under rare earthquakes, the structure starts to yield and exploits its ductility capacity which should not exceed a ductility limit fixed in an interval of values between 2 and 4. The last behavior of the structure is designed to be under a very rare earthquake where the structure may present severe damage, but structural collapse is prevented and non-structural elements might fall.

4.4. HORIZONTAL SYSTEM

From the simplified assumption of the elastic - perfectly plastic systems, this curve will be of course bilateral and characterized by the following

parameters:

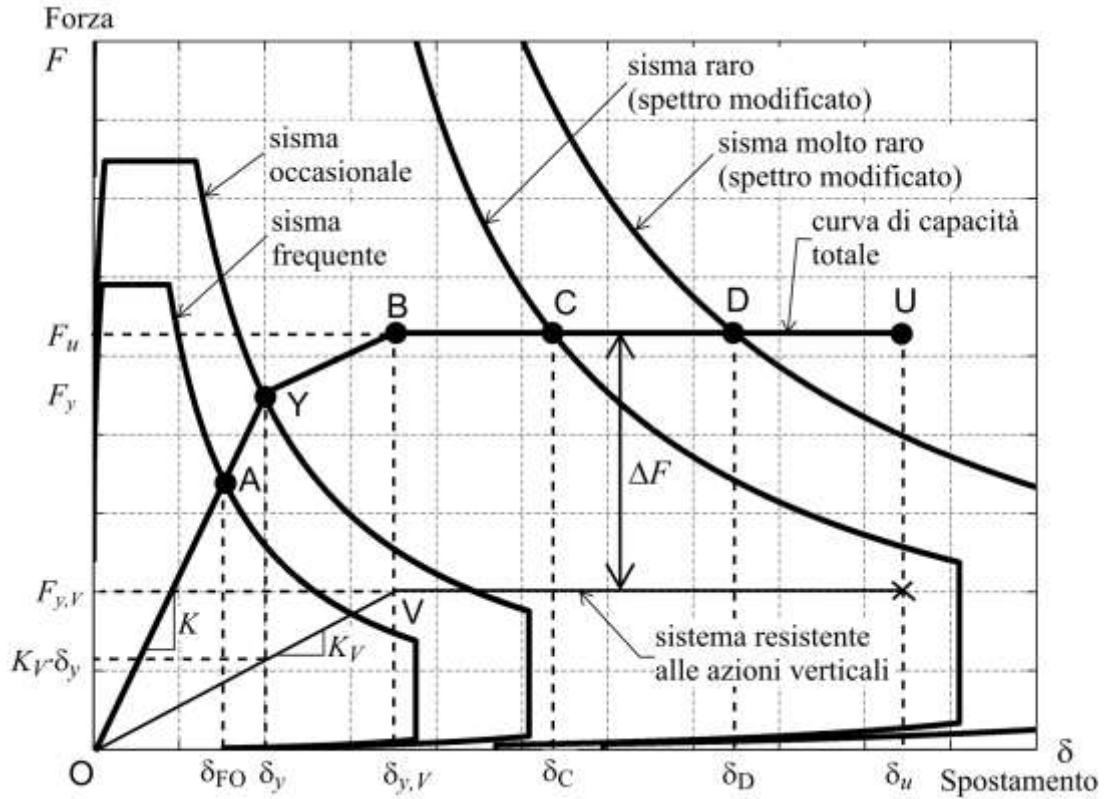


Figure 4.2 The difference between the VRS capacity curve and the objective curve

$$\delta_{y,H} = \delta_y \quad F_{y,H} = F_y - K_V \delta_y \quad K_H = K - K_V \quad \delta_{u,H} > \delta_D$$

Where $\delta_{y,H}$ is the limit of the elastic displacement, $F_{y,H}$ is the limit of the elastic resistance and $\delta_{u,H}$ is the ultimate displacement of the horizontal resistant system.

Based on this curve that in general - also taking account of the effects of the second order - will have a bi-linear form (elastic - hardening) or tri-linear, the individual dissipative elements that form the horizontal resistant system can be dimensioned. Assuming for example that these elements are all equal and in the number of n , it is sufficient to divide the ordinates of the curve by n and thus, the optimum capacity curve of the single dissipative component is obtained.

4.5. CSB DEVICES TO FULFILL THE PERFORMANCE OBJECTIVES

Following what we obtained from sections 4.2, 4.3 and 4.4, the horizontal dissipative devices should have a certain curve shape to mitigate the objective curve of the structure. From chapter 2, after showing all possible retrofitting techniques, it is possible to say that the solution for this problem can be founded in the supplemental damping device, the displacement activated device, and specially metallic, yielding and friction devices (Figure 2.2).

As the behavior curve of those devices should be similar to the objective curve as was explained before, many innovations were done to develop such new devices. Few are the metallic hysteretic device that can achieve this goal. To mention, the Cast Steel Yielding Fuse (CSF) device, as the one manufactured by Cast Connex Corporation (under the commercial name of Scorpion Yielding Devices), is a steel device for concentrically braced frames that dissipates energy through inelastic flexural yielding of special elements. The system exhibits a full, symmetric hysteresis characterized by an increase in stiffness at brace elongations larger than the design level. This increase in stiffness is a result of the second-order change in geometry of the yielding fingers, each of which is shaped to promote the spread of plasticity along its entire length. This effect can limit peak drifts and residual drifts and mitigate the likelihood that, in the event of a large earthquake, the inelastic demand will collect at a single story.

As well, the Crescent Shaped Brace, developed in this thesis is a new dissipative device that can have a desirable behavior and it can be inserted in the first story as a horizontal resisting system, like the first example studied here, or as dissipative diagonals for the other two examples.

Some examples have been developed in previous studies using the benefits of those new devices, before studying it deeply in analytically, numerically and experimentally in the following chapters.

FIRST EXAMPLE: SOFT STORY ISOLATION

A five-story steel frame to be built in Bologna (Italy) is the case study which was studied in previous study [57]. The building structure has a rectangular plan with dimensions equal to 36.00 m x 18.00 m. It is composed of 3 bays in x-direction and 6 bays in y-direction. The inter-story height is equal to 3.5 m while the roof height is equal to 17.5 m. From a design point of view, the structural system can be assumed as regular both in plan and elevation. The design of the structure is developed according to the Italian building code prescriptions. All the structural members (beams, columns, braces...) are supposed to be built adopting a S355 structural steel (yield strength equal to 355 MPa). The upper stories are braced using traditional concentric X-braces, which are sized in order to remain in the elastic field on the basis of Capacity Design criteria. The building has the same first-story lateral stiffness (referred to as k_{VRS}) in both principal directions. It should be noted the beams are all pin connected to the columns. The seismic weight per unit of area is equal to 10.0 kN/m^2 at the typical floor and 6.25 kN/m^2 at the roof leading to a seismic building mass equal to $m = 3055 \text{ t}$. For seismic design purpose the building is supposed to be located on a type-C soil and on a S1 (i.e. plane) topographic surface.

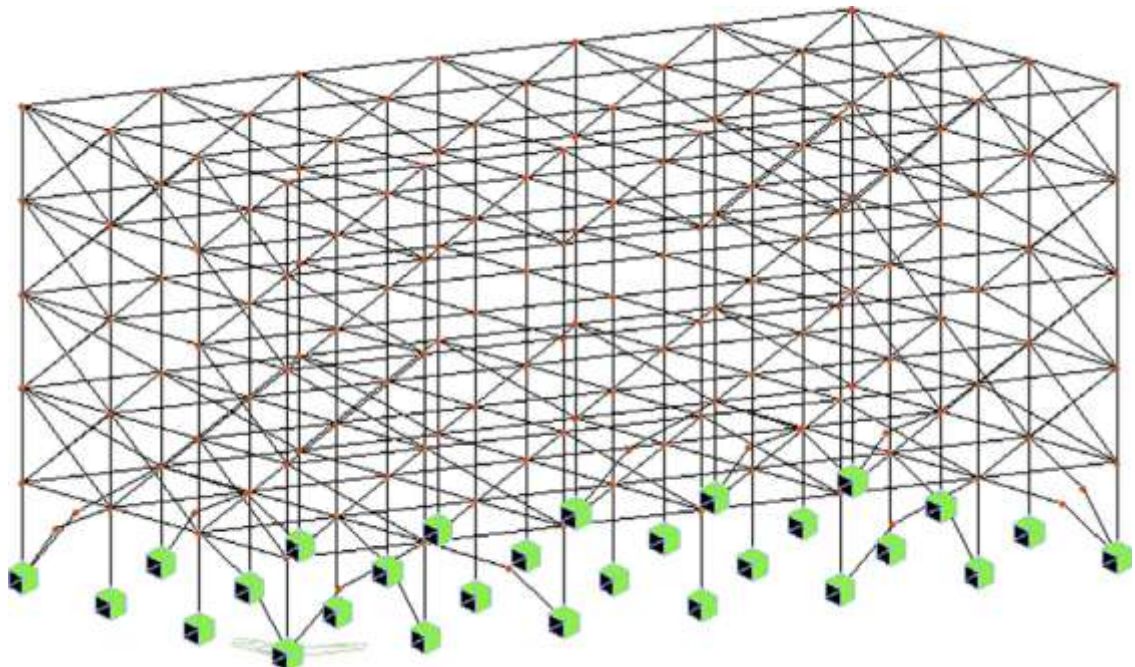


Figure 4.3 The CSB are inserted at the first level based on the concept of enhanced first story

Without repeating the same example, the conceptual approach was presented and fully detailed with reference to a specific case study in which the story seismic isolation system is realized through the insertion of special braces, called “crescent shaped braces”, at the first story, while traditional cross stiff braces are used at the upper storeys. The proposed design/verification approach involves a first phase of structure dimensioning by fitting the actual pushover curve of the structure to a “target pushover curve”, which is representative of the seismic idealized behavior of the structure. It is showed that the design process may be easily represented within the Capacity Spectrum Method, also accounting for P–D effects.

The second phase lies in the verification of the actual seismic behavior of the building structure under the design ground motions and is carried out through the development of non-linear time-history analyses. The results of non-linear time history analyses performed on the present case study building, as well as the results of previous analyses on similar case studies, show a good agreement between design and verification. Thus, the proposed approach may represent a valid option for the practitioner in order to design a building structure characterized by specific seismic performances. [57]

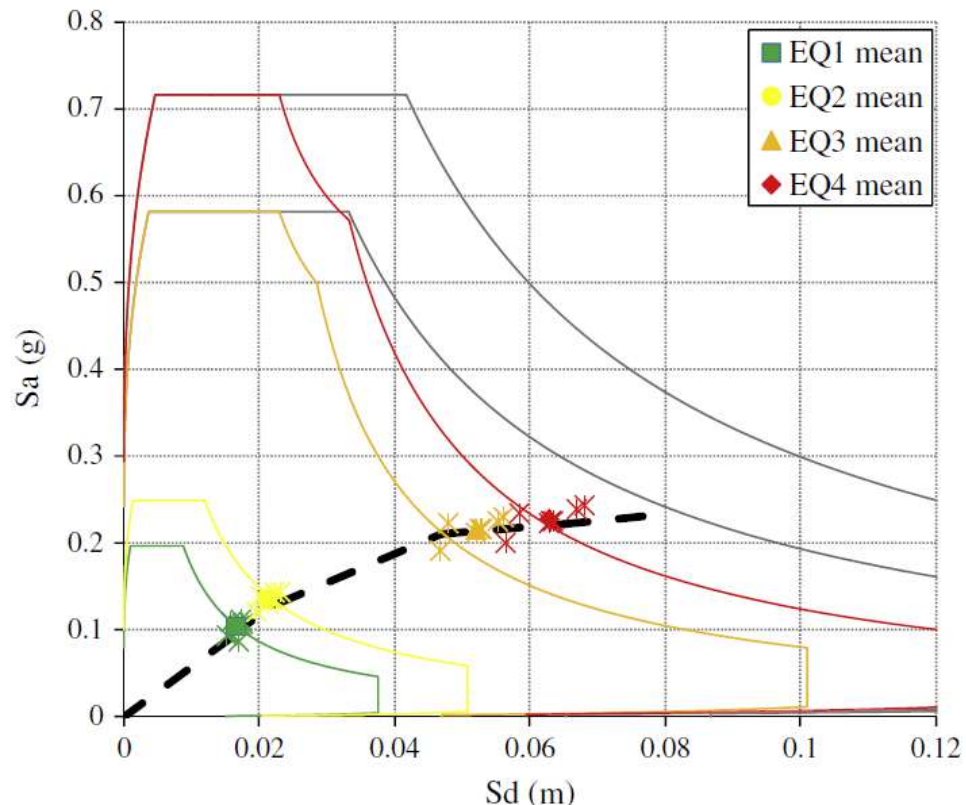


Figure 4.4 The building designed to verify the PBSO objectives using CSB

SECOND EXAMPLE: Retrofitting of an existing RC school

The building under study is the elementary school "Castle Hill" of Bisignano (CS), Italy, which was put to use in 1983. [5]

The building is made of three stories with a roof pavilion on the top. The geometry of the plan is rectangular. The backbone consists of four four-bay frames in the secondary direction. The frames are connected in the transverse direction by clay hollow-block floors and edge beams, while the only internal secondary beams are those that support the stairwell. The roof rests on walls and curbs, which is in turn supported by the floor of the attic (3rd level). [5]



Figure 4.5 The Castel Hill School in Bisignano

A complete study has been done on the equipped and the unequipped systems in terms of performance under the two ground motion levels SLD and SLV [5]. The results of the pushover and the time history analyses for both systems are plotted together in one graph so the comparison will be possible Figure 4.6. and Figure 4.8 and the effect of the inserted CSB is clear.

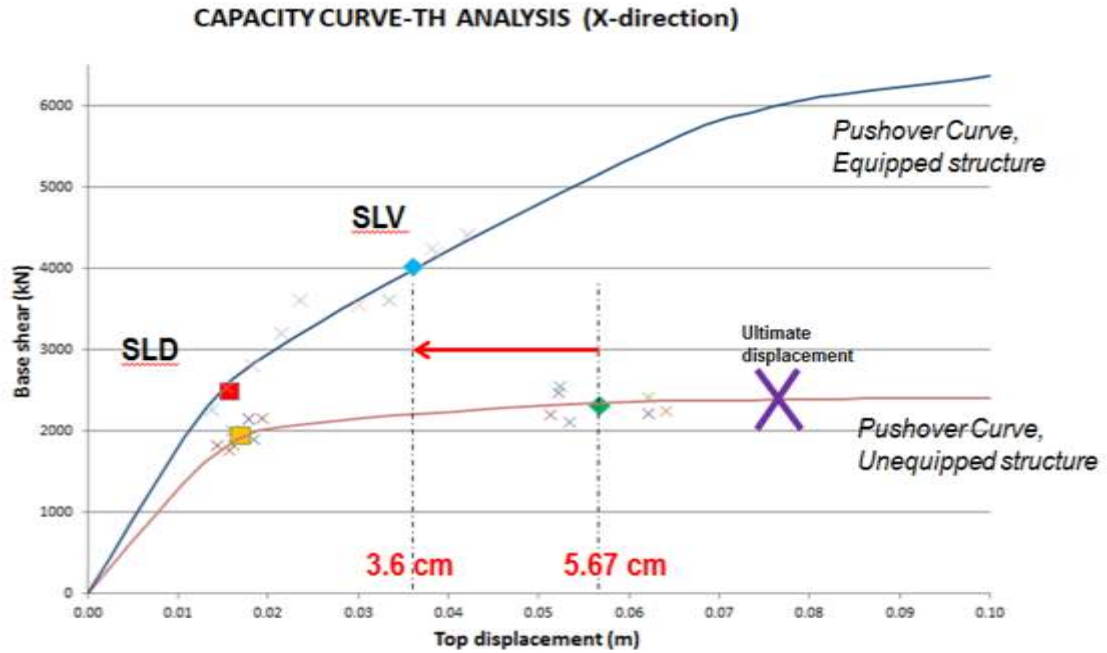


Figure 4.6 The behavior difference between the naked and the equipped structure in X direction

It is clear that we have improvements in the elastic and plastic regions. The structure is now able to stand the same force with less displacement. In the x-direction, the displacement is reduced from 5.67 cm to 3.6 cm (36 % improvement). Similarly, in the y-direction the displacement has reduced from 12.3 cm to 5.6 cm (54 % improvement). The results indicate how efficient the devices were, especially in the y-direction. Now after this significant reduction in displacement, the safety margin between the actual displacement and the ultimate displacement became larger.

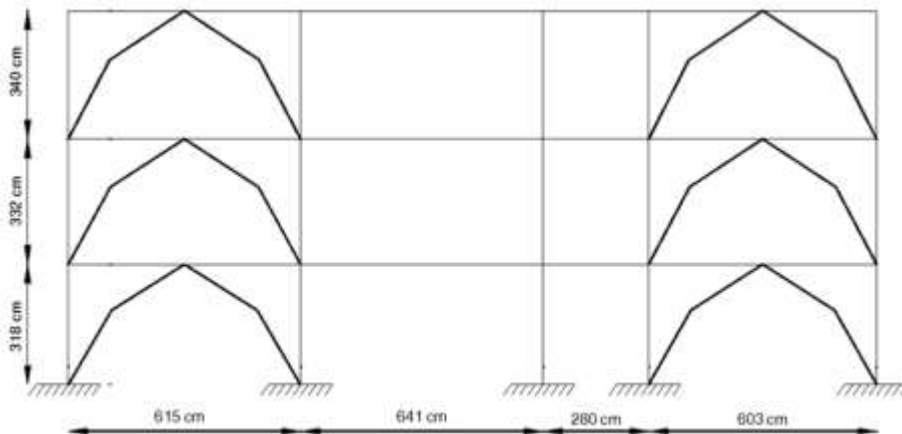


Figure 4.7 Example of the inserted CSB in X direction

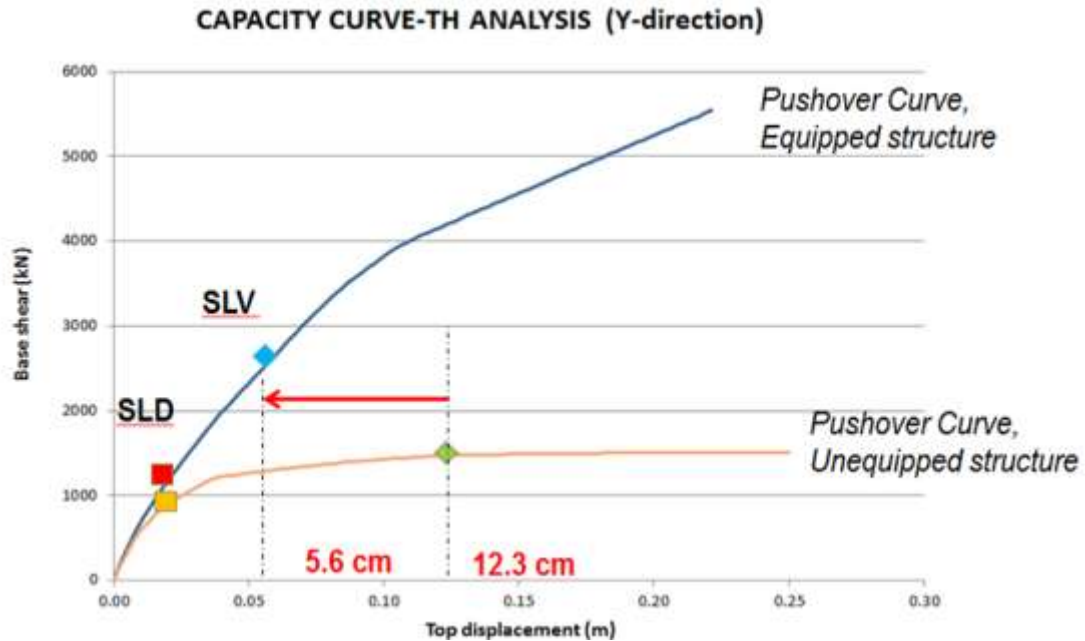


Figure 4.8 The behavior difference between the naked and the equipped structure in Y direction

Two types of analysis are performed in this work: The dynamic time-history and the static pushover analyses. [5]

4.6. CONCLUSIONS

This chapter presents a seismic design approach which allows exploiting all the potentialities offered by both the PBSD framework and the CSC methodologies at their best.

This approach leads to the identification of the characteristics of the structural system resisting to horizontal loads which enables to satisfy given seismic performance objectives. This is achieved by considering a total conceptual separation between structural systems resisting to vertical loads and another parallel one resisting to horizontal loads and by the use of specific braces as horizontal resisting system.

The original aspect of the proposed approach relies mainly in the combined use of the following recent contributions in the field of seismic engineering:

- Structural characteristics are designed in a way to give the building response a predefined seismic behavior (active role of the structural process).

- The designer may impose/select the stiffness, the strength and the ductility of the structure in order to achieve the desired seismic performances;
- Satisfaction of a multiplicity of performance objectives within a PBSO approach. The structural seismic performances are determined either upon strength and resistance or displacement capabilities of the horizontal system, depending upon the considered limit state;
- Conceptual separation between the structural systems resisting to vertical and horizontal loads. This opens the ground for new structural solutions for the seismic design of structures;
- Proposal of use of specific braces, mentioning the peculiar crescent shaped steel braces (Part B), which seem to have good behavior and independency between stiffness, resistance and ductility.

PART B: Constitutive Behavior of the Crescent Shaped Brace

Part B is focused on verification of the validity of the Crescent shaped Brace. Chapter 4 defines analytically the behavior of a CSB element, under tensile and compressive loads, for both elastic and plastic fields. Chapter 5, is a numerical verification of the behavior of the device. Moreover, the influence of the picked cross section and the angle of inclination of the device are investigated in this chapter. Chapter 7 forms the main core of part B. It is a fully description of the experimental tests applied on thirteen specimens. Geometrical and mechanical properties of specimens, protocol of tests and the used machine are described in the first segment of this chapter. Then, the force displacement results are shown before an analysis of the results, the effect of welding, the ductility and energy dissipation capacities and local deformation seen on some tested tests.

5. Behavior of CSB: Analytical Developments

5.1. INTRODUCTION

This chapter describes the analytical model developed in general terms. It distinguishes between the behavior in traction and in compression. Also, it shows the behavior of two coupled devices. The problem of instability is studied as well for the case of compressed Crescent Shaped Brace. As the double devices can have more advantages, analytical studies of such disposition will be presented too.

5.2. GEOMETRICAL AND MECHANICAL PROPERTIES

Crescent Shaped Braces are steel hysteretic devices which connect two generic points of the structure (e.g. two points at the same storey or two points at different storeys). The fundamental feature of these devices lies in their geometrical configuration, which is “ad hoc” defined in order to provide a desired behavior, as it will be clarified later. CSBs can be used as “enhanced” diagonal braces for common frame structures. Figure 5.2 displays a CSB (thick solid line) inserted into a single frame (thick dotted line). The frame is characterized by a height H_f and a length B_f , the diagonal length is indicated as L . The specific CSB geometrical configuration of Figure 5.1 will be referred to as “bilinear configuration”. [21]

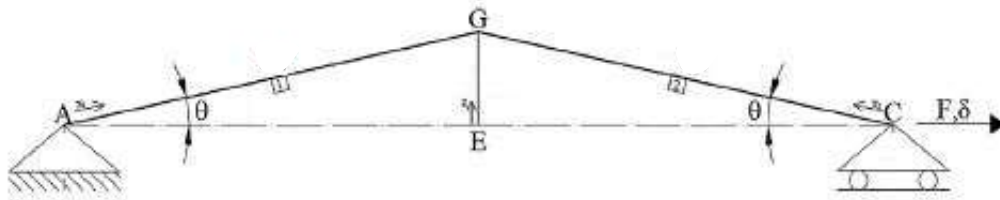


Figure 5.1 A single Crescent Shaped Brace

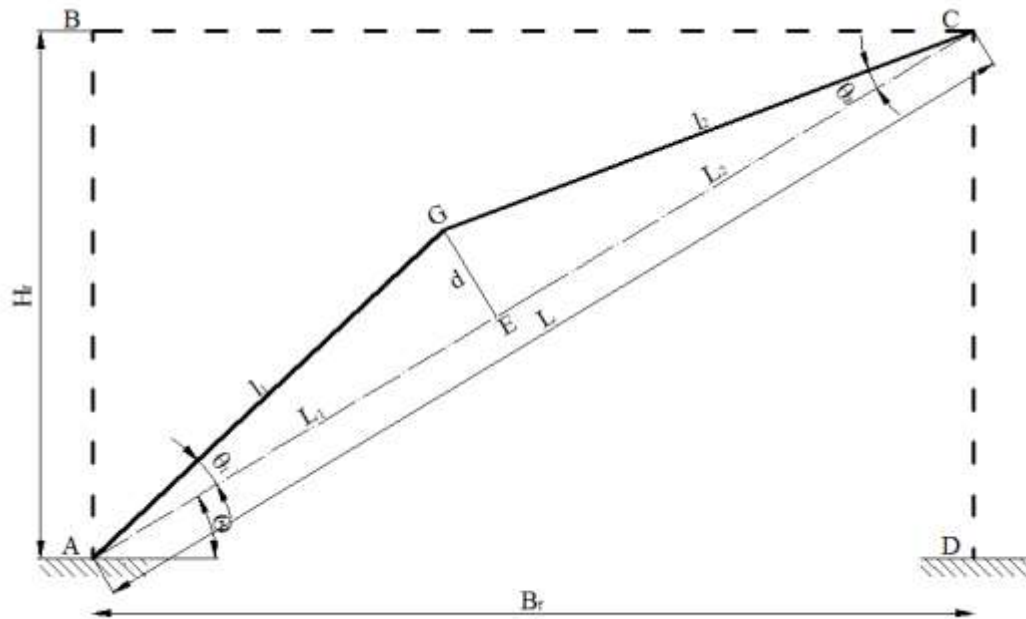


Figure 5.2 A single Crescent shaped Brace inserted in a frame

The following notation is introduced and presented in Figure 5.1 and Figure 5.2:

- Θ represents the inclination of the reference diagonal line with respect to the horizontal direction;
- l_1 and l_2 are the lengths of the two straight elements, indicated as 1 and 2, respectively (the total CSB length is equal to $l=l_1+l_2$, L_1 and L_2 are the projection of l_1 and l_2 . For a symmetrical crescent shaped brace, l_1 is equal to l_2).
- θ along the diagonal; θ_1 and θ_2 are the inclinations of element 1 and 2 with respect to the reference diagonal line, respectively; in all the next studies, the CSB will be symmetrical, thus: $\theta_1 = \theta_2$
- d indicates the orthogonal distance between the knee point G and the reference diagonal line and will be referred to as “arm”.

It is supposed that elements 1 and 2 have the same cross-section, characterized by area A , moment of inertia J and section modulus W ($W=2J/h$, where h is the depth of the cross-section).

With reference to the bilinear configuration displayed in Figure 5.2, the independent geometrical and mechanical parameters, which govern the CSB response, are:

•With reference to the geometry:

1. the diagonal length L
2. the diagonal projection L_1 ($L_2 = L - L_1$), or equivalently the L_1
3. the diagonal inclination Θ / L ratio
4. the arm d , or equivalently the d/L ratio (indicated also as ξ)

•With reference to the cross-section:

5. the depth of the cross-section h
6. the cross-section area A
7. the moment of inertia J , or equivalently the i/h ratio, where i is the radius of gyration of the cross-section ($i^2 = J/A$)

•With reference to the material (a bilinear stress-strain relationship is assumed):

8. the elastic modulus E
9. the yield strength f_y
10. the hardening ratio, r , as defined as the E_p/E ratio, where E_p is the tangent of the stress-strain curve after the yielding point.

Typically, i/h values are between 0.2 and 0.5. Compact profiles exhibit lower i/h values, while I profiles (IPE, HE) exhibit higher i/h values. Table 5-1 provides the i/h values for some typical steel profiles.

Profile	Full Circular	Full Rectangular	Tubular Circular	Tubular Rectangular	I sections
i/h	0.25	0.29	0.35	0.39	0.44

Table 5-1 i/h of typical steel profiles

Based on the above observations, the total number of independent engineering parameters governing the CSB behavior is equal to ten.

It will be shown that L_1 practically does not affect, for seismic design purposes, the CSB behavior. Thus, the remaining independent parameters become equal to nine.

5.3. EQUILIBRIUM EQUATIONS

The behavior of a bilinear CSB system under lateral loads is studied with reference to the geometrical configuration represented in Figure 5.3 with the specific purpose of deriving analytical expression of the lateral stiffness and the yield strength. It is supposed that the CSB is pinned at node A, while it is rolled at node C. A horizontal load F is applied at node C.

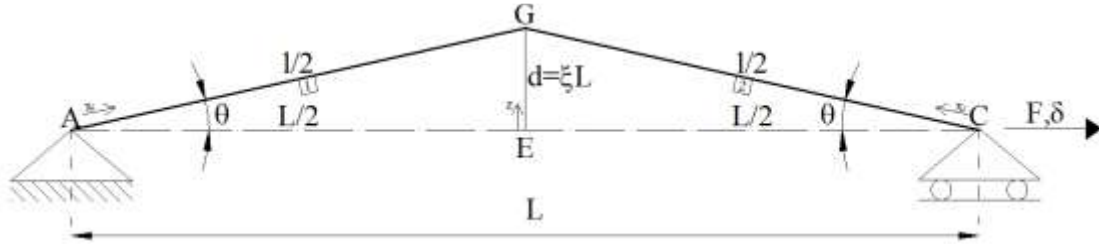


Figure 5.3 Geometrical characteristics of a CSB device

From simple equilibrium considerations, the axial force, the shear force and the bending moment acting along the two elements are equal to:

$$\begin{cases} N_1(x_1) = F \cdot \cos \vartheta \\ V_1(x_1) = F \cdot \sin \vartheta \\ M_1(x_1) = \int_0^{x_1} V_1(x_1) dx_1 = \int_0^{x_1} F \cdot \sin \vartheta dx_1 = F \cdot z \end{cases} \quad \text{Eq. 5.1}$$

$$\begin{cases} N_2(x_2) = F \cdot \cos \vartheta \\ V_2(x_2) = F \cdot \sin \vartheta \\ M_2(x_2) = \int_0^{x_2} V_2(x_2) dx_2 = \int_0^{x_2} F \cdot \sin \vartheta dx_2 = F \cdot z \end{cases} \quad \text{Eq. 5.2}$$

Where x_1 and x_2 represent the local longitudinal axes of the elements, z represents the abscissa along segment EG.

The axial and shear forces are constant along the elements (thus can be simply indicated as N_1 , N_2 and V_1 , V_2 , respectively), while the bending moment varies linearly and achieves its maximum value at the knee point G:

$$M_G = F \cdot d \quad \text{Eq. 5.3}$$

5.4. THE LINEAR ELASTIC BEHAVIOR

The lateral displacement δ due to the horizontal force F can be evaluated by applying the principle of virtual works:

$$\delta = \delta_N + \delta_M = \int_0^{l_1} \frac{N_1}{E \cdot A} \cdot \cos \vartheta_1 dx_1 + \int_0^{l_2} \frac{N_2}{E \cdot A} \cdot \cos \vartheta_2 dx_2 + \int_0^{l_1} \frac{M_1(x_1)}{E \cdot J} \cdot z(x_1) dx_1 + \int_0^{l_2} \frac{M_2(x_2)}{E \cdot J} \cdot z(x_2) dx_2$$

Where, δ_N and δ_M are the axial and the flexural contributions to total deformation. It should be noted that the deformation due to shear has been neglected. The assumption is reasonable in the case of slender steel members, say span-to-depth ratio larger than 5 (for ordinary span-to-depth ratios, e.g. 10-30, the error due to shear deformations become negligible).

By introducing $\rho = L_1/L$ e $\xi = d/L$, after simple mathematical developments, the equation becomes:

$$\delta = \delta_N + \delta_M = F \cdot \left[\frac{L}{E \cdot A} (\rho \cdot \cos \vartheta_1 + (1 - \rho) \cdot \cos \vartheta_2) + \frac{L^3 \cdot \xi^2}{3E \cdot J} \left(\frac{\rho}{\cos \vartheta_1} + \frac{(1 - \rho \cdot \cos \vartheta_1)}{\cos \vartheta_2} \right) \right]$$

Where the expressions of δ_N and δ_M are:

$$\delta_N = F \cdot \left[\frac{L}{E \cdot A} (\rho \cdot \cos \vartheta_1 + (1 - \rho) \cdot \cos \vartheta_2) \right] \quad \text{Eq. 5.4}$$

$$\delta_M = F \cdot \left[\frac{L \cdot d^2}{3E \cdot J} \left(\frac{\rho}{\cos \vartheta_1} + \frac{(1 - \rho \cdot \cos \vartheta_1)}{\cos \vartheta_2} \right) \right] \quad \text{Eq. 5.5}$$

It should be noted that the expressions inside the square brackets in Equations 5.4 and 5.5 are the inverses of the lateral stiffness of the CSB. In order to obtain a more compact notation, the following two functions of ρ and ξ are introduced:

$$f_1(\rho, \xi) = \sqrt{\rho^2 + \xi^2} + \sqrt{1 - \rho^2 + \xi^2}$$

$$f_2(\rho, \xi) = \frac{\rho^2}{\sqrt{\rho^2 + \xi^2}} + \frac{1 - \rho^2}{\sqrt{1 - \rho^2 + \xi^2}}$$

Which allow expressing the first equation as follows:

$$\delta = \delta_N + \delta_M = F \cdot \left[\frac{L}{E \cdot A} \cdot f_2(\rho, \xi) + \frac{L \cdot d^2}{3E \cdot J} \cdot f_1(\rho, \xi) \right] \quad \text{Eq. 5.6}$$

It should be noted that f_1 and f_2 are close to one for most values of ρ and, as first approximation, for design purposes, they can be assumed both equal to 1. This justifies the statement anticipated at the end of section 5.2, regarding the negligible influence of L_1 .

After some mathematical manipulations, the lateral stiffness of the CSB can be expressed as follows:

$$K = \frac{F}{\delta} = \left(\frac{E \cdot A}{L} \right) \cdot \left(\frac{1}{f_2(\rho, \xi) \cdot \left(1 + \frac{\delta_M}{\delta_N} \right)} \right) = K_N \cdot \gamma$$

Where:

$$K_N = \frac{E \cdot A}{L}$$

It can be recognized that the first term (K_N) represents the axial rigidity of an ideal straight member, while the second term (γ) is a reduction factor due the geometry of the system. Figure 5 displays γ as function of $\xi = d/L$ for different cross-section profiles (i.e. different values of i/h ; for sake of simplicity, $f_2(\rho, \xi)$ is taken equal to 1.0). Inspection of the graph clearly shows that the lateral stiffness rapidly decreases as the d/L ratio increases.

If the diagonal reference line of the CSB configuration is inclined with an angle ϑ with respect to the horizontal line, the inclination should be taken into account as follows:

$$K = \left(\frac{E \cdot A}{L} \right) \cdot \cos^2 \vartheta \cdot \left(\frac{1}{f_2(\rho, \xi) \cdot \left(1 + \frac{\delta_M}{\delta_N} \right)} \right) = K_N \cdot \cos^2 \vartheta \cdot \gamma$$

From the equilibrium considerations discussed in the previous section, it clearly appears that the CSB reaches the first yielding condition at the knee point G. By imposing the yielding condition ($\sigma_{\max} = f_y$, i.e. the maximum stress equals the yield stress of the material), the following expression of the yield strength can be obtained:

$$F_y = f_y \cdot \frac{W}{\xi \cdot L} \cdot \left(\frac{1}{1 + \frac{L}{h} \cdot \frac{2}{\xi} \cdot \left(\frac{i}{h} \right)^2} \right) = f_y \cdot \frac{W}{\xi \cdot L} \cdot \mu$$

Or alternately:

$$F_y = A \cdot f_y \cdot \left(\frac{1}{1 + \frac{L}{h} \cdot \frac{\xi}{2 \cdot \left(\frac{i}{h} \right)^2}} \right) = A \cdot f_y \cdot \eta$$

Where:

$$\mu = \left(\frac{1}{1 + \frac{h}{L} \cdot \frac{2}{\xi} \cdot \left(\frac{i}{h}\right)^2} \right)$$

$$\eta = \left(\frac{1}{1 + \frac{L}{h} \cdot \frac{\xi}{2 \cdot \left(\frac{i}{h}\right)^2}} \right)$$

The coefficients μ and η represent the reduction factors that are to be applied to the pure flexural strength or to the axial strength ($N_y = A \cdot f_y$) of the member in order to obtain the effective yield strength. Figure 6 displays η as a function of d/L for various steel profiles, (i.e. for various i/h ratios) for a fixed h/L ratio equal to 0.04.

In particular, analytical expressions of the initial lateral stiffness and lateral force leading to the first yielding has been derived studying the equilibrium in the initial undeformed configuration considering both the axial and flexural contributions to the total elastic deformation. As observed before, increasing ξ leads to a rapid reduction of the axial contribution. Practically, for ξ larger than 0.10, the yield strength can be assumed equal to the pure flexural strength. In such a case, the following simplified analytical expressions of the lateral stiffness and lateral force leading to the first yielding can be used for design purposes (in the following, the subscript indicates that the quantities are evaluated with respect to the initial undeformed configuration):

$$K_{L0} = \frac{3}{2} \frac{EJ}{L^3 \sin^2 \theta_0} \tag{Eq. 5.7}$$

$$F_{y0} = \frac{M_y}{d_0} \tag{Eq. 5.8}$$

Where $M_y = W_{el} \cdot f_y$ the bending yielding moment of the cross section is (W_{el} is the elastic strength modulus of the cross-section).

5.5. THE POST ELASTIC BEHAVIOR

This section analyzes the post-yielding behavior of CSBs under both monotonic (in tension and compression) and cyclic reversed increasing loadings with the specific

purpose of providing useful information related to the seismic design of such systems. Without loss of generality, for sake of conciseness, the results presented here are referred to the case of the symmetric bilinear configuration (Figure 5.3). The lateral force leading to the full plasticization of the knee cross-section is given by:

$$F_{pl0} = \frac{M_{pl}}{d_0} \quad \text{Eq. 5.9}$$

Where M_{pl} is the plastic bending moment of the cross section ($W_{pl} = \beta \cdot W_{el}$ is the plastic benefit of the member cross-section).

5.6. APPLICATIVE EXAMPLE

In the present section, an explicit calculation is done on a Crescent shaped Brace example with a rectangular cross section (4.14*1.5 cm), L=104 cm, d=0.1*L=10.4cm, E=210000MPa.

Section 5.6 is composed of two subsections: the first one describes the behavior of the CSB element in tensile field and the second one describes the behavior of the same element under compression loads.

In the section related to the tensile loads, it is divided into four parts: the first part treats the elastic behavior of the element in three different analytical methods. Two of them, the first and the third, are explained in section 5.4. The second one is a development of the first one with an addition of the angle variation, for this reason a MATLAB code is developed to have the results. The other three parts in the tensile section are dedicated to describe the plastic, hardening and ductile behavior of the device after the yielding point.

The second big subsection is dedicated to the behavior under compression. This part as well is composed of two parts. First one describes the elastic behavior in two methods: first one is a long one, based on the formulas of Merchant-Rankine. The second method is the simple one described in section 5.4. The plastic behavior is described in the second part.

In the end of each section, the obtained behavior was plotted.

5.6.1. Behavior under Tensile Loads

The behavior of structural steel subjected to a tensile test is represented, in generic form, in the stress-strain diagram represented in Figure 5.4

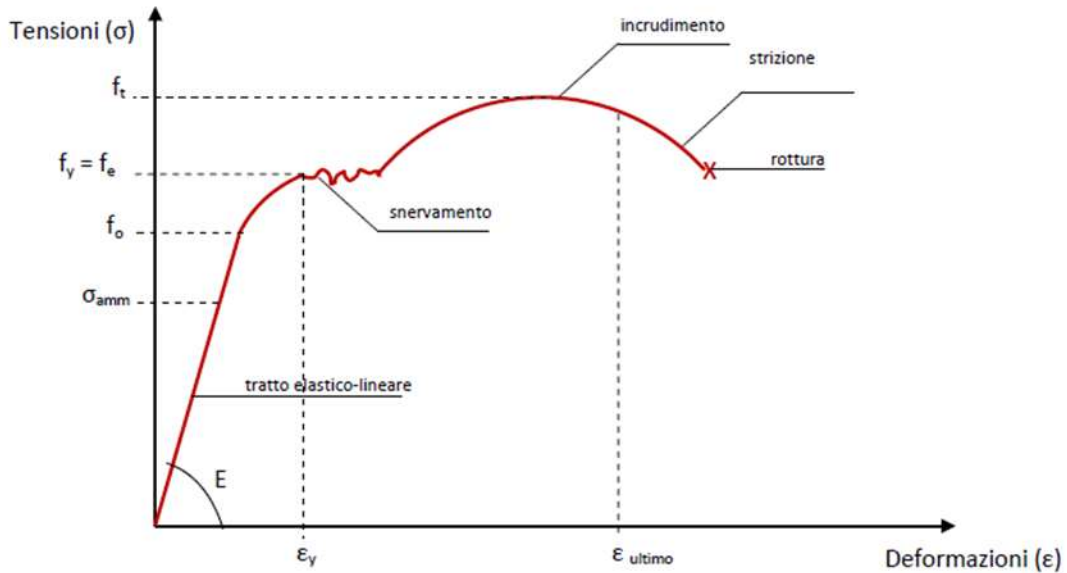


Figure 5.4 The stress-strain steel behavior

The adopted model for our calculation refers to the elastic-plastic model. Where σ_y reaches the yield stress, the load should increase in order to increase the deformation due to the hardening of the material. [9]

Theoretical anticipation of the non-linear behavior of the device can be obtained by referring to the followed idealization:

Regarding the initial elastic response, we consider that the continuous system is composed of two deformable rods connected rigidly to the knee point;

Regarding the non-linear response after the knee point yielding, we consider the discrete equivalent system consisting of two rods with different inertia, in a part with elastic behavior and in another with plastic comportment.

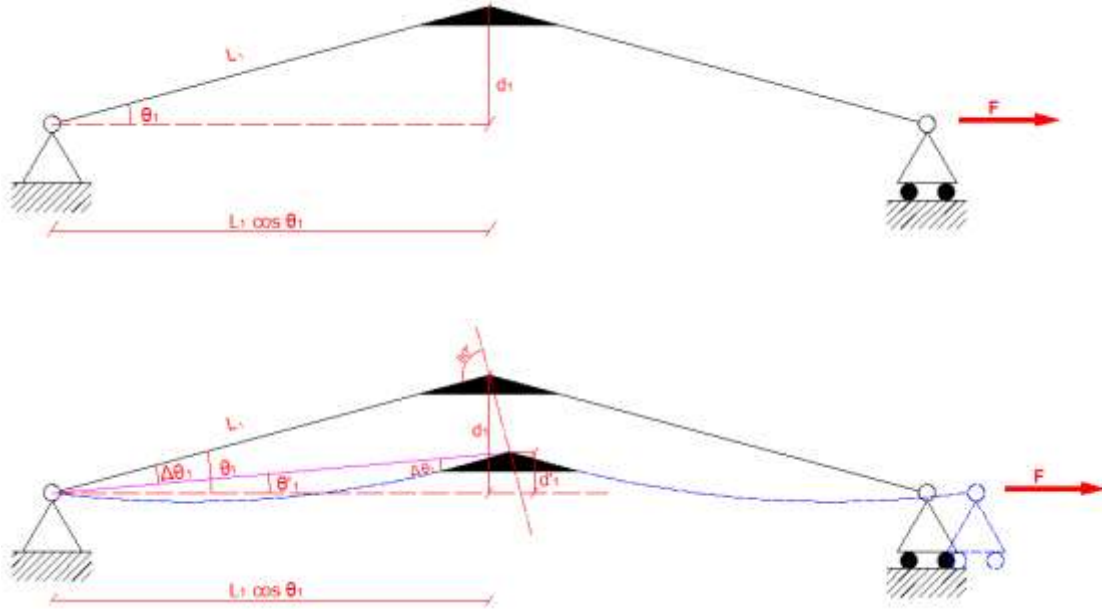


Figure 5.5 the deformation of a CSB device under tensile loads

1) Elastic Range

Before developing the calculations for the first section, it occurs that the use of the Principle of Virtual Work gives consistent results. For this purpose we calculate the slope of the curve obtained by applying the PLV in the case of small deformation, making the following assumptions:

The initial angle θ_1 is constant angular variations negligible within the elastic range of the structure;

The maximum applied force F is the first yielding point of occurrence of yielding.

$$\sigma_y = \frac{N_y}{A} + \frac{M_y}{W_{el}} = \frac{F_{y,flex} \cdot \cos(\theta_{1y,flex})}{A} + \frac{F_{y,flex} \cdot L_1 \cdot \sin(\theta_{1y,flex})}{W_{el}} \quad \text{Eq.5.7.}$$

The results of the Table 5-2 are obtained using the equations of virtual work developed in the section 5.4.(Eq. 5.4, Eq 5.5, Eq 5.6).

F [kN]	θ_1 [°]	δ [cm]
0	11,3100	0
5	11,0269	0,10133
8	10,8663	0,15771
10	10,7629	0,19359
12	10,6621	0,22821
15	10,5158	0,27789
17	10,4213	0,30962

Table 5-2 Deformation values under elastic tensile loads

Taking in consideration the angle deformation during elastic range, we get out with this new equation based on the previous ones:

$$2 \cdot \left(\frac{F \cdot L_1^3 \cdot (\sin(\vartheta_1'))^2}{3 \cdot E \cdot J} + \frac{F \cdot L_1 \cdot (\cos(\vartheta_1'))^2}{E \cdot A} + \frac{F \cdot L_1 \cdot (\sin(\vartheta_1'))^2}{A \cdot G} \right) = 2 \cdot L_1 \cdot \cos(\vartheta_1') - 2 \cdot L_1 \cdot \cos(\vartheta_1)$$

Thus, for the same elastic range, after using a MATLAB script to calculate the equation above, we obtain a new table describing the behavior of the element under tensile loads:

F [kN]	ϑ_1' [rad]	δ [cm]
0	0,197297	0
5	0,192359	0,10133
8	0,189557	0,15771
10	0,187752	0,19359
12	0,185994	0,22821
15	0,183442	0,27789
17	0,181794	0,30962

Table 5-3 Deformation values under elastic tensile loads (second method)

The value of $F_y=17$ comes from equation 5.7, using the following calculation:

$$40 \left[\frac{kN}{cm^2} \right] = \frac{17 [kN] \cdot \cos(0.181794)}{6.21 [cm^2]} + \frac{17 [kN] \cdot 53 [cm] \cdot \sin(0.181794)}{4.28 [cm^3]}$$

In the other hand, using the last simple equations, without taking in consideration the geometrical non linearity, we obtained the value of $K_0 = 49$ kN/cm and $F_y=16.2$ kN.

2) Post-Elastic Range

The yield configuration identified above and shown schematically in Figure 5.7 represents the departure for the study of this second section between the yield strength (equal to 17 kN) and a maximum load that implicates the attainment of the last moment M_u on the knee section.

The following diagram is solved by imposing a load increase of 1 kN, starting from the carrying value of $F_{y, flex}$. Figure 5.6 represents a discrete equivalent system consisting of two rods having a different inertia, in which the non-mechanical linearity is taken into

account. More precisely, the length of the elastic rod is equal to ηL_1 , while the remaining part of the rod, which includes the knee area, with a length equal to $(1-\eta)L_1$, is already plasticized.

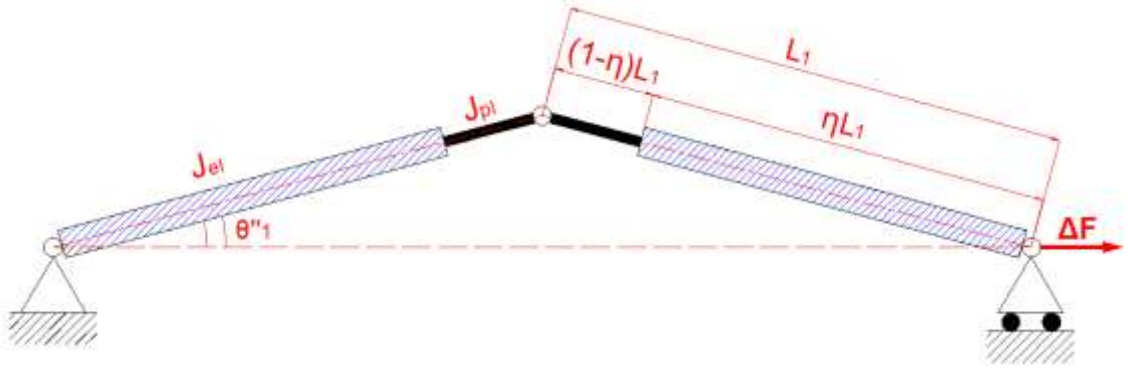


Figure 5.6 The change of the section characteristics after the yielding point

Once the value of angle $\theta_{1y, flex}$ is known, the displacement is obtained by the following kinematic equation:

$$\delta_{y, flex} = 2 \cdot L_1 \cdot \cos(\vartheta_{1y, flex}) - 2 \cdot L_1 \cdot \cos(\vartheta_1)$$

Increasing the load after flexural yielding, they are obtained the following effects:

- Cross sections start to plasticize, in fact, the stress diagram is modified;
- The curvature of the deformation diagram is modified and, consequently, the value of J decreases, but is assumed homogenous in each section of the device.

The device is in a situation where a part is elastic and a part is plastic, so it is necessary to introduce the parameter η , which is indicative of the percentage of the elastic structure.

The analytical formulation that detects the displacement of an elastic beam composed of two portions having different inertia is:

$$\delta'' = \delta''_{M, PLV} = \frac{2 \cdot F \cdot L_1^3}{3 \cdot E \cdot J_{el}} \cdot \left(\eta^3 + \frac{1 - \eta^3}{\beta} \right) \cdot (\sin(\vartheta_1''))^2$$

Where:

J_{el} = moment of inertia of the elastic sections

$$\beta = \frac{J_{pl}}{J_{el}}$$

J_{pl} = moment of inertia of the plasticized section

For details see Appendix A.

It is possible to evaluate the variation of the plasticized rod length as a function of the reduction of inertia of the cross section.

For $F = F_{y,flex}$ we have $J_{el} = J_{pl}$, thus $\beta = \infty$ and $\eta = 1$, so the plasticized part of the device is nothing;

For $F > F_{y,flex}$, we find the value of \bar{x} which attribute to the length of the elastic rod, thus identifying the section where $M(F, \bar{x}) = M_y$

$$\begin{cases} M_y = F_{y,flex} \cdot L_1 \cdot \sin(\vartheta_{1y,flex}) \\ M(F, \bar{x}) = F \cdot \bar{x} \cdot \sin(\vartheta_1'') = (F_{y,flex} + \Delta F) \cdot \bar{x} \cdot \sin(\vartheta_1'') \end{cases}$$

Imposing $M_y = M(F, \bar{x})$ we obtain:

$$F_{y,flex} \cdot L_1 \cdot \sin(\vartheta_{1y,flex}) = (F_{y,flex} + \Delta F) \cdot \bar{x} \cdot \sin(\vartheta_1'')$$

Imposing:

$$\bar{x} = \frac{F_{y,flex}}{(F_{y,flex} + \Delta F)} \cdot \frac{\sin(\vartheta_{1y,flex})}{\sin(\vartheta_1'')} \cdot L_1$$

Thus:

$$\eta = \frac{\bar{x}}{L_1} = \frac{F_{y,flex}}{(F_{y,flex} + \Delta F)} \cdot \frac{\sin(\vartheta_{1y,flex})}{\sin(\vartheta_1'')}$$

Applying the following hypothesis:

1. $\eta = 0.8$;
2. $\bar{\beta}(\Delta F) = \beta(\Delta F)$, for a constant increase along the plasticized part of the CSB element, we have the same value of β .

We consider now the system with a homogenized moment of inertia thus:

$$\begin{aligned} \delta'' = \delta_{M,PLV}'' &= \frac{2 \cdot F \cdot L_1^3}{3 \cdot E \cdot J_{el}} \cdot \left(\eta^3 + \frac{1 - \eta^3}{\beta} \right) \cdot (\sin(\vartheta_1''))^2 \\ &= \frac{2 \cdot F \cdot L_1^3}{3 \cdot E \cdot J_{el}} \cdot \left(\frac{1}{2} + \frac{1}{2 \cdot \beta} \right) \cdot (\sin(\vartheta_1''))^2 \\ &= \frac{F \cdot L_1^3}{3 \cdot E \cdot J_{el}} \cdot \left(1 + \frac{1}{\beta} \right) \cdot (\sin(\vartheta_1''))^2 \\ &= \frac{F \cdot L_1^3}{3 \cdot E \cdot J_{el}} \cdot (\sin(\vartheta_1''))^2 + \frac{F \cdot L_1^3}{3 \cdot E \cdot J_{pl}} \cdot (\sin(\vartheta_1''))^2 \end{aligned}$$

Going from elastic to plastic behavior, it is possible to have the following equations:

- Yielding Moment:

$$M_y = F_{y,flex} \cdot L_1 \cdot \text{sen}(\vartheta_{1y,flex})$$

- Moment variation:

$$\Delta M = \Delta F \cdot L_1 \cdot \text{sen}(\vartheta_1'')$$

- Plastic benefit:

$$\xi = \sqrt{\frac{1}{4} - \frac{\Delta M}{2 \cdot M_{y,flex}}}$$

- Curve corresponding to yielding

$$\chi_y = \frac{\varepsilon_y}{h/2} = \frac{2 \cdot \sigma_y}{E \cdot h}$$

- Plastic curve:

$$\chi = \frac{\varepsilon_y}{\bar{y}} = \frac{\sigma_y}{E \cdot \bar{y}} = \frac{\sigma_y}{E \cdot \xi \cdot h}$$

where \bar{y} is distance between the neutral axis and the first yielded fiber of the cross section

- Reduced moment of inertia:

$$\tilde{J} = \frac{b \cdot h^3}{8} \cdot \left(\frac{\chi_y}{\chi}\right) \cdot \left(1 - \frac{1}{3} \cdot \left(\frac{\chi_y}{\chi}\right)^2\right) = \frac{3}{2} \cdot J \cdot \left(\frac{\chi_y}{\chi}\right) \cdot \left(1 - \frac{1}{3} \cdot \left(\frac{\chi_y}{\chi}\right)^2\right)$$

Again, using the Principal of Virtual Work, it is possible to determine the value of the displacement where the element is subjected to a force equal to ΔF :

$$\delta_{\Delta}'' = \delta_M'' + \delta_N'' + \delta_T''$$

$$\delta_{\Delta}'' = 2 \cdot \int_0^{\eta \cdot L_1} M' \cdot \frac{M}{E \cdot J} dx + 2 \cdot \int_{\eta \cdot L_1}^{L_1} M' \cdot \frac{M}{E \cdot \tilde{J}} dx + 2 \cdot \int_0^{L_1} \left(N' \cdot \frac{N}{E \cdot A} + T' \cdot \frac{T}{E \cdot A}\right) dx$$

$$\begin{aligned} \delta_{\Delta}'' = 2 \cdot \int_0^{\eta \cdot L_1} & \left(1 \cdot \text{sen}(\vartheta_1'') \cdot x \cdot \frac{\Delta F \cdot \text{sen}(\vartheta_1'') \cdot x}{E \cdot J}\right) dx + 2 \\ & \cdot \int_{\eta \cdot L_1}^{L_1} \left(1 \cdot \text{sen}(\vartheta_1'') \cdot x \cdot \frac{\Delta F \cdot \text{sen}(\vartheta_1'') \cdot x}{E \cdot \tilde{J}}\right) dx + 2 \\ & \cdot \int_0^{L_1} \left(1 \cdot \text{cos}(\vartheta_1') \cdot \frac{\Delta F \cdot \text{cos}(\vartheta_1')}{E \cdot A} + 1 \cdot \text{sen}(\vartheta_1'') \cdot \frac{\Delta F \cdot \text{sen}(\vartheta_1'')}{A \cdot G}\right) dx \end{aligned}$$

$$\delta_{\Delta}'' = 2 \cdot \left(\frac{\Delta F \cdot (\sin(\vartheta_1''))^2}{E \cdot J} \cdot \left[\frac{x^3}{3} \right]_0^{\eta \cdot L_1} + \frac{\Delta F \cdot (\sin(\vartheta_1''))^2}{E \cdot \tilde{J}} \cdot \left[\frac{x^3}{3} \right]_{\eta \cdot L_1}^{L_1} + \frac{\Delta F \cdot (\cos(\vartheta_1''))^2}{E \cdot A} \cdot [x]_0^{L_1} + \frac{\Delta F \cdot (\sin(\vartheta_1''))^2}{A \cdot G} \cdot [x]_0^{L_1} \right)$$

However, to take into consideration that the section near and in the knee zone are partially yielded, the moment of inertia J is calculated imposing $\eta^3 = 0.5$, as it was verified before, we obtain:

$$\delta_{\Delta}'' = \frac{\Delta F \cdot L_1^3 \cdot (\sin(\vartheta_1''))^2}{3 \cdot E \cdot J} + \frac{\Delta F \cdot L_1^3 \cdot (\sin(\vartheta_1''))^2}{3 \cdot E \cdot \tilde{J}} + 2 \cdot \frac{\Delta F \cdot L_1 \cdot (\cos(\vartheta_1''))^2}{E \cdot A} + 2 \cdot \frac{\Delta F \cdot L_1 \cdot (\sin(\vartheta_1''))^2}{A \cdot G}$$

Due to geometrical consideration, we neglect the flexural effect along the device and the following kinematic equation is obtained:

$$\delta_{\Delta}'' = 2 \cdot L_1 \cdot \cos(\vartheta_1'') - 2 \cdot L_1 \cdot \cos(\vartheta_{1y,flex})$$

Putting together the last two equations, we obtain, as we seen before, the main equation which describes the problem:

$$\frac{\Delta F \cdot L_1^3 \cdot (\sin(\vartheta_1''))^2}{3 \cdot E \cdot J} + \frac{\Delta F \cdot L_1^3 \cdot (\sin(\vartheta_1''))^2}{3 \cdot E \cdot \tilde{J}} + 2 \cdot \frac{\Delta F \cdot L_1 \cdot (\cos(\vartheta_1''))^2}{E \cdot A} + 2 \cdot \frac{\Delta F \cdot L_1 \cdot (\sin(\vartheta_1''))^2}{A \cdot G} - 2 \cdot L_1 \cdot \cos(\vartheta_1'') + 2 \cdot L_1 \cdot \cos(\vartheta_{1y,flex}) = 0$$

From here, it is possible to calculate the unique unknown ϑ_1'' and then the requested displacement δ_{Δ}'' , using the kinematic equation.

Knowing $\delta_{y,flex}$ and δ_{Δ}'' , it is possible to determine the value of the lengthening of the CSB device for a force higher than the yielding force:

$$\delta'' = \delta_{y,flex} + \delta_{\Delta}''$$

F	ΔF	ϑ''1	ΔM	My	ξ	χ	χy	Jreduced	δ
[kN]	[kN]	[rad]	[kN*cm]	[kN*cm]				[cm^4]	[cm]
17	0	0,18179	0,00	162,90	0,500	0,00092	0,00092	8,870	0,310
18	1	0,18085	9,58	162,90	0,470	0,00098	0,00092	8,822	0,328
19	2	0,1799	19,07	162,90	0,438	0,00105	0,00092	8,671	0,346
20	3	0,17893	28,45	162,90	0,403	0,00114	0,00092	8,404	0,364

21	4	0,17791	37,73	162,90	0,366	0,00126	0,00092	8,003	0,383
22	5	0,1768	46,90	162,90	0,326	0,00141	0,00092	7,440	0,404
23	6	0,1755	55,93	162,90	0,280	0,00164	0,00092	6,669	0,428
24	7	0,17381	64,78	162,90	0,226	0,00203	0,00092	5,608	0,459
25	8	0,17088	73,32	162,90	0,158	0,00291	0,00092	4,062	0,513
26	9	0,16836	81,12	162,90	0,032	0,0144	0,00092	0,849	0,558

Table 5-4 Deformation values of CSB device under post-elastic tensile loads

3) The hardening behavior

It suspends the data analysis calculated with the above analytical formulation as, for an applied load of more than 26 kN, the value of J which represents the reduced moment of inertia of the elastic section, instead of decreasing, tends to increase, manifesting such a contradiction and describe well the hardening behavior of the device.

F	ΔF	ϑ''_1	$J_{reduced}$	δ
[kN]	[kN]	[rad]	[cm ⁴]	[cm]
26	0	0,168364	0,849	0,5576
27	1	0,163694	0,849	0,6394
28	2	0,159384	0,849	0,7129
29	3	0,155391	0,849	0,7792
30	4	0,151679	0,849	0,8394
35	9	0,136371	0,849	1,0723
40	14	0,124858	0,849	1,2312
45	19	0,115791	0,849	1,3466
50	24	0,108411	0,849	1,4341
55	29	0,10225	0,849	1,5028
65	39	0,092569	0,849	1,6026
75	49	0,084972	0,849	1,6740
85	59	0,078985	0,849	1,7259
90	64	0,076409	0,849	1,7471
100	74	0,071898	0,849	1,7825
120	94	0,064747	0,849	1,8343
150	124	0,056966	0,849	1,8845
180	154	0,051283	0,849	1,9170
200	174	0,048239	0,849	1,9331
248	222	0,042505	0,849	1,9607

Table 5-5 Deformation values of CSB device under plastic tensile loads

4) Phase of the Material Hardening

At the end of the phase of the tensile yielding, the process continues with the hardening phase which starts from a previous deformation, neglecting the necking of the section.

Taking advantage of the expression:

$$\Delta\varepsilon' = \frac{\Delta u}{L^*}$$

Where:

Δu = increasing of the displacement;

L^* = linearized length of the entire device.

For each of Δu value, it corresponds:

$$\sigma_y(\varepsilon) = \sigma_y + E \cdot \alpha \cdot \Delta\varepsilon'$$

Where α represents the work hardening factor, in this case set equal to 0.002.

Calculated $\sigma_y(\varepsilon)$, for a given displacement value you can find the corresponding value of force:

$$F(\Delta u) = A \cdot \sigma_y(\varepsilon)$$

δ	$\Delta\delta$	$\Delta\varepsilon'$	$\sigma_y(\varepsilon)$	F
[mm]	[mm]		[kN/mm ²]	[kN]
31	1	0,0094340	40,396	250,861
32	2	0,0188679	40,792	253,321
33	3	0,0283019	41,189	255,782
34	4	0,0377358	41,585	258,242
35	5	0,0471698	41,981	260,703
36	6	0,0566038	42,377	263,163
37	7	0,0660377	42,774	265,624
38	8	0,0754717	43,170	268,085
39	9	0,0849057	43,566	270,545
40	10	0,0943396	43,962	273,006
50	20	0,1886792	47,925	297,611
60	30	0,2830189	51,887	322,217
70	40	0,3773585	55,849	346,823
75	45	0,4245283	57,830	359,125

Table 5-6 The values of the hardening response of a (4.14x1.5 cm) CSB devicce

The total response is plotted in Figure 5.7 showing four phases of different comportment: elastic field, yielding and ductility, hardening then last yielding behavior accompanied with hardening.

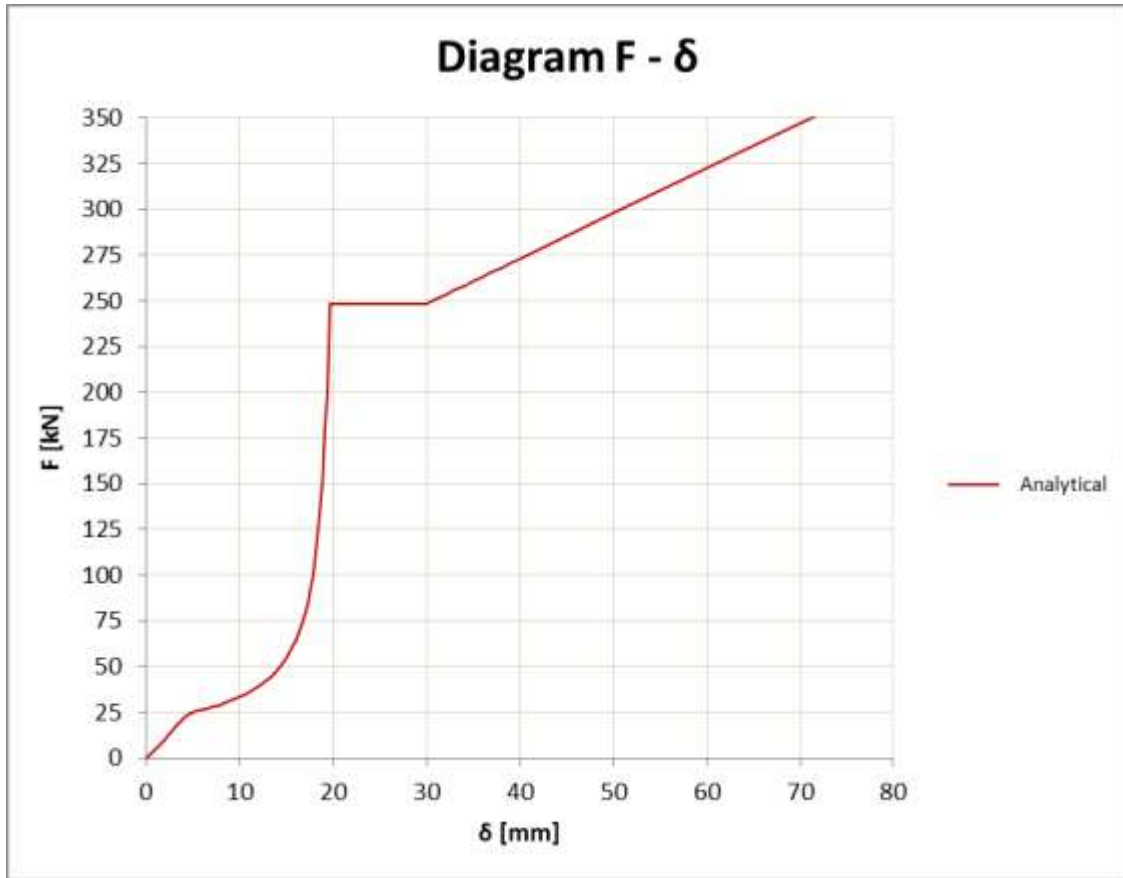


Figure 5.7 Analytical response of a rectangular cross section CSB device under tensile loads

5.6.2. Behavior under Compressive Loads

The simple equations described at the end of the section 5.4 can be used very well in this section, but we preferred to show another way of analysis.

1) Elastic Range

The steel is a material practically with a symmetric constitutive law in traction and in compression. It can be shown schematically, structural purposes, as in Fig. 5.13

Regarding the non-linear response, in case of compression, it is considered the discrete system (elasticity model concentrated) of two rods hinged to each other in the non-

deformable knee point and connected with a rotational spring, characterized by a non-linear constitutive law. [63]

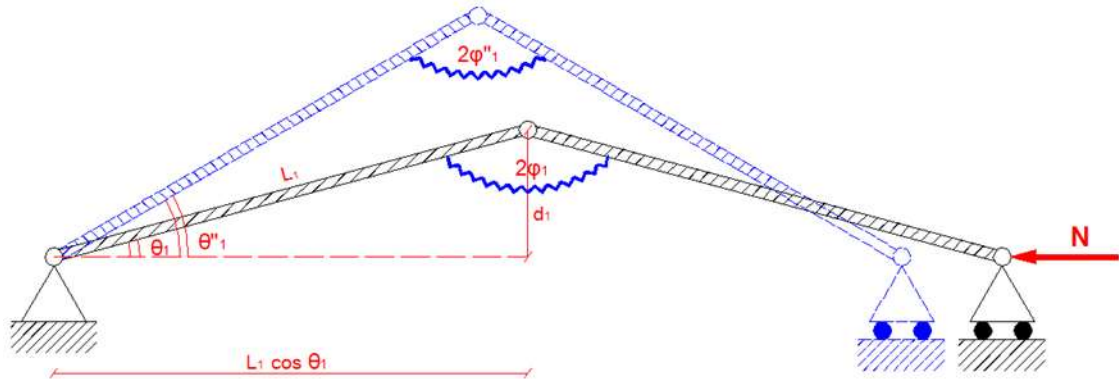


Figure 5.8 The deformation of a CSB device under compression

Based on Merchant-Rankine studies, the intern equilibrium equations presenting the non-mechanical linearity are presented here:

$$\begin{cases} 1) & N = 2 \cdot f_y \cdot b \cdot \bar{y} \\ 2) & M = f_y \cdot b \cdot \left(\frac{h^2}{4} - \bar{y}^2 \right) \end{cases}$$

Where:

\bar{y} = distance between the first plasticized fiber and the neutral axes;

f_y = tensione di snervamento;

b = width of the cross section;

h = height of the cross section.

The external equilibrium is written as follows, describing the non-geometrical linearity:

$$\begin{cases} 3) & N = \frac{4 \cdot K}{L^*} \cdot \left(\frac{\vartheta_1' - \vartheta_1}{\sin(\vartheta_1')} \right) \\ 4) & M = N \cdot \frac{L^*}{2} \cdot \sin(\vartheta_1') \end{cases}$$

Where:

$$K = \frac{3 \cdot E \cdot J}{L^*};$$

ϑ_1' = angle correspondent to the elastic configuration;

ϑ_1 = angle correspondent to the initial phase;

L^* = projected length of the entire device.

Using equations 1), 2) and 4) we obtain 5):

$$5) 2 \cdot f_y \cdot b \cdot \bar{y} \cdot \frac{L^*}{2} \cdot \sin(\vartheta'_1) = f_y \cdot b \cdot \left(\frac{h^2}{4} - \bar{y}^2 \right)$$

Using 3) and 1) we obtain 6:

$$6) 2 \cdot f_y \cdot b \cdot \bar{y} = \frac{4 \cdot K}{L^*} \cdot \left(\frac{\vartheta'_1 - \vartheta_1}{\sin(\vartheta'_1)} \right)$$

And then:

$$7) \bar{y} = \frac{2 \cdot K}{L^* \cdot f_y \cdot b} \cdot \left(\frac{\vartheta'_1 - \vartheta_1}{\sin(\vartheta'_1)} \right)$$

Putting the value of \bar{y} in equation 5) we obtain:

$$\begin{aligned} 2 \cdot f_y \cdot b \cdot \frac{2 \cdot K}{L^* \cdot f_y \cdot b} \cdot \left(\frac{\vartheta'_1 - \vartheta_1}{\sin(\vartheta'_1)} \right) \cdot \frac{L^*}{2} \cdot \sin(\vartheta'_1) \\ = f_y \cdot b \cdot \left(\frac{h^2}{4} - \left(\frac{2 \cdot K}{L^* \cdot f_y \cdot b} \cdot \left(\frac{\vartheta'_1 - \vartheta_1}{\sin(\vartheta'_1)} \right) \right)^2 \right) \end{aligned}$$

$$2 \cdot K \cdot (\vartheta'_1 - \vartheta_1) = f_y \cdot b \cdot \left(\frac{h^2}{4} - \frac{4 \cdot K^2}{L^{*2} \cdot f_y^2 \cdot b^2} \cdot \left(\frac{\vartheta'_1 - \vartheta_1}{\sin(\vartheta'_1)} \right)^2 \right)$$

From the equation above, it is possible to have the value of the unknown angle $\vartheta'_1 = \vartheta_{cr}$. knowing ϑ_{cr} , and using the equation 7), \bar{y} is obtained, as consequence, using equation 3), we obtain $N_{cr} \cong 23 \text{ kN}$.

The plastic moment is obtained assuming $\bar{y} = 0$ in equation 2), where all the fibers of the section are plasticized:

$$M_{pl} = f_y \cdot b \cdot \frac{h^2}{4}$$

In parallel, the axial normal force is obtained assuming $\bar{y} = \frac{h}{2}$ in equation 1) as follows:

$$N_{pl} = 2 \cdot f_y \cdot b \cdot \frac{h}{2}$$

Knowing N_{cr} and N_{pl} , we can use the formula of Merchant-Rankine:

$$\frac{1}{N_{lim}} = \frac{1}{N_{pl}} + \frac{1}{N_{cr}}$$

$$N_{lim} = \frac{N_{pl} \cdot N_{cr}}{N_{pl} + N_{cr}}$$

From this equation, the limit force in the elastic range applied to the device is equal to 20.86 kN.

Once N_{lim} is calculated, the curve force-displacement can be obtained using the following equations:

$$\vartheta_1' = \frac{\frac{4 \cdot K}{L^*}}{\left(\frac{4 \cdot K}{L^*} - N\right)} \cdot \vartheta_1 \quad \text{where } N < N_{lim}$$

$$\delta = 2 \cdot L \cdot \cos(\vartheta_1) - 2 \cdot L \cdot \cos(\vartheta_1') + 2 \cdot \frac{N \cdot L \cdot (\cos(\vartheta_1'))^2}{E \cdot A} \quad \text{Where } N < N_{lim}$$

F [kN]	ϑ_1' [rad]	δ [cm]
0	0,1972967	0
5	0,2022649	0,1084
8	0,2053678	0,1773
12	0,2096562	0,2741
13	0,2107564	0,2992
14	0,2118683	0,3247
15	0,2129919	0,3506
16	0,2141275	0,3768
17	0,2152753	0,4035
18	0,2164354	0,4306
19	0,2176082	0,4582
20	0,2187937	0,4861
20,86	0,2198236	0,5105

Table 5-7 Deformations value of a CSB device under elastic compressive loads

2) Post-Elastic Range

After a certain value of rotation or forces, the knee point starts to enter the plastic field and a moment rises up from the following equation:

$$M = \alpha \cdot M_{pl}$$

Where:

$$\alpha = 1 + \frac{(N_{lim} - N)}{100}$$

The equilibrium of the device reported in Figure 5.8 is verified by the following equation:

$$\alpha \cdot M_{pl} = N \cdot \frac{L^*}{2} \cdot \sin(\vartheta_1'')$$

Knowing M_{pl} , it is possible to calculate ϑ_1'' correspondent to the plastic configuration in function of the applied force N, where $N < N_{lim}$:

$$\vartheta_1'' = \arcsin\left(\frac{\alpha \cdot M_{pl}}{2 \cdot N \cdot L^*}\right)$$

At the end, the displacement is obtained from the following relation:

$$\delta = \delta_{lim} + 2 \cdot L \cdot \cos(\vartheta_{lim}') - 2 \cdot L \cdot \cos(\vartheta_1') + 2 \cdot \frac{N \cdot L \cdot (\cos(\vartheta_1'))^2}{E \cdot A}$$

Where δ_{lim} represents the displacement correspondent to the limit applied force:

F [kN]	ϑ_1' [rad]	δ [cm]
20,86	0,219824	0,5105
20	0,249694	1,2623
19	0,265811	1,6969
18	0,283802	2,2135
17	0,304023	2,8335
16	0,326926	3,5858
15	0,353101	4,5102
14	0,383329	5,6625
13	0,418674	7,1239
12	0,460629	9,0156
11	0,511374	11,5268
10	0,574260	14,9685
9	0,654819	19,8896

Table 5-8 Deformation values of a CSB device under post-elastic compressive loads

The sum of the results obtained by the analytical treatment of the different sections is graphically depicted by the curve in Figure 5.9.

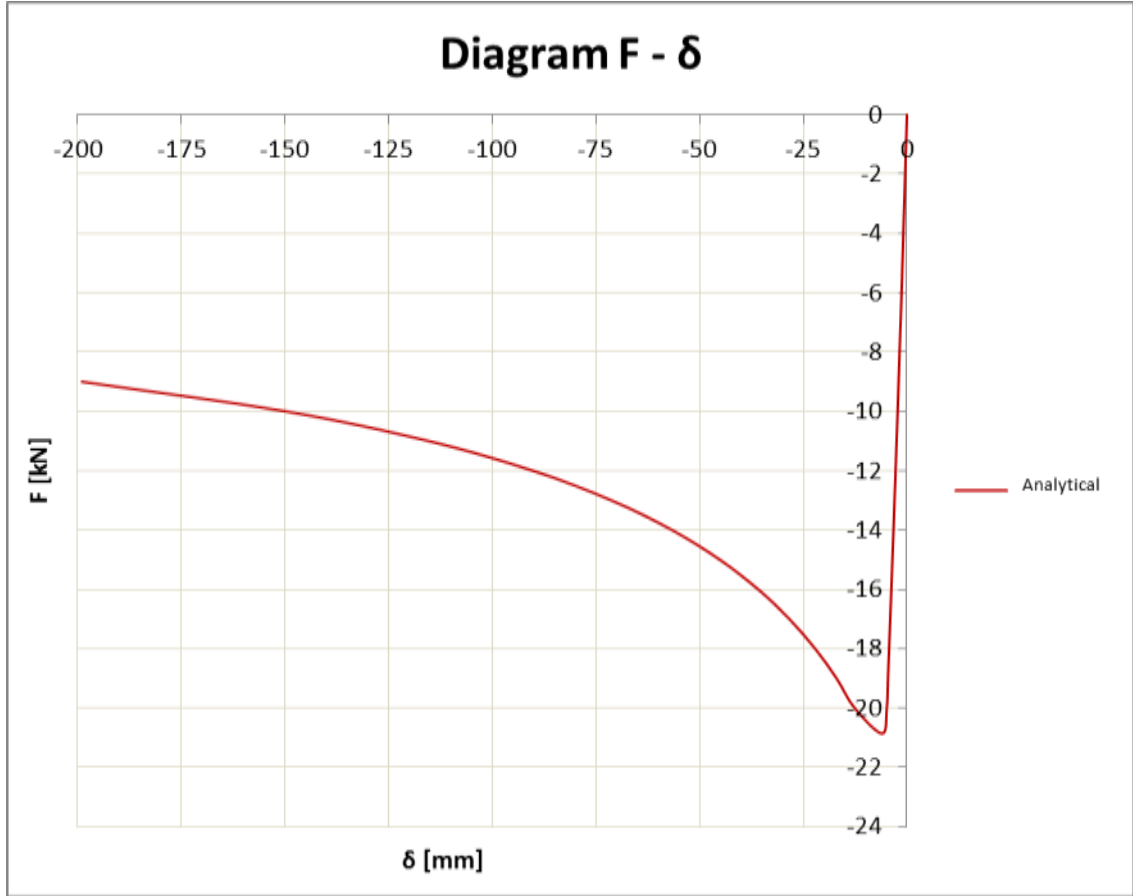


Figure 5.9 Analytical response of a CSB device under compressive loads

5.7. THE DOUBLE CSB EQUATIONS

For the case of the double Crescent Shaped Braces, the composed element, formed of two fixed crescent shaped braces, as seen in the Figure 5.10 , has bigger stiffness than the single element.

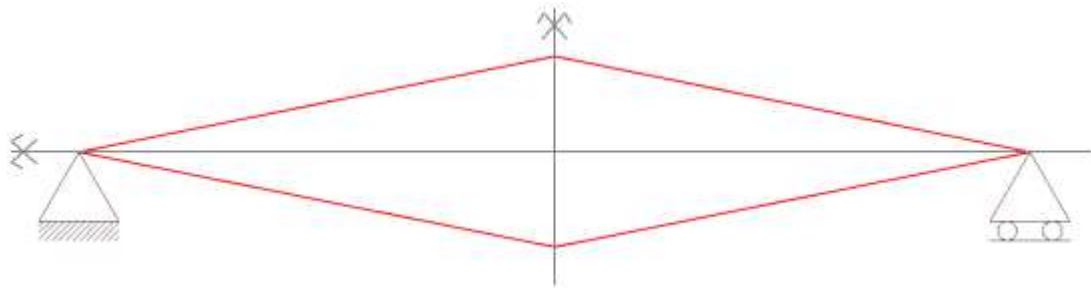


Figure 5.10 Double CSB devices inserted together

Considering now for one element and $d \geq 0.1L$, thus the axial deformations are negligible:

$$\delta = \delta_N + \delta_M = 0 + \int_0^{L^*} \frac{F \cdot \sin\theta \cdot x}{E \cdot J} \cdot x \cdot (\sin\theta) dx$$

$$\delta = \frac{F \cdot \sin^2 \theta}{E \cdot J} \int_0^{L^*} x^2 dx$$

Where L^* is equal to $l/2$.

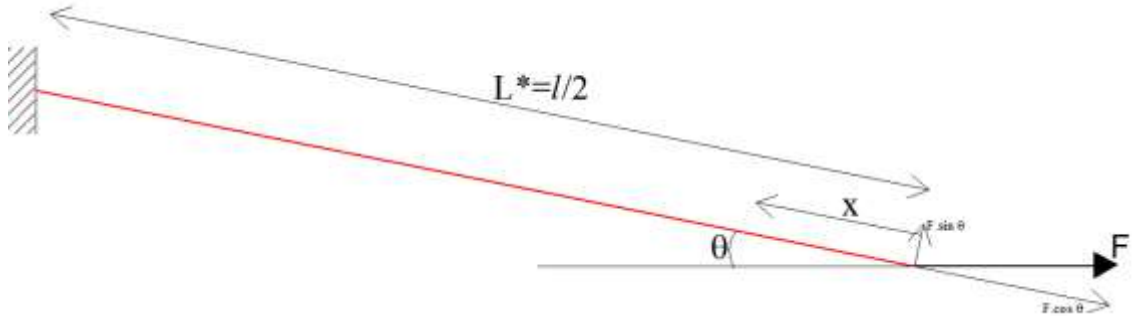


Figure 5.11 The force acting on one half of one CSB device from a double disposition

Thus, δ for one element of the double device, assuming a force of value F is acting on each CSB device, is equal to:

$$\delta = \frac{F \cdot \sin^2 \theta \cdot L^{*3}}{3 \cdot E \cdot J}$$

And due to the symmetry of the two CSB elements, F will be multiplied by 2, and the final result of K_{L0} is four times bigger than the single CSB K_{L0} :

$$K_{L0} = \frac{12}{2} \frac{EJ}{L^{*3} \sin^2 \theta_0}$$

And for the whole double device, the stiffness will be 8 times bigger, and the total displacement will be less by the double and the strength higher by four times.

For a double CSB device, where the cross section is the same of the single CSB studied before, a fully circular cross section ($r= 1.75\text{cm}$ and $L=110\text{cm}$, steel S275), the stiffness is 134 kN/cm for one element of the double device which means 270 kN/cm for the whole device.

5.8. CONCLUSIONS

An analytical description of the crescent shaped brace was presented in this chapter. First, geometrical and mechanical characteristics of the element were detailed. It was clear that such element can be symmetrical or no. even so, our studies were oriented

toward the symmetric device. Thus, equilibrium equations describing the forces acting upon the device were developed, other than its behavior described both in elastic and post elastic fields.

From the equations of yielding force and stiffness, it is evident that the CSBs are characterized by a lateral stiffness uncoupled from the yield strength and by an overall symmetric hysteretic behavior with a hardening response at large drifts (due to non-linear geometrical effects) which may prevent from global structural instability due to second-order effects (such as P- Δ effects). The overall behavior is correspondent to the required idea idealized in previous chapter to be implemented in new device which is the CSB.

Those equations were applied to a clear example of the rectangular section and its behavior is totally plotted, under tensile and compressive forces, in elastic and post elastic zones. It is worth to say that the graphs were as expected to be.

Exploiting some symmetrical benefits, the idea of inserting double crescent shaped braces was developed analytically, and it was clear that the stiffness of the ensemble its four times higher than the single one, or in another way, putting two crescent shaped braces separately will have the half stiffness of putting them together as described in section 5.7.

•

6. Behavior of CSB: Numerical Simulation

6.1. INTRODUCTION

This chapter analyzes the behavior of CSBs under both monotonic (in tension and compression) and cyclic reversed increasing loadings with the specific purpose of providing useful information related to the seismic design of such systems. Without loss of generality, the results presented here are referred to the case of the symmetric bilinear configuration (Figure 5.1).

First, the main features of the force-displacement behavior are discussed in section 6.2 and section 6.3. Then the following specific aspects, which can be of interest for the practitioners, are investigated:

- the influence of the section profile (section 6.4);
- the influence of the geometrical configuration (section 6.5);
- the influence of the double CSB (section 6.6);
- the material behavior (6.5).

The constitutive law of the crescent shaped brace is controlled by the configuration of the device (angle of force with respect to the line connecting the device's both extremities), the device's geometry (lever arm, diagonal length, etc...), and the section characteristics (hardening ratio, yielding strength, stiffness, etc...).

The post-yielding behavior of CSBs has been studied through extensive numerical analyses carried out on fully non-linear finite element models developed using the research software SeismoStruct v7. Each straight member is modeled with a single beam element using the force-based formulation. Material non linearity is accounted using the Menegotto-Pinto law with the isotropic hardening behavior for its ability to model the experimental hysteretic behavior of the steel.

Menegotto-Pinto Model:

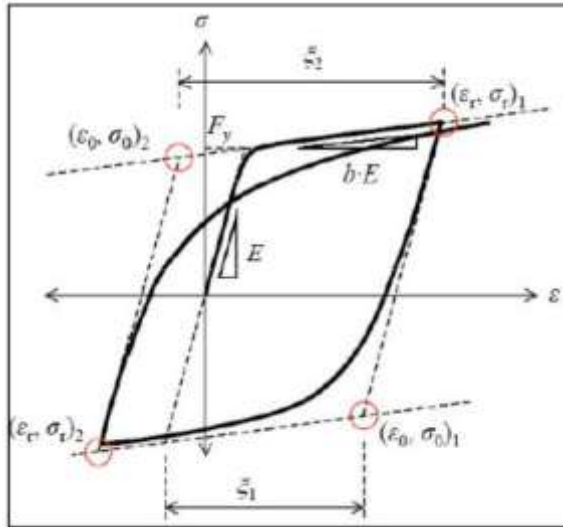


Figure 6.1 The Menegotto-Pinto Model

The Menegotto-Pinto model is an evolution of the model proposed by Giuffrè and Pinto (1970).

The general Menegotto-Pinto law is written as follows:

$$\sigma^* = b \cdot \varepsilon^* + \frac{(1-b) \cdot \varepsilon^*}{(1 + \varepsilon^{*R})^{1/R}}$$

With:

$$\varepsilon^* = \frac{\varepsilon - \varepsilon_r}{\varepsilon_0 - \varepsilon_r}$$

$$\sigma^* = \frac{\sigma - \sigma_r}{\sigma_0 - \sigma_r}$$

$$R = R_0 - \frac{a_1 \cdot \xi}{a_2 + \xi}$$

Where:

σ is the normal Stress;

ε is the axial deformation;

$(\varepsilon_0, \sigma_0)$ are the stress and the strain at the point where the initial tangent and the asymptotes of the curve meet;

B is the hardening ratio;

R_0, a_1, a_2 are constants equal, respectively, to 20.0, 18.5, and 0.15;

ξ is the difference between the maximum value of the deformation in the direction of the load and ε_0 ; [21]

6.2. BEHAVIOUR UNDER TENSILE LOADS

The behavior of CSB under tension loading is firstly studied. The isotropic hardening parameter was set equal to 0.005. The section profile has been chosen to be fully rectangular cross section with dimensions (4.14*1.5cm).

The system is subjected to an increasing horizontal force F up to the complete elongation condition. Figure 6.2 displays the response of force versus horizontal displacement.

Due to the special geometrical shape of the CSB, the device is able to resist the elongation through its axial as well as its moment capacity at the knee point G, unlike the conventional braces that resist through their axial stiffness only.

Referring to Figure 6.2, it is possible to identify five different regions of behavior:

Region A: The response of the system in the elastic field. The behavior is mostly flexural.

Region B: The bending moment at knee section reaches the yielding strength F_y and the axial force slightly increases up to 0.2 Np.

Region C: The axial force significantly increases. The behavior is both flexural and axial.

Region D: The axial force rapidly increases up to the axial capacity Np. The behavior is mainly axial with the hardening behavior presented.

Region E: The axial force is constant and equal to the axial capacity Np. The system behaves as a straight bar under tension.

When the normalized arm reaches zero, the system will continue resisting through its axial capacity only, like a conventional brace or a truss in tensile configuration.

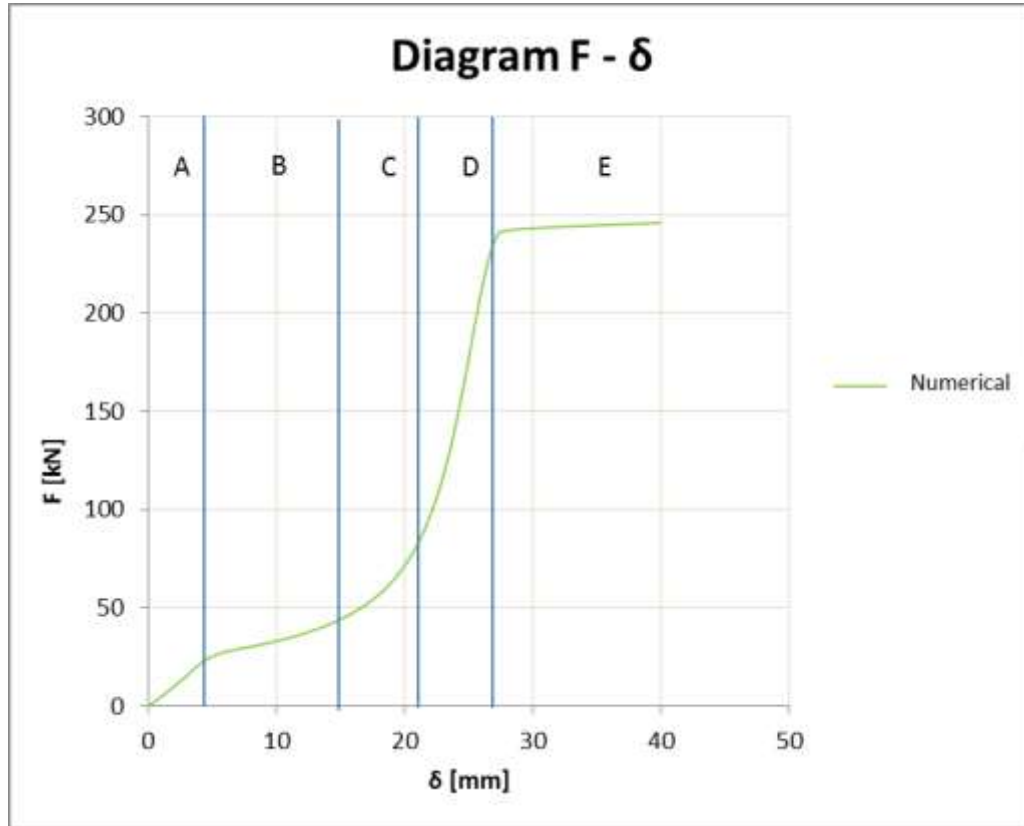


Figure 6.2 Force-Displacement curve of a rectangular cross section CSB under tensile loads

For the studied case, a fully rectangular cross section (4.14*1.5 cm) CSB device with $L=104$ cm, and $d=0.1 L$, the yielding point corresponds to a value equal to 19 kN and displacement of around 4 mm, with a linear stiffness equal to around 50 kN/cm.

6.3. BEHAVIOUR UNDER COMPRESSIVE LOADS

Similarly, the device has been tested under compressive monotonic force while keeping the same geometrical configuration and section profile. Both mechanical and geometrical nonlinearities are included in the analysis. Figure 9 displays the response of compression force versus horizontal displacement.

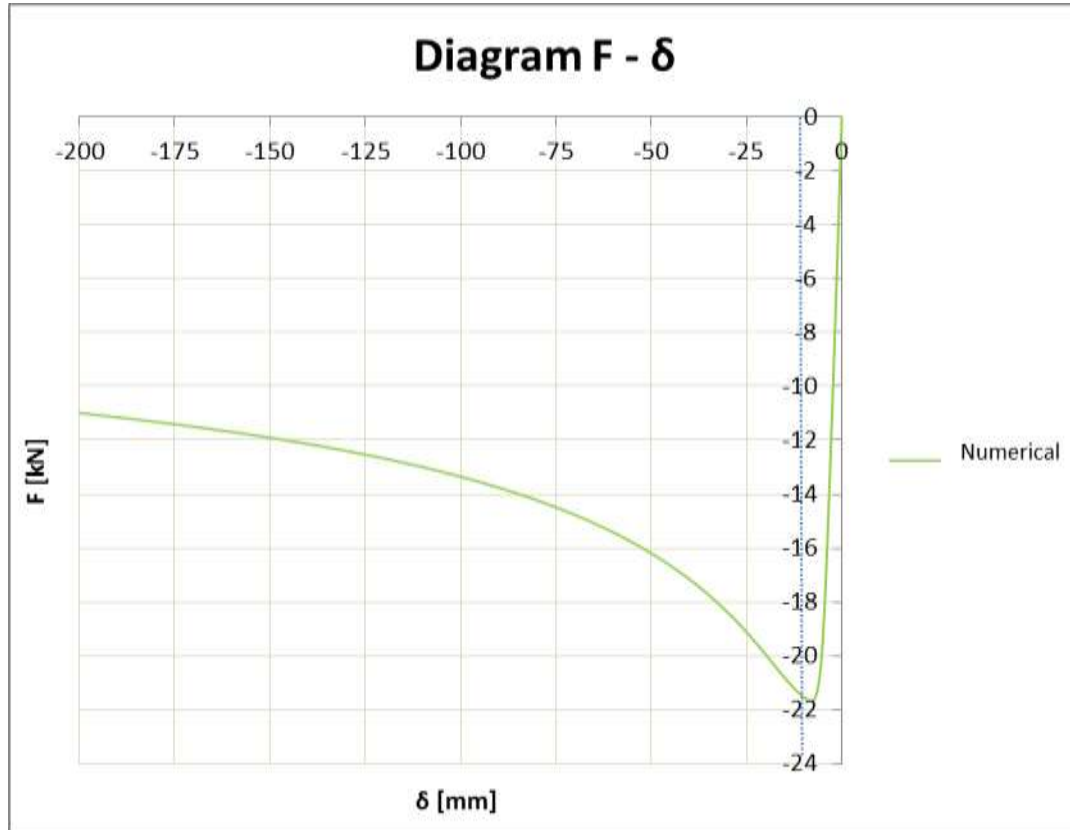


Figure 6.3 Force-Displacement curve of a rectangular CSB under compressive loads

It is possible to divide the obtained behavior curve into two different parts:

The first one to the right of the dotted blue line is the elastic part. The left part is the post elastic part which is characterized by a softening behavior and a large value of displacement. From theoretical point of view, the maximum displacement which can be reached by the device under compressive loads is $\delta=L$, until one end touches the other end.

The yielding force is around 22 kN with a displacement of around 4.5 mm. The stiffness is almost equal to 50 kN/cm. Those values are compatible with the values obtained in the elastic part of the response curve under tensile loads due to the symmetry of the elastic behavior under tensile and compressive loads of the steel.

6.4. INFLUENCE OF THE CROSS SECTION

As in the previous sections, the system will be subjected to an increasing horizontal force F up to the complete elongation condition. Figure 6.4 and Figure 6.5 display the response of force versus horizontal displacement for all section profiles.

The choice of the cross section (keeping the same geometrical parameters of the CSB device: L and d) has an impact of course on the elastic behavior of the Crescent-Shaped Brace.

Using numerical simulations, different cross-sections are tested in order to identify the influence of the change of the cross section profile on the system behavior. The profiles may be classified based on the i/h ratio.

In order to have a comparable results, all sections are set to have the same inertia J as well as the same section depth h . the lever arm ratio $\xi=d/L$ is set equal to 0.1 for all analyses. The steel yield strength has been assumed equal to 355 MPa (S355), while the hardening ratio $r=0.005$. The mechanical parameters of the section profiles are listed in Table 6-1.

Profile	Full circular	Full rectangular	Tubular circular	Tubular rectangular	HE200 B
$J(cm^4)$	5696	5696	5696	5696	5696
H or $D(cm)$	18.46	20.00	20.00	20.00	20.00
$A(cm^2)$	267.54	170.88	149.03	77.44	65.30
A/A_{HE200B}	4.10	2.62	2.28	1.19	1.00
β	1.70	1.50	1.27	1.25	1.14
β/β_{HE200B}	1.49	1.32	1.11	1.10	1.00
i/h	0.25	0.29	0.31	0.43	0.47
$M_p(kN.m)$	372.50	303.31	256.27	252.76	225.46
$M_p/M_{p_{HE200B}}$	1.65	1.35	1.14	1.12	1.00
$N_p(kN)$	9497.70	6066.24	5290.54	2749.22	2318.15
$(M_p/h)/N_p * 100$	0.21	0.25	0.24	0.46	0.49
$F_y(kN)$	351.67	319.28	316.21	300.21	294.24

Table 6-1 Geometrical and mechanical properties of the studied profiles

Figure 6.4 represents the behavior under tensile loads while Figure 6.5 represents the behavior of the same profiles under compressive loads.

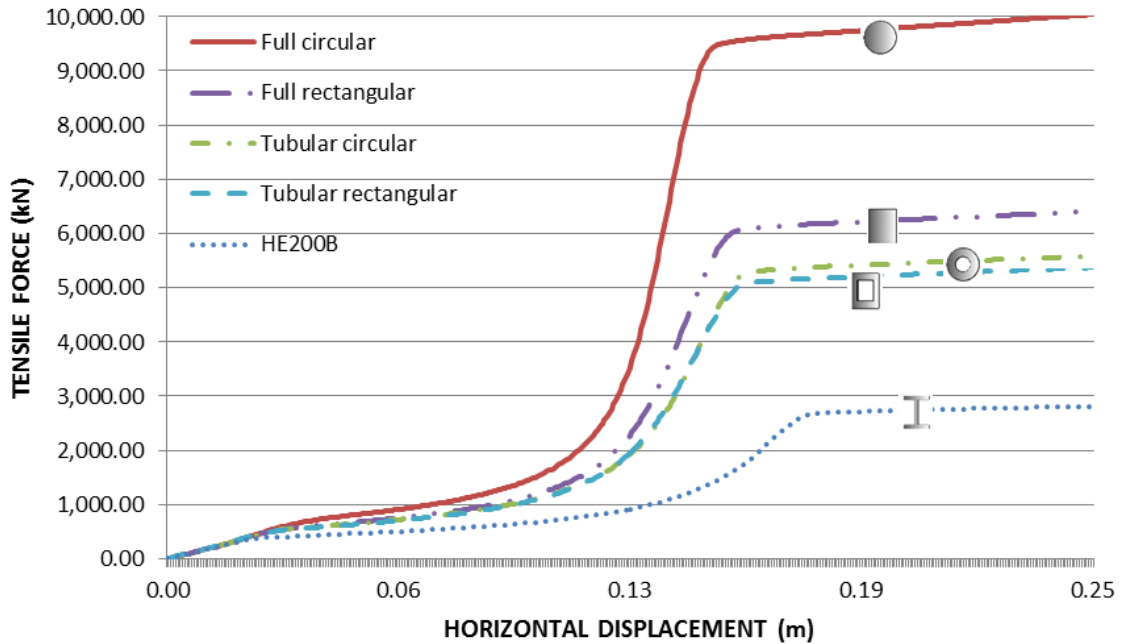


Figure 6.4 The tensile response of different cross section CSBs

An assessment of Figure 6.1 and Table 6.1 allows noticing that all profiles undergo the same qualitative post-yielding response. In detail:

Qualitatively, all profiles are characterized by the same elastic behavior and stiffness.

Qualitatively, all profiles are characterized, under tensile loads, by almost the same ductility capacity (3/3.5).

The strength between yielding (PO-2) and substantial hardening (PO-3) is proportional to the plastic benefit of the cross-section β .

The HE profile exhibits a limited hardening behavior with respect to those showed by the other profiles, whilst the full circular profile exhibits the largest hardening behavior. The two tubular profiles exhibit a quite similar hardening behavior. The full rectangular profile shows a response similar to that of the tubular profiles with a slightly larger global hardening.

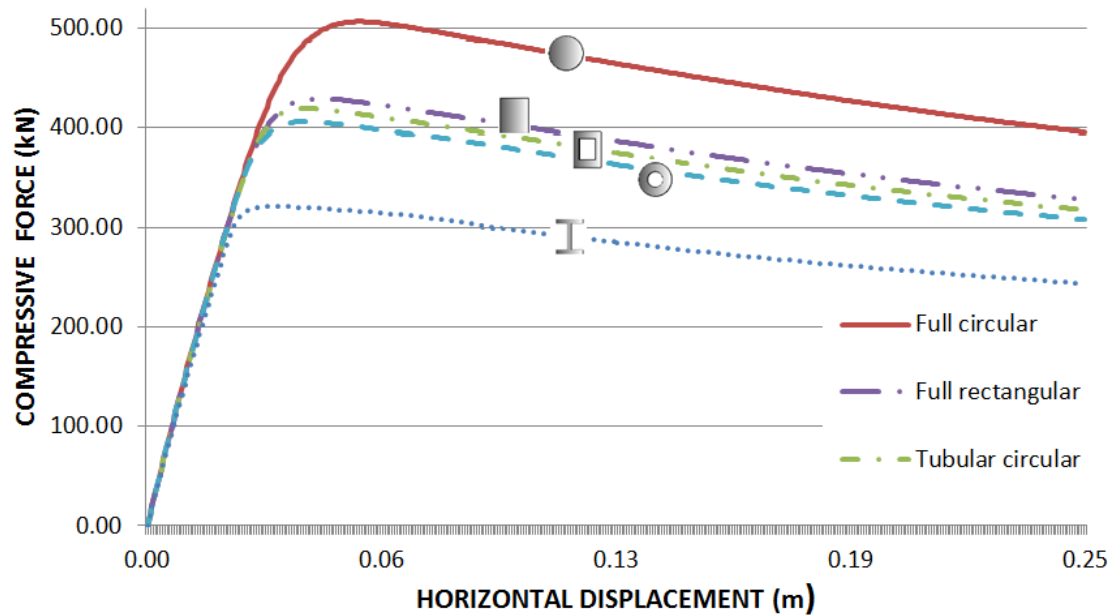


Figure 6.5 The compressive response of different cross section CSBs

The five section profiles have been studied under monotonic compressive forces. Figure 6.5 shows the results of the static pushover analysis of all sections. As in the tension test, the full circular section is the most resisting one, while HE200B is the first one to reach yielding point. The three other profiles, respectively, full rectangular, tubular circular and tubular rectangular show similar elastic and post yielding behavior. All of the tested profiles exhibit softening behavior due to the geometrical non-linear effects and a big ductility capacity almost equal to 5.

6.5. INFLUENCE OF THE COUPLED CSB

One of the important aspects is to figure out the best configuration of the device. There are plenty of configurations but not all of them are equally effective. Bracings transform lateral forces from earthquakes and wind into axial forces in the columns, and this force is not to be neglected. The best solution within the engineering spirit is to find the configuration that minimizes the amount of forces transmitted.

Another issue lies in the modeling of the device. The crescent shaped brace behaves differently in tension and compression, and for this reason when two CSBs are coupled together, one in front of the other as in Figure 6.6, their behavior will not be the same. This is due to the fact that when the first is working in tension, the other will be

working in compression, so each of the two braces will produce different reaction under the same displacement, and thus the axial force transmitted to the adjacent columns will be different.

Summing the CSB response subjected to traction with that of the one subjected to compression, the force-displacement diagram shown in Figure 6.7 is obtained. By that, it might be better to get the objective force-displacement curve of the system resistant to the horizontal actions (HRS), which allows the structure to meet the predetermined seismic performance targets.

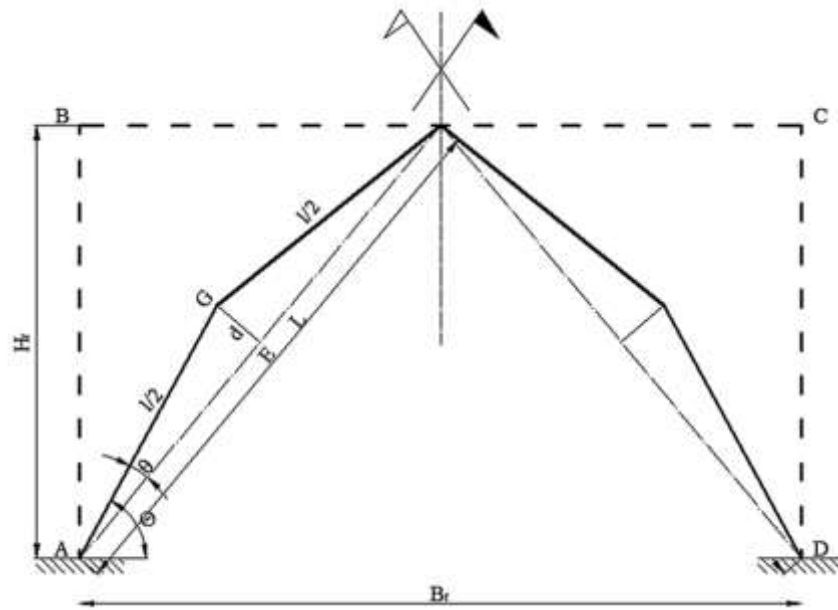


Figure 6.6 A couple CSBs inserted in a generic frame

Due to the symmetry in the elastic part of the compressive and tensile response, the sum of the two curves will double the response in the elastic field, but the effect in the post-yielding part is a little bit limited regarding the ductility or the hardening part, because the major part of the total ductility and hardening responses go back to the tensile response and not to the compressive one which is characterized by a softening behavior after yielding point.

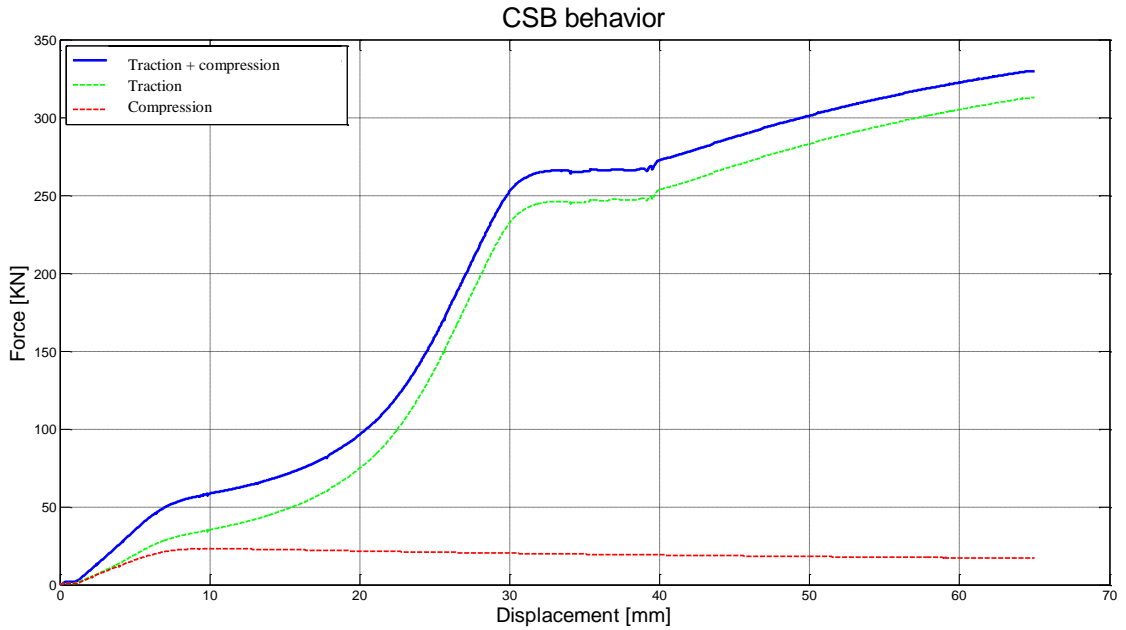


Figure 6.7 The behavior force-displacement of coupled CSBs inserted in a generic frame

6.6. INFLUENCE OF THE DOUBLE CSB

As we have seen in the analytical part, taking advantages of the symmetrical properties of double CSB devices, the stiffness increases and the response of the composed element becomes more resistant. The studied cross section is a fully circular cross section with radius 1.75 cm, $L=110$ cm and $d=0.1 L$, Steel S275.

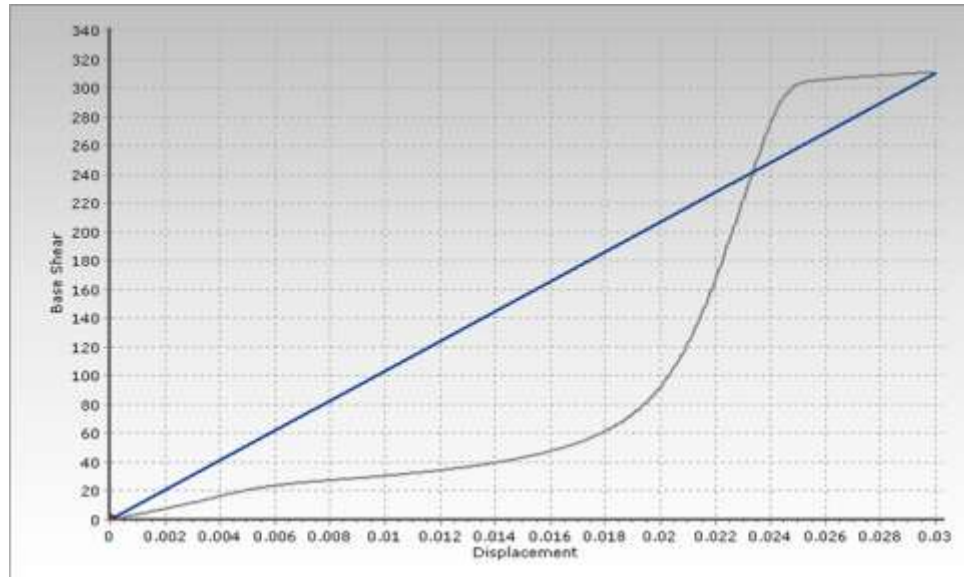


Figure 6.8 The Force(kN)-Displacement(m) curve (grey) of a single circular cross section CSB under tensile loads

As we can see from Figure 6.8, the response of a single circular cross section CSB, is composed of five sections, as the rectangular one in section 6.2. Here, the yielding force is around 19 kN, the correspondent displacement is around 0.0052 m, which means a stiffness of around 36 kN/cm.

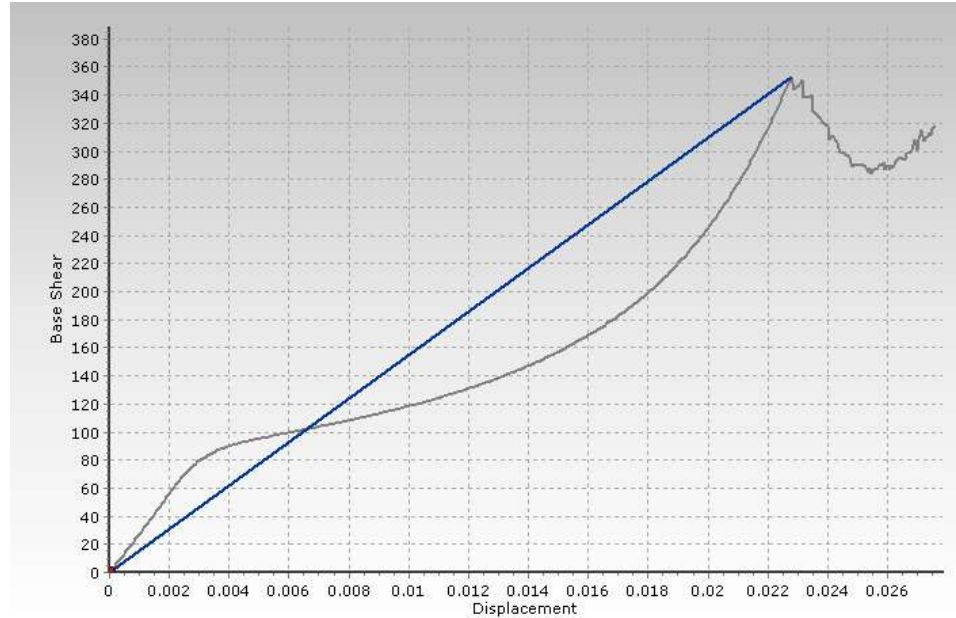


Figure 6.9 The Force-Displacement curve (grey) of a double circular cross section CSB under tensile loads

From Figure 6.9, the response of a double circular cross section CSB has almost the same behavior of the single CSB device with a difference in the last axial response. Anyway, regarding the elastic part, the yielding force is around 79 kN, the correspondent displacement is around 0.0028 m, which means a stiffness of around 282 kN/cm.

It is possible to remark that the stiffness of the double CSB is 8 times bigger than the one of the single device: $K_{D,CSB}=8*K_{S,CSB}=8*36=288kN/cm$

The yielding force of the double one is almost four times bigger than the yielding force of the single one: $F_{y,D}=4*F_{y,S}=4*19=76 kN$

And the displacement, as a consequence, in the case of the double CSB will be the half of the displacement in the case of the single one:

$$\delta_{y,D}=0.5*\delta_{y,S}=0.5*0.0052=0.0026 m$$

Regarding the post-yielding part, the ductility of the single device is around 5, while it is around 8 times for the case of the double CSB.

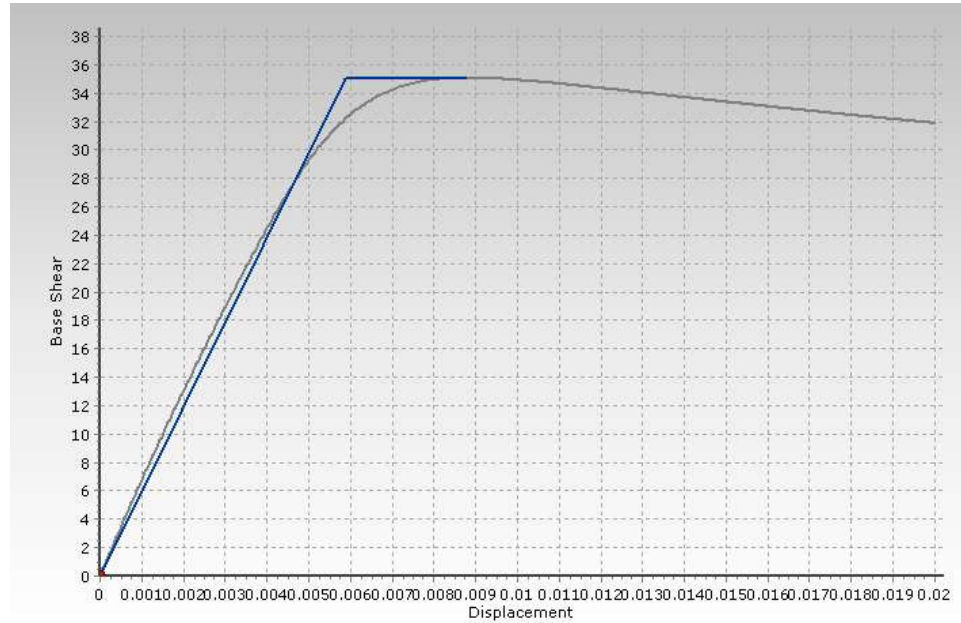


Figure 6.10 The Force(kN)-Displacement(m) curve (grey) of a single circular cross section CSB under compressive loads

Regarding the behavior of the same studied case under compressive loads, the yielding force is about 28 kN with a stiffness equal to 58 kN/cm.

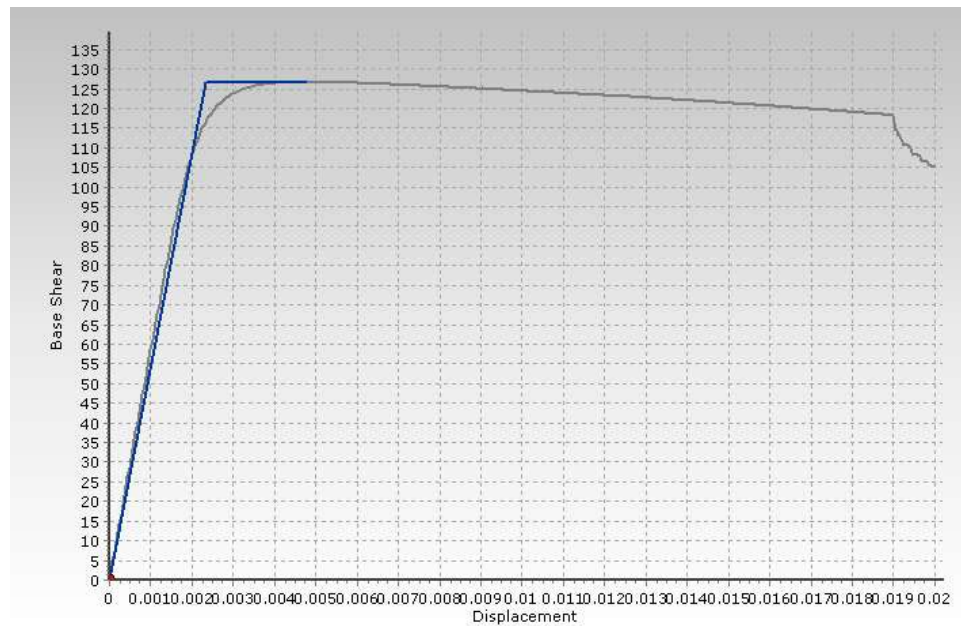


Figure 6.11 The Force(kN)-Displacement(m) curve (grey) of a double circular cross section CSB under compressive loads

While for the case of a double CSB, the yielding force is about 112 kN with a stiffness equal to 560 kN/cm. This value is around 10 times bigger than the case of the single

CSB. The ductility is also around 10 which is bigger than the ductility for the case of the single CSB which is around 5.

6.7. THE MATERIAL BEHAVIOR

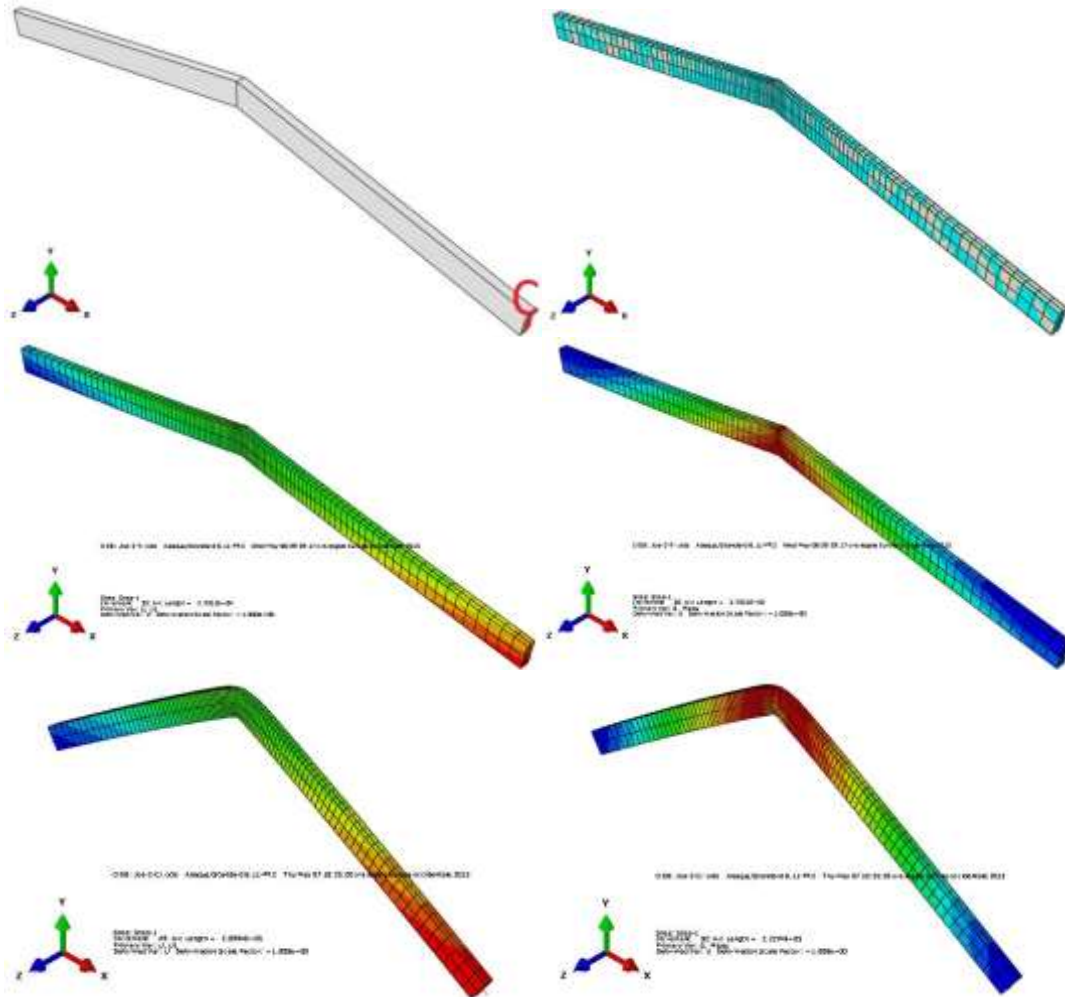


Figure 6.12 The material response under cyclic loading (ABAQUS)

To check the response of the material via numerical models, we used ABAQUS software, which by means of elements Brick type, allows a three-dimensional study of the most accurate device. The section studied is a rectangular section S275 of dimensions 4.14*1.5 cm.

Such modeling makes a real modeling of the device, in the sense that it does not make a device linearization, but rather it will discretize the same one in three-dimensional finite element.

The creation of the model with Brick elements follows the usual steps used in every numerical model; choosing material behavior, material, section, forces...

Figure 6.12 shows the deformed configuration of the device, by displaying a profile color map that shows the trend of the displacements along the direction X of the device. In particular, the red color refers to the maximum displacements while the blue one refers to the smaller displacements. It is clear that the more stressed zone of the device is the knee zone, both under the maximum tensile loads and the maximum compressive loads. The before last figure shows how the energy starts to dissipate along the device to reach the knee zone under maximum compressive loads. This is the extremity where the device is loaded. Instead, the opposite extremity is always colored by blue because extremities should be the most relaxed zones in this device, and the knee zone is the most stressed as it is clear.

6.8. CONCLUSIONS

In this section, the behavior of different section profiles CSB under monotonic (in tension, compression and reversed cyclic) loading is studied, assuming the Menegotto-Pinto material behavior.

Many important results can be extracted from this numerical analysis:

Inspection of Figure 6.2 allows identifying the following “regions” of behavior:

- Region A ($0.095 < d/L < 0.10$): the response of the system is in the elastic field. The behavior is mainly flexural, the lateral stiffness and yield strength are analytically provided by elastic equations.
- Region B ($0.07 < d/L < 0.095$): the bending moment at knee section reaches the plastic moment M_p and remains constant. The axial force slightly increases up to $0.2 N_p$

- Region C ($0.02 < d/L < 0.07$): the bending moment at knee section decreases while the axial force significantly increases. The behavior is both flexural and axial. The behavior is still mainly flexural.
- Region D ($0 < d/L < 0.02$): the bending moment at the knee section rapidly decreases up to vanish, while the axial force rapidly increases up to the axial capacity N_p .
- Region E ($d/L = 0$): the axial force is constant and equal to the axial capacity N . The behavior is mainly axial.

It is worth recalling here that, from a design point of view and with reference to the Performance Objectives reported in the idealized “objective curve” of Figure 3.2, the transition between Regions A and B corresponds to point PO-2, the transition between Regions B and C should correspond to point PO-3, and point PO-4 should fall in Region C or D before the transition between Regions D and E.

In the part referring to the effect of the cross section, in the tension test, the full circular section resists the most, while HE200B is the first one to reach the yielding point. The 3 other profiles, respectively, full rectangular, tubular circular, and tubular rectangular show similar pre and post yielding behavior. All of the tested profiles exhibit softening behavior under compressive loads due to the geometrical non-linear effects.

Two different dispositions of the Crescent Shaped Braces have been studied, the coupled CSBs and the Double CSBs.

Regarding the first disposition, it is possible to say that the total response of a coupled CSBs inserted in a generic frame is improve especially in the elastic part where the stiffness is increased to the double. The effect of the compressive device is limited on the post-yielding part.

Regarding the second disposition, the double CSBs, the behavior is enhanced clearly. The stiffness is increased around eight times for the elastic phase, both under tensile and compressive loads. The yielding force is increased four times which means as consequence a decrease of the correspondent displacement to the half. The ductility as well is increased both under tensile and compressive loads. Thus, if double CSBs are coupled in a generic frame, the stiffness of the composed devices (four single CSBs)

will be sixteen times the stiffness of one single CSB element and the ductility will increase as well.

The last phenomenon studied in this section was the behavior of the material and the diffusion of stresses along the device while it was tested under tensile and compressive loads. As it was expected, the most stressed zone is the knee zone, both under tensile and under compressive loads. The last stressed zones are the two extremities of the device. To pay attention that under tensile loads, the most stressed part of the knee zone is the down part, while under compressive loads the upper part was the most stressed and this result verify what it was expected.

7. Behavior of CSB: Experimental Tests

7.1. DESCRIPTION OF THE EXPERIMENTAL TESTS

Intending to assess the non-linear cyclic behavior of crescent shaped braces, an experimental campaign has been carried out between 2014 and 2016 at the Structural Engineering and Geotechnical Laboratory (LISG) of the University of Bologna. A total of thirteen 1/10-scale tests were performed: three tests were performed on fully rectangular cross section, three on fully circular cross section; three tests were performed on welded fully rectangular cross section without ribs, two on fully rectangular cross section with ribs and the other two on tubular cross section. Each specimen underwent cyclic load (tensile, compressive or reversed) and the obtained force displacement curves were studied in order to understand some seismic characteristics like energy dissipation, deformation zones, ductility and hardening behavior. This chapter contains a full description of the experimental results and tests. [8]

7.1.1. Geometrical and mechanical properties of the specimens

Thirteen scaled CSB specimens have been tested. All the specimens are characterized by a symmetric bilinear geometrical configuration with a normalized lever arm $d=0.1L$ and scaling factors set to be representative of a device inserted in a frame having dimensions of 6 x 3 m (diagonal length of about 7 m), in that way, they are consistent with the numerical and analytical simulations developed in previous chapters. In each end of the two extremities of the CSB device, there is a connection plate with a central hole (nominal diameter of 32 mm) with a main function of connecting the device to the testing machine. The specimens have been produced using different manufacturing processes, depending on the exigency of each specimen and on the possible available techniques: (i) The technique of laser-cutting of one element from a flat steel plate of uniform thickness was used for rectangular cross section specimens; (ii) welding together two straight segments at the knee section was the technique used for the

tubular cross section specimens; (iii) welding two straight elements (cut by laser) to the V-shaped knee element, so in total three components compose the device was used for the welded rectangular cross section specimens; (ii) The technique of bending with a spindle an initial straight element having a length equal to the length of the two straight segments was the only available solution to prepare the circular cross-section specimens. Due to the standard commercial cross section and the straight circular bar, this solution was the most logical one, even if the knee zone is suggested to stresses before the test. In more details, the following cross-sections were utilized: (i) fully rectangular (symbol R) with a height-to-width ratio equal to 3; (ii) fully circular (symbol C); (iii) fully rectangular welded in the middle of each straight part of the device; (iv) fully rectangular with central stiffening ribs (symbol RR) and (v) tubular circular (symbol T). Some specimens were tested under monotonic cyclic loadings (tension, T, or compression, C), while others were tested under cyclic reserved loadings (R). In one case, after imposing a cyclic loading history in compression the specimen has been subjected to a final monotonic loading in tension (C+T) up to the failure.

Structural steel S275JR (with nominal characteristic yielding stress $f_{yk} = 275 \text{ MPa}$ and characteristic ultimate stress $f_{uk} = 410-560 \text{ MPa}$, according to EN 10025-2 2004) has been used for all specimens. Tests on small steel specimens have been carried out to evaluate the actual material properties. The actual yield stress varied between 300 MPa and 400 MPa.

Table 7-1 identifies all the tested specimens summarizing their main geometrical properties, the protocol under which they have been tested and the manufacturing technique. For instance, R1-T indicates a full rectangular cross-section which has been tested under cyclic loadings in tension. Figure 7.1, Figure 7.2 and Figure 7.6 shows all specimens before testing. [25], [26], [27], [29], [55], [56], [57],

Name	Cross Section	Manufacturing	Protocol	a(mm)	A(mm ²)	J(mm ⁴)	L(mm)	ξ
R1-T	Full Rectangular	Laser-Cut	Tensile	41.4	621	88700	1040	0.1
R2-C	Full Rectangular	Laser-Cut	Compression	42.8	672	88700	1040	0.1
R3-R	Full Rectangular	Laser-Cut	Reversed	42.5	672	88700	1040	0.1
RW1-	Full	Laser-Cut and	Reversed	41.4	623	88700	1040	0.1

C+T	Rectangular	welded at the middle of each straight segment						
RW2-R	Full Rectangular	Laser-Cut and welded at the middle of each straight segment	Reversed	41.5	630	88700	1040	0.1
RW3-R	Full Rectangular	Laser-Cut and welded at the middle of each straight segment	Reversed	42	630	88700	1040	0.1
RR1-R	Full Rectangular with Ribs	Laser-Cut and welded ribs	Reversed	41.5	770	89200	1040	0.1
RR2-R	Full Rectangular with Ribs	Laser-Cut and welded ribs	Reversed	41.5	770	89200	1040	0.1
C1-T	Full Circular	Bent	Tensile	35	962	73625	980	0.1
C2-C	Full Circular	Bent	Compression	35	962	73625	980	0.1
C3-R	Full Circular	Bent	Reversed	35	962	73625	980	0.1
TW1-R	Tubular Circular	Welded at the Knee section	Reversed	42	333	37804	1060	0.1
TW2-R	Tubular Circular	Welded at the Knee section	Reversed	42	333	37804	1060	0.1

Table 7-1 Geometrical properties of the studied specimens

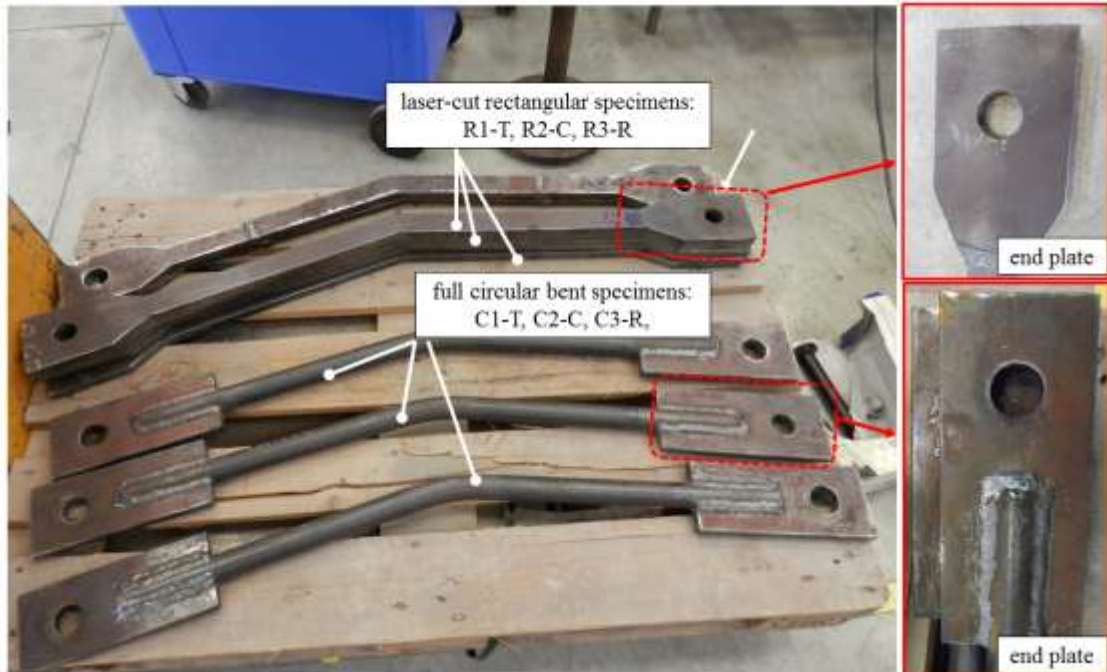


Figure 7.1 Six Specimens (rectangular and circular cross section) before testing with ends details

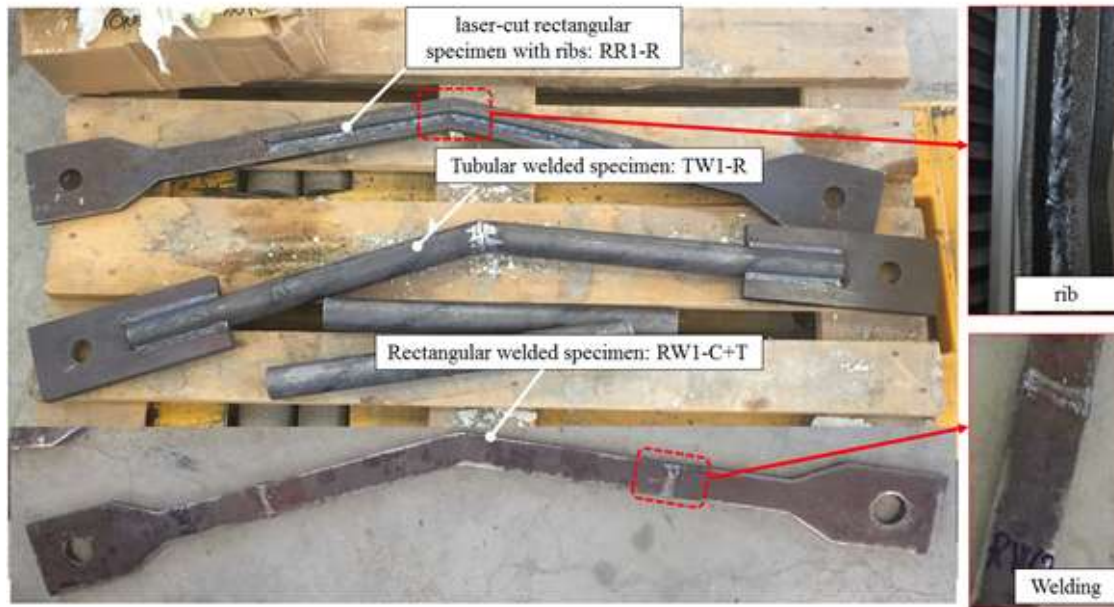


Figure 7.2 RW1R, RR1R, TW1R before testing with welding details

7.1.2. Test set-up and protocols

1. Test set-up and machine

The monotonic and reversed cyclic pseudo-static tests were performed using a universal traction machine realized by METRO COM (company based in Novara, specializing in the construction of equipment for laboratories, both electromechanical and electrohydraulic Figure 7.3). Specifically, the machine at the university laboratories has a maximum rated capacity of 600 kN. The machine has a steel structure; it is equipped with a lower fixed base and a movable upper head driven by an oil-dynamic piston. This piston enters in pressure when a hydraulic fluid reaches it by a pump driven by an electric motor. To fix the device into this machine, two U-shaped box connectors aligned along the vertical direction are presented. The specimen is inserted between those two boxes through $\varnothing 30$ mm high strength bolts, so that rotations are permitted (pinned connections). The loads/displacements are applied to the top U-shaped box by mean of a hydraulic actuator (displacement increments of 2 mm/min – 5 mm/min). The machine allows adjusting the test conditions, varying both the load, through the pressure of the fluid, and the speed, through a flow regulator. The machine used is equipped with a computer which analyzes the parameters and two displays: in

one are the instantaneous values of the applied load and the elongation values, while the other shows the force-displacement diagram.

With this machine it is possible to make both tensile and compression tests, with variable speed displacement.



Figure 7.3 The universal traction machine

The Digital Image Correlation (DIC) technique is used to monitor the surface deformation field and in order to use it and emphasize the displacement occurred upon the element, the surface of the specimen is treated with white painting and black dots. The monitoring is performed using a VIC-3D HR system, with a hardware composed by two cameras with a resolution of 14 Megapixel (in terms of deformation the resolution is around $50 \mu\epsilon$).



Figure 7.4 Details of the bolts used at the extremities

2. Effects of the bolts

The displacement recorded during the test is principally due to two important factors:

1. Deformation of the specimen
2. Lengthening of the bolts used to fix the studied element to the machine

Each end of the specimen was fixed between two boxes as we said before. Each box of them is fixed to the machine using two bolts M20 (Table 7-3), thus, four in total for each end. Each bolt takes $\frac{1}{4}$ of the load applied from the machine. The bolts are fabricated from steel property class 8.8. Referring to ISO 898-1: 2009, property class 8.8 means that this bolt is guaranteed to support a stress up to $f_{tb} \geq 800 \text{ N/mm}^2$, and yield strength is equal to 0.8 of the ultimate strength thus $f_{yb} = f_{tb} \cdot 0.8 = 649 \text{ N/mm}^2$.

The maximum load applied by the test machine is 600 kN, in the case of those specimens; here, every bolt takes a load equal to:

$$P = \frac{600}{4} = 150 \text{ kN}$$

Assuming that the diameter of each bolt is equal to 20 mm, each one will have a resistant section of 314 mm^2 . Thus, the maximum stress applied on the section is equal to:

$$\sigma_{max} = \frac{P}{A} = \frac{150000}{314} = 477.7 \text{ N/mm}^2$$

This value is less than the yielding value found before for a bolt of property class 8.8 ($f_{yb} = 649 \text{ N/mm}^2$) and assure that those bolts will behave elastically during the tests.

The maximum lengthening of the bolts is calculated here as well:

$$\Delta l = \frac{\sigma_{max} \cdot l}{E} = \frac{477.7 \cdot 200}{210000} = 0.46 \text{ mm}$$

As the deformation hits both the bolts of the upper and lower end, the maximum total deformation related to the bolts will be:

$$\Delta l_{max} = \Delta l \cdot 2 = 0.92 \text{ mm}$$

This value is less than the 1.5% of the total deformation registered during the traction test of the first specimen R1T which is around 65 mm, thus the effect of the deformation of the bolts cannot be taken in consideration.

During the compressive test, the bolts are not stressed which means that no deformation along them.

3. Preparation of the tests

To prepare each test, different steps have been followed:

1. Preparing the specimens following the geometrical details and the predefined technique of manufacturing;
2. In the case of the use of the DIC technique, the specimen should be colored by white background dotted by black points and keep it a part a while in order to dry the colors;
3. Implementing of the connection boxes described above;
4. Preparing the necessary video-camera to register the local deformation of the specimen;
5. Fixing the device in question;
6. Application of a pre-force of 1.4 kN necessary to take out of the initial not significative deformation registered by the machine;
7. Choosing the velocity (mm/min) and other parameters of the test;
8. Start of the test;
9. Registration of the force-displacement results;
10. Analyzing of the obtained results.

4. Protocols of all tests

The typical loading protocols used for the monotonic tests and reversed cyclic is summarized, in Figure 7.5 in terms of maximum imposed displacement δ_{\max} (absolute value) at each cycle as normalized with respect to the first yielding displacement δ_y . Clearly, the actual imposed loading histories vary from one specimen to another as is shown in the following tables. All the applied loading histories are displacement controlled. The amplitudes of the first cycles are set in order to investigate the initial

elastic behavior, and then they progressively increase up to large amplitudes (higher than $8 \delta_y$) or until reaching failure point. [27]

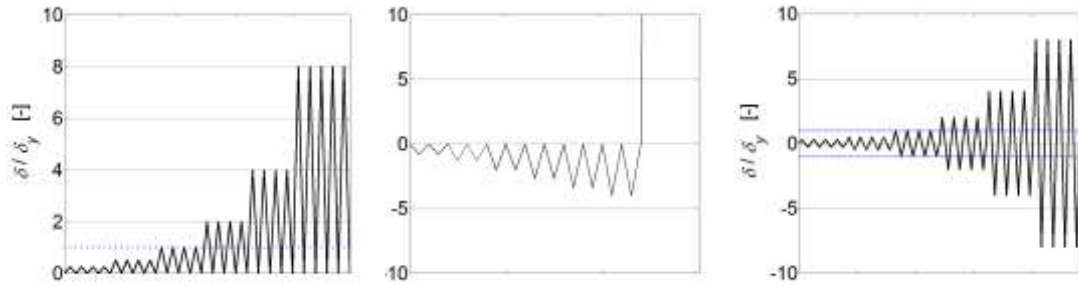


Figure 7.5 The typical loading protocols: left) traction, middle) compression, right) reversed

For the rectangular

	Cycle	Number	Velocity (mm/min)	Force (kN)	δ (mm)	Force (kN)	δ (mm)
R1-T	I	2	8	5	1		
	II	2	8	8	1.9		
	III	2	15	12	2.7		
	IV	2	25	15	3.1		
	V	1	25	20	4.1		
	VI	1	40	35	9.5		
	VII	1	40	60	16.8		
	VIII	3	40	150→326	25→76		

Table 7-2 The applied protocol at the R1T specimen

	Cycle	Number	Velocity (mm/min)	Force (kN)	δ (mm)	Force (kN)	δ (mm)
R2-C	I	1	8			-5	-1
	II	1	15			-8	-1.9
	III	1	25			-12	-3
	IV	1	25			-15	-3.5
	V	1	40			-20	-5.8
	VI	1	40			-23	-8.6
	VII	1	40	290	62		

Table 7-3 The applied protocol at the R2C specimen

	Cycle	Number	Velocity (mm/min)	Force (kN)	δ (mm)	Force (kN)	δ (mm)
R3-R	I	5	8	13	3.4	-13.5	-3.5
	II	5	15	42	9	-20	-6
	III	5	25	52	16	-23	-11
	IV	3	40	195	27	-22	-13
	V	1	25	270	45	-22	30

	VI	1	40	326	79		
--	----	---	----	-----	----	--	--

Table 7-4 The applied protocol at the R3R specimen

C1-T	Cycle	Number	Velocity (mm/min)	Force (kN)	δ (mm)	Force (kN)	δ (mm)
	I	2	8	4.2	1.4		
	II	2	15	7.3	2.4		
	III	2	25	13.6	3.4		
	IV	2	25	26.5	7.7		
	V	1	40	75	18		
	VI	1	40	150	23		
	VII	1	40	430	190		

Table 7-5 The applied protocol at the C1T specimen

C2-C	Cycle	Number	Velocity (mm/min)	Force (kN)	δ (mm)	Force (kN)	δ (mm)
	I	2	8			-9	-3
	II	2	15			-19.6	-6
	III	2	25			-20.2	-9
	IV	1	25			-18	-15
	V	1	40			-16.5	-28
	VI	1	40			-14	-55
	VII	1	40			-14.6	-85

Table 7-6 The applied protocol at the C2C specimen

C3-R	Cycle	Number	Velocity (mm/min)	Force (kN)	δ (mm)	Force (kN)	δ (mm)
	I	5	15	15	3.5	-17	-4.8
	II	5	25	30	9	-22.3	-5.6
	III	5	40	49	14	-23	-7
	IV	5	25	88	19	-28	30
	V	5	40	150 → 250	23 → 29	-53	17
	VI	1	40		20		

Table 7-7 The applied protocol at the C3R specimen

RW1-C+T	Cycle	Number	Velocity (mm/min)	Force (kN)	δ (mm)	Force (kN)	δ (mm)
	I	1	8			-5	-1.6
	II	1	15			-8	-2.3
	III	1	25			-12	-3
	IV	1	40			-15	-4.2
	V	1	40			-18	-6.5
	VI	1	40			-19	-7
	VII	1	40	10	19		
	VIII	1	40	20	51		

	IX	1	40	50	83		
	X	1	40	205	102		
	XI	1	40	290	172		

Table 7-8 The applied protocol at the RW1(C+T) specimen

	Cycle	Number	Velocity (mm/min)	Force (kN)	δ (mm)	Force (kN)	δ (mm)
RW2-R	I	5	8	16	5	-14	-5
	II	5	15	27.5	9	-19.5	-9
	III	5	25	35	13.5	-19.7	-13.5
	IV	5	40	46.5	18	-17	-18
	V	4	40	100-->212	36	-17	-29
	VI	1	40	280	110		

Table 7-9 The applied protocol at the RW2R specimen

	Cycle	Number	Velocity (mm/min)	Force (kN)	δ (mm)	Force (kN)	δ (mm)
RW3-R	I	5	15	17	5	-13.5	-5
	II	5	25	31.5	10.5	-20.5	-10.5
	III	5	40	36	14	-21.5	-14
	IV	3	40	62	21	-20.8	-21
	V	3	40	94-->132	28	-15	-28
	VI	2	40	254-->280	100		

Table 7-10 The applied protocol at the RW3R specimen

	Cycle	Number	Velocity (mm/min)	Force (kN)	δ (mm)	Force (kN)	δ (mm)
RR1-R	I	3	8	5	2	-5	-2
	II	3	15	25	4	-20	-7
	III	3	25	40	10.4	-24	-12.6
	IV	2	25	91	20	-28.5	-2
	V	1	40	248	30	-52	4.9
	VI	1	40	213	30	-44	3.3
	VII	1	40	286	40	-54.5	13
	VIII	1	40	314	48.5	-58.2	42

Table 7-11 The applied protocol at the RR1R specimen

	Cycle	Number	Velocity (mm/min)	Force (kN)	δ (mm)	Force (kN)	δ (mm)
RR2-R	I	4	8	21	5	-13	-5
	II	5	15	31	10	-18.5	-10
	III	5	25	41	15	-20	-15
	IV	1	40	152	25	-38	18
	V	3	40	200	40	-48	60

	VI	1	40	260	118		
--	----	---	----	-----	-----	--	--

Table 7-12 The applied protocol at the RR2R specimen

	Cycle	Number	Velocity (mm/min)	Force (kN)	δ (mm)	Force (kN)	δ (mm)
TW1-R	I	3	10	2	1	-2	-1
	II	3	15	5	2.5	-5	-2.5
	III	3	15	10	4.7	-10	-4.3
	IV	2	25	15	12	-10	-10
	V	2	25	25	15	-12	-18
	VI	4	25	38→60	25	-20 → -12	-25
	VII	1	25	40	30		

Table 7-13 The applied protocol at the TW1R specimen

	Cycle	Number	Velocity (mm/min)	Force (kN)	δ (mm)	Force (kN)	δ (mm)
TW2-R	I	3	10	4	2.2	-3.7	-2.3
	II	3	15	11	4.3	-9	-4.5
	III	3	15	14	8.6	-9.3	-8.5
	IV	3	25	16	12.3	-6	-12.5
	V	1	25			-3.2	-26

Table 7-14 The applied protocol at the TW2R specimen

As it is seen in all the tables above, every specimen had its own protocol, but following a general rule indicated in Figure 7.5, for tension the left part, for compression the middle part and for reversed cycles the right part of the indicated figure.

7.1.3. Main goals of the experimental tests

The main objective of the experimental campaign is to provide a complete experimental assessment of the pseudo-static cyclic response of CSB devices and to verify the effectiveness of the design formulations. To achieve the objective, the following specific aspects are discussed in the following sections:

- An overview of the experimental force-displacement response (section 7.2);
- The comparison between the experimental responses and the prediction provided by the analytical formulas of chapter 4 (chapter 8);
- The effects of the welding on the global behavior of the device (section 7.3);
- The assessment of the ductility capacity (section 7.4);

- To assessment of the non-linear cyclic response in terms of energy dissipation capacity (section 7.5);
- The monitoring of the local deformation fields through the DIC technique (section 7.6).

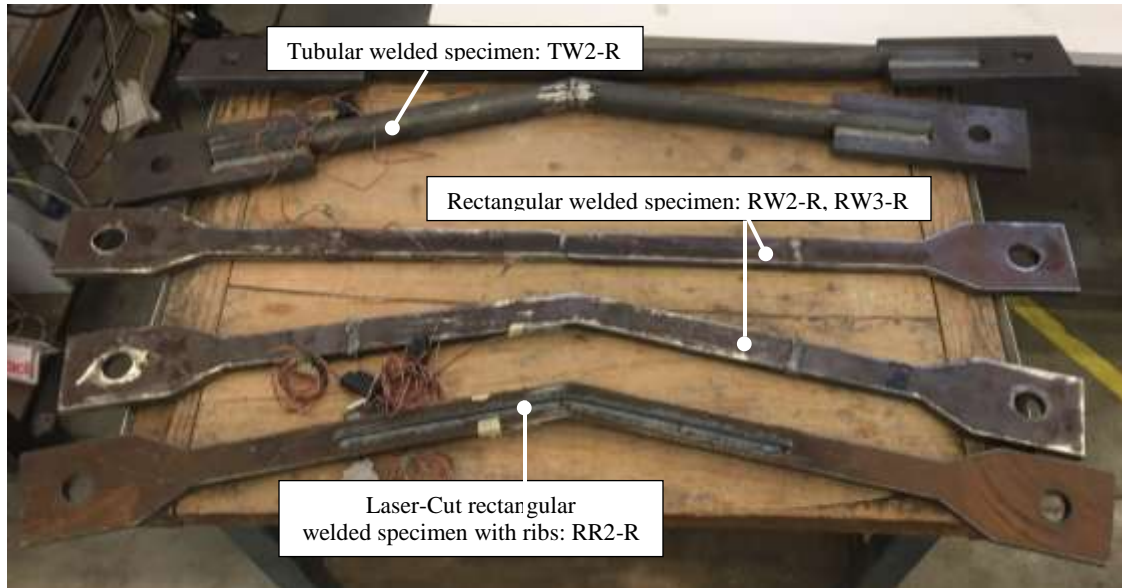


Figure 7.6 RR2R, RW2R, RW3R and TW2R before testing



Figure 7.7 RW2R inserted in the test machine during the test loading

7.2. THE FORCE – DISPLACEMENT RESPONSE

The main results of the tests conducted on the thirteen specimen described above were the force-displacement response. With some specimens, we reached the failure, with others, the test was stopped before. In all cases, in this section we are going to show all the results divided into four parts; first one is related to the fully rectangular cross section specimens, or first three specimens. Second part shows the results of the fully circular cross section specimens. While the third one concentrates on the fully rectangular welded and with ribs, in other words, four specimens, the fourth part is dedicated to the ultimate two specimens done by the circular tubular cross section.

1- Fully rectangular cross section specimens

The first specimen or R1T was subjected to pseudo-static cyclic tensile loads. As it was described in the protocol section, the first two cycles underwent with a load of 5kN, the second two cycles were under 8 kN, than 2 cycles for 12 kN, 2 cycles for 15 kN, one under 20 kN, one for 35 kN where the knee section knew flexural yielding, another cycle was conducted under 60kN. The test finished with three cycles, one under 150 kN, second one under 245 kN which corresponds to the yielding under traction and the last one was under 326 kN corresponding to the ultimate tensile force corresponding to the point of total yielding of the device.

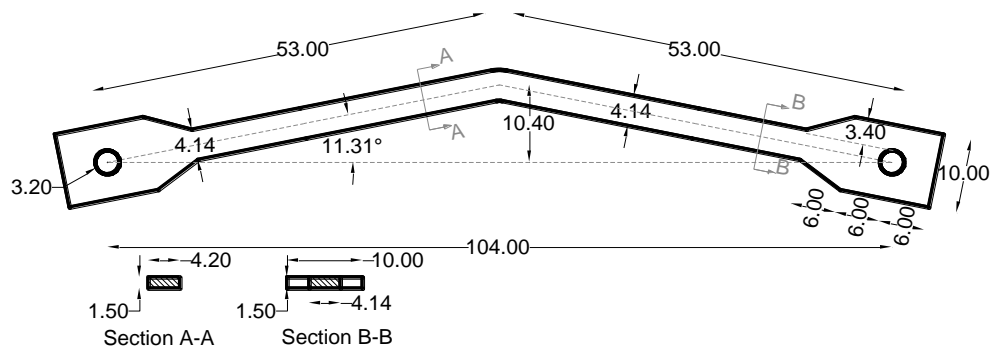


Figure 7.8 The adopted measures for the rectangular cross section specimens

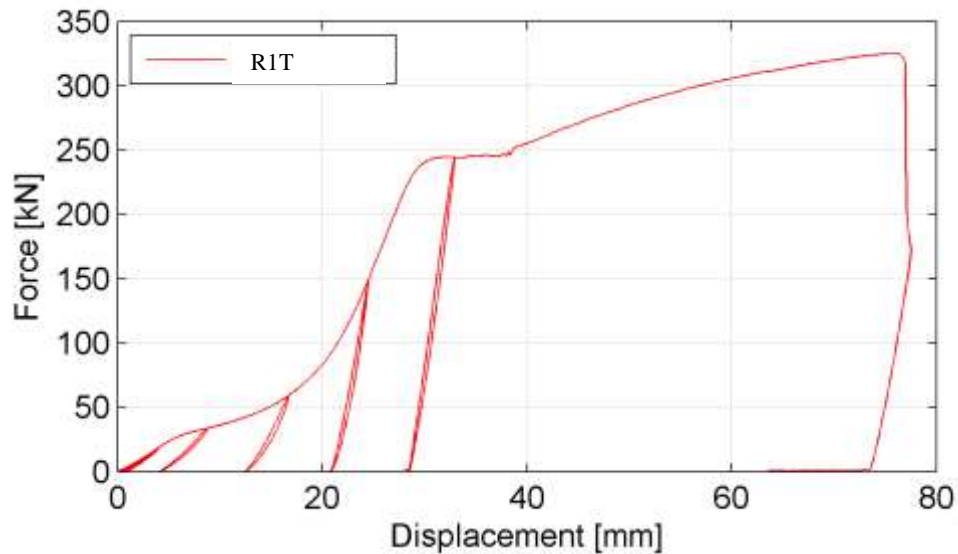


Figure 7.9 The force-displacement response of R1T

To note that the stiffness corresponding to the elastic part is equal to 5kN/mm, while in the hardening part is around 20 kN/mm.

R2C, as its name describes, is the second fully rectangular cross section specimen, studied under compressive loads. The first cycle was performed with an interval of loads finished at 5kN. The second cycle was done under 8 kN load, then 12 kN, 15 kN, the fifth cycle was under 20 kN, the sixth one under 23 kN. As well in this test, the yielding started from the knee point. The last cycle was done under tensile load which reached the value of 290 kN. It is logic in this test to think that the specimen reaches the failure due to the failure of the knee point under the last tensile load.

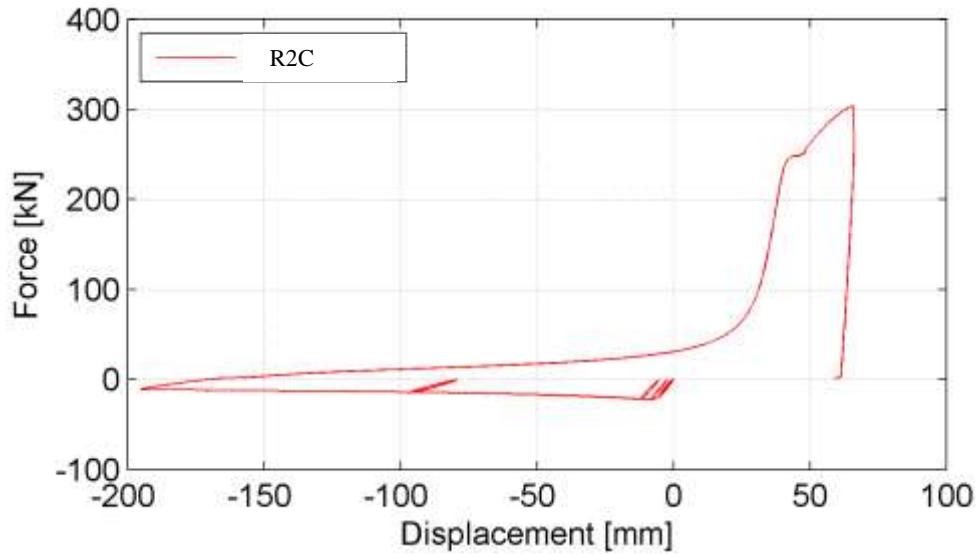


Figure 7.10 The force-displacement response of R2C

As we expected, due to the symmetry in the elastic field of the steel, the stiffness in the compression elastic field was as well around 5 kN, the same as the specimen R1T.

From the analysis of the specimens R1T and R2C, it was clear that:

R2C loaded by compressive loads and then a final tensile one knew a shorter lengthening than the R1T tested only under tensile loads.

The behavior of R2C under tensile load, after the compressive cycles, was different than the R1T which was subjected only to tensile loads.

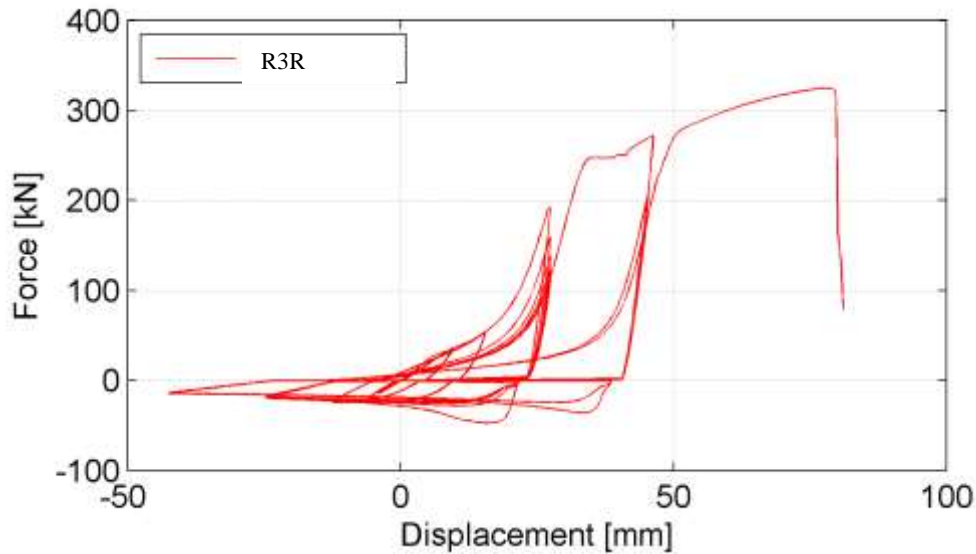


Figure 7.11 The force-displacement response of R3R

Concerning the specimen R3R, the pseudo-static cyclic reversed test under tensile and compressive loads was performed as was described in the protocol section: 5 cycles

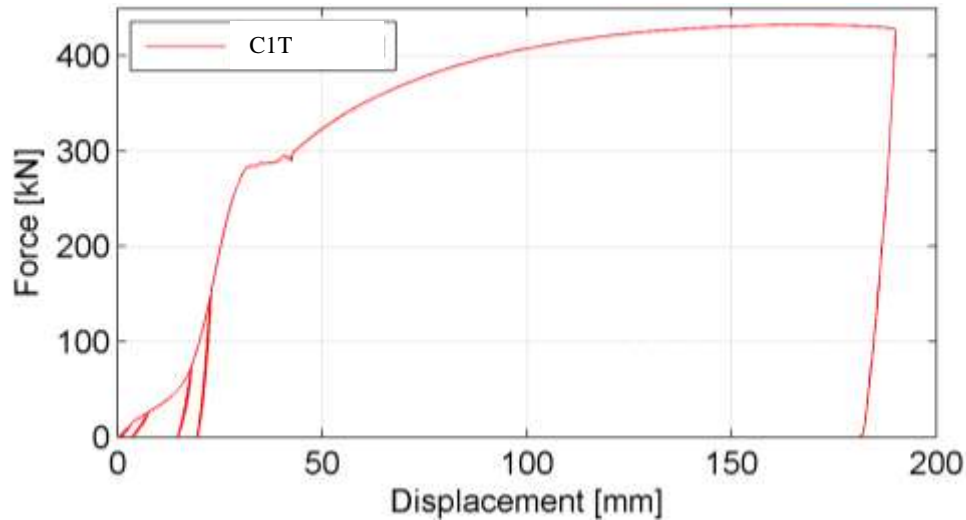


Figure 7.13 The force-displacement response of C1T

At around 16 kN, the force-displacement curve starts to show a change in its progress, at 18 kN this change becomes clearer. This means that at this point the first yielding starts to manifest upon the knee zone of the device. In the interval of forces going from 100 kN to 150 kN, the specimen was almost straight, it knew the hardening behavior and it is clear from the curve above. The hardening behavior is clear until a value of force equal to 287 kN where a new change of the progress of the curve appears. At around 295 kN, the new trend of the curve starts to manifest explaining the behavior of a straight bar under tensile axial loads, or in other words, increasing of deformation under almost a constant load.

From 300 kN, another hardening part appears with an increase of deformation and loads reaching 430 kN where we decide to stop the test after a sudden decrease in the behavior curve.

To note that the stiffness corresponding to the elastic part is equal to 3kN/mm, while in the hardening part is around 7 kN/mm. The first flexural yielding point corresponds to 10.25 kN, while it is around 284 kN for the axial yielding and the failure force is around 430kN.

We noticed the final lengthening of the specimen. The initial length was 1320mm while it increased to 1460 mm at the end of the test for a total displacement of 15%.

What it was clear in the second part was the deformation of the whole of the bolt. The diameter was increased transversally from 31 mm to 35 mm by a total increase of 11%.



Figure 7.14 The ovalisation of the bolt hole

The second specimen of this part is the C2C, a fully circular cross section specimen tested under compressive loads. In total, eleven cycles were performed on this specimen. The first two went from 0 to 8.5 mm, the second two cycles were performed until a displacement of 10 mm was reached. The third two cycles reached the 13 mm of displacement. After that, five different cycles were applied reaching respectively 16mm, 21 mm, 35mm, 63 mm and 95 mm.

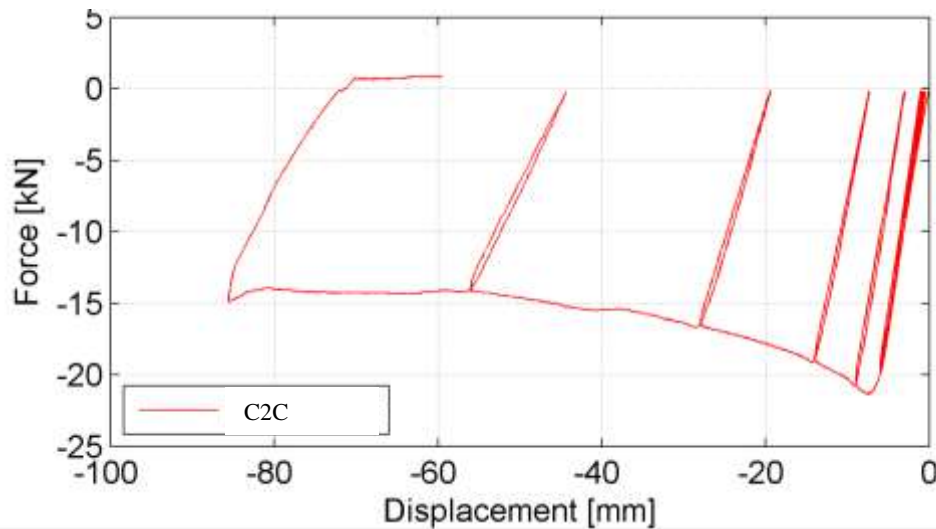


Figure 7.15 The force-displacement response of C2C

As we were expecting, the stiffness corresponding to the elastic part is equal to 3 kN, the same stiffness of the C1T due the symmetry of the behavior of the steel in elastic filed under compressive and tensile loads. The yielding force is around 12 kN. An ovalization of the hole was detected in one end of the specimen.

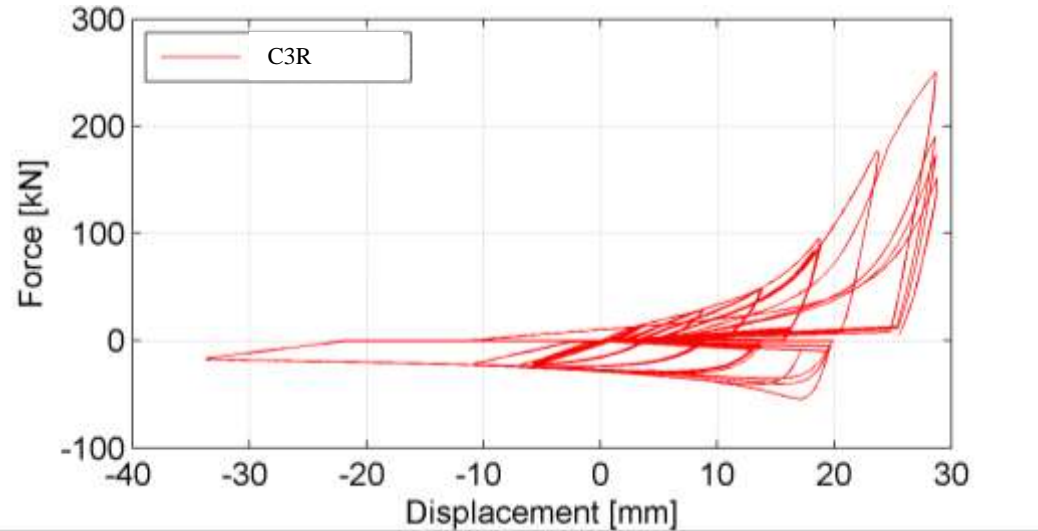


Figure 7.16 The force-displacement response of C3R

Specimen C3R was subjected to a reversed cyclic test. The test has been conducted in terms of displacement. 26 cycles in total have been performed on this specimen. The first 5 cycles reached 5mm of displacement under tensile and under compressive loads. The second five cycles reached a displacement of 10 mm for both cases. After that, 15mm was reached by other consecutive five cycles and then 20 mm with the next five cycles. One cycle was applied and the displacement was 25 mm, other three cycles were applied to reach 30mm. The test end with different two cycles, the first one reached in compression the 48 mm of displacement while the second one stopped at 20mm of displacement.

At around 8 kN, the first changing of the progressing of the elastic curve starts to appear. hysteretic cycles were been observed both in tension and in compression, even if they are small cycles. The same observations were been done for the next 5 cycles were hysteretic cycles have been detected with a higher displacement in tension, around 11.2 mm and in compression, 19mm.

The cycles went in this mode; every increasing in the displacement corresponds to an increase of the force and of the area of the hysteretic cycle.

3- Fully rectangular welded and with ribs cross section specimens

This part contains two types of specimens, three fully rectangular cross section welded, all of them subjected to reversed cycles, tension and compression, and two specimens

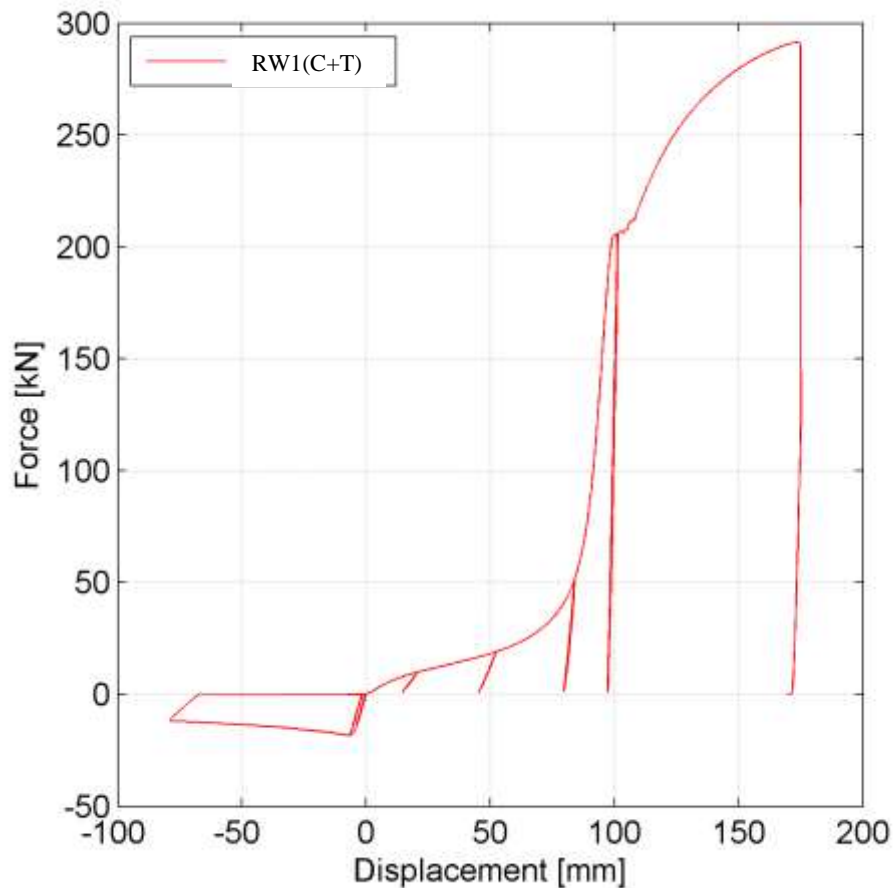


Figure 7.18 The force-displacement response of RW1(C+T)

For this reason, the energy dissipation capacity of some specimens will be studied in the section 7.5.

The specimen RW2R has been subjected to almost the same test of RW1R, with the difference that RW2R was surmounted with an extensimeter to check more precisely the effect of welding. Until the writing of these lines, the data was not elaborated to be studied. Thus, other papers will deal with this matter and its results.

It is remarkable the clearness of the cycles of this specimen. It was subjected in total to 25 cycles without reaching the rupture. First five cycles were in elastic field, with 16 kN in tension and 14 kN in compression and a displacement of around 5.5 mm and 5 mm, which lead us to a stiffness equal to 3.2 kN/mm. Next five cycles hit 27 kN in tension and 20 kN in compression going out of the elastic field. Other two types of cycles have been performed reaching for the first five cycles the value of 35 kN in

tension and 20 kN in compression with a larger shortening than before, around 13.5 mm. The second five cycles hit 47 kN in tension with a displacement of around 18 mm and -18 mm in compression with 18 kN of loads

Last five cycles were with different values especially for tensile case where they went from 212 kN to 150, then 115 and 100 kN to finish with 280 kN with a total displacement of around 110 mm.

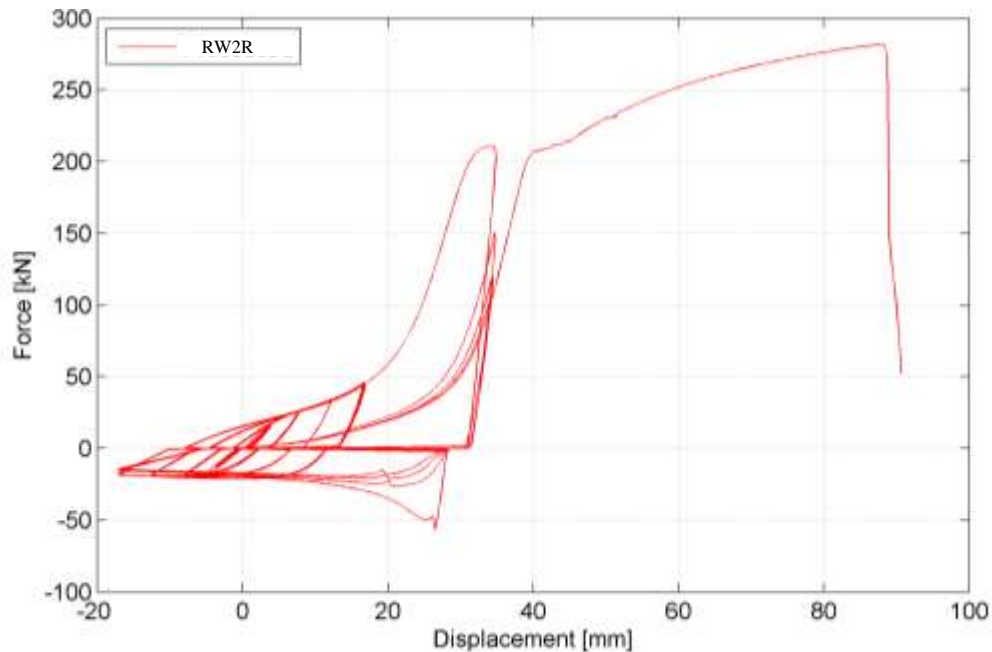


Figure 7.19 The force-displacement response of RW2R

It is possible to say that RW3R was a twin to RW2R. It was subjected to total number of 25 cycles. An extensimeter was implemented on it to check the effects of welding and the correspondent behavior of the constitutive material. First five cycles were achieved hitting a final force of 17 kN in tension and 13.5 kN in compression. For the next five cycles, a 32 kN of tensile force was the range of the test and 21 kn in compression with a total displacement of 22 mm. To remember that after 20 kN the plastic phase starts. Same procedure was done for the rest of the ten cycles. The most important result is the result of the final result which was a 100 mm of displacement under a tensile load of 280 kN. It is almost the same result of the specimen RW2R. The results are plotted in the followed figure, Figure 7.20. The stiffness of this specimen is equal to 3.3 kN/mm in the elastic field and around 20 kN/mm for the first hardening and 2 kN/mm for the last hardening.

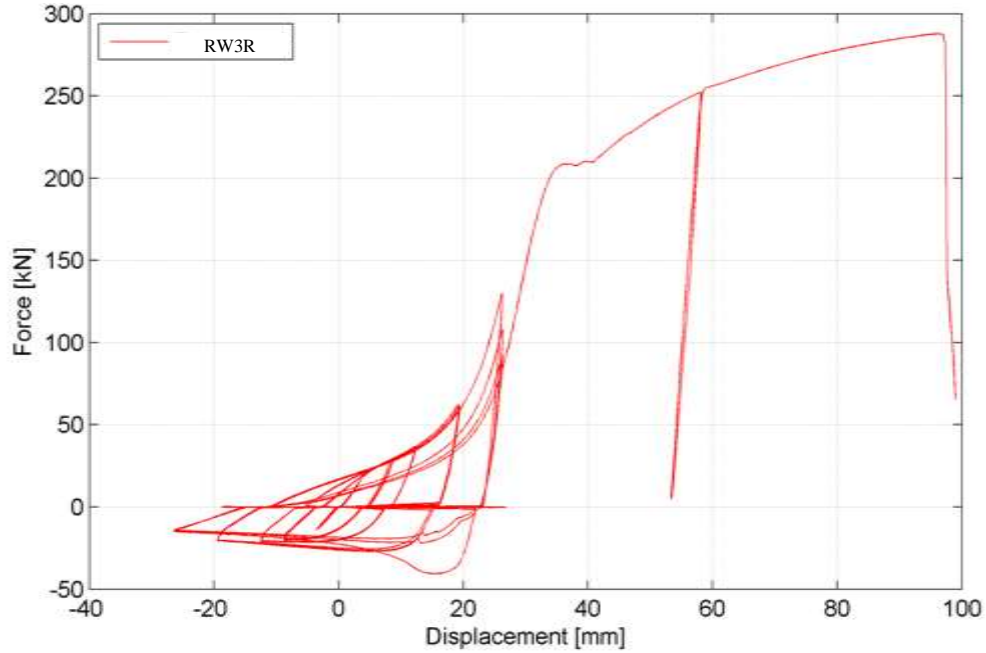


Figure 7.20 The force-displacement response of RW3R

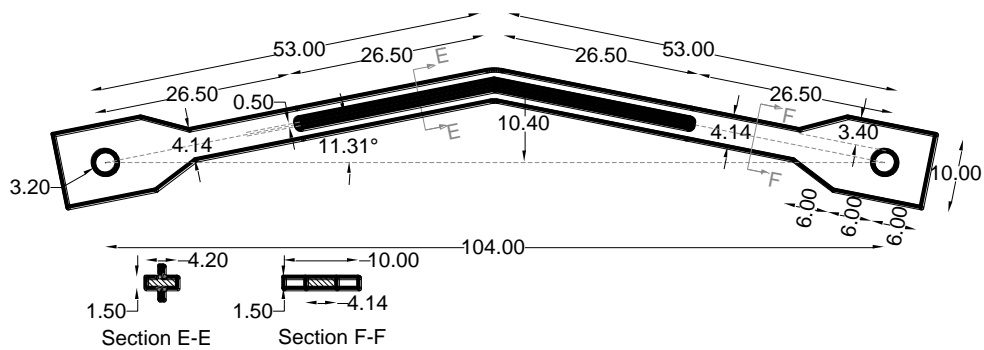


Figure 7.21 The applied geometry for the rectangular cross section with ribs specimens

The RR1R was the first specimen of fully rectangular section with ribs to be tested. The main objective of this test was to check the effect of the increased inertia on the out of plan buckling. The inertia is increased and so the stiffness which is around 6.2 kN/mm, higher than 5 kN/mm, the stiffness of the fully rectangular specimens.

This specimen was loaded first by small loads in tension and compression, around 5 kN, for three cycles. After that, another three cycles were applied arriving to 25 kN in tension and 20 kN in compression, with a total displacement of 5.5 mm in tension and around 7 mm, even on the graph its seems around 13 mm, this is due to the initial phase of calibration. Another three cycles have been performed reaching 91 kN in tension with 20 mm of lengthening and 29 kN in compression.

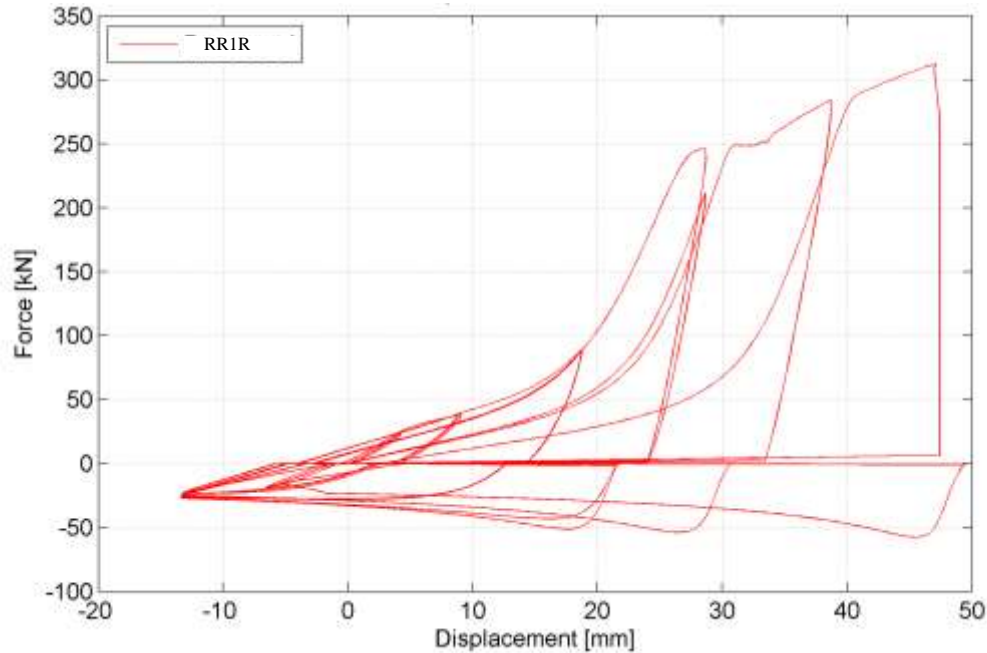


Figure 7.22 The force-displacement response of RR1R

Four last different cycles have been performed in tension and compression, reaching respectively 248 kN, 213 kN, 286 kN and the last one was 314 kN in tension and 52 kN, 44 kN, 55kN and 58kN in compression with a total displacement of around 40 mm. The test has been stopped without reaching the rupture of the specimen, but of course passing by the flexural yielding point corresponding to a force of 23 kN and the axial yielding point at around 250 kN which was the point of the end of the first hardening, and the start of a plateau, where displacement was increasing, and then a last hardening which ends at around 314 kN starting from 248 kN and 31mm of displacement ending at 48.5 mm of total lengthening, with a hardening stiffness equal to 3.8 kN/mm.

The second fully rectangular cross section with ribs specimen studied RR2R was subjected to almost the same protocol. The difference between the two tests is that we put extensimeter for the RR2R to check the macro displacement of the welded part with the ribs. The data until the date of the writing of this thesis was not elaborated, for this reason it will be subject of another studies.

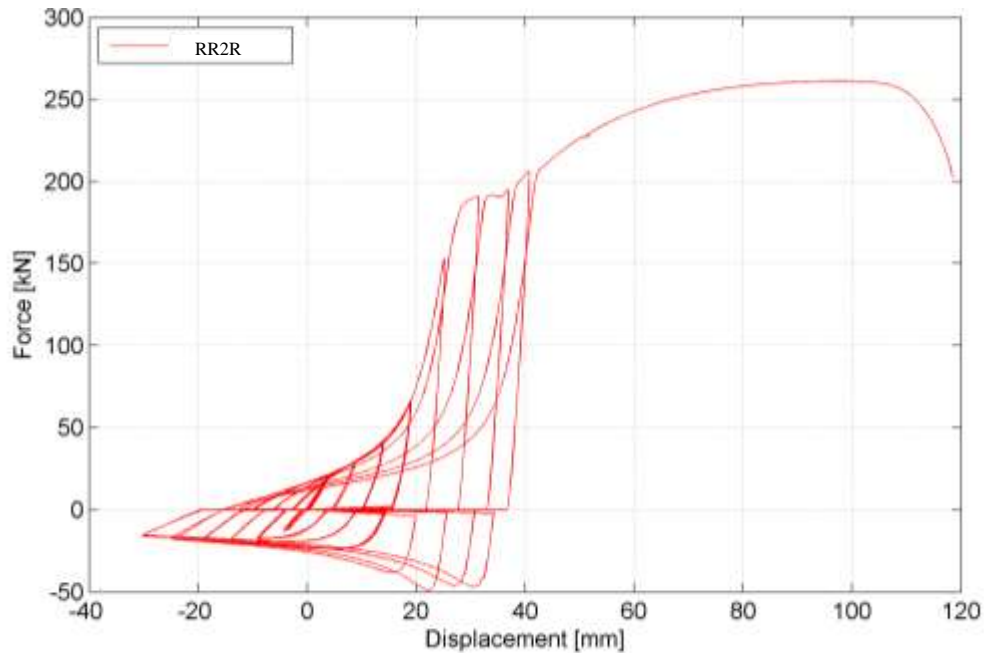


Figure 7.23 The force-displacement response of RR2R

The test started with four cycles in tension and in compression reaching a force of around 21 kN in tension and 13kN in compression. The stiffness is around 6 kN/mm. Other three types of cycles, each one of five cycles have been performed, reaching in tension respectively 31, 41 and 68 kN in tension, 18.5, 20, 26 kN in compression. The last five cycles correspond to 150kN in tension and this value correspond to the first hardening. And then 195, 195 and 203 kN corresponding to the plateau or the ductility where the displacement increases from 25 to 40 mm. The last cycle reaches a maximum of 260 kN to decrease again to 200 kN. For the compression part, it is evidence the big value of shortening or displacement which correspond to around 60mm reaching values of 50 kN. The test was stopped before the rupture of the device.

4- Tubular Circular cross section specimens

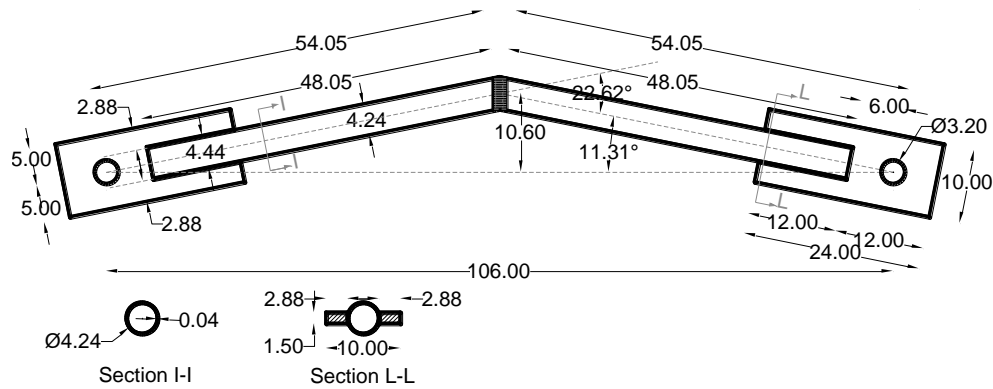


Figure 7.24 The applied geometry for the tubular cross section specimen

The first specimen in this part is the TW1R, it was subjected to reverse tensile and compressive cycles. As it was expected, it has a poor behavior due to its small moment of inertia, as seen in

Table 7-1. The first three cycles were performed with a small velocity to check the behavior of the device. Reaching a force of 2 kN in tension and -2kN in compression, the displacement was around 1 mm in both cases. The next three cycles were performed symmetrically until a 5kN of loading with a displacement equal to 2.5 mm. The third three cycles hit the 10 kN of force with a displacement of around 4.5 mm and the flexural yielding point was hit in this interval. After that, always speaking symmetrically, two cycles were performed in tension phase with a force of 15 kN and 12 mm of displacement, and -10 kN in compression with around 10 mm of displacement. Next two cycles reached 25 kN in tension and 12 kN in compression. And after reaching by 4 cycles 60kN in tension with a total displacement of 25 mm and 12 kN in compression as well with 25 mm of displacement, the last cycle was under tensile loads which reached 40 kN and a total of 30mm of displacement arriving to the rupture point of the device on the knee point due to the failure of the welding (Figure 7.25). The elastic stiffness of this specimen is around 2 kN/mm.

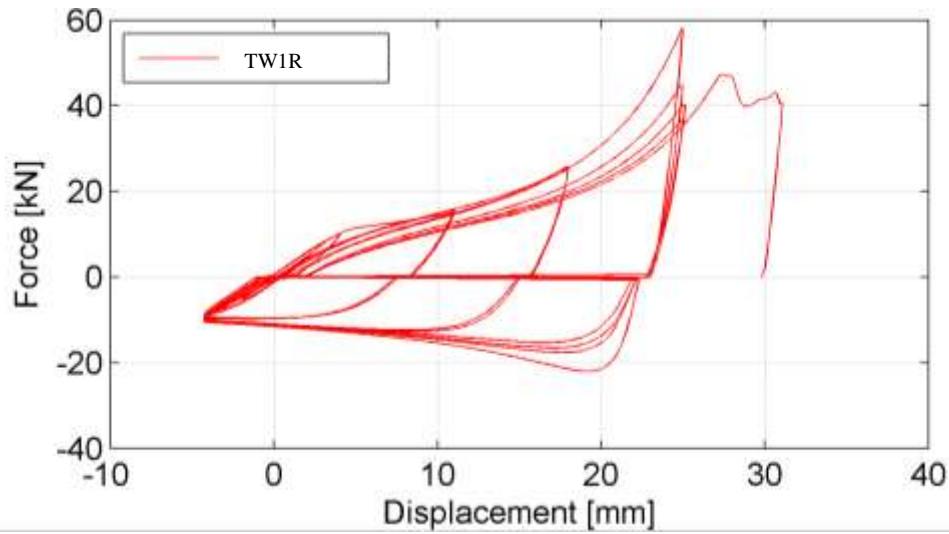


Figure 7.25 The force-displacement response of TW1R

The last studied specimen is the TW2R. The objective of this specimen is to study the failure under compressive loads even it was subjected to reversed cyclic ones.

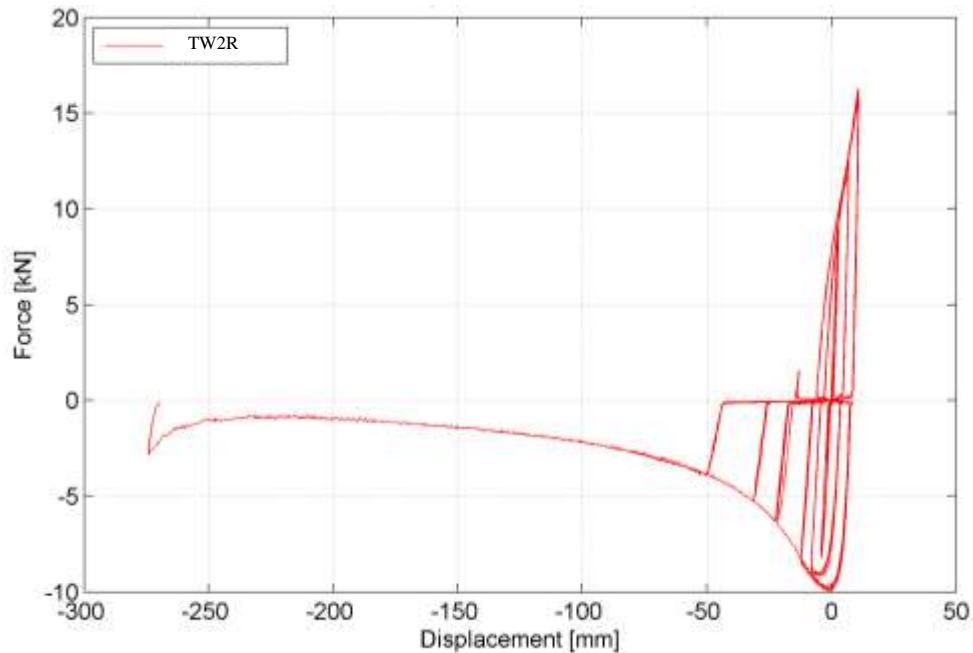


Figure 7.26 The force-displacement response of TW2R

As we remark from the Figure 7.26, TW2R was subjected to pseudo-static cycles varied between tension and compression zones. The first three cycles reached 4 kN in tension and -3.7 in compression. The second three cycles reached 11 kN in tension and -9 in compression with a total displacement of 4.5 mm in both cases. The displacement became symmetrical for 8.8 mm in tension with 14 kN of loading and in compression with 9.3 kN. Last cycle was applied in tension arriving to 16 kN and 12.3 mm of

displacement and then the test continues in compression reaching 12.5 mm of displacement. The idea was to assess the behavior under excessive compression loads. Applying a load of around 12 kN, the displacement was increasing until it reached 25mm and the test has been stopped. At this point, the welding in the knee zone knew two different zones: the upper part of the knee was under tensile loads and started to fail and the lower part was under compression. This part under compression played the role of barrier and it was impossible to continue after that the compression because the force was stable and the displacement as well.

7.3. THE EFFECT OF WELDING ON THE CRESCENT SHAPED BRACE

As some specimens (RW1R, RW2R) were welded in the middle of each straight element of the CSB device, it was necessary to study the effects of the welding on the test results.



Figure 7.27 The RW1 before being welded

7.3.1. Analysis of the tensional state

The CSB used in this test were made with three pieces joined by means of electrical welding by full penetration, positioned in the center of both rods of the device, approximately at a distance of about 26.5 cm from the knee point.

First we calculate, as follows, the theoretical maximum elongation due to the axial strength of one of the two oblique portions of the device:

$$\Delta l = \frac{N \cdot L}{E \cdot A} = \frac{291 \cdot 53}{21000 \cdot 6.21} = 0.12 \text{ cm}$$

The value is, in first approximation, negligible. With this assumption, it can be stated that the length of the oblique sections remains constant during the traction and compression phases.

7.3.2. Identification of the situation of highest stress and calculation of the maximum stress in the tensile cycle

Having available the experimental values of the displacement as a function of the load applied, and by simple geometric considerations, it was possible to calculate first the angle at the vertex:

$$\vartheta'_1 = \arccos\left(\frac{L}{L_1}\right)$$

Where L is the inclined rod length which, by assumption, it is considered constant, and L_1 is the half of the distance between the two points of anchorage of the device, which varies in function of the applied load.

Knowing ϑ'_1 , it is possible to express the moment at the point affected by the welding, using the following expression:

$$M = N \cdot \frac{L}{2} \cdot \text{sen}(\vartheta'_1)$$

In function of M and N, through the expression:

$$\sigma_{max} = \frac{N}{A} + \frac{M}{W_{el}}$$

It is possible to calculate the maximum applied stress.

The development of the calculations allows identifying that, in the point of the maximum stress, in the traction phase; the applied load is of 24.55 kN, which corresponds to a displacement of 0.311 cm. In this position the maximum tensile stress in the area affected by the welding is 30.98 kN / cm²; this value is less than the elastic limit of the yield strength, equals to 40 kN / cm², in the present case.

Therefore, with the used assumptions, the affected area remains completely in the elastic range.

If all the section was, instead, in the plastic phase, W_{pl} should be used instead of W_{el} , thus the maximum stress value would be equal to 21.95 kN/cm².

7.3.3. Identification of the situation of the highest stress and the calculation of the maximum stress in the compression cycle

In the case of normal compressive force, the maximum moment is obtained at the position where the axial load is the maximum, and, therefore, the greater displacement is also of the knee point. In this situation too, it is possible to identify the geometric dimensions necessary to the calculation of the bending moment in the area affected by the welding.

The greatest stress corresponds to a situation where the load is approximately -20 kN with a displacement or shortening of around of 1.62 cm.

In function of M and of N, through the expression:

$$\sigma_{max} = -\frac{N}{A} + \frac{M}{W_{el}}$$

It is possible to calculate the maximum stress, which for the highest values of stresses is equal to 34.82 kN / cm². Since this value is less than the elastic yielding stress value (40 kN / cm²), the outer areas of the section (those most stressed) remain in the elastic range.

If all the section was, instead, in the plastic phase, W_{pl} should be used instead of W_{el} , thus the maximum stress value would be equal to 24.24 kN/cm².

7.3.4. Remarks

From the theoretical studies, it was clear that the areas of the device subjected to welding remain in the elastic phase during both traction and compressive loadings.

It is curious to know that during the carrying out of the experimental tests, the specimens are collapsed in the areas around the knee, both in the traction and in the compression phase but not in the welded zones.

Therefore, the results obtained from the theoretical analysis confirm what was obtained in the experimental tests; thus, the welding, if it was well executed, it does not show any critical issue for the CSB devices.

As already described in section 4.2., the specimens were covered with a particular two-tone paint (black dots on a white background). A special device, consisting of a number of sensors connected to the CSB and by a special camera, detects the change of distance between the colored points, thus allowing identifying the deformation present in the various areas of the structure, associating to each value of the deformation a different coloring. The result is represented in the subsequent figures of immediate interpretation and, through the chromatic scale present to the right of each image, it allows to have an immediate assessment of the deformation state of the different areas of the CSB in each stage of the test.

7.4. ASSESSMENT OF THE DUCTILITY CAPACITY

The displacement ductility capacity of the CSB is here evaluated with respect to the condition of the first yielding at the knee section by considering the response of the equivalent bilinear system characterized by equal area (i.e. dissipated energy) under the force-displacement response. The stiffness of the equivalent bilinear system is given by section 5.4. For instance, Figure 7.28 and Figure 7.29 display the normalized force-displacement response of the full rectangular and full circular specimens in terms of normalized force (F/F_y^*) vs displacement ductility μ . Values of F_y^* have been obtained from the experimental responses by imposing equal areas under the experimental envelope (black solid lines) and the idealized bilinear responses (red dotted lines).

In tension, the ductility capacity is limited (values around 2) and depends mainly on the specific geometry of the CSB (lever arm and cross-section) rather than the material ductility, as also noted in the analytical part. However, as above mentioned, it has to be remarked that the ductility under tensile loadings is here evaluated with respect to the first yielding force which is quite less (even 10 times) with respect to the ultimate tensile capacity of the device.

At ultimate conditions under tensile loadings, the CSB behaves as a conventional steel member subjected to a tensile axial load whose ultimate ductility capacity is mainly

governed by the material ductility already plasticized (stress-strain material behavior). In compression, CSBs exhibit larger values of ductility capacity (around 5). This capacity can be seen clearly in the TW2R specimen who knew a big value of ductility reaching a big value of displacement, around 25 cm. While under tensile loads, it failed at the knee section before knowing any important ductility.

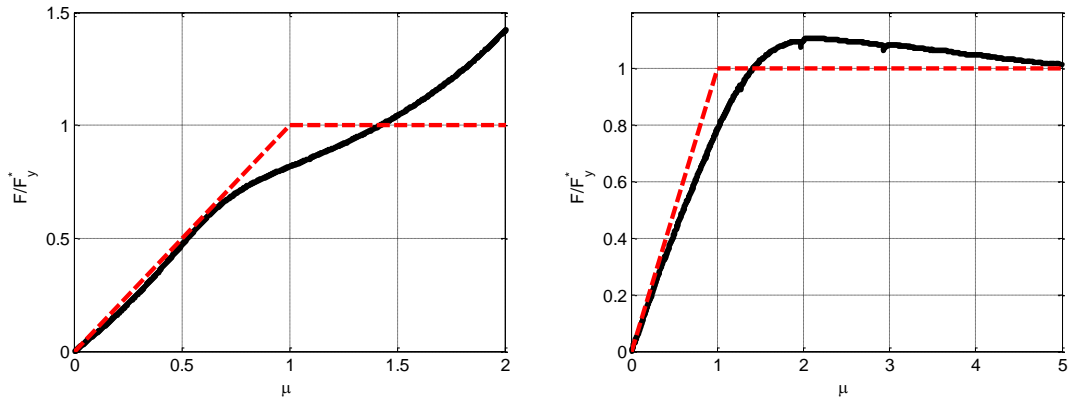


Figure 7.28 Ductility capacity of the R3R specimen left) in tension, Right) in compression

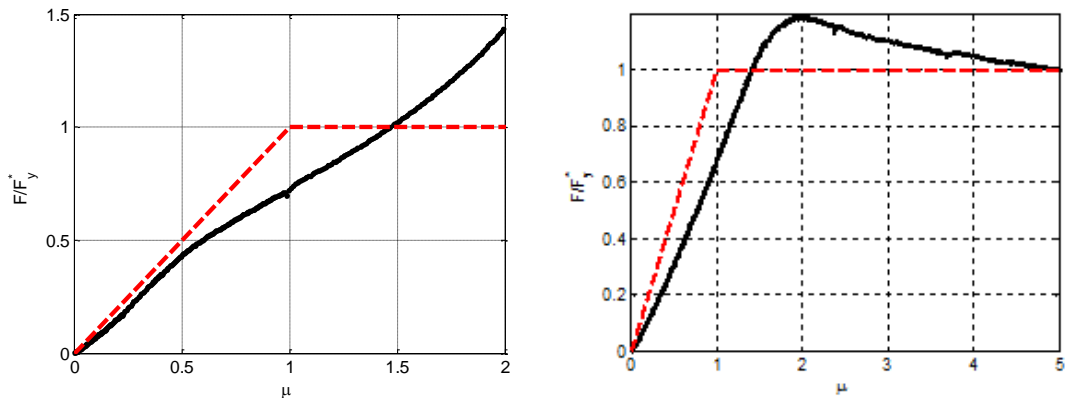


Figure 7.29 Ductility capacity of the C3R specimen left) in tension, Right) in compression

7.5. ENERGY DISSIPATION CAPACITY

One of the important characteristics of any hysteretic device is its ability to dissipate energy, as was explained previously in chapter 2. Therefore, the energy dissipation capacity of the CSB is here evaluated by means of the equivalent damping ratio $\zeta_{eq,i}$ according to Jacobsen (1930), referring to the i -th half hysteresis cycle:

$$\zeta_{eq,i} = \frac{1}{\pi} \cdot \frac{A_{half,i}}{F_{max,i} \cdot \delta_{max,i}}$$

Where $A_{half,i}$ is the area of half of the cycle where the energy is dissipated by the CSB in the i -th hysteresis cycle; $F_{max,i}$ and $\delta_{max,i}$ are the maximum recorded force and displacement in the i -th half cycle, respectively. A cycle means a complete trajectory in compressive zone and in tensile zone. Thus, the equivalent damping ration does not take into consideration the whole cycle, but just the part corresponding to one type of loads, or tensile or compressive. For this reason, our study was based on specimens who were subjected to reversed pseudo-static test where cycles are composed of two half-cycles, one in the compressive zone and the other in the tensile one. Figure 7.30 R3R equivalent damping ratio Left) Tension; Right) Compression Figure 7.31 C3R equivalent damping ratio Left) Tension; Right) Compression, Figure 7.32, Figure 7.33, Figure 7.34 show the average values (along the cycles at the same imposed displacement) of the equivalent damping ratio as resulted from tests R3-R, C3-R, RR1R, RW2R, TW2R. The values of the equivalent damping ratios obtained from the half cycles in tension and the half cycles in compression are indicated with $\zeta_{eq,i}^+$ and $\zeta_{eq,i}^-$ respectively. From the section 7.2, we remarked that the areas of the tensile cycles are bigger than those of the compressive cycles. However, the corresponding tensile forces are bigger as well then the compressive forces. The following calculation can show us that the equivalent energy dissipation capacity in the case of compression has a bigger equivalent damping ratio then the one of the tensile case.[25]

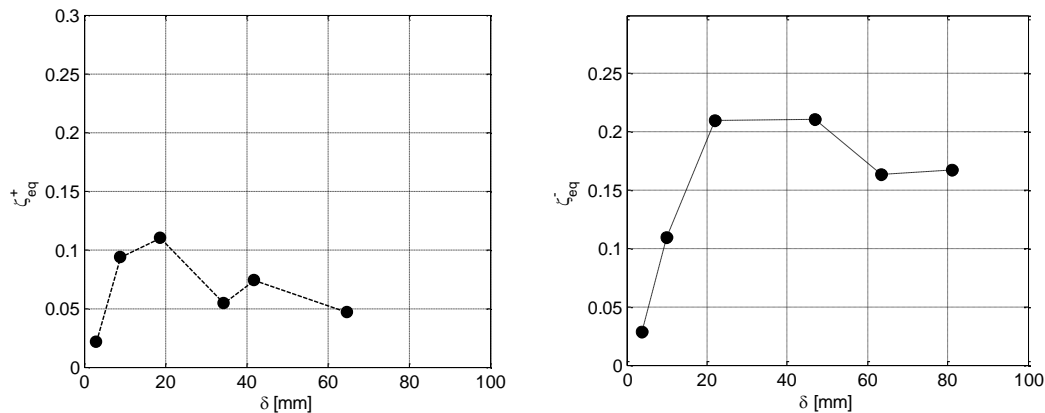


Figure 7.30 R3R equivalent damping ratio Left) Tension; Right) Compression

In the case of the rectangular specimen, it is clear that the dissipation in the tensile case is poor in comparison with the compressive case. To note that the first damping ration, corresponding to the elastic field is equal for both cases due to the symmetrical elasticity in the case of compression and tension.

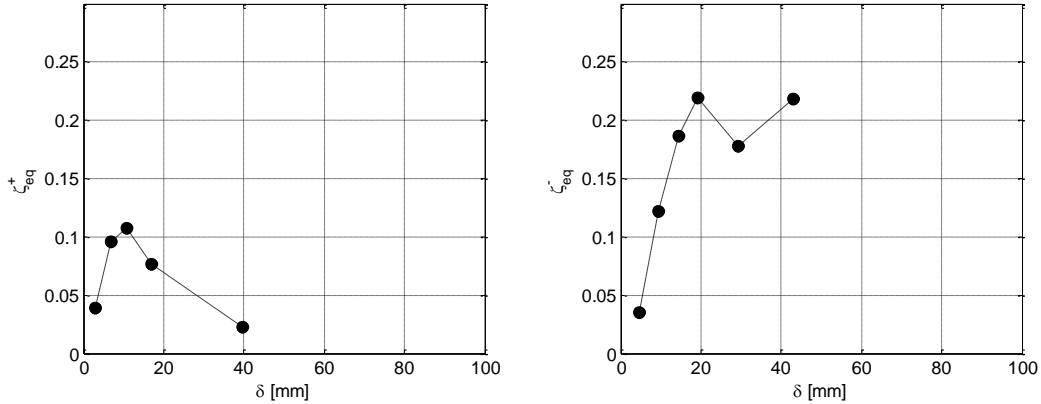


Figure 7.31 C3R equivalent damping ratio Left) Tension; Right) Compression

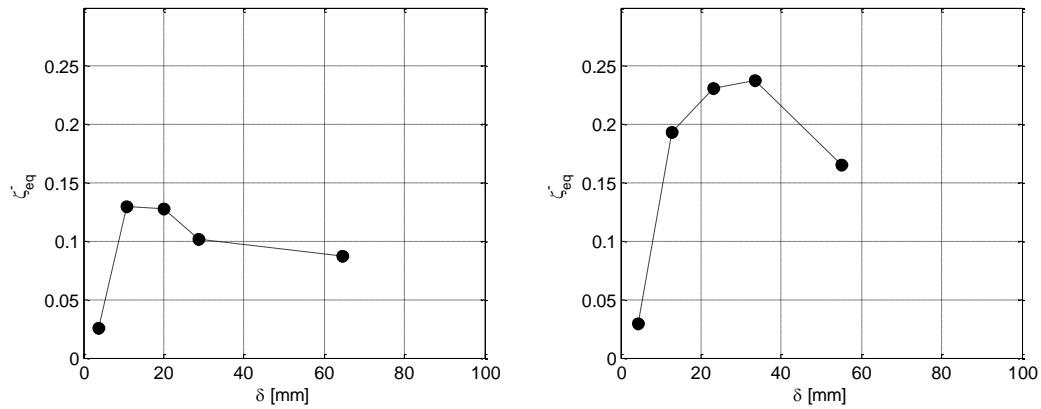


Figure 7.32 RR1R equivalent damping ratio Left) Tension; right) Compression

It is possible to remark the decrease of the equivalent damping ratio for the last cycles even for tension and compression. In the tensile case, this can be return to the fact that the device knows a hardening so a fast increase in the resisting force which is not proportional to the increase of the lengthening or displacement.

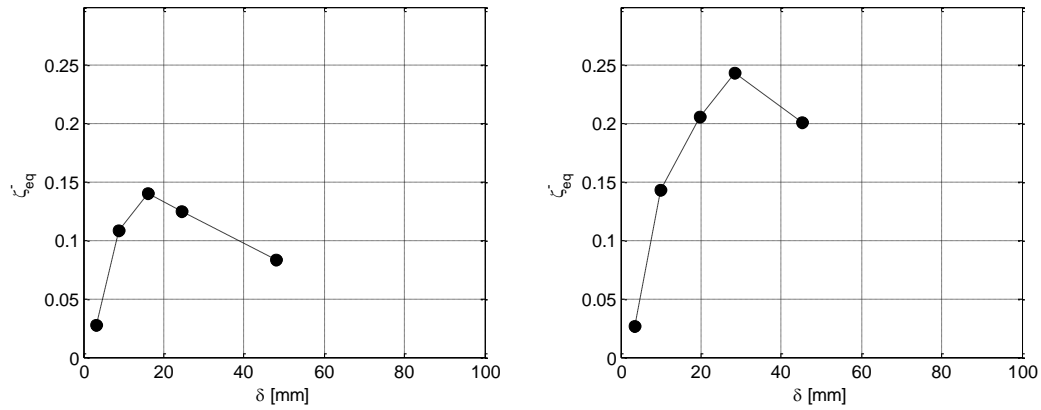


Figure 7.33 RW2R equivalent damping ratio Left) Tension; Right) Compression

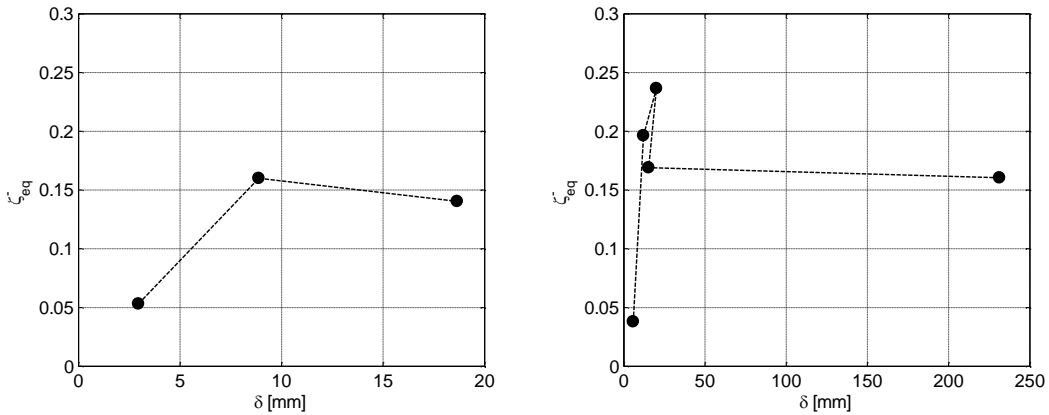


Figure 7.34 TW2R equivalent damping ratio Left) Tension; Right) Compression

From all results shown in the figures above, as expected, due to the asymmetric behavior in tension and compression, the CSBs exhibit quite different dissipative capacities when subjected to cyclic loadings in compression or tension. The maximum values are around 0.25 in the case of compression, while the maximum values remain around 0.15 for the tensile case.

It is worth to note that the last damping ratio of the TW2R in the compressive phase is 0.16, less than 0.24, the maximum value in the same condition. Even if the area was quite big, the shortening was around 200 mm, which is a big value and it was the cause of this decrease. This value is almost equal to the dissipation under tensile loads for the same specimen when it was subjected to 14 kN and a lengthening of 8mm.

In conclusion, it is possible to say that values of the energy dissipation capacity under tensile loadings are limited. In compression a good dissipative response is obtained, even though the softening response does not allow exploiting the “full plastic

dissipation capacity” (i.e. the dissipation capacity of an elastic-perfectly plastic device). From a practical point of view, the overall dissipation capacity could be enhanced by adopting the symmetric disposition (see Figure 6.6).

7.6. LOCAL DEFORMATIONS THROUGH THE DIC TECHNIQUE

7.6.1. The digital image correlation (DIC)

Digital Image Correlation (DIC) is an innovative non-contact optical method that employs image registration techniques for accurate 2D and 3D measurements of changes in images. This is often used to measure deformation, displacement, strain, and optical flow.

DIC is simple to use and cost effective compared to other techniques such as speckle interferometry, and more accurate and subjective than manual measurement methods, leading to a huge range of potential applications.

Its use is expanding into challenging areas, such as to be used over a period of time without a need for a permanent set up, or to apply it to hard to reach areas via small unmanned helicopters carrying camera and relocation equipment.

DIC has several advantages over other optical techniques such as laser shearography and speckle interferometry, which are generally more expensive and more difficult to use outside the laboratory as they require precise setup and low vibrational environments, also the equipment is not always suitable for use outdoors. In contrast

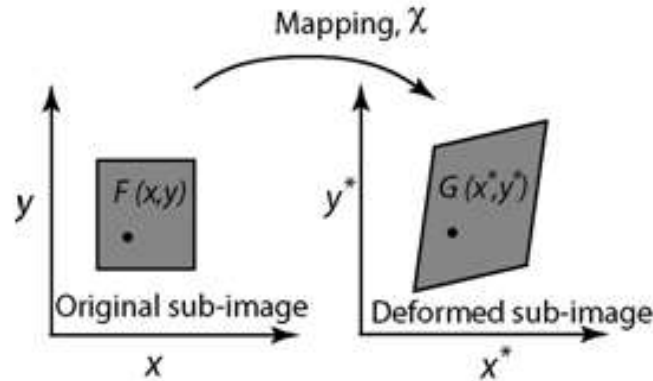


Figure 7.35 Basic concept of the image correlation

DIC works by comparing digital photographs of a component or test piece at different stages of deformation. By tracking blocks of pixels, the system can measure surface displacement and build up full field 2D and 3D deformation vector fields and strain maps. For DIC to work effectively, the pixel blocks need to be random and unique with a range of contrast and intensity levels. It requires no special lighting and in many cases the natural surface of the structure or component has sufficient image texture for DIC to work without the need for any special surface preparation.

Software techniques have been developed to obtain sub-pixel resolutions and allow efficient execution of the algorithms. These allow high-resolution measurements to be made such that with commercially available digital photography, surface deformation can be measured down to one part per million of the field of view.

Images can be obtained from a wide variety of sources including conventional CCD or consumer digital cameras, high-speed video, macroscopes, and microscopes, including scanning electron and atomic force microscopes. The DIC correlation process is not restricted to optical images and can also be applied to other datasets such as surface roughness maps and 2D surfaces of structures like tunnels

7.6.2. The deformation fields through the DIC technique

Deformation fields have been obtained through the DIC technique. To highlight better the state of deformation during the test phase, the specimen was covered with a white paint as a base color and then dotted by a black paint. The specimen has been finally positioned under an incandescent lamp to accelerate the drying process of the paint.



Figure 7.36 R3R and RW1R colored to be tested by the DIC technique

This procedure has been conducted on five different specimens: R3R, RW1R, C1T, C2C, and C3R. In this section, we will present some illustrative results.

The result can be an immediate interpretation and, through the chromatic scale present on the right side, it allows to have an immediate assessment of the deformation state of the different areas of the CSB at each stage of the test.

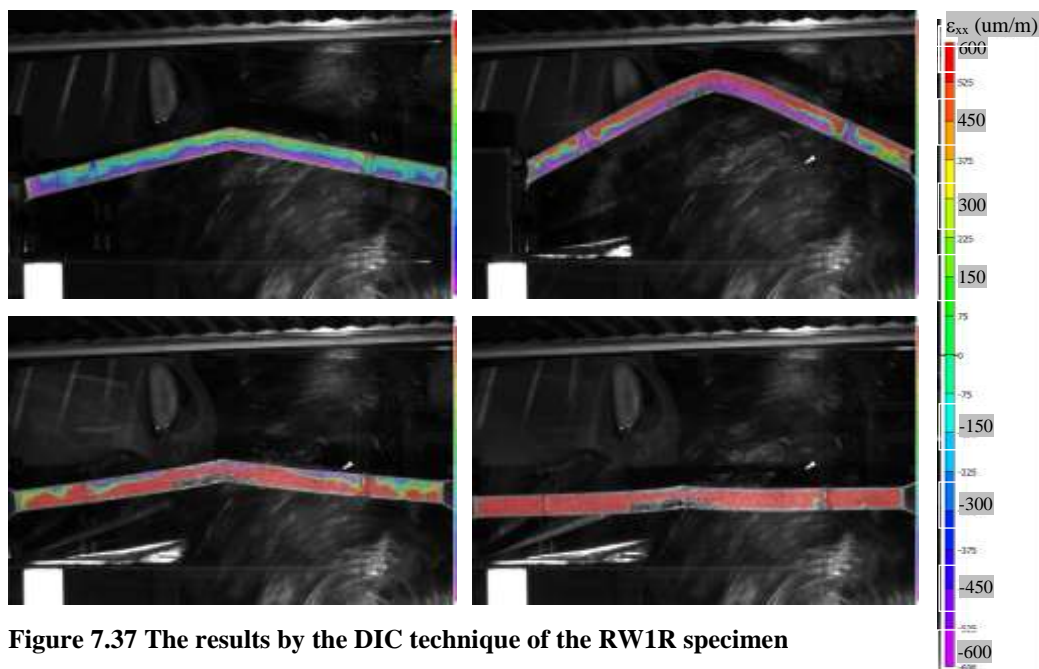


Figure 7.37 The results by the DIC technique of the RW1R specimen

For the specimen RW1R, Figure 7.34 displays the strain contour maps corresponding to the force-displacement response.

The strain field within the elastic range is shown for the full rectangular specimen RW1R in the moment when it was subjected to a negative or compressive lateral force. As expected, the maximum strains are concentrated at the top and bottom of the knee region. It is important to note that the concentration of stresses in the welding zones is less than those along the device. Maybe this fact is due to the thickness of the welding material and in the way of art it was executed.

The deformation field of specimen C1-T within the elastic and plastic range (well beyond the first yielding) under a positive lateral force is displayed in Figure 7.38. It is shown in a different way than the previous specimen to show the correspondence of the qualitative deformation to its location in the force-displacement curve. The deformation field corresponding to the first photo is after crossing the elastic field, it is clear the mostly homogeneous color of the entire device. The second photo corresponds to the hardening behavior of the device and allows to appreciate the extension of the plastic zone. From a simple visual inspection, it appears around 1/3 of the length of the specimen. The deformation fields representative of the third photo in the plateau zone of the force-displacement response allow capturing the evolution of plastic deformations up to the rupture.

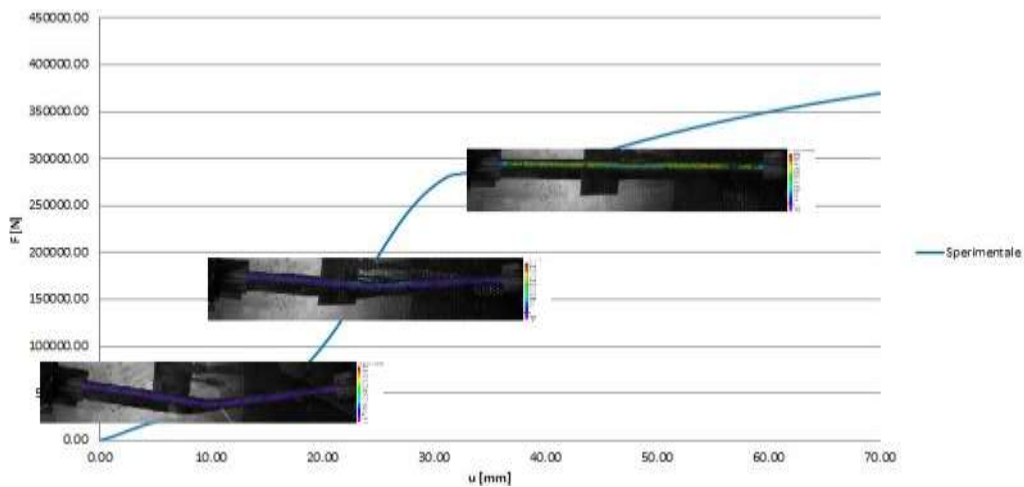


Figure 7.38 The correspondent DIC technique results to the force-displacement behavior curve of the specimen C1T

Figure 7.39 shows the deformation fields within the elastic and plastic range under a negative lateral force for specimen C2C. It can be noted that the deformation field remains quite uniform even up to an imposed lateral displacement of 10 cm corresponding to an increase of 100% in the lever arm.

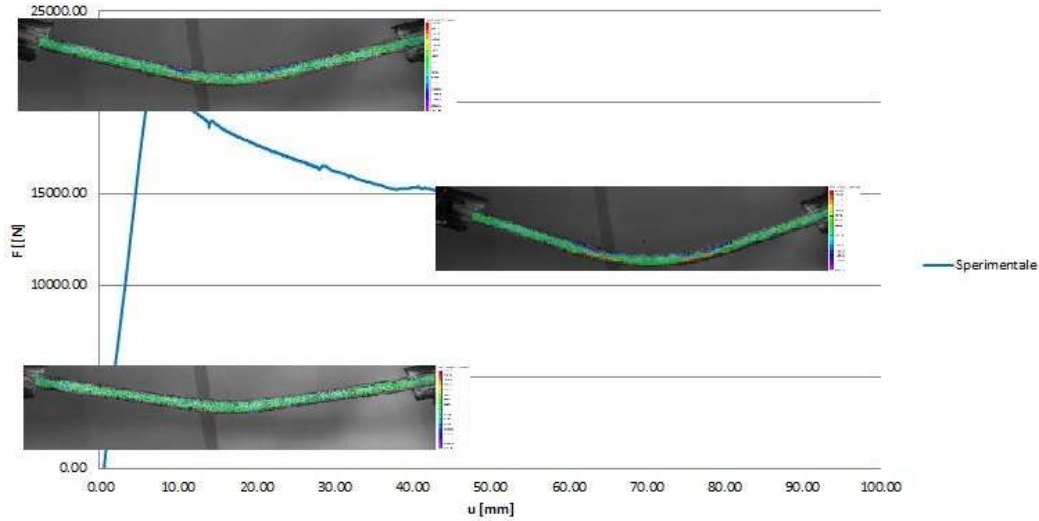


Figure 7.39 The correspondent DIC technique results to the force-displacement behavior curve of the specimen C2C

What is curious about the third photo is that the concentration of stresses are not in the knee zone, but near it. This is due to the fact that the bar, to give the crescent shaped geometrical form, was bended before the test and so it was yielded before the other parts of the element.

In the sequence of photos of Figure 7.37, it is seen clearly the deformation of the material of the specimen C3R which was subjected to reverse cyclic loads. The concentration of stresses is located in the knee zone. It is clear in the last photo that the bottom part of the knee zone is subjected to tension (red color). This is due to the fact that the specimen is subjected to tension and it is in a lengthening part, and the fibers that were under compression before due to compression force, now are under tension stresses.

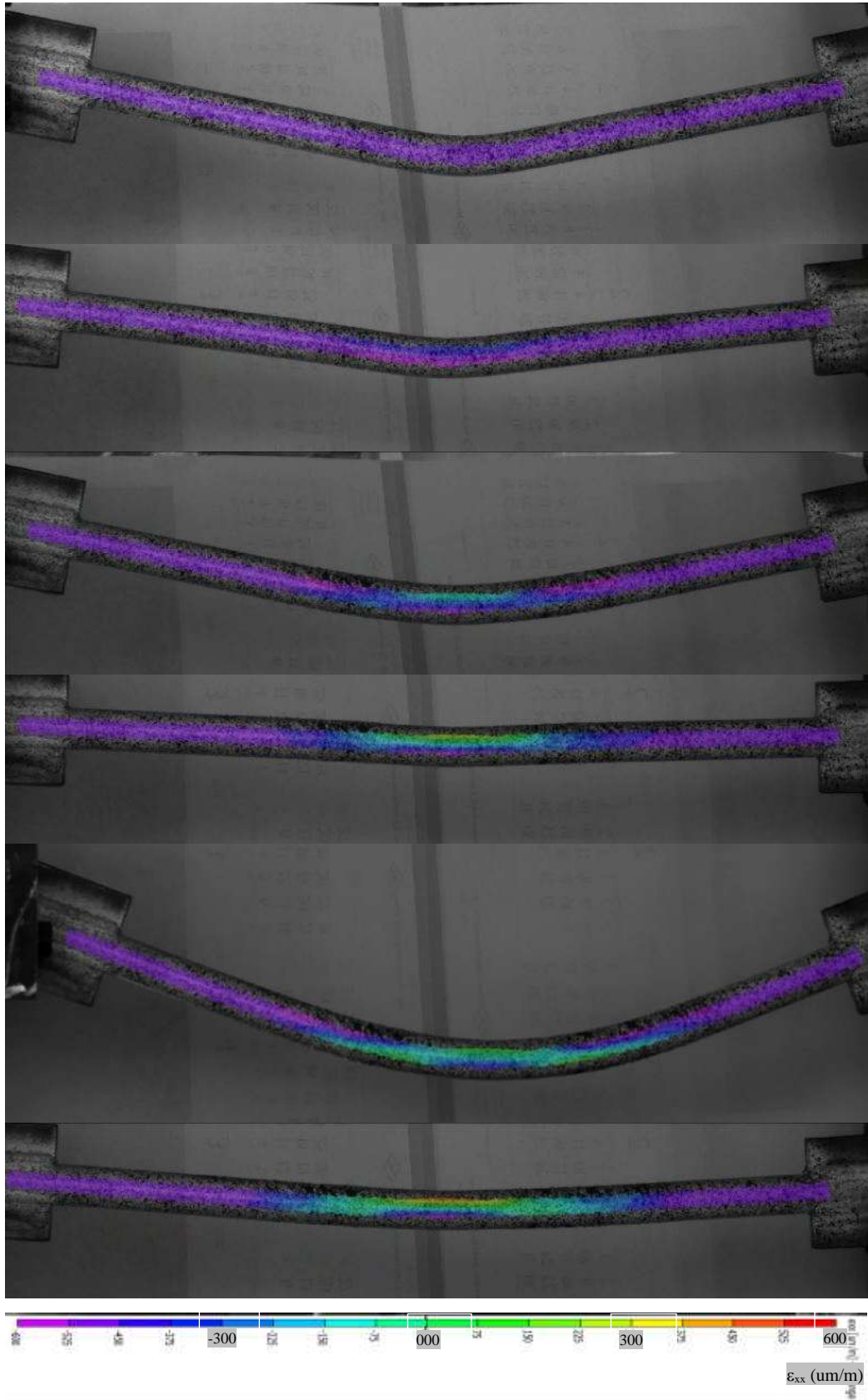


Figure 7.40 The material behavior of the C3R specimen under reversed test

7.7. CONCLUSIONS

In this chapter, different pseudo-static tests conducted on thirteen different specimens of Crescent shaped Brace were presented. The main purpose of those tests was to assess the nonlinear cyclic behavior of those novel steel hysteretic bracing device.

In previous chapters, it was indicated that, from a theoretical point of view, the device, thanks to its geometrical shape, has a number of desirable seismic properties, such as the initial lateral stiffness uncoupled from the first yield strength, a significant ductile capacity and a final hardening to prevent from P- Δ induced collapses.

The device was developed, as we have seen in part A and chapters 5 and 6, to mitigate some predisposed performance. The CSB is constituted by a metallic element made starting from standard profiles. The CSB can be used to resist horizontal actions inserting it in a system dimensioned to behave in a predicted way in a controlled soft-story (so-called floor insulation) under the umbrella of the PBS (Performance Based Seismic Design). In addition, the main results of the experimental campaign may be summarized as follows:

- All specimens, without any exception, have a force-displacement curve similar to the desired one. In tension, it is characterized by an elastic part, ductility, hardening and final ductility before reaching the collapse. In compression, the curve is composed of two different phases, the elastic one which is symmetrical to the elastic part under tensile loads, and a post elastic part which characterizes the softening of the device.
- the rectangular profiles with a large height-to-width ratio tend to experience significant out-of-plane buckling after exposed to large elongations in tension. Such effect is prevented by using cross sections with larger out-of-plane moment of inertia (such as the circular and the rectangular with ribs cross sections);
- CSB made by two straight members welded at the knee cross-section experienced a sudden premature fragile failure at the knee section under tensile load TW1R. Thus, when it is not possible to obtain a device from a unique element (e.g. laser-cut manufactured), the welding should be realized far from the knee sections and

from the ends of the members, like the case of the three specimens RW1R, RW2R, RW3R which behaved as it was expected.

- Regarding the stresses on the welding part, from the DIC technique, it seems that the welded part of the RW1R for example was less stressed than the other part, and the failure came first on the knee zone not on the welded parts.
- The initial elastic stiffness seems to be less the stiffness in the hardening phase of the element which gives the device a good behavior under P- Δ effects.
- The ductility of the system is higher under compressive loads than under tensile loads. For this reason, to exploit the properties of this new device, it is better to insert it in a frame coupled with another one. Thus, when a single device resists to compression and shows a softening behavior, the coupled device will resist tensile loads and shows a hardening behavior. From coupling two crescent shaped braces, it can result a favorable force-displacement curve
- The equivalent damping ratio is higher for compression loadings. In fact, the correspondent values under tensile loads seem to be maximum around 15% while in compression they reach 25%. To notice that under the value of the damping ratio under a softening cycle of compressive load cannot increase the equivalent damping ratio, but it will decrease. It was kind of verification that the dissipative energy in elastic phase, for tensile and compressive loads, was equal. This is due to symmetry of the material behavior for both types of loadings.
- From the final results of the tests carried out on those specimens, all the obtained failures were due to the element, especially failure in the knee section under tensile loadings. Under compression, no failure has been detected. One final observation from the experimental results is to make attention on the way of connection of the device to a real structure. One of the curious results was the deformation and ovalization of the holes where the CSB element has been connected to the machine; even the CSB did not reach the rupture. In real cases, if the connection is not designed in a way to support those deformations, it can be the main cause of failure of the system.

Thirteen tests have been conducted on different Crescent shaped braces following a precise protocol of pseudo-static cycles of tensile and compressive loads. In order to

complete the experimental assessment, future experimental tests will be carried out on different CSBs dispositions, like the coupled CSB or the double CSB that seems to have stiffer behavior.

8. Analytical Numerical Experimental Correlation Study

This chapter provides the comparison between the results from experimental test, analytical and numerical analyses carried out in the present work. Through this comparison, it is possible to validate the accuracy of the analytical model developed and the adequacy in simulating the real behavior of the model analyzed. For sake of simplicity, the case of the rectangular cross section for the Crescent Shaped Brace device is investigated and validated. And then, other comparison will take part like the response of the double CSB and the local deformation of the material.

8.1. THE NUMERICAL RESULTS

The comparison between the experimental results and the analytical ones are displayed in the Table 5-1 . It is possible to remark that for the yielding point, the results of the simple equations developed in chapter 5, Eq. 5.7 and Eq. 5.8, match pretty well the experimental real results. The stiffness as well as the yielding strength describes for the first two columns an elastic behavior. The ultimate strength can change a little bit due to the changeable admitted protocol for each specimen. In general, it is clear that the analytical formulas describing the critical points of the behavior curve of the CSB are compatible with the experimental results.

Specimen	Error! Objects cannot be created from editing field codes. [kN/mm]		Error! Objects cannot be created from editing field codes. [kN]		Error! Objects cannot be created from editing field codes. [kN]		
	Experimental	Eq. 5.7	Experimental	Eq. 5.8	Experimental	Eq. 5.9 (C)	Eq. 5.9 (T)
R1-T	4.2	4.8	17	15.5	324	23.2	248
R2-C	4.0	4.8	16	15.5	22	23.2	248
R3-R	3.4(C) / 4(T)	4.8	10(C) / 15(T)	15.5	22(C) / 320(T)	23.2	248
RR1-R	4.1(C) / 6(T)	4.9	15(C) / 20(T)	15.7	57(C) / 300(T)	23.6	308

RR2-R	4.1(C) / 6(T)	5.8	15(C) / 20(T)	15.7	57(C) / 300(T)	23.6	308
RW1-C+T	3.6 (C)	4.8	15 (C)	15.5	18(C) / 290(T)	23.2	248
RW2-R	3.6 (C)	4.8	15 (C)	15.5	18(C) / 290(T)	23.2	248
RW3-R	3.6 (C)	4.8	15 (C)	15.5	18(C) / 290(T)	23.2	248
C1-T	3.9	4.7	18	16.3	420	27.7	385
C2-C	3	4.7	15	16.3	21.3	27.7	385
C3-R	3.3(C) / 4.7(T)	4.7	10(C) / 11(T)	16.3	54(C) / 250*(T)	27.7	385
TW1-R	2.7(C) / 2.7(T)	3.4	6(C) / 8(T)	10.7	22(C) / 58(T)	14.4	133
TW2-R	2.7(C) / 2.7(T)	3.4	6(C) / 8(T)	10.7	22(C) / 58(T)	14.4	133

Table 8-1 Comparison between analytical and experimental numerical results

8.2. THE FORCE-DISPLACEMENT CURVES

Comparing the graphical results of the analytical formulations, numerical models and experimental tests for the rectangular cross section specimen (4.14x1.5 cm, L=110cm, d=0.1L), the three different curves show a similar trend. In particular, in the elastic phase, both in tension and compression, the three curves are almost the same. The analytical curve shows a yielding point a little bit smaller than the other two curves which coincide perfectly, but the stiffness or the trend is the same. Regarding the post-yielding behavior under tensile loads, the numerical curve shows less ductility than the experimental one while analytical formulas couldn't take in consideration very well this aspect. It shows directly a brittle hardening. The hardening represented by the numerical curve is stiffer than the experimental one. The last part, yielding and hardening behavior of the CSB device under tensile axial load after the ultimate yielding point, is presented by the experimental curve. Numerical curve missed this part while the analytical curve is represented after a long calculation shown in 5.5 which is not easy to do for every type of cross section. In summary, the ultimate yielding point can be described by the analytical formula if we are not taking in consideration the real trend of the force-displacement curve under tensile loads. Figure 8.2

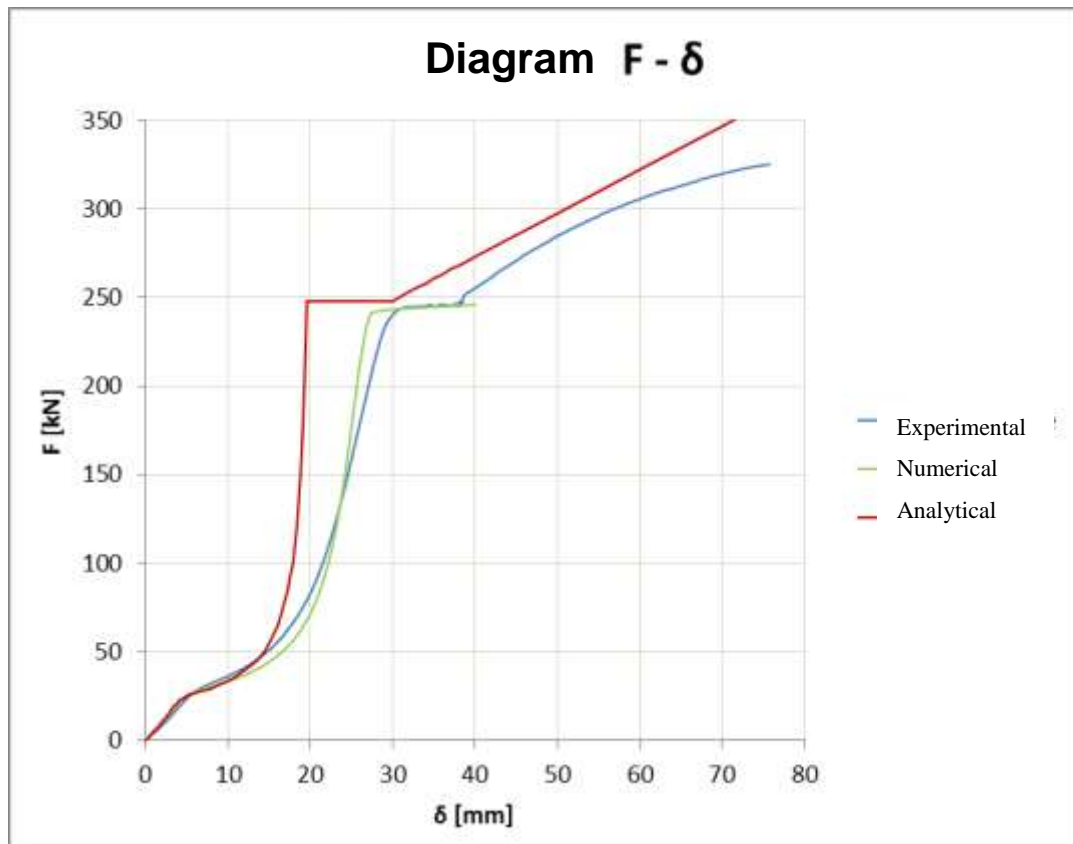


Figure 8.1 The force-displacement curve under tensile loads

If the analytical formula could calculate the exact yielding strength, the compression curve could come as the numerical and experimental curve. However, due to this small difference, the post-yielding curve came with the same difference then before but with the same decreasing trend. Numerical curve and experimental curve are almost equal. Figure 8.2

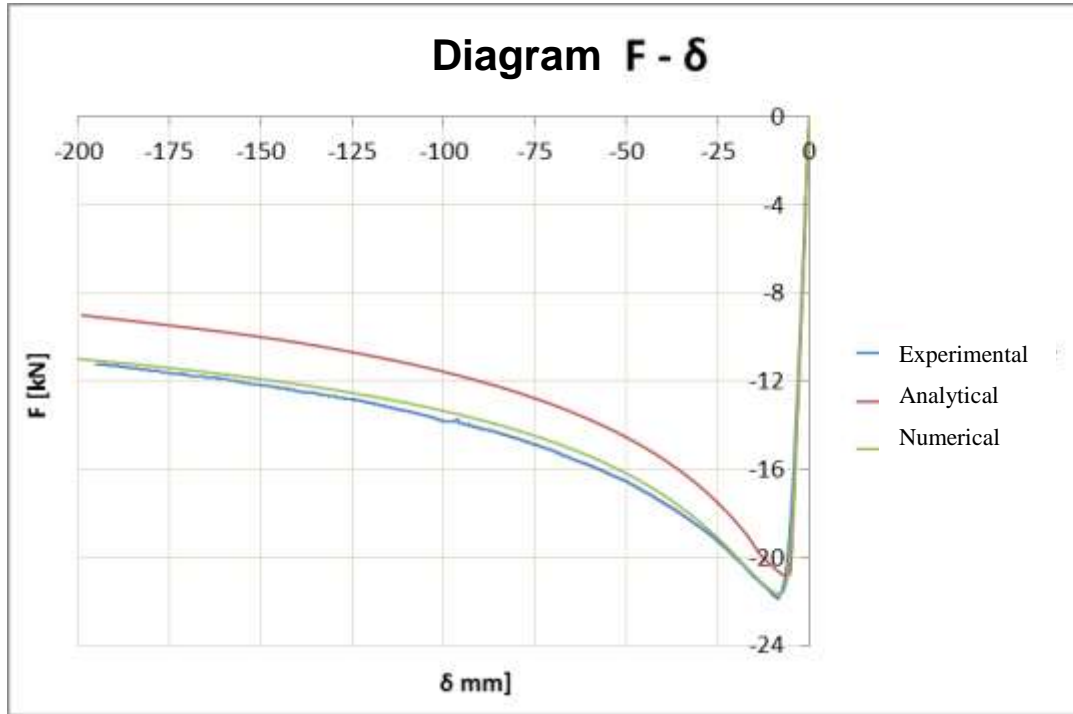


Figure 8.2 The force-displacement curve under compressive loads

8.3. THE MATERIAL BEHAVIOR

The behavior of the material, hardening or softening, stretching or shortening could be detected experimentally through the DIC technique. Using ABAQUS, brick property, it was possible to detect as well the theoretical behavior of the material under similar loading. The results for the rectangular cross section came equal to the experimental results as shown in Figure 8.7. Under tensile loads, the most stressed part is the knee zone, especially the bottom fibers which stressed positively, and the upper fibers are stressed negatively. The knee zone becomes stressed positively when the behavior of the device arrives to only axial behavior. The effect of compression is the same, but the upper part of the knee zone becomes stressed positively. As we remark from the experimental photos, this specimen is the RW1R, and the stresses on the welded parts are less than the other device. This fact depends on the way of welding. However, the numerical model seems as an homogenous isotropic element.

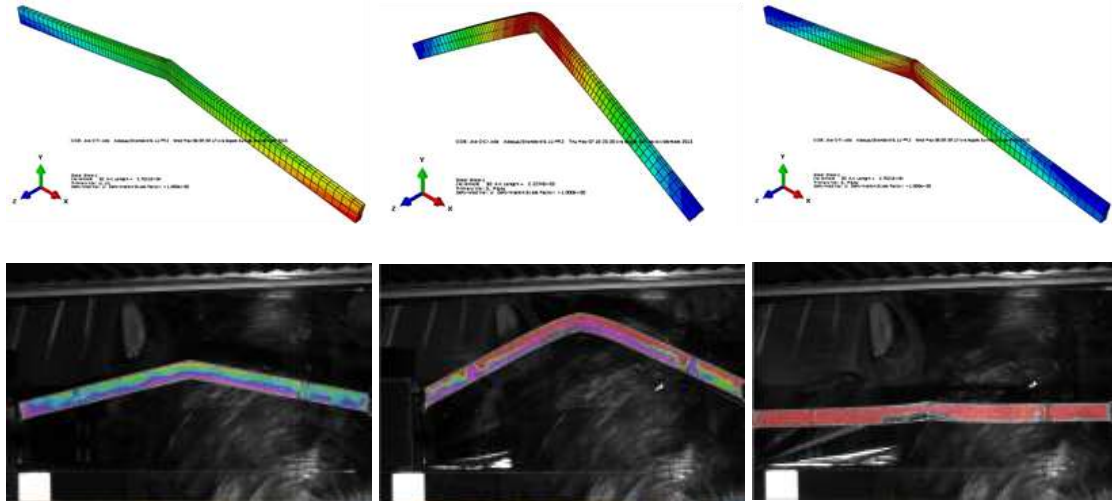


Figure 8.3 Comparison between numerical and real material behavior

The results obtained from circular cross section specimens give different observations. First observations are similar to the one done for the rectangular case, that during tensile and compressive loadings, theoretically the most stressed zone is the knee zone. This is clear from the red color concentrated on the knee zone for the case of C1T (right) and C2C (left). However it is possible to remark that the concentrated stresses are not in the knee zone for the experimental tests, but in the zones near the knee zone. This fact is related to the way of manufacturing the experimental specimens. The circular cross section specimens were bent from a straight circular bar to give the crescent shape, thus, the knee zone where the bar was bent, knew before the other parts of the specimens kind of yielding and the fibers at this zone were already yielding when the test started.

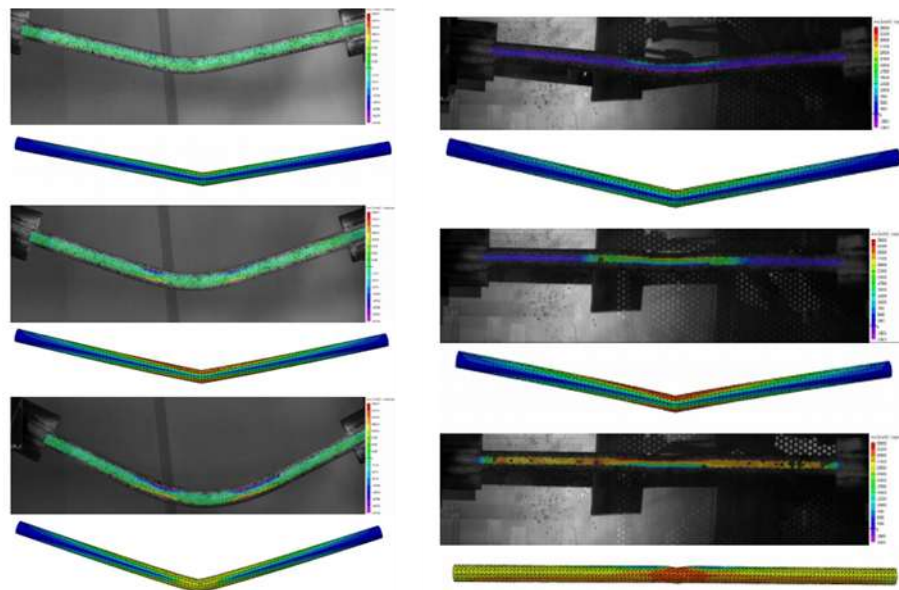


Figure 8.4 Comparison between numerical and real material behavior

8.4. CONCLUSIONS

This chapter presents a correlation between analytical, numerical and experimental results obtained in previous chapters. For sake of simplicity, the study has been developed on just one type of cross section, the fully rectangular cross section.

From theoretical point of view, the Crescent shaped Brace, thanks to its geometrical shape, has a number of desirable seismic properties, such as the initial lateral stiffness uncoupled from the first yield strength, a significant ductile capacity and a final hardening behavior to prevent from P- Δ induced collapses.

First, the experimental findings confirm the expected theoretical behavior of the device, thus suggesting that CSBs could be efficiently used as an enhanced resisting device. In addition, the main results of the done comparisons may be summarized as follows:

- the analytical formulation developed to describe the elastic behavior of the Crescent Shaped Brace can be adopted by engineers and designers to choose the desirable profiles, regarding that the stiffness, ductility and strength are uncoupled

the analytical formulation developed to describe the post-elastic behavior of the Crescent Shaped Brace loaded by compressive loads describe pretty well the real behavior obtained from experimental tests and numerical models.

the analytical formulation developed to describe the post-elastic behavior of the Crescent Shaped Brace loaded by tensile loads cannot describe with accuracy the ductility and hardening behavior, however, a general indications can be taken through those formulas. The difference is due to the formulas which do not take in consideration axial deformability, just the geometrical one.

- the theoretical material behavior of the circular cross section is different than the experimental one. The difference rises from the technique of manufacturing the tested specimen. It was bended on the knee section, thus this zone knew yielding before the test and the zones near the knee point seems the most stressed. The theoretical behavior confirmed what it was expected; the knee zone is the most stressed one.
- the theoretical material behavior of the rectangular cross section confirm the experimental one. The tested specimen was prepared by a laser cut from a rectangular plate, thus all the points of the tested specimen had the same properties before the start of the test, and thus the most stressed zone was the knee zone.
- the material behavior of the rectangular cross section on the welded zone of the fully rectangular welded cross section specimen knew less stresses than the surrounded zones, maybe the main reason go to the way of welding.
- the behavior curve of the single CSB obtained from numerical models confirmed the curve obtained from experimental test. Both curves showed a desirable seismic behavior. The curve is composed of five zones; zone A is the elastic part of the curve correspond to the PO-1 of the objective curve, PO-2 can be placed in the transition zone between zone A and zone B, the transition between Regions B and C should correspond to point PO-3, and point PO-4 should fall in Region C or D before the transition between Regions D and E.
- the behavior of the double CSB has a lot of advantages regarding the high stiffness it showed, the high yielding strength and the ductility capacity. This result was confirmed by analytical and numerical developments.

At the end of this part, it is possible to say that the analytical formulas developed to describe the Crescent Shaped Brace are simple and useful to define in a fast way the characteristics of CSB device. They can be developed more to describe more accurately

the post-yielding part or the other possible dispositions like the double one. However, numerical models, using different commercial software define precisely the global behavior of this device if we put a part the real imperfections and human error. Though, further models can be developed to understand more the behavior of the CSB especially the ductility under tensile and compressive loads for the double disposition. At the end, future experimental tests in order to complete the experimental assessment of different CSBs dispositions will be carried out to exploit the overall non-linear behavior of different CSB dispositions.

PART C: Design Solutions and Procedures

Part C is focused on some possible disposition of the Crescent Shaped Brace elements in different types of structures. Chapter 9 put lights on how the Crescent Shaped Brace can be inserted in a real structure putting light on two types of SDOF structures, the first soft story concept and the Backbone structure. Of course other few examples will be presented as well as a future development. Chapter 10 describes the proposed procedure and an applicative example with a classical disposition of CSB as diagonal braces at the level of the first floor.

9. Possible Dispositions of The Crescent Shaped Braces

After verifying the validity of the Crescent shaped Brace device through analytical and numerical verification and experimental assessment, our study will refer to the possible disposition of the Crescent shaped Brace in some types of structures referring especially to the single degree of freedom structures. For the first hence, it seems that our building will be composed of one floor level, or it will be a water tower for example. However, some multi-levels structures can be considered as single degree of freedom and in this section, we will present briefly two concepts about structures considered as SDOF. The first one is enhanced first soft story and the second one is the Backbone or Strongback structure. After what, a fast possible use of the CSB outside the first story isolation will be presented.

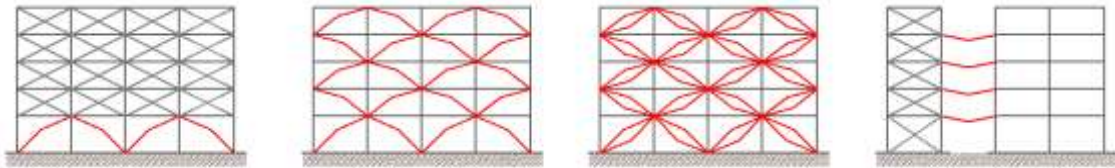


Figure 9.1 Possible dispositions of the CSB: from left to right: first story isolation, Diagonal dissipative elements, double diagonal dissipative elements, and horizontal links

9.1. THE FIRST SOFT STORY CONCEPT

A soft story or a weak story is defined as a story in a building that has considerably low resistance or stiffness or energy dissipation capacity (ductility) to resist the earthquake induced building energy. Weak story structures are characterized by having a floor which has a lot of open space like parking garages, large retail spaces or floors with a lot of windows. [25], [34], [35], [55]

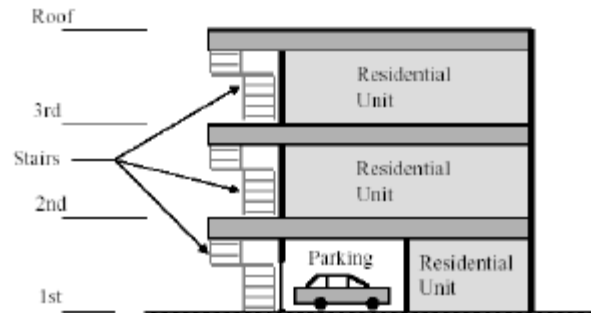


Figure 9.2 An example of a residential building with a weak first story

If a building has a floor which is 70% less stiff than the floor above it, it is considered a soft story building (UBC-1997, IBC-2003 and ASCE-2002). This soft story creates a major weak point during an earthquake, and since soft stories are classically associated with retail spaces and parking garages, they are often on the lower stories of a building, which means that when they collapse, they can take the whole building down with them, causing serious structural damage which may render the structure totally unusable. [38], [64]

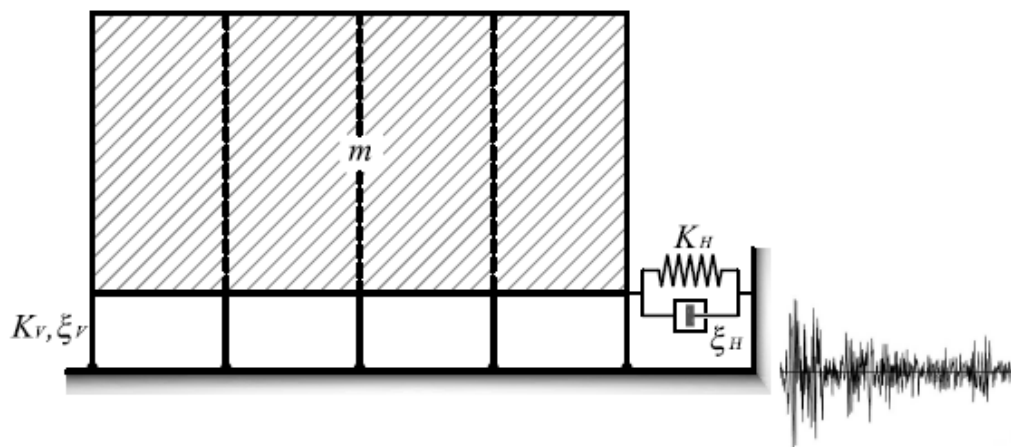


Figure 9.3 The above residential building idealized as a SDOF with the mass of the upper-structure m

The concept of the soft story has been idealized by Fintel and Khan (1969). Researchers had pointed out some aspects of a flexible first story in the 1930s (Martel 1929, Green 1935, Jacobsen 1938). This concept is an effort to reduce acceleration in a building by letting the first floor columns yield during an earthquake and dissipate earthquake energy. However, excessive drifts in the first story coupled with P- Δ effects on the yielded columns may drive buildings to collapse.[38], [40]

The concept of soft first story is extended to incorporate seismic isolation system for separation between the first story and the rest of the building.

The Olive View Hospital damaged in the 1971 after San Fernando earthquake was an example of the behavior of the soft first story. The building survived without major damage to the upper stories, but it could not be repaired because the first story drift was excessive for such a structure without any special arrangement.

The concept has been studied further since then and it is now well understood and discussed in texts. Those buildings with soft first stories and without the necessary additional arrangements are not appropriate for earthquake prone regions. But the practical advantages of having an open first story is often too tempting for architects and even engineers and these types of buildings continue to emerge even today.

Some of the engineers who had to design such an arrangement and who were also conscious of the consequences had to come up with innovative solutions to the potential problems. Chen and Constantinou (1988) describe a building of the Science University of Tokyo where the steel columns are enclosed in hollow concrete casings with gaps between them. There are also dampers at the top of the casings for additional energy dissipation and stability of the steel columns. The Union House in Auckland, New Zealand is supported on long slender piles passing through tubes in the basement which is independently supported on the soft harbor mud. Energy dissipaters located between the columns and the basement using non-sympathetic motions of the piles and the basement to provide the isolation. The Wellington Central Police Station, completed in 1990, uses the same concept. The police station has a 10-story tower block above a separate basement. The tower block was isolated by supporting it on pin-ended piles separated from the ground by hollow sleeves, with horizontal displacement control in the form of lead extrusion dampers located at ground level and pinned between the base of the tower block and the basement.

The reinforced concrete superstructure was stiffened by diagonal bracing which enables the building to move as a rigid body.

Chen and Constantinou (1988) proposed a modified soft first story concept. Their arrangement included Teflon sliders placed at top of some of the first story columns. These columns are tied together with tie beams and are designed to carry a major portion of the vertical load and the lateral load determined by the frictional

characteristics of the Teflon sliders. The remaining columns, usually the least loaded columns along the perimeter, are designed for ductile behavior in order to accommodate large drifts. It is shown that the system provides effective protection to the superstructure. While the rotational hinge demand required of the ductile columns is large, the stability of the system is maintained by the columns fitted with Teflon sliders which may be designed to remain elastic.

Another variation of the soft first story concept is proposed by Todorovska (1999) using inclined rubber base isolators or inclined soft first story columns. The system behaves as a physical pendulum, pivoted above the center of the mass and is more stable than the standard system. Another advantage of the inclination is that the inertia forces of the structure due to rotation about the pivot point cancel to some degree the inertia forces due to the base translation. This should result in smaller relative deformations of the building and smaller inertial forces.

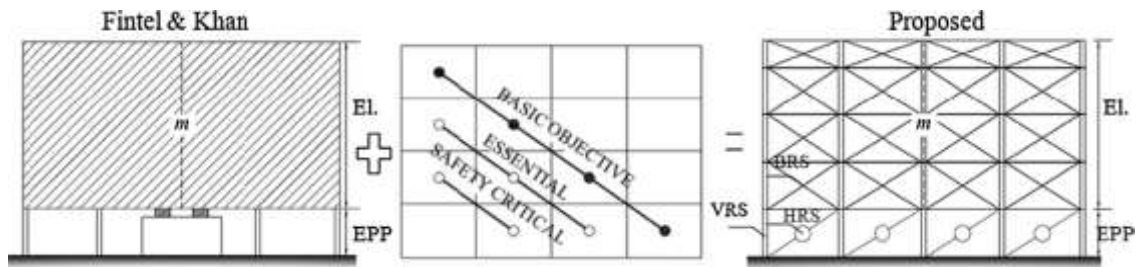


Figure 9.4 The proposed approach is the combination of the Fintel & Khan concept and the PBSO

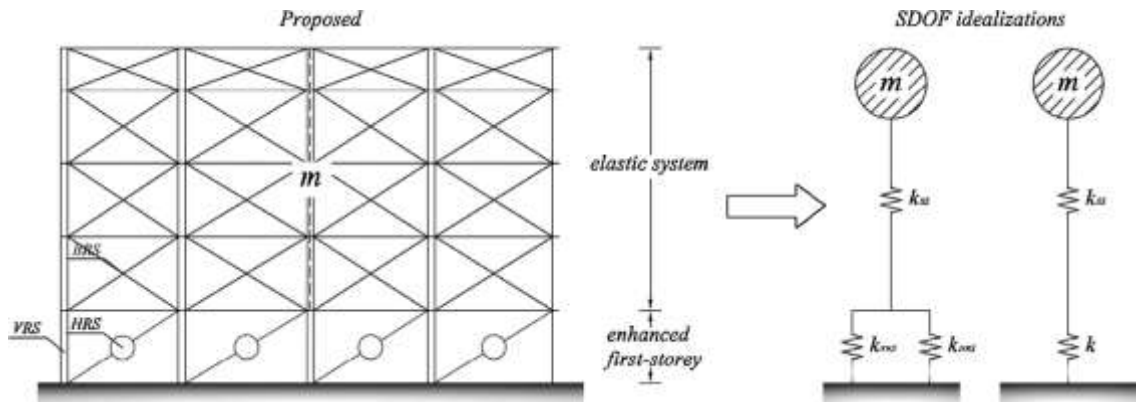


Figure 9.5 The idealization of a building as a simple oscillator or SDOF

From all examples cited above, the conceptual structural design that will be proposed is based on the original idea of the soft story concept for the mitigation of the seismic effects, which is revised and developed within the PBSO framework. The coupling of

these two fundamental concepts leads to the structural solution that may be referred to as “enhanced first-story seismic isolation” (right-hand scheme of Figure 9.4).

An enhanced first-story seismic isolated building is characterized by the following resisting systems:

- Vertical-load Resisting System (VRS), typically beams and columns, which is specifically designed to withstand the static vertical loads.
- First-story Horizontal-load Resisting System (HRS), consisting of special dissipative devices located only at the first story, which is specifically designed in order to accomplish multiple seismic performance objectives.
- Bracing Rigid System (BRS) of the superstructure, consisting in common stiff braces, which is designed in order to behave in the elastic field and provide the superstructure with enough lateral stiffness with respect to the stiffness of the bottom story.

The Stiffening System of The Superstructure:

With regard to the stiffening system of the superstructure, it shall achieve the essential function of making the upper floors over the ground floor sufficiently rigid, with the purpose that:

- The structure can be modeled as a system of one degree of freedom (SDOF);
- The ground floor can actually act as a seismic isolation for the superstructure. It cannot be determined in advance the type and the manner in which to be achieved, by the moment, the only requirements of the superstructure is to remain in the elastic range and possess stiffness sufficiently higher than that of the ground floor.

In practice this bracing system can be dimensioned by applying both the principles of Capacity Design and by checking that the entire performance of the total system is similar to that of a system with one degree of freedom.

Finally, the validity of the calculation procedure described above resides in the fact that the horizontal elements can be considered infinitely rigid in their plan.

The fundamental advantage which emerges from this rationale is the separation (from a design point of view) of the VRS and HRS systems. In such a way the HRS can be

designed specifically to accomplish only seismic requirements (without accounting also for static design issues, which are provided by the VRS only).

9.2. THE STRONGBACK OR BACKBONE CONCEPT

The strongback system is a newly developed seismic force-resisting system that combines aspects of a traditional concentric braced frame with a mast to form a hybrid system that achieves improved seismic performance.

The mast acts like a strong back to help resist the tendency of concentric braced frames to concentrate damage in one or few stories during severe seismic excitations. Therefore, the purpose of the strongback system is to promote uniform story drifts over the height of the structure. [19]

Thanks to the presence of the Strongback system, as part of the bracing system that ensures a uniform distribution of loads and displacements along the height of the building, hence resulting to behave within the elastic field, the overall structure can be idealized as a Single-Degree-Of-Freedom (SDOF).

This schematization can be considered reasonable if the global rotation of the superstructure (assumed as a rigid body system due to the presence of the Strongback system that acts as a mast) is limited.

According to this idealization, the analogy between the actual structural system and its equivalent SDOF idealization can be made. The mass m of the SDOF is equal to the total building mass, while the lateral stiffness K is equal to the total lateral stiffness, which is given by the sum of the HRS lateral stiffness, k_{HRS} , that typically represents the predominant contribution, and the VRS lateral stiffness k_{VRS} , represented in this case by the Strongback contribution.

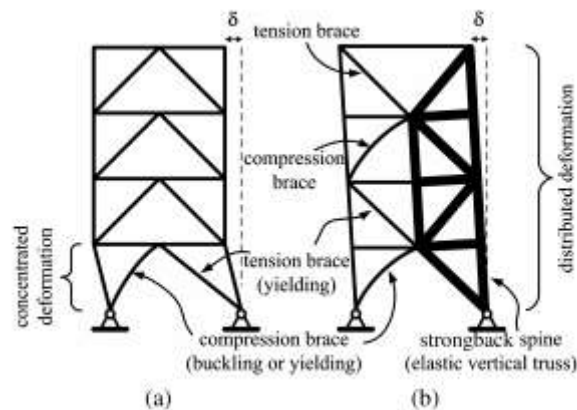


Figure 9.6 Difference between the response of a backbone and soft first story structures

These connect the locations where the diagonal braces intersect along the span of the beams. As illustrated in Figure 9.6, segments of the augmented braced bay are proportioned to provide a continuous vertical truss that is designed to remain essentially elastic during levels of excitation where soft story mechanisms are likely to occur. This vertical truss provides an elastic strongback or mast that imposes a nearly uniform lateral deformed shape over the height of the structure Figure 9.6.

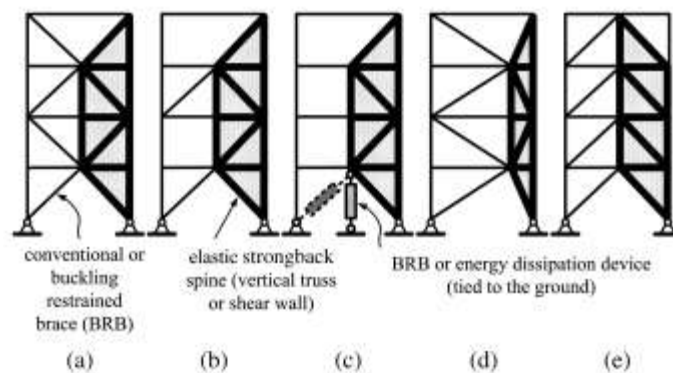


Figure 9.7 Different backbone structures types

The versatility of the SBS systems is twofold: (1) a pinned connection or fixed connection appropriately detailed to develop the required plastic rotations can be provided at the base of the strongback truss; and (2) the braces and beam outside of the strongback truss are sized and detailed to yield, and either conventional buckling or buckling restrained braces (BRBs) can be used in conjunction with the SBS system. Several possible bracing configurations and strongback spines are shown in Figure 9.7. With proper sizing of the strongback mast system, the designer may have greater flexibility in locating and orienting the braces that yield. This system is not limited to

vertical trusses, and other essentially elastic systems, such as steel or reinforced concrete structural walls, large plate girders, and so on, could be used for the strongback mast. For braces with significant differences in tension and compression capacities, it is expected that the overall structural system for a structure would include two strongback bays along each frame line so that an equal number of yielding braces at a floor are loaded in tension and compression. As shown in Figure 9.7 (d) the intersection of the braces at the floor beams can be shifted from the midspan of the beam, which can facilitate proportioning the load to various members in the SBS. In the cases considered herein, the vertical elastic truss portion of the bay is narrower than half the bay width, making the inelastic elements longer so that they have greater length over which to yield. Reducing the inclination of the inelastic braces has the benefit that they can be smaller yet able to resist the same lateral load on the structure. Moreover, for large lateral displacements of the frame, the increased length of the beam in the inelastic portion of the bay will be longer, reducing its shear and the plastic hinge rotations that might form at the ends of the beams. [19],

The Strongback System is not intended to provide supplemental lateral resistance to the structure. In fact, the only purpose of this hybrid solution is to impose a uniform drift distribution through the elastic truss, so that every story is able to contribute to the frame's energy dissipation capacity. The structure outside of the elastic strongback is designed and detailed to yield, controlling the inelastic behavior in the system through either Buckling-Restrained Braces (BRB) or conventional brace yielding and buckling behavior.

The benefit of the Strongback System lies in its tendency to impose nearly uniform drifts in each story. However, it should be noted from simple kinematic considerations that special attention should be placed in the design of the end of the first-floor beam, due to the local concentration of inelastic demand caused by the strongback retrofit. Due to these rotational demands, the peak story drift demand would also be reduced significantly in this configuration. The versatility of the hybrid system is that at the base a pinned or fixed connection can be designed, in order to develop the required plastic rotations, and the braces and beams outside of the strongback truss are sized and detailed to yield. Either conventional buckling or Buckling Restrained Braces (BRB) can be used in conjunction with the SBS.

With proper sizing of the strongback mast system the designer has greater flexibility in locating and orienting the braces that yield. Moreover, this system is not limited to vertical trusses, but other essentially elastic systems could be used for the strongback mast, such as steel or reinforced concrete structural walls, large plate girders, and so on. The vertical truss-like mast frame is a stiff vertical element that enforces a uniform drift profile. This essentially acts as a mode-shaping spine, which straightens out a brace frame's double-curvature deformed shape into a firstmode rocking displaced shape.

The ASCE load protocol for new buildings has been applied to this structure, compared with the Normal Concentric Braced Frame (NCBF), and it successfully completed the standard procedure, mitigating the “soft-story” and “weak-story” behavior as expected. However, the analysis shows that this hybrid solution is more likely to have large residual drifts, of about 0.6%, which leads to the necessity to add re-centering systems to be more resilient after a seismic event. Moreover, large vertical midspan displacements of the beams result to be difficult to repair after high-intensity earthquakes.

9.3. OTHER SOLUTION (EXTERNAL FACADES, SINGLE DISPOSITION, DOUBLE DISPOSITION)

The crescent shaped brace has not been developed to be used only in structures idealized as a SDOF, but to substitute, if it is possible, the classical dissipative braces due to the independency between its stiffness, strength and ductility that gives engineers and designers more freedom in designing and choosing the dissipative systems. Briefly, we will present some other displacement of the CSB, from angle reinforcement, to horizontal links, as dissipative elements inserted in the façade in a single or in a double disposition:

9.3.1. CSB AS A BEAM-COLUMN JOINT

Moment resisting frames are usually used in seismic design. Even they have high strength against horizontal actions; a lot of failures have been detected. Those failure are related to a failure of beam-column connection due to the fractures of the welded connections and brittle failure under heavy stress concentration in these zones.

The semi-rigid frames using bolt connections reduce the brittle failure, however insufficient energy dissipation in the bolt connections can be a reason of failure under cyclic loads.

The Crescent shaped Brace can be proposed to improve this systems structural performance regarding the high energy dissipation capacities they have, the ductile behavior and their easiness of fabrication, assemblage and the low production cost. Of course this is a raw idea, to be studied in details in the future.

9.3.2. CSB AS A HORIZONTAL LINK

The Crescent Shaped Brace devices can be used as horizontal two different structures, like a main core building and seismic dissipative towers. This connecting system not only plays a vital role in alleviating the differential thermal variations between core and dissipative frame, but also has a role in seismic behavior of the structure.

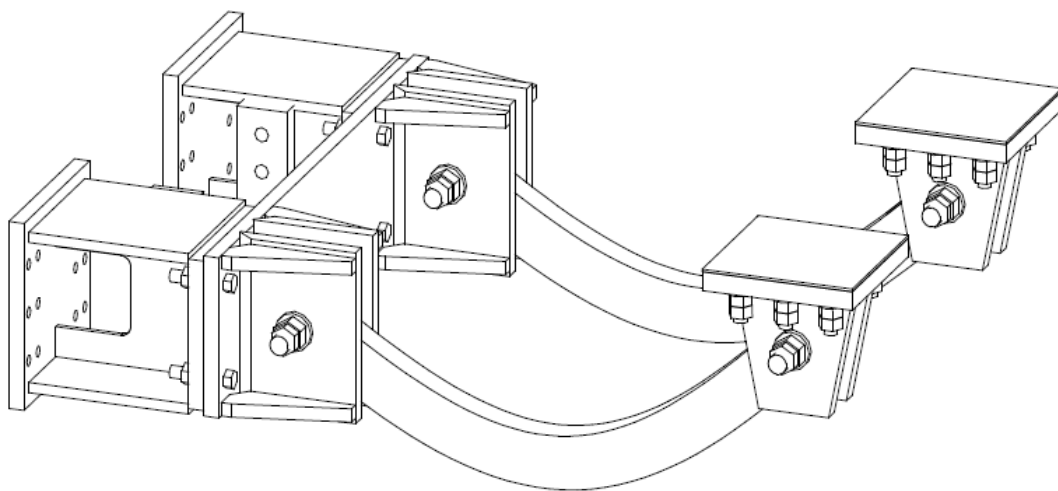


Figure 9.8 Crescent Shaped Brace Element can be used as horizontal link or angle reinforcement

The non-linear behavior of the connection system of type Crescent shaped Brace CSB may lead to a reduction of stresses on the structure.

9.3.3. CSB AS DISSIPATIVE DEVICES ALONG THE STRUCTURE

While writing this thesis, we were developing in parallel a retrofit system for an existing building in Bologna, dating back to 1960 (**Figure 9.9**).



Figure 9.9 VIII Agosto Building in Bologna City

Two possible solutions until now are proposed:

The first one (Figure 9.10) is to insert in every floor, single but coupled crescent shaped braces. The advantages of this disposition are:

- Every level will have its own horizontal resisting system (described in chapter 4) and as consequence the capacity curve of this system which is equal to the sum of the number of CSB installed at this level. As we have seen before, the behavior curve of CSB is favorable for the PBSB performance objectives.
- Every CSB couple is connected in a node connecting beam to column which reduces excessive axial drift on beams.
- Aesthetic geometrical shape

Maybe the only disadvantage of this disposition is the need of calculation for each level the correspondent horizontal resisting system which require some time for sizing it.



Figure 9.10 single coupled CSBs inserted in VIII Agosto building

The second solution is to use double CSB device as described in section 5.7.

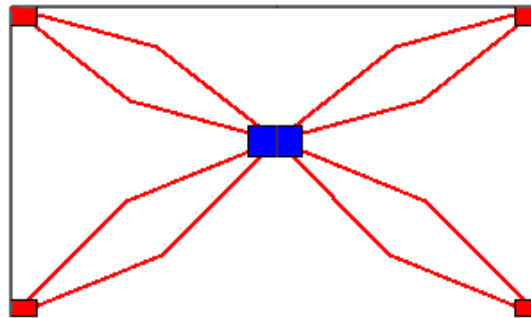


Figure 9.11 A double coupled CSB devices inserted in a frame as a Pall Friction Damper

The double CSB device can be inserted in each bay of the frame as a diagonal Figure 9.12, or it can be inserted as is shown in Figure 9.11, as a pall friction damper.

For the first glance, the advantages of this double disposition seem to be same of the first disposition, but in fact there is another one relying in the fact that this disposition has a high stiffness in comparison with the single disposition, which is 4 times bigger, and the strength of each CSB is multiplied by two without applying any moment at the column/beam node.



Figure 9.12 VIII Agosto enhance by double CSB devices

10. Design Procedure

10.1. INTRODUCTION

The design procedure proposed in this study leads to separate between resisting system to vertical loads and resisting system to horizontal loads, so that no damage arises in structural and non-structural elements. The applicative examples clarify the design steps and show, with numerical results, the effectiveness of this separation in terms of improvement of the seismic response achieving many performances objectives. To achieve this result, a specific hysteretic devices have been used, the Crescent shaped Braces which have been developed in the part B of the thesis.

10.2. THE PROPOSED APPROACH AND THE CONCEPT OF THE FIRST STOREY ISOLATION

The propose method refers to a case study of a multilevel frame enhanced on the level of the ground floor with the new dissipative elements studied within this thesis, the Crescent Shaped Brace, and enhanced by classical rigid braces in all the other floors of the superstructure. The method can be applied for other type of structures of single degree of freedom like one floor structure as industrial structures.

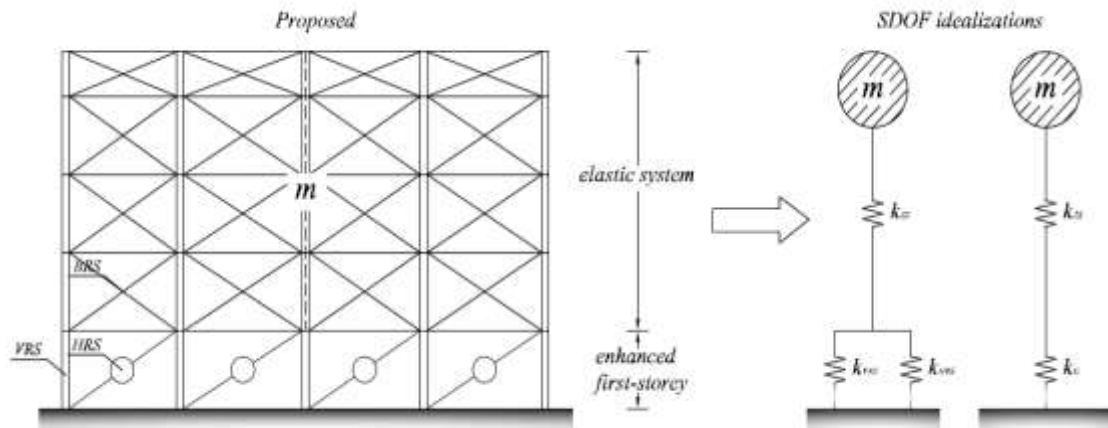


Figure 10.1 The SDOF idealization of the ‘enhanced first story’ isolated structure

The method consists on a modern review of the concept of the “shock-absorbing soft story”, obtained by inserting in the first floor of the structure, a horizontal resisting system designed in terms of rigidity, stiffness and ductility in such a way that it can satisfy the multi-performance objectives of the seismic design within the PBSO.

As it was said before, the structure is assimilated, at least for the first approximation, to a simple oscillator of masse m (equal to the total mass of the upper-structure) with the entire first story which has a function of seismic isolation for the all above upper-structure.

The stiffness and the resistance of the first story are obtained from the sum of the characteristics of the two existing systems which work in parallel:

- The vertical resistance system (VRS) and in particular the columns of the first floor
- The horizontal resisting system (HRS) composed of the dissipative elements CSB in the same floor

The stiffness and the resistance of the upper levels rely on the characteristics of the classical braces inserted in those levels (BRS).

The phases of the design procedure, which to be followed by a proper verification of the seismic behavior of the structure through numerical non-linear dynamic time-history analysis, are as follows:

PHASE 1:

Sizing of the vertical resistance system (VRS) for just the vertical static loads and determination of the capacity curve of this system (VRS) assuming a highly rigid behavior of the upper-structure (or the correspondent structure above the first floor level) due to the inserting bracing system (BRS) which will be designed in phase 3.

The capacity curve of the VRS means the response in terms of base shear – Total displacement of the first floor (where the base shear is transferred due to the VRS only). This curve can be obtained through a non-linear static analysis of the VRS stiffened at the higher levels by classical bracing system (BRS), and like this, the structure without the HRS at the first level takes in consideration the effect of II order.

PHASE 2:

Determination of the objective curve of the objective targets in order to satisfy the following established objectives:

Objectives	Description		
	Protection Level (Limit State)	Condition	Involved Structural capacity
PO-1 (SLO) (SLS)	No –non- structural damage under frequent earthquake	$d_{SLO} < \bar{d}_1$	Lateral stiffness
PO-2 (SLD) (SLS)	No structural damage under occasional earthquake	$F_{SLD} \leq \bar{F}_y$	Strength (yielding shear base)
PO-3 (SLL) (SLU)	Moderate structural	$d_{SLL} \leq \bar{\mu} \cdot d_y$	Ductility

	damage, but the structure is stable and. life safety is protected under rare earthquake		
PO-4 (SLC) (SLU)	Structural collapse is prevented under very rare earthquake	$d_{SLC} \leq \bar{d}_u$	Ultimate displacement

Table 10-1 the performance objectives

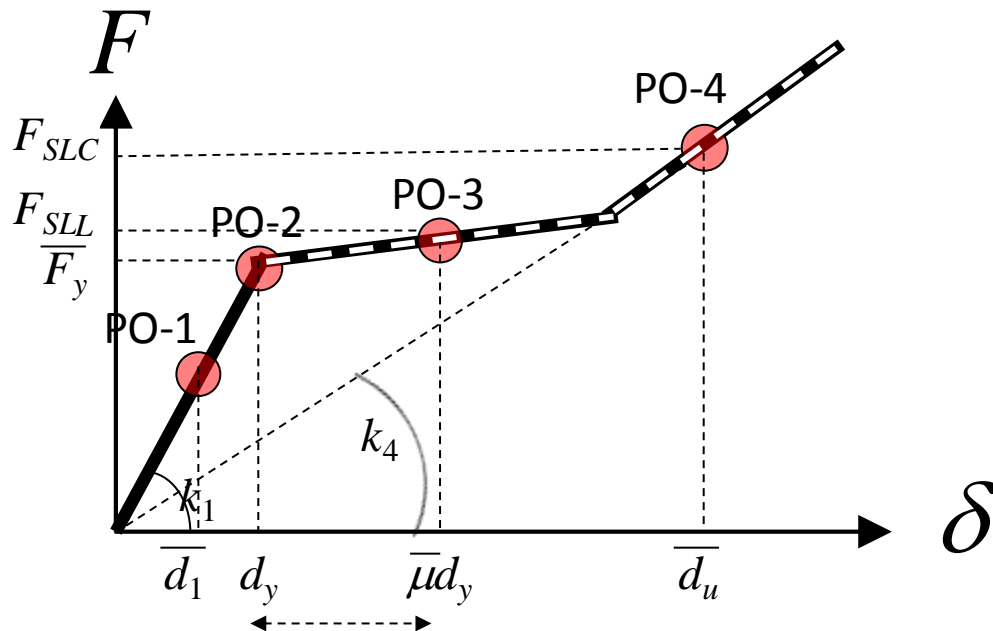


Figure 10.2 The objective curve in terms of stiffness, strength ductility and earthquake levels

The objective curve or the capacity curve of the structure refers to the response in terms of total base shear –lateral displacement of the first floor.

In details, the four performance objectives which determine the objective curve are as follows:

PO-1:

The objective lateral stiffness of the structure is determined imposing that the target displacement under an earthquake SLO is less than a predefined limit displacement of reference \bar{d}_1 :

$$d_{SLO} \leq \bar{d}_1$$

$$S_{d,SLO}(T_1) \leq \bar{d}_1$$

$$S_{a,SLO}(T_1) \left(\frac{T_1}{2\pi} \right)^2 \leq \bar{d}_1$$

$$\left(a_{g,SLO} \cdot S_{SLO} \cdot F_{0,SLO} \right) \frac{T_{C,SLO}}{T_1} \cdot \left(\frac{T_1}{2\pi} \right)^2 \leq \bar{d}_1$$

$$\left(a_{g,SLO} \cdot S_{SLO} \cdot F_{0,SLO} \cdot T_{C,SLO} \right) \cdot \frac{1}{2\pi} \sqrt{\frac{m}{k_1}} \leq \bar{d}_1$$

$$k_1 \geq \frac{m}{4\pi^2} \cdot \frac{\left(a_{g,SLO} \cdot S_{SLO} \cdot F_{0,SLO} \cdot T_{C,SLO} \right)^2}{\bar{d}_1^2}$$

Where m is the total mass of the building, $a_{g,SLO}$, S_{SLO} , $F_{0,SLO}$, $T_{C,SLO}$ are the seismic parameters provided by the Italian norm (D.M. 14/01/2008) for the correspondent studied site under a frequent earthquake of Operational Limit State (SLO) and \bar{d}_1 is the limit displacement of reference (for example: $\bar{d}_1 = 0.005h$ or $\bar{d}_1 = \frac{2}{3}0.005h$, with h is the height of the first floor level).

For applicative cases, we can use the following equality:

$$k_1 = \frac{m}{4\pi^2} \cdot \frac{\left(a_{g,SLO} \cdot S_{SLO} \cdot F_{0,SLO} \cdot T_{C,SLO} \right)^2}{\bar{d}_1^2}$$

Once k_1 is known, the fundamental period of the structure assumed as a simple oscillator is obtained from the following simple equation:

$$T_1 = 2\pi \sqrt{\frac{m}{k_1}}$$

PO-2:

The objective strength of the structure, in terms of total base shear, is determined imposing that the demand in terms of the total base shear under an earthquake SLD is less than the yielding strength:

$$\begin{aligned}
 F_{SLD} &\leq \overline{F}_y \\
 k_1 \cdot S_{d,SLD}(T_1) &\leq \overline{F}_y \\
 m \cdot \left(\frac{2\pi}{T_1} \right)^2 \cdot S_{d,SLD}(T_1) &\leq \overline{F}_y \\
 m \cdot S_{a,SLD}(T_1) &\leq \overline{F}_y \\
 \overline{F}_y &\geq m \cdot S_{a,SLD}(T_1)
 \end{aligned}$$

Where $S_{a,SLD}(T_1)$ is the ordinate of the elastic spectrum under the correspondent acceleration for a period T_1 provided by the Italian norm (D.M. 14/01/2008) for the correspondent studied site under an occasional earthquake of damage Limit State (SLD).

For applicative case, it is possible to consider the following equality:

$$\overline{F}_y = m \cdot S_{a,SLD}(T_1)$$

The yielding displacement of the structure corresponds to:

$$d_y = \frac{\overline{F}_y}{k_1}$$

PO-3:

The system should guarantee a ductile capacity $\bar{\mu}$ in a way that:

$$\begin{aligned}
 d_{SLL} &\leq \bar{\mu} \cdot d_y \\
 S_{d,SLL}(T_1) &\leq \bar{\mu} \cdot d_y \\
 \bar{\mu} &\geq \frac{S_{d,SLL}(T_1)}{d_y} = \frac{S_{d,SLL}(T_1)}{S_{d,SLD}(T_1)} = \frac{(a_{g,SLL} \cdot S_{SLL} \cdot F_{0,SLL}) \cdot \frac{T_{C,SLL}}{T_1}}{(a_{g,SLD} \cdot S_{SLD} \cdot F_{0,SLD}) \cdot \frac{T_{C,SLO}}{T_1}} \cong \frac{a_{g,SLL}}{a_{g,SLD}}
 \end{aligned}$$

In the applicative cases, the verification of the validation of this condition can be done through numerical non-linear analysis like pushover analysis.

Without loose of generality, in order to point out the PO-3 point in a concrete way on the curve, we will assume the following equality:

$$\bar{\mu} = \frac{S_{d,SLV}(T_1)}{S_{d,SLD}(T_1)} \cong \frac{a_{g,SLV}}{a_{g,SLD}}$$

And in order to limit the effects of the second order II, we will hypothesize a certain hardening behavior $\alpha \cong 1 \div 1.3$:

$$F_{SLV} = \alpha \cdot \bar{F}_y$$

PO-4:

To avoid excessive displacement under high seismic actions correspondent to a limit state of collapse (SLC), it is better to have an effective stiffness equals to:

$$\begin{aligned} d_{SLC} &< \bar{d}_u \\ S_{d,SLC}(T_4) &\leq \bar{d}_u \\ S_{d,SLC}(T_4) \left(\frac{T_4}{2\pi} \right)^2 &\leq \bar{d}_u \\ (a_{g,SLC} \cdot S_{SLC} \cdot F_{0,SLC}) \cdot \frac{T_{C,SLC}}{T_4} \cdot \left(\frac{T_4}{2\pi} \right)^2 &\leq \bar{d}_u \\ (a_{g,SLC} \cdot S_{SLC} \cdot F_{0,SLC} \cdot T_{C,SLC}) \cdot \frac{1}{2\pi} \sqrt{\frac{m}{k_4}} &\leq \bar{d}_u \\ k_4 &\geq \frac{m}{4\pi^2} \cdot \frac{(a_{g,SLC} \cdot S_{SLC} \cdot F_{0,SLC} \cdot T_{C,SLC})^2}{\bar{d}_u^2} \end{aligned}$$

For applicative example, it is possible to consider the following equality:

$$k_4 = \frac{m}{4\pi^2} \cdot \frac{(a_{g,SLC} \cdot S_{SLC} \cdot F_{0,SLC} \cdot T_{C,SLC})^2}{\bar{d}_u^2}$$

To which correspond an elastic shear base, for the SLC case, equal to:

$$F_{SLC} = k_4 \cdot \bar{d}_u = \frac{m}{4\pi^2} \cdot \frac{(a_{g,SLC} \cdot S_{SLC} \cdot F_{0,SLC} \cdot T_{C,SLC})^2}{\bar{d}_u}$$

Where: $a_{g,SLC}$, S_{SLC} , $F_{0,SLC}$, $T_{C,SLC}$ are the seismic parameters provided by the Italian norm (D.M. 14/01/2008) for the correspondent studied site under a very rare earthquake of Limit State of collapse (SLC) and \bar{d}_u is the limit ultimate displacement at the SLC (for example $\bar{d}_u = 0.025h$, with h is the height of the first floor).

PHASE 3:

Design of the stiffening system of the Upper-structure (BRS)

The fundamental period of the upper-structure defined as the structure above the first floor level, stiffened by a diagonal bracing system should satisfy the following condition:

$$\frac{T_1}{T_{upper-structure}} > 3$$

From this formula, it is possible to have the necessary stiffness of the BRS and then to calculate the characteristics of the dissipative diagonals.

PHASE 4:

Determination of the capacity curve of the system resisting to the horizontal actions (HRS) will be done as the difference between the objective curve already known from phase 2 and the capacity curve of the vertical resisting system already known from phase 1. The capacity curve of the HRS means the response in terms of base shear transferred through the HRS and lateral displacement of the first floor level.

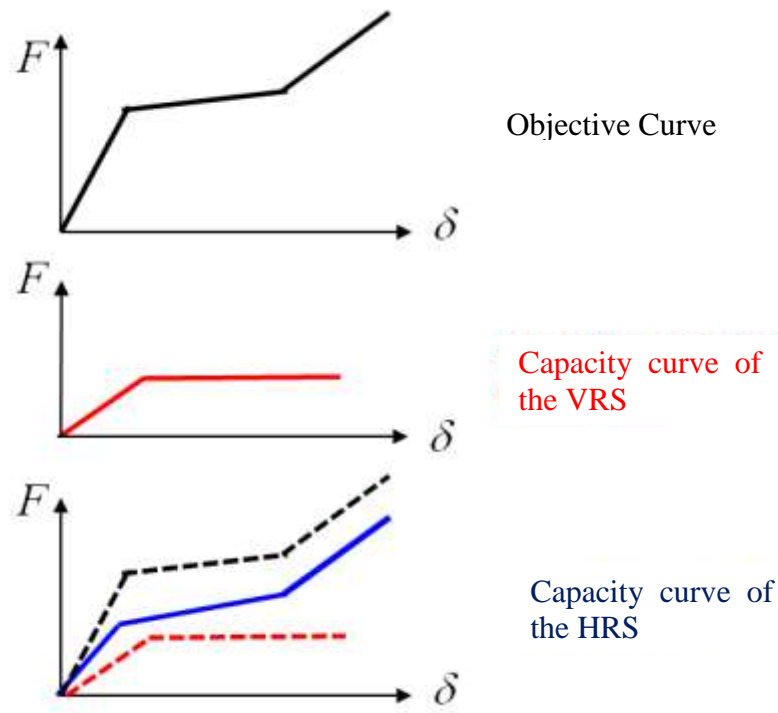


Figure 10.3 The different resisting systems of the proposed approach

PHASE 5:

Design of the HRS composed of n couples of hysteretic dissipative element of CSB, based on the capacity curve of the HRS determined already in phase 3.

Once the capacity curve of the HRS is obtained, the elastic stiffness of this system k_{HRS} and the yielding strength $F_{y,HRS}$ are known, and so the stiffness and the yielding force of each element CSB can be calculated as follows:

$$k_{CSB} = \frac{k_{HRS}}{2n}$$

$$F_{y,CSB} = \frac{F_{y,HRS}}{2n}$$

Where n represents the number of the coupled CSB devices.

The geometrical characteristics of a single CSB device (in terms of section and form) can be calculated through the following two equations:

$$k_{CSB} = \frac{3EJ \cos^2 \theta}{L^3} \cdot \frac{1}{\left(\frac{d}{L}\right)^2 \left(1 + 2\left(\frac{d}{L}\right)^2\right)}$$

$$F_{y,CSB} = \frac{W_{el} f_y \cos \theta}{d}$$

Where: E is the steel Young's Modulus, J is the moment of inertia of the CSB cross section, θ is the angle between the diagonal joining the two extremities of the CSB element and the horizontal level, L is the length of this diagonal or the segment joining the two extremities of the CSB, d is the distance between the knee point of the CSB and the diagonal ("arm" of the device), W_{el} is the elastic resistance modulus of the correspondent cross section, f_y is the steel yielding force (of the design).

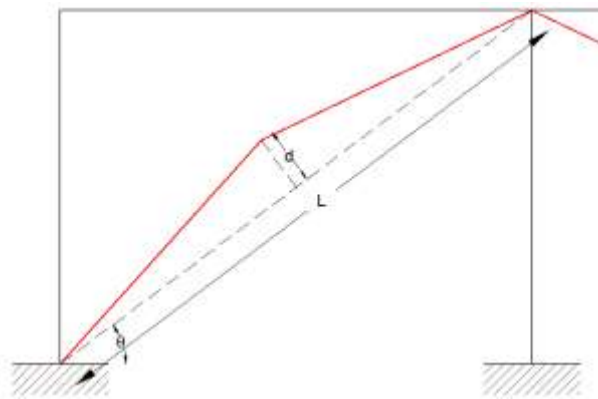


Figure 10.4 CSB inserted in a frame

Those two equations enable to calibrate the HRS composed by CSB elements in a way to satisfy the first to performance objectives: PO-1 and PO-2. In particular, by the use of those two equations, it is possible to calculate the moment of inertia J and the arm d , two necessary parameters to design the CSB

The peculiarity of the geometrical shape of the CSB and their coupled disposition as indicated in the Figure 10.5 permit (through changing J and d) to calibrate the non-linear response and obtain a curve which satisfy the other two performance objectives PO-3 and PO-4 and then reach the entire desired curve.

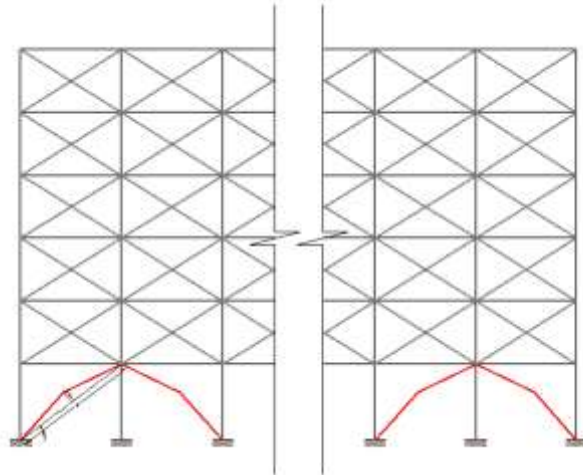


Figure 10.5 Coupled CSB inserted in an ‘enhanced first-story’ building

VERIFICATION:

It is advisable to do a final verification of the designed structure through non-linear dynamic analysis using accelerograms compatible with the spectra representing the different levels of the seismic intensity. The verification should be done through a representation of the effective non-linear response in terms of base shear and the lateral displacement of the VRS of the first floor.

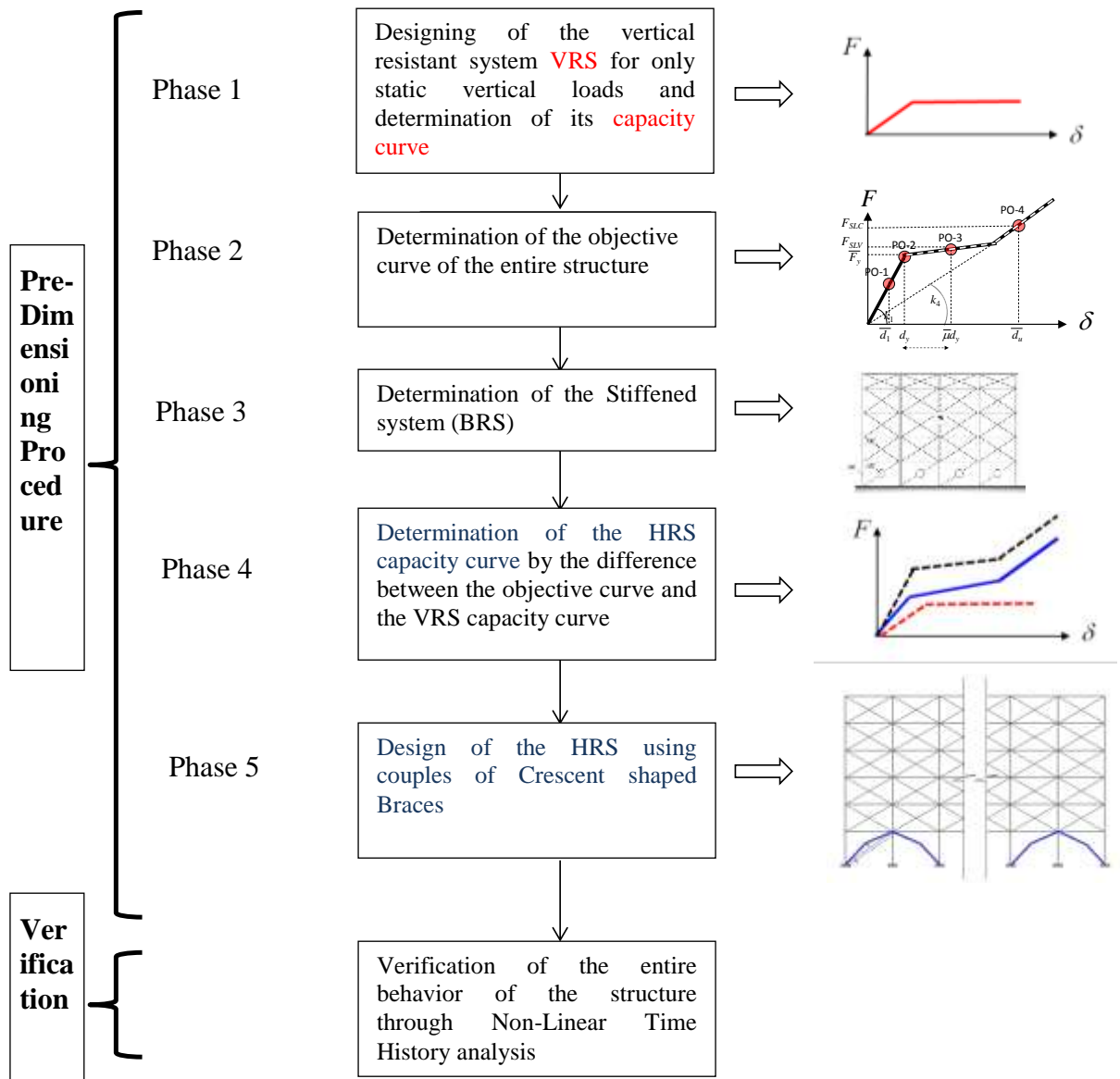


Figure 10.6 Flow-chart of the proposed procedure

10.3. APPLICATIVE EXAMPLE

The applicative example refers to a steel structure residential building, composed of five floors with a rectangular plan of dimensions (36,00m x 18,00m). the structure is composed of six bays in the longitudinal direction and three in the transversal one, each bay has a width of 6.00 m. with a height of each floor equal to 3.50 m. The structure is a regular one, without any irregularities in horizontal or in vertical, from this point, it is possible to study the seismic effect on each direction separately. The structure is built using structural steel grade S355.

The building is supposed to be built in the city of Bologna, based on a terrain of topographical category T1 and soil category C, as it is defined in the §3.2.2 of the D.M. 14/01/2008.

The intension of this procedure is not to do a complete design ready for the execution of this structure, but it is just an example to simplify the design procedure presented before in. section 4.6.

As it was mentioned before in the proposed procedure, the structure is composed of three different resisting systems, separated physically and functionally one from each other:

- Vertical Resisting System (VRS) with the main aim to resist to vertical loads, composed of bays in the two directions, with beams connected at the extremities to columns, which in their turn are fixed to ground.;
- Horizontal Resisting System (HRS) with the main aim to resist to horizontal loads, inserted totally at the first floor in order to be the floor seismic isolation and it is composed of specific dissipative elements with special mechanics characteristics to be determined later;
- A stiffening system of the upper-structure (BRS), installed along the structure above the first floor.

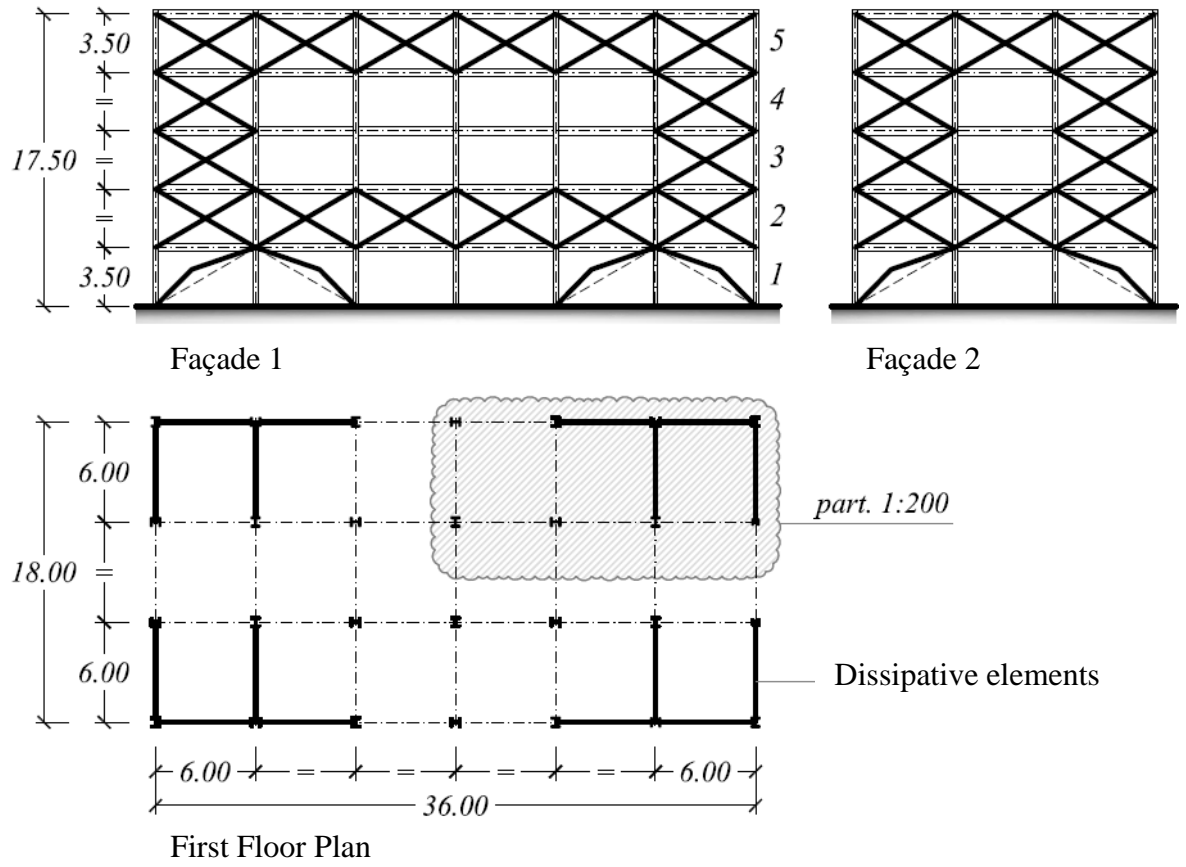


Figure 10.7 Plan and Facades of the first floor of the studied example

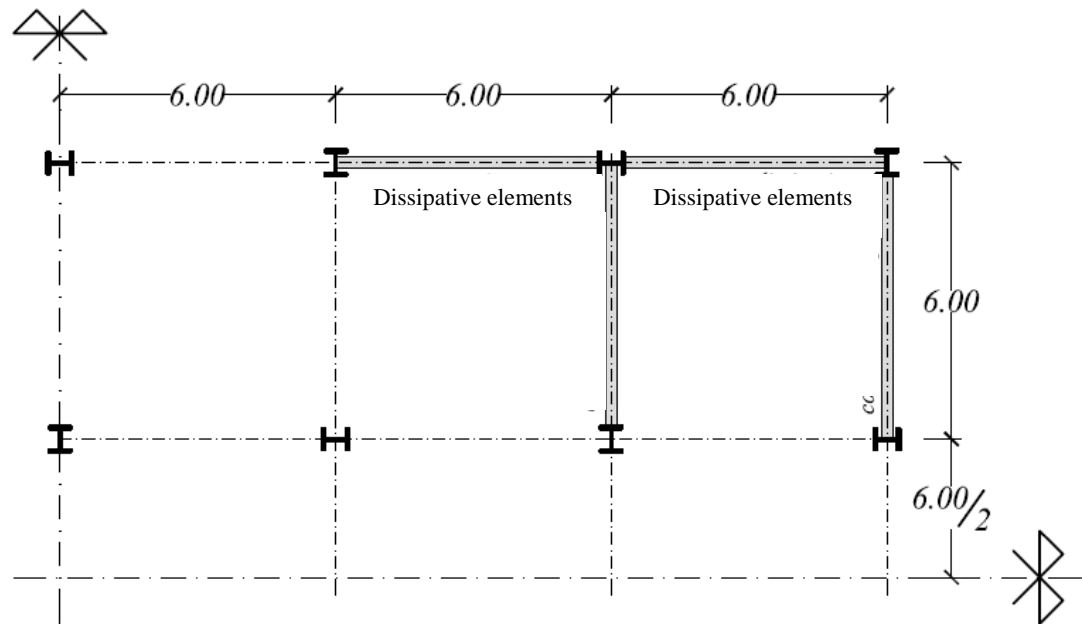


Figure 10.8 Plan Details

Earthquake	T_R (years)	P_{VR} (%)	A_g/g	F_0	T_C^* (S)
Frequent	30	81	0.053	2.478	0.258
Occasional	50	63	0.067	2.482	0.272
Rare	475	10	0.166	2.404	0.310
Very rare	975	5	0.212	2.436	0.315

Earthquake	T_R (years)	S_S	S_T	S	PGA (g)	C_C	T_B (s)	T_C (s)	T_D (s)
Frequent	30	1.500	1.0	1.500	0.080	1.641	0.141	0.424	1.812
Occasional	50	1.500	1.0	1.500	0.101	1.641	0.146	0.439	1.868
Rare	475	1.461	1.0	1.461	0.243	1.545	0.160	0.479	2.264
Very rare	975	1.390	1.0	1.390	0.295	1.538	0.161	0.484	2.448

Table 10-2 Parameters to define the seismic hazard for the city of Bologna

10.3.1. Load Analysis

Generic Slab			
Slab Self Weight:		3,00 kN/m ²	G ₁
Plasterboard Ceiling		0,20 kN/m ²	
Plaster	0,10 m × 8,00 kN/m ³ =	0,80 kN/m ²	
Pavement	0,06 m × 20,00 kN/m ² =	1,20 kN/m ²	
Partitions		1,20 kN/m ²	
		<hr/>	
		3,40 kN/m ²	G ₂
Overload (Life Load)		2,00 kN/m ²	Q _{k1}
Roof Slab			
Slab Self Weight:		3,00 kN/m ²	G ₁
Plasterboard Ceiling		0,20 kN/m ²	
Insulation		0,15 kN/m ²	
Waterproofing		0,05 kN/m ²	
Cover		0,60 kN/m ²	
Solar Energy System		0,25 kN/m ²	
		<hr/>	
		1,25 kN/m ²	G ₂
Overload (snow)	0,8 × 1,50 kN/m ² =	1,20 kN/m ²	Q _{k2}
External walls (1m of height)			
Brick wall	0,30 m × 12,00 kN/m ³ =	3,60 kN/m ²	
Interior Plaster	0,015 m × 20,00 kN/m ² =	0,30 kN/m ²	
Insulation		0,10 kN/m ²	
		<hr/>	
		4,00 kN/m ²	G ₂
Structural elements			
Beams		0,50 kN/m ²	
Columns		0,25 kN/m ²	
Other (Braces, etc)		0,25 kN/m ²	
		<hr/>	
		1,00 kN/m ²	G ₁

10.3.2. Numerical Application:

Phase 1:

The sizing of the vertical resisting system was done in an order to satisfy the norm regarding the SLU and SLE.

The following sections have been used for the different structural elements:

- I-shaped cross section IPE500 for the beams
- H-shaped cross section HEB400 for the columns

Capacity curve of the vertical resisting system VRS:

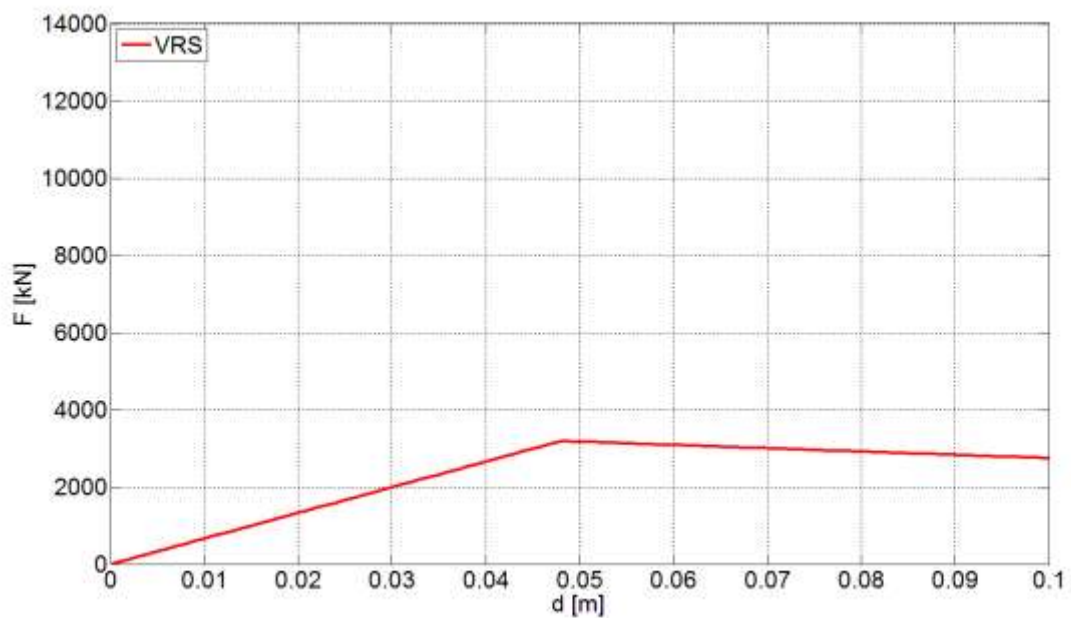


Figure 10.9 VRS Capacity curve

Phase 2:

PO-1:

Displacement limit of reference:

$$\bar{d}_1 = 0.005h = 0.005 \cdot 3.50 \text{ m} = 0.0175 \text{ m}$$

Lateral Objective Stiffness:

$$k_1 = \frac{m}{4\pi^2} \cdot \frac{(a_{g,SLO} \cdot S_{SLO} \cdot F_{0,SLO} \cdot T_{C,SLO})^2}{\bar{d}_1^2} = \frac{29970 \text{ kN}}{4\pi^2 \cdot g} \cdot \frac{(0.08g \cdot 2.478 \cdot 0.424)^2}{(0.0175 \text{ m})^2} \cong 173000 \frac{\text{kN}}{\text{m}}$$

Natural Period of the structure:

$$T_1 = 2\pi \sqrt{\frac{m}{k_1}} = 2\pi \sqrt{\frac{\frac{29970 \text{ kN}}{9.81 \frac{\text{m}}{\text{s}^2}}}{173000 \frac{\text{kN}}{\text{m}}}} = 0.835 \text{ s}$$

PO-2:

Objective Strength of the structure (in terms of the total base shear)

$$\bar{F}_y = m \cdot S_{a,SLD}(T_1) = m \cdot \frac{(a_{g,SLD} \cdot S_{SLD}) \cdot F_{0,SLD} \cdot T_{C,SLD}}{T_1} = \frac{29970 \text{ kN}}{g} \cdot \frac{0.101g \cdot 2.482 \cdot 0.439 \text{ s}}{0.835 \text{ s}} \cong 3960 \text{ kN}$$

Displacement correspondent to the yielding point:

$$d_y = \frac{\bar{F}_y}{k} \cong \frac{3960 \text{ kN}}{173000 \frac{\text{kN}}{\text{m}}} \cong 0.023 \text{ m}$$

PO-3:

Minimum needed ductility capacity $\bar{\mu}$:

$$\bar{\mu} \geq \frac{a_{g,SLV}}{a_{g,SLD}} = \frac{0.166g}{0.067g} = 2.48$$

Assuming $\alpha = 1.3$ we obtain:

$$F_{SLV} = \alpha \cdot \bar{F}_y = 1.3 \cdot 3960 \text{ kN} = 5148 \text{ kN}$$

PO-4:

Ultimate displacement to not be exceeded for the SLC:

$$\bar{d}_u = 0.025h = 0.025 \cdot 3.50 \text{ m} = 0.0875 \text{ m}$$

Efficacy stiffness:

$$k_4 = \frac{m}{4\pi^2} \cdot \frac{(a_{g,SLC} \cdot S_{SLC} \cdot F_{0,SLC} \cdot T_{C,SLC})^2}{\bar{d}_u^2} = \frac{29970 \text{ kN}}{4\pi^2 \cdot g} \cdot \frac{(0.295g \cdot 2.436 \cdot 0.484)^2}{(0.0875 \text{ m})^2} \cong 118000 \frac{\text{kN}}{\text{m}}$$

To which corresponds a total elastic base shear for the SLC equal to:

$$F_{SLC} = k_4 \cdot \bar{d}_u = 118000 \frac{\text{kN}}{\text{m}} \cdot 0.0875 \text{ m} = 10325 \text{ kN}$$

FASE 3:

The period of the upper-structure (the structure above the first floor level) stiffened by classical diagonal braces should verify the following condition:

$$T_{sovrastuttura} < \frac{T_1}{3} = \frac{0.835 \text{ s}}{3} = 0.28 \text{ s}$$

To guarantee this condition, it is sufficient to use profiles type UPN 320 for the bracing system.

Phase 4:

The capacity curve of the resistant system to the horizontal actions (HRS) is obtained from the difference between the objective curve obtained in phase 2 and the capacity curve of the vertical resistant system obtained in phase 1.

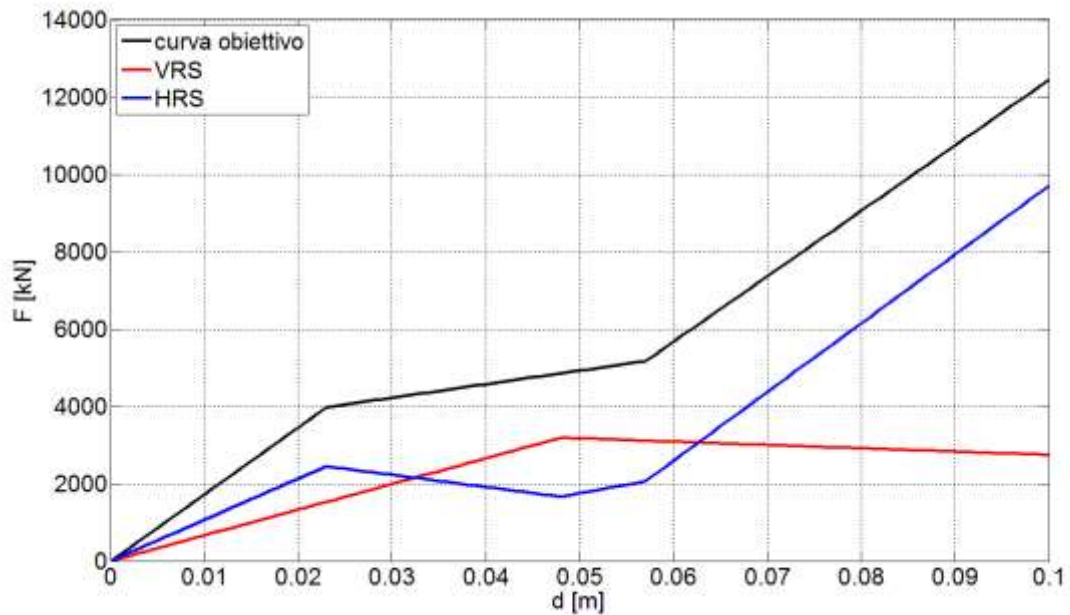


Figure 10.10 The objective curve (black), VRS capacity curve (Red) and the HRS capacity curve (Blue)

In particular, we obtain:

$$F_{y,HRS} = 2450 \text{ kN}$$

$$k_{HRS} = \frac{2450 \text{ kN}}{0.023 \text{ m}} \cong 106500 \frac{\text{kN}}{\text{m}}$$

Phase 5:

Supposing that four couples ($n=4$) of CSB in each of the two directions are inserted, the following specified characteristics are obtained:

$$k_{CSB} = \frac{k_{HRS}}{2n} = \frac{106500 \frac{\text{kN}}{\text{m}}}{2 \cdot 4} \cong 13300 \frac{\text{kN}}{\text{m}}$$

$$F_{y,CSB} = \frac{F_{y,HRS}}{2n} = \frac{2450 \text{ kN}}{2 \cdot 4} \cong 300 \text{ kN}$$

Adapting cross section type HEB 240 for the single CSB, we obtain the following results:

$$k_{CSB} = \frac{3EJ \cos^2 \theta}{L^3} \cdot \frac{1}{\left(\frac{d}{L}\right)^2 \left(1 + 2\left(\frac{d}{L}\right)^2\right)} =$$

$$= \frac{3 \cdot 2.1 \cdot 10^8 \frac{\text{kN}}{\text{m}^2} \cdot 11260 \cdot 10^{-8} \text{m}^4 \cdot \cos^2 30^\circ}{(6.95 \text{ m})^3} \cdot \frac{1}{(0.1)^2 (1 + 2(0.1)^2)} \cong 15500 \frac{\text{kN}}{\text{m}}$$

$$F_{y,CSB} = \frac{W_{el} f_y \cos \theta}{d} = \frac{938 \cdot 10^3 \text{ mm}^3 \cdot \frac{355}{1.05} \frac{\text{N}}{\text{mm}^2} \cdot \cos 30^\circ}{(0.1 \cdot 6950 \text{ mm})} \cong 395 \text{ kN}$$

The results obtained above validate very well the previous specifications.

The following figures show the relation force-displacement of the single CSB (as designed) under tensile loads, under compressive loads and so the total response of a couple of CSB when one is subjected to tension and the other to compression.

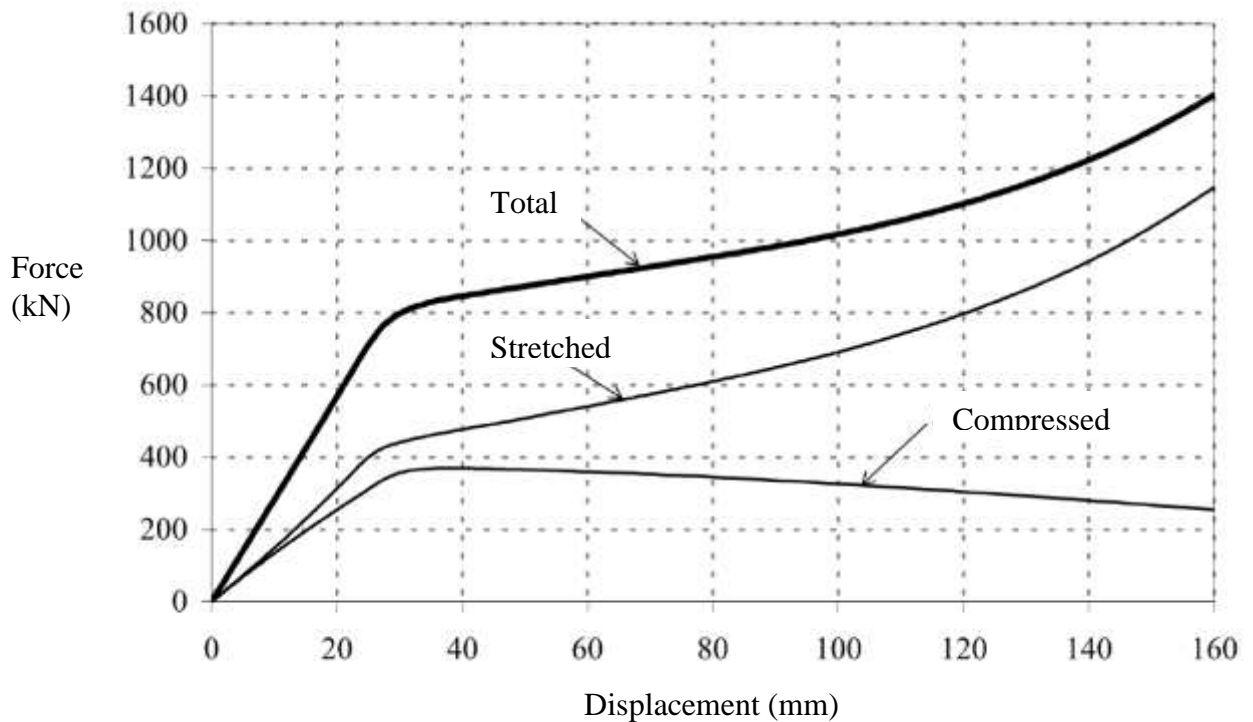


Figure 10.11 the total response F-d of a couple of CSB, one is stretched under tensile loads, the other is compressed under compressive loads (cross section HE240B, $d/L=0.1$)

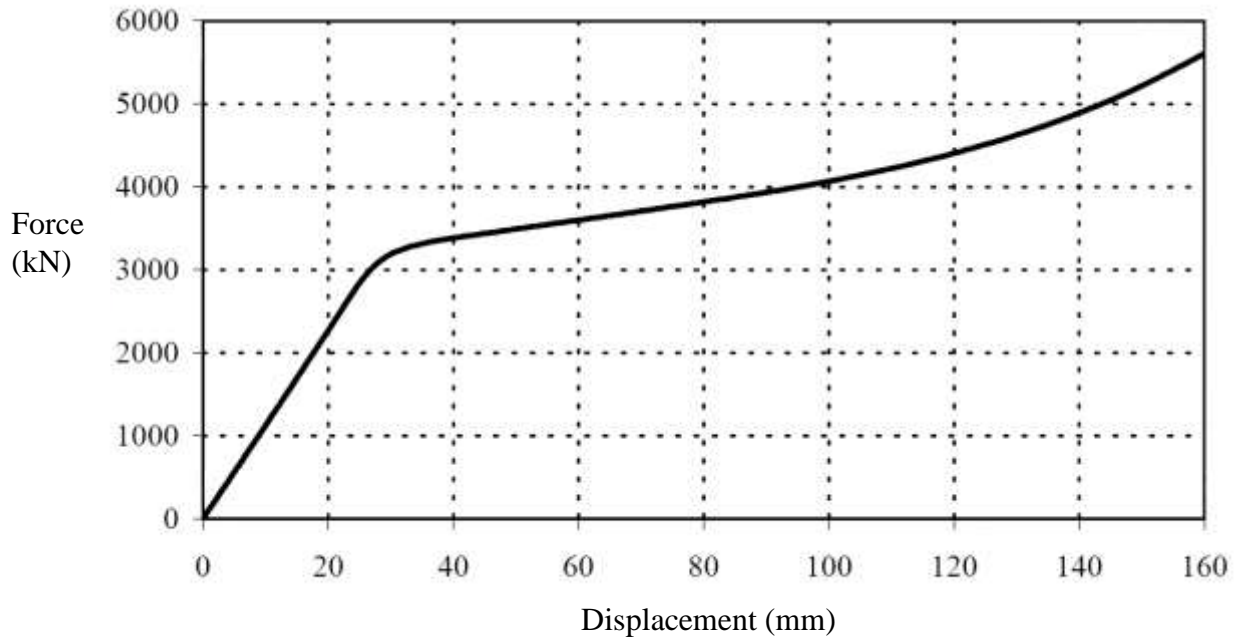


Figure 10.12 Capacity curve of the Horizontal Resisting System (HRS) composed of four couples of Crescent shaped Braces stretched/compressed in every direction

After following this procedure for pre-dimensioning the horizontal resisting system and the different structural elements, it is desirable to do a final verification through a finite element model using non-linear time history dynamic analysis and correspondent accelerograms spectra.

10.4. CONCLUSIONS

In this chapter, the original idea of the soft story seismic isolation, originally proposed in the 1960s by Fintel and Khan is revised and enhanced in light of the recent developments in the earthquake engineering field. The rationale of the proposed approach lies in the concept of the “enhanced first-story seismic isolation”, which results into a structural system which is able to provide a predefined behavior under multiple seismic intensity levels.

For sake of clearness, the conceptual approach is presented and fully detailed with reference to a specific case study in which the story seismic isolation system is realized through the insertion of special braces, the “crescent shaped braces”, at the first story, while traditional cross stiff braces are used at the upper stories.

The proposed design approach relies on a total separation between the Horizontal Resisting System HRS and the Vertical Resisting System VRS. It involves a structure dimensioning by fitting the actual pushover curve of the structure to a “target pushover curve”, which is representative of the seismic idealized behavior of the structure. It is showed that the design process may be easily represented within the Capacity Spectrum Method, also accounting for P–D effects.

Thus, the proposed approach may represent a valid option for the practitioner in order to design a building structure characterized by specific seismic performances.

11. Conclusions and Future Developments

11.1. MAIN CONCLUSIONS

With this thesis, a new steel hysteretic dissipative device has been presented. It is the Crescent shaped Brace or CSB. Its behavior has been analyzed in detail by subjecting thirteen different specimens to different pseudo-static cyclic tests of traction and compression.

The idea behind the Crescent shaped Braces came as a solution to a new conceptual structural design proposed in the first chapters based on the coupling of two fundamental concepts of the PBSB and the soft-first story building.

The main philosophy of the proposed procedure is to separate vertical resisting system (VRS) from horizontal resisting system (HRS) in order to study separately the behavior of the HRS against horizontal loads in order to accomplish multiple seismic performance objectives within the PBSB.

In part A and C, this conceptual approach is presented and fully detailed with reference to a specific SDOF case study, more precisely an enhanced first-storey seismic isolated building in which the storey seismic isolation system is realized through the insertion of special braces, called “crescent shaped braces”, at the first storey, while traditional cross stiff braces are used at the upper storeys. Thus, the studied structure is characterized by the following resisting systems:

Vertical-load Resisting System (VRS), typically beams and columns, which is specifically designed to withstand the static vertical loads.

First-storey Horizontal-load Resisting System (HRS), consisting of special dissipative devices located only at the first storey to resist horizontal forces.

Bracing Rigid System (BRS) of the superstructure, consisting in common stiff braces, which is designed in order to behave in the elastic field and provide the superstructure

with enough lateral stiffness with respect to the stiffness of the bottom storey. Thanks to the presence of the superstructure bracing system, the upper storeys can be considered as a single rigid block compared to the first floor, thus allowing a single-degree-of-freedom (SDOF) idealization.

The proposed design/verification approach involves a first phase of structure dimensioning by fitting the actual pushover curve of the structure to a “target pushover curve”, which is representative of the seismic idealized behaviour of the structure. It is showed that the design process may be easily represented within the Capacity Spectrum Method, also accounting for P–D effects. Thus, the proposed approach may represent a valid option for the practitioner in order to design a building structure characterized by specific seismic performances.

The fundamental advantage which emerges from this rationale approach is the separation from a design point of view of the VRS and HRS systems. In such a way the HRS can be designed specifically to accomplish only seismic requirements without accounting also for static design issues, which are provided by the VRS only.

From here, a specific device with a certain behavior was developed to accomplish those seismic requirements; it is the Crescent Shaped Brace. The behavior curve of the CSB arose as a curve composed of elastic part, a ductility phase followed by a strong hardening phase to finish with the final ductility performance leading to the failure or rupture of the system. The boomerang shape of the CSB gives it a similar behavior curve and permits engineer to choose independently between stiffness, ductility and strength.

In the part B of this thesis, we developed analytical formulas to describe the behavior of the Crescent shaped Brace. Numerical models have been developed as well and verified the simplified analytical prediction. Not to forget the thirteen tests performed at the laboratories of the university present results that verified our predictions about the global response of these new devices.

By comparing the curves obtained from the analytical formulas, by numerical modelling and from the experimental tests it is possible to make some observations:

The tensile curve is distinguished by different phases:

The first phase is the elastic phase under flexural behavior, then it is followed by a ductility phase when the element behaves under flexural and axial loads, until reaching the end showing practically an axial behavior passing through a strong hardening behavior.

For the compression instead the curve is characterized by a first linear elastic section followed by descending phase or softening behavior corresponding to a shortening of the device.

In addition to the tensile and compressive strength, it was also investigated for the coupled behavior. The equilibrium path, obtained by summing the tensile and compression curves, is characterized by an ideal curve which can describe well the imposed objective curve by the PBSB design: a first phase of linearity, followed by ductility phase and then a hardening behavior before the ultimate failure.

The double CSB disposition shows as well a similar behavior, even stiffer.

From the results obtained, The Crescent-Shaped Braces can be a good solution for strengthening existing structures or even designing new structures to match certain predefined performance objectives.

It can be deduced that the established hypothesis, the constitutive models and analytical treatment used are appropriate to describe the real behavior of the CSB.

The ease of realization of the device, retrieval of the initial material and the low production costs, allow hypothesizing a rapid production even for high quantities;

11.2. FUTURE DEVELOPMENTS

The new approach of separating VRS from HRS was established in this thesis referring to one type of structure, the first enhanced soft story. In the future, other developments can be done to this procedure to apply it for other typologies of structure.

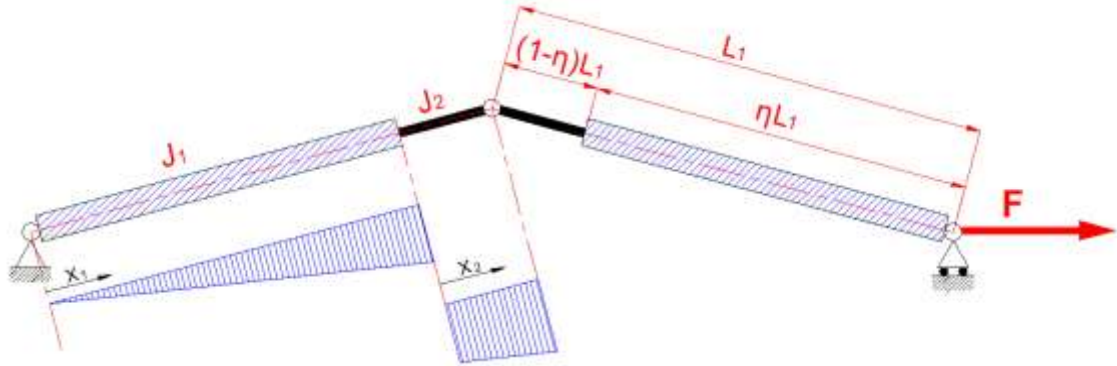
Regarding the CSB, in light of the foregoing, it is possible to say that these new devices have remarkable potentials regarding seismic control and more effort can be put in the design of the crescent-shaped braces to meet other performance objectives which are not studied in this work, such as ductility.

Other typologies of disposition of crescent shaped braces can be developed in the future, like horizontal links, angle reinforcement, the double disposition and the coupled disposition which can be displaced in different ways.

Furthermore, different types of structures equipped with the CSB devices can be of a concern. For instance, the precast reinforced concrete structure might be interesting to study since they are characterized by large displacement, so our devices might show effectiveness in reducing the displacement and thus increasing the performance.

Thanks to these considerations, this study will lead to a further development in the seismic engineering world, developing better structures with higher anti-seismic characteristics.

Appendix A: Calculation of δ (under flexion) of a system composed of single element with two different inertia.



$$M(x_1) = F \cdot x_1 \cdot \sin(\vartheta_1'') \quad x_1 \in [0, \eta \cdot L_1]$$

$$M(x_2) = F \cdot x_2 \cdot \sin(\vartheta_1'') \quad x_2 \in [\eta \cdot L_1, L_1]$$

$$\begin{aligned}
 1 \cdot \delta_{M,PLV} &= \int_0^{L_1} M' \cdot \frac{M}{E \cdot J} dx \\
 &= \int_0^{\eta \cdot L_1} F \cdot x_1 \cdot \sin(\vartheta_1'') \cdot \frac{1 \cdot x_1 \cdot \sin(\vartheta_1'')}{E \cdot J_1} dx_1 \\
 &+ \int_{\eta \cdot L_1}^{L_1} F \cdot x_2 \cdot \sin(\vartheta_1'') \cdot \frac{1 \cdot x_2 \cdot \sin(\vartheta_1'')}{E \cdot J_2} dx_2 \\
 &= \frac{F \cdot (\sin(\vartheta_1''))^2}{E} \cdot \left[\frac{1}{J_1} \cdot \int_0^{\eta \cdot L_1} x_1^2 dx_1 + \frac{1}{J_2} \cdot \int_{\eta \cdot L_1}^{L_1} x_2^2 dx_2 \right] \\
 &= \frac{F \cdot (\sin(\vartheta_1''))^2}{E} \cdot \left[\frac{1}{J_1} \cdot \left[\frac{x_1^3}{3} \right]_0^{\eta \cdot L_1} + \frac{1}{J_2} \cdot \left[\frac{x_2^3}{3} \right]_{\eta \cdot L_1}^{L_1} \right] \\
 &= \frac{F \cdot (\sin(\vartheta_1''))^2}{3 \cdot E} \cdot \left[\frac{(\eta \cdot L_1)^3}{J_1} + \frac{L_1^3 - (\eta \cdot L_1)^3}{J_2} \right] \\
 &= \frac{F \cdot (\sin(\vartheta_1''))^2}{3 \cdot E} \cdot \left[\frac{(\eta \cdot L_1)^3}{J_1} + \frac{L_1^3 \cdot (1 - \eta^3)}{J_2} \right]
 \end{aligned}$$

- For $J_1 = J_2$ we have:

$$\delta_{M,PLV} = \frac{F \cdot (\sin(\vartheta_1^*))^2 \cdot L_1^3}{3 \cdot E \cdot J_1}$$

- For $J_1 \neq J_2$ we have:

$$\delta_{M,PLV} = \frac{2 \cdot F \cdot L_1^3}{3 \cdot E \cdot J_1} \cdot \left(\eta^3 + \frac{1 - \eta^3}{\beta} \right) \cdot (\sin(\vartheta_1^*))^2$$

where:

$$\beta = \frac{J_2}{J_1} \quad \beta \in [0, 1]$$

$$\eta \in [0, 1]$$

References

1. Aiken ID, Nims DK, Whittaker AS, Kelly JM. Testing of passive energy dissipation systems. *Earthquake Spectra* 1993; 9(3):335 –369.
2. AISC. (1997), *Seismic Provisions for Structural Steel Buildings*, American Institute of Steel Construction, Chicago, Illinois.
3. AISC. (2005), *Seismic Provisions for Structural Steel Buildings*, American Institute of Steel Construction, Chicago, Illinois.
4. American Association of State Highway Officials “Guide Specifications for Seismic Isolation Design”, Washington, D.C., American Association of State Highway Officials , (1999)
5. “Application Of Crescent-Shaped Braces In Reinforced Concrete Structures” Master Thesis, Omar Kammouh, University of Bologna, 2015
6. ASCE-ACI Committee 445 on Shear and Torsion, 1998. Recent approaches to shear design of structural concrete. *J Struct Eng* 124:1375–1417.
7. ASCE 7 (2005), *ASCE Standard Minimum Design Loads for Buildings and Other Structures*, ASCE 7-05, American Society of Civil Engineers, Reston, VA.
8. ATC (2007), *Interim Testing Protocols for Determining the Seismic Performance Characteristics of Structural and Nonstructural Components*, FEMA 461 Report, prepared by Applied Technology Council for the Federal Emergency Management Agency, Washington, D.C.
9. Ballio G., Mazzolani F. M., *Strutture in acciaio*, Editore Ulrico Hoepli Milano 1994.

10. Black, C. J., Makris, N., & Aiken, I. D. (2004). Component testing, seismic evaluation and characterization of buckling-restrained braces. *Journal of Structural Engineering*, 130(6), 880-894.
11. Carpinteri A., *Analisi non lineare delle strutture*, Pitagora Editrice Bologna 1998. (Ministero delle Infrastrutture 2008)
12. M.G. Castellano, G.P. Colato, and S. Infanti, Use Of Viscous Dampers And Shock Transmission Units In The Seismic Protection Of Buildings, Published in: *Proceedings of 13th World Conference on Earthquake Engineering Vancouver, B.C., Canada, August 1-6, 2004 Paper No. 2172*
13. CEN., 2003a. Eurocode 8: Design of structures for earthquake resistance - Part 1: General rules, seismic actions and rules for buildings, prEN 1998-1, December 2003, Brussels.
14. Andrew Charleson, *Seismic Design for Architects, Outwitting the Quake*, Architectural Press, imprint of Elsevier, Linacre House, Jordan Hill, Oxford OX2 8DP, UK, first Edition 2008
15. Anil K. Chopra, 'Dynamics of Structures – Theory and Applications to Earthquake Engineering' Prentice-Hall, Berkeley, 1995.
16. Chopra, A.K., Goel, R.K., 2002. A modal pushover analysis procedure for estimating seismic demands for buildings. *Earthq. Eng. Struct. Dyn.* 31, 561–582.
17. C. Christopoulos and A. Filiatrault, "Principles of passive supplemental damping and seismic isolation," in IUSS Press, Pavia, 2006.
18. Chui-Hsin Chen, Jiun-Wei Lai and Stephen Mahin, *Seismic Performance Assessment of Concentrically Braced Steel Frame Buildings*, The 14th World Conference on Earthquake Engineering, October 12-17, 2008, Beijing, China.

19. "Comparison Of Earthquake-Related Consequences Through Loss Analysis Of Different Braced Frame Structural Systems", Tesi di laurea, Vittoria Laghi, Università di Bologna, 2016
20. "Comparisons of Energy Dissipation in Structural Energy Dissipation Devices with Foundation Elements during Seismic Loading", Thesis, Duraisamy S. Saravanathiiban, Faculty of the North Dakota State University of Agriculture and Applied Science, 2010
21. "Crescent Shaped Brace: Dispositivo Metallico Di Dissipazione Isteretica", Tesi di Laurea, Benedetta Ferri, Università di Bologna, 2016
22. DASSE (2007), Cost Advantages of Buckling Restrained Braced Frame Buildings, DASSE Design Inc.
23. Dargush GF, Soong TT. Behaviour of metallic plate dampers in seismic passive energy dissipation systems *Earthquake Spectra* 1995; 11(4):545–568.
24. T. Datta, *Seismic Analysis Of Structures*, Delhi, India: John Wiley & Sons (Asia) Pte Ltd, 2010.
25. A. Dib, M. Palermo, S. Silvestri, T. Trombetti, Experiments on Crescent Shaped Brace, a New Simple Hysteretic Bracing Device, 16th World Conference on Earthquake Engineering, 16WCEE 2017, Santiago Chile, January 9th to 13th 2017
26. A. Dib, M. Palermo, S. Silvestri, T. Trombetti, Experimental assessment of a new steel hysteretic device: Crescent Shaped Brace, 19th IABSE Congress Challenges in Design and Construction of an Innovative and Sustainable Built Environment, Stockholm, Sweden, September 2016
27. A. Dib, M. Palermo, S. Silvestri, G. Gasparini, T. Trombetti, L. Pieraccini, Experiments on Crescent Shaped Braces, 2015, ISEC-8, The Eighth International

- Structural Engineering and Construction Conference, Sydney, Australia, November 23-28, 2015
28. Roger M. Di Julio Jr., Ph.D., Linear Static Seismic Lateral Force Procedures,
29. EN, C. (2004). 10025–2: Hot rolled products of structural steels–Part 2: Technical delivery conditions for non-alloy structural steels. *Brussels, Belgium: European Committee for Standardisation.*
30. Eurocode 2:Design of concrete structures-Part 1-1:General rules and rules for buildings, Brussels: CEN national Members, 2004.
31. Eurocode 8: Design of structures for earthquake resistance -Part 1: General rules, seismic actions and rules for buildings, Brussels: CEN national Members, 2004.
32. P. Fajfar and M. EERI, "A Nonlinear Analysis Method for Performance Based Seismic Design," *Earthquake Spectra*, vol. 16, no. 3, pp. 573-592, 2000.
33. Fierro E, Perry CL, Varner TR. Damping system aids seismic retro. *Modern Steel Construction*, July 1992.
34. Fintel, M., & Khan, F. R. (1968). Shock-Absorbing Soft Story Concept for Multistory Earthquake Structures. *Portland Cement.*
35. Gagliardi S., Trombetti T. (2012). Tesi di Dottorato: Utilizzo di dispositivi isteretici per l'isolamento di piano: strategie per una progettazione sismica di tipo multi-prestazionale.
36. Gray, M. G., Christopoulos, C., & Packer, J. A. (2010, July). Cast steel yielding fuse for concentrically braced frames. In *Proceedings of the 9th US National and 10th Canadian Conference on Earthquake Engineering (Vol. 9)*. Oakland, CA, USA and Ottawa, ON, Canada: Earthquake Engineering Research Institute and the Canadian Association for Earthquake Engineering.

37. Gray, M. G., Christopoulos, C., Packer, J. A., & Lignos, D. G. (2014). Development, Validation and Modeling of the new Cast Steel Yielding Brace System. In Proceedings of Structures Congress 2012 (pp. 71-82).
38. F. Hejazi, S. Jilani, J. Noorzaei, C. Y. Chieng, M. S. Jaafar, A. A. Abang ,Effect of Soft Story on Structural Response of High Rise Buildings, University Putra Malaysia, doi:10.1088/1757-899X/17/1/012034
39. Hwang, J.S. and Sheng, L.H. “Equivalent elastic seismic analysis of base-isolated bridges with lead-rubber bearings”, Engineering Structures, Vol.16, No.3, pp. 201-209(1994).
40. A. Iqbal, Soft First Story with Seismic Isolation System, Bangladesh Consultants Ltd. Dhaka, Bangladesh. 2006 NZSEE Conference
41. Samuele Infanti, M. Gabriella Castellano, Viscous Dampers: A Testing Investigation According To The Hitec Protocol, Published in: Proceedings of Fifth World Congress on Joints, Bearings and Seismic Systems For Concrete Structures, Rome (ITALY), 7-11 October 2001
42. Journal of the seismic rehabilitation of existing buildings 360-2006 instructions “Department of Engineering Management and Planning”,(2006)
43. Ju, J., 1989. Energy-based coupled elastoplastic damage models at finite strains. J. Eng. Mech
44. Theodore L. Karavasilisa and Choung-Yeol Seob, “Seismic structural and non-structural performance evaluation of highly damped self-centering and conventional systems”, Engineering Structures, [VOL33, ISSUE8, August 2011, DOI: 10.1016/j.engstruct.2011.04.001

45. Khatib, I., Mahin, S. and Pister, K. (1988), Seismic behavior of concentrically braced steel frames, UCB/EERC-88/01, Earthquake Engineering Research Center, University of California, Berkeley, 1988-01, 222 pages
46. Krawinkler, H., Gupta, A., Medina, R., and Luco, N. (2000), Loading history for seismic performance testing of SMRF components and assemblies, Sacramento, Calif.: SAC Joint Venture. (SAC/BD-00/10)
47. Jiun-Wei Lai and Stephen A. Mahin, Strongback System: A Way to Reduce Damage Concentration in Steel-Braced Frames, M.ASCE2, J. Struct. Eng., 2015, 141(9): 04014223
48. McKenna, F. (1997). Object Oriented Finite Element Programming: Frameworks for Analysis, Algorithms and Parallel Computing, University of California, Berkeley, Berkeley, CA 94720.
49. Naeim, F. & Kelly, J. M, John Wiley and sons. “Design of seismic isolated structures from theory to practice”,(1999).
50. NEHRP (1997), Recommended Provisions for the Development of Seismic Regulations for New Buildings (and other Structures), Building Seismic Safety Council, Washington, D.C.
51. “Norme Tecniche per le Costruzioni” adottate con il D.M. del 14 gennaio 2008 e pubblicate sul S.O. n. 30 alla G.U. n. 29 del 04/02/2008.
52. Newmark N, Rosenblueth E. Fundamentals of Earthquake Engineering. Prentice-Hall, Inc.: New York, 1971.
53. “Optimal Insertion of viscous dampers in shear type structures for maximum efficiency in mitigation of the seismic effects: the mass proportional damping (MPD) system”, Tesi di laurea di dottorato, Dott. Ing. Stefano Silvestri (2003)

54. M. Palermo, A. Dib, S. Silvestri, G. Gasparini, T. Trombetti, Application of the Equivalent Static Analysis procedure for the seismic design of buildings with added viscous dampers, 19th IABSE Congress Challenges in Design and Construction of an Innovative and Sustainable Built Environment, Stockholm, Sweden, September 2016
55. Palermo M., Silvestri S., Gasparini G., Trombetti T. (2014). Crescent shaped braces for the seismic design of building structures. *MATERIALS AND STRUCTURES*, vol. 47, p. 1-18, ISSN: 1359-5997, doi: 10.1617/s11527-014-0249-z, Codice SCOPUS: 2-s2.0-84893180235.
56. M. Palermo, S. Silvestri, G. Gasparini and T. Trombetti, "Crescent shaped braces for the seismic design of building structures," *Materials and Structures*, vol. 48, no. 5, pp. 1485-1502, 2014.
57. Palermo M., Ricci I., Gagliardi S., Silvestri S., Trombetti T., Gasparini G. (2014). Multi-performance seismic design through an enhanced first-storey isolation system. *ENGINEERING STRUCTURES*, vol. 59, p. 495-506, ISSN: 0141-0296, doi: 10.1016/j.engstruct.2013.11.002, Codice ISI: 000331920700042, Codice SCOPUS: 2-s2.0-84890285603.
58. Avtar s. Pall, Rashmi Pall, Friction Dampers for Seismic Control of Buildings, "A Canadian Experience", 11th world Conference on earthquake Engineering, paper No. 497, Elsevier 1996
59. Paulay, T., Priestley, M.J.N., 1992. *Seismic Design of Reinforced Concrete and Masonry Buildings*, Structural Safety.
60. Pinho, R., & Antoniou, S. (2009). *SeismoStruct Computer Program*.

61. M. C. Phocas and A. Pocanschi, Steel frames with bracing mechanism and hysteretic dampers, Institute of Structural Systems and Structural Building Design; University of Stuttgart; Keplerstrasse 11; 70174 Stuttgart; Germany
62. F. Ponzo, D. Cesare, D. Nigro, A. Vulcano, F. Mazza, M. Dolce and C. Moroni, "JETPACS project: dynamic experimental tests and numerical results obtained for a steel frame equipped with hysteretic damped chevron braces," *J Earthq Eng*, vol. 16, pp. 662-685, 2012.
63. P. Pozzati, C. Ceccoli, 'Teoria e tecnica delle strutture', Vol. 2 'Sistemi di travi - L'interpretazione elastica', UTET Torino, 1980.
64. I. Ricci, S. Gagliardi, G. Gasparini, S. Silvestri, T. Trombetti and M. Palermo, "First-storey isolation concept for multi-performance seismic design of steel buildings," in *Proceedings of the 15th world conference on earthquake engineering*, Lisbon, 2012.
65. F. Ricciardelli, A. D. Pizzimenti, M. Mattei, Passive and active mass damper control of the response of tall buildings to wind gustiness, University of Reggio Calabria, March 2003, *Engineering Structures* 25 (2003) 1199–1209
66. Robert. D. Hanson, TSU T. Soong; "Seismic design with supplemental energy dissipation devices" published by Earthquake Engineering Research Institute, 145-156(2003)
67. Robinson, W., & Greenbank, L. (1976). An extrusion energy absorber suitable for the protection of structures during an earthquake. *Earthquake Engineering & Structural Dynamics*, 4(3), 251-259.
68. Sabelli, R. (2000), *Research on Improving the Design and Analysis of Earthquake Resistant Steel Braced Frames*, FEMA / EERI.
69. Sabetta, F., Pugliese, A., 1996. Estimation of Response Spectra and Simulation of Nonstationary Earthquake Ground Motions. *Bull. Seismol. Soc. Am.* 86, 337–352.

70. Somerville, P. G. (1997). Development of ground motion time histories for phase 2 of the FEMA /SAC Steel Project. SAC BD/97-04, SAC Steel Joint Venture, Sacramento California.
71. Soong, T. T., & Spencer, B. F. (2002). Supplemental energy dissipation: state-of-the-art and state-of-the-practice. *Engineering Structures*, 24(3), 243-259.
72. Tremblay, R. (2002). Inelastic seismic response of steel bracing members. *Journal of Constructional Steel Research*, 58(5), 665-701.
73. Trevor E Kelly Holmes Consulting Group, Damper Design Guidelines, (2001)
74. T. Trombetti, S. Silvestri, Gasparini G and I. Ricci, "Stiffness-strength-ductility design approaches for crescent-shaped braces," *Open Constr Build Technol J*, vol. 3, pp. 127-140, 2009.
75. T. Trombetti, M. Palermo, A. Dib, G. Gasparini, S. Silvestri and L. Landi, Application of a direct procedure for the seismic retrofit of an R/C school building equipped with viscous dampers, 2015. *Front. Built Environ.* 1:14., doi: 10.3389/fbuil.2015.00014, September 2015
76. Tsai, K. C., Chen, H. W., Hong, C. P., & Su, Y. F. (1993). Design of steel triangular plate energy absorbers for seismic-resistant construction. *Earthquake spectra*, 9(3), 505-528.
77. Tsai K-C, Chen H-W, Hong C-P, Wang T-F. Steel plate energy absorbers for improved earthquake resistance. *Proceedings of the ASCE Structures Congress*, Irvine, CA, 1993.
78. Uriz, P (2005), Towards earthquake resistant design of concentrically braced steel structures, Ph.D. Dissertation, Department of Civil and Environmental Engineering, University of California, Berkeley, CA.

79. Vanmarcke, H. Erik, Cornell, C. Allin, Gasparini, A. Dario, Hou and Shou-nien, "The Earthquake Engineering Online Archive," Department of Civil Engineering, Massachusetts Institute of Technology, Cambridge, Massachusetts, 2011. [Online]. Available: <http://nisee.berkeley.edu/elibrary/Software/SIMQKE1ZIP>.
80. Warn, G. P. and Whittaker, A. S. "Performance estimates in seismically isolated bridges", Engineering Structures, Vol.26, pp. 1261-1278(2004).
81. E. Wilson and R. Clough, "Seismic analysis," [Online]. Available: https://en.wikipedia.org/wiki/Seismic_analysis#endnote_IDA
82. Whittaker AS, Bertero VV, Thompson CL, Alonso LS. Seismic testing of steel plate energy dissipation devices. Earthquake Spectra 1991; 7(4):563– 604.

1